Micro Injection Moulding:

Process Monitoring and Optimisation

A thesis

Submitted to Cardiff University

For the degree of

Doctor of Philosophy

by

Steffen Gerhard Scholz

Institute of Mechanical and Manufacturing Engineering

Cardiff School of Engineering

Cardiff University

Cardiff, Wales

United Kingdom

2011

ABSTRACT

The advances in micro engineering and especially micro products and micro components with functional micro and nano structures / features are directly dependent on the advances in manufacturing technologies for their scale up production. Micro injection moulding is one of the key technologies for cost effective serial production of micro components. In this thesis, the process capabilities and constraints of this technology were studied systematically. More specifically, new tool making process chains and various process factors affecting the micro injection moulding process were investigated. The manufacturing capabilities of this technology were further analysed by investigating the filling behaviour of micro cavities, the influence of air in micro cavities and the forces occurring during the demoulding stage.

Chapter 2 of this thesis reviews the state of the art in micro tooling and micro injection moulding.

In Chapter 3 an advanced condition monitoring system was developed to better understand the behaviour of the injection moulding process. In particular, cavity pressure sensors were utilised to analyse interdependences between process conditions and key characteristics of cavity pressure curves.

Chapter 4 investigates the influence and effects of air inside micro cavities. A design of experiments' study was carried out to identify process settings for achieving an optimum filling of micro cavities. In particular the flow length inside the cavity was investigated to judge about the process performance.

Next, the demoulding stage of the injection moulding cycle was studied in Chapter 5. In particular, ejection forces were analysed to investigate the influence of different

process settings on demoulding behaviour of polymer parts. This is especially important in order to avoid any part damage during demoulding.

In Chapter 6 micro stereolithography was used to fabricate mould inserts for micro injection moulding. Experiments were carried out with such mould inserts, and the tool life in relation to process settings for both the manufacture of the inserts and their replication performance, was studied systematically.

Finally, Chapter 7 summarises the main conclusions and contributions to knowledge of this research. Also, future research directions in the area of micro injection moulding are proposed and briefly discussed.

The main findings of this research can be summarised as follows:

- Indirect measurement methods can be utilised to monitor cavity pressure conditions in micro injection moulding and it was shown that P_{max}, P_{work} and P_{rate} were dependent on the materials and processing conditions.

- The performance of the µ-IM process can be improved by understanding the effects of V_i and air evacuation on Q_{max} , Q, and the part flow length. High µ-IM process settings and a limited venting through the primary split line have a significant impact on the filling performance. The µ-IM process performance can be improved by incorporating secondary vents and by applying vacuum methods for air evacuation.

- P_{max}, P_{work} and F^e_{max} were dependent on the processing conditions and there is a direct correlation between cavity pressure and demoulding force. The position of the pressure sensors is important, but the readings of both sensors correlate.

The holding pressure has the highest impact on the maximum demoulding forces.

- Rapid tooling can be applied successfully in µ-IM and offers a faster, cheaper and highly flexible manufacturing route for producing prototypes in the final material. Only the µSL inserts produced with a layer thickness of 20 µm (less undercuts) survived during the demoulding stage. The best results were achieved with PP, followed by PC. ABS polymer parts couldn't be replicated successfully.

ACKNOWLEDGEMENTS

Initially I would like to express my gratitude to Cardiff University for accepting my application to carry out my PhD research in the Manufacturing Engineering Centre at the School of Engineering.

It has been my privilege to work under the guidance of my supervisors Professor S.S. Dimov and Professor D.T. Pham. My enthusiasm during the study was fuelled by the high standard of work and scientific expertise of my supervisors. I am grateful for their advice, support and encouragement.

I would like to thank my colleague Chris Griffiths for the fruitful cooperation and the endless discussions of my research and the results of our joint work which was stimulating and at the same time indispensable for the completion of this work. I hope that this successful cooperation will continue.

I would like to thank Chris Matthews for the thorough review of this thesis and for keeping me motivated even at times when I thought that there was no light at the end of the tunnel.

My thanks also go to my colleagues in the Manufacturing Engineering Centre, especially to Emmanuel, Andrew, Petko, Todor, Krastimir, Hassan, Roussi, Ekaterin and Samuel for their friendship and technical advice.

My gratitude goes to my wife Julia and my daughter Ronja. Their love and support over the years have been pivotal in allowing me to reach my goals.

Finally, I would like to thank my Father for introducing me into the world of injection moulding when I was only a boy. In recognition of his support I dedicate this research to him.

The research reported in this thesis was funded by the FP7 programmes “Converging technologies for micro systems manufacturing” (COTECH, CP-IP 214491-2, http://www.fp7-cotech.eu/) and ‘‘Integrating European research infrastructures for the micro-nano fabrication of functional structures and devices out of a knowledge-based multimaterials’ repertoire” (EUMINAfab, FP7-226460, http://www.euminafab.eu/), the UK Engineering and Physical Sciences Research Council (EP/F056745/1) and the MicroBridge programme supported by Welsh Assembly Government and the UK Department for Business, Enterprise and Regulatory Reform.

DECLARATION

This work has not previously been accepted in substance for any degree and is not concurrently submitted in candidature for any degree

Signed……. (Candidate)

Date ……

Statement 1

This thesis is the result of my own investigation, exception where otherwise stated. Other sources are acknowledged by footnotes giving explicit references. A bibliography is appended.

Signed…….. (Candidate)

Date ……

Statement 2

I hereby give consent for my thesis, if accepted, to be available for photocopying and for inter-library loan, and for the title and summary to be made available to outside organisations.

Signed…….... (Candidate)

Date ……..

CONTENTS

LIST OF FIGURES

LIST OF TABLES

NOTATION:

ABS		Acrylonitrile Butadiene Styrene
Al		Aluminium
ANOVA		Analysis of Variance
COC		Cyclic Olefin Copolymer
d	[mm]	Measuring Pin Diameter
DLP		Digital Light Processor
DOE		Design of Experiments
E_a		Air evacuation
E_a^R		Resistance to Air Evacuation
E_f	[pC/N]	Force Sensitivity
E_p	[pC/MPa]	Pressure Sensitivity
FEA		Finite Element Analysis
F^e	[N]	Demoulding Force
F^e_{max}	[N]	Maximum Demoulding Force
FIB		Focused Ion Beam
IBM		Ion Beam Machining
IM		Injection Moulding
Int_{max}	[MPa s]	Maximum Integral Value
k	[W/(m K)]	Thermal Conductivity
LBM		Layer-Based Manufacturing
OA		Orthogonal Array
P	[MPa]	Pressure
P^c	[MPa]	Cavity Pressure

P^c_{max}	[MPa]	Maximum Cavity Pressure
P^c_{work}	[MPa ms]	Cavity Pressure work done
pd(x)	[-]	Probability Density
P^i / P_i	[MPa]	Injection Pressure
P^i_{max}	[MPa]	Maximum Injection Pressure
P^i_{work}	[MPa ms]	Injection Pressure work done
P_h	[MPa]	Holding Pressure
P_{max}	[MPa]	Maximum Cavity Pressure
PP		Polypropylene
P_{start}	[MPa]	Pressure at start of interval
P_{rate}	[MPa/ms]	Pressure rate of change
P_{work}	[MPa ms]	Pressure work done
$\dot{Q}$	[ml/s]	Air flow rate
Q	[ml]	Air flow volume
$\dot{Q}_{max}$	[ml/s]	Maximum air flow rate
$\dot{Q}_{start}$	[ml/s]	Air flow rate at start
$\dot{Q}_{end}$	[ml/s]	Air flow rate at end
R_a	[µm]	Surface roughness
RMF		Rapid Micro Fabrication
RP		Rapid Prototyping
RT		Rapid Tooling
SEM		Scanning Electron Microscope
SL		Stereo lithography
SV_R		Surface to Volume Ratio

t	[ms] / [s]	Time
t^{e}_{max}	[ms]	Time when demoulding force reaches Maximum
t_{end}	[s]	Time end of Air flow rate integral
t_h	[s]	Holding Pressure Time
t_i	[s]	Injection Time
t_{max}	[ms] / [s]	Time to Maximum Cavity Pressure
$t_{mould\_opening}$	[ms]	Time when mould starts opening
t_{start}	[ms] / [s]	Start Time
T	[°C]	Temperature
T_b	[°C]	Melt / Barrel Temperature
T_{cr}	[°C]	Critical Temperature Range
T_g	[°C]	Glass Transition Temperature
T_m	[°C]	Tool / mould Temperature
TR	[-]	Transcription fidelity
T_t	[°C]	Polymer Transition Temperature
V	[mm^3/g]	Specific volume
V_i	[mm/s]	Injection Speed
W	[mg]	Part Weight
WLI		White Light Interferometer
Δt	[ms]	Time Step of Data Acquisition System
Δ	[-]	Relative effect
σ	[-]	Standard Deviation
µ-IM		Micro-Injection Moulding
µSL		Micro-Stereolithography
μ_k	[-]	Kinetic friction coefficient

μ_s	[-]	Static friction coefficient

1 INTRODUCTION

1.1 Motivation

In recent years the number of commercialised products with micro scale components or features has been increasing rapidly. For example, this includes from highly specialised technical products such as lab on chip devices to mass-produced products for daily use such as mobile phones and cameras that incorporate hundreds of micro scale mechanical components. The demand and market for such products has been growing quickly over recent years (Eloy 2008). To support this demand, multi-functional, multi-material micro components must advance from the laboratory to low-cost and high volume manufacture.

Ratchev and Turitto reported in 2008 that Europe has outstanding competence and infrastructure for conquering successfully a good fraction of the expanding Micro and Nano Manufacturing (MNMT) market. Nevertheless, the transition from Research and Development (R&D) to products for this highly specialised market has to be accelerated (Ratchev and Turitto 2008).

Micro and nanotechnology manufacturing processes are highly cost intensive. This is due to the fact that very low tolerances are required, materials are expensive and often a cleanroom environment is demanded. This underlines the importance of replication technologies which employ very expensive masters to produce hundreds of thousands of components in a cost effective way. In this context, micro injection moulding (µ-IM) is one of the most important high throughput replication technologies. Micro tool making and micro and nano replication by injection moulding (IM) are among the most

commonly used process chains for the production of micro products and micro components. To meet the growing demands for such products/components it is essential to understand and characterise the capabilities and limitations of viable micro and nano manufacturing technologies. New emerging applications necessitate the production of thinner parts (for weight reduction), smaller components, micro parts with smaller features or polymer parts with higher aspect ratios, and hence are dependent on technology advances in micro tool making and micro replication.

Micro injection moulding is a complex process with many factors affecting the quality of the final polymer parts. In particular, the quality of the replicated parts depends on materials' characteristics, process and machine processing parameters, production environment and the quality of the IM tools. In order to design and implement a viable process for micro replication all of these factors have to be taken into account and their constrains studied systematically. In this thesis the behaviour of air inside the mould cavities, the monitoring of process conditions, the forces during demoulding of the polymer part, and finally, a new mould making process chain were investigated.

In order to keep this study focused, the investigation of the µ-IM process is based on a comprehensive state of the art survey of latest research and developments in this area.

1.2 Research Objectives

The overall aim of this research was to investigate the factors affecting the performance of the µ-IM process and by applying empirical and analytical methods to characterise and reduce the uncertainties associated with the µ-IM process. Due to the

large number of factors affecting this process and the complexity of the process, a subset of process parameters was selected and thoroughly investigated in this thesis. For the empirical part of this research mould inserts with micro cavities were produced using different micro tool making technologies. These moulds were designed purposely to investigate certain aspects of the µ-IM process, which are of particular interest for this research, especially:

- The cavity pressure behaviour during the filling stage of polymer micro parts;
- The cavity air flow behaviour in micro injection moulds;
- The demoulding forces on polymer micro parts;
- The use of micro stereo lithography (µSL) polymer mould inserts for IM.

After identifying the main factors affecting the µ-IM process in the context of the topics above, a number of process conditions were selected to investigate their effects on the replication process of polymer micro parts. Design of experiments techniques, condition monitoring experimental setups and statistical methods were applied innovatively to quantify specific moulding conditions that were viewed as crucial in understanding the µ-IM process. To achieve the overall aims, the following objectives were set:

- To perform a detailed analysis of the filling stage of the µ-IM process. This includes an assessment of the effect of process parameters on the melt flow behaviour of different polymers with a particular focus on the relationship between process parameters and the achievable flow length and part quality.

- To systematically investigate the effect of air traps in micro cavities and their effects on the part quality. In particular, to identify process conditions which can be chosen to minimise the effects of trapped air and the so called “diesel” effect.

- To investigate both the filling and the demoulding stages of the µ-IM process by conducting a systematic experimental study. A special emphasis was set on analysing the forces applied on the polymer part during the demoulding stage and their interdependence with process conditions and materials characteristics.

- To investigate a new tool making process chain that utilises µSL to fabricate moulding inserts. To identify the best set of µ-IM parameters to maximise tool life.

In order to achieve these objectives empirical investigations of the µ-IM process were carried out by employing design of experiment studies and statistical methods. The results of the experimental tests were analysed, quantified, and their influence on different sets of process parameters identified. Further to that, recommendations for the improvement of the process performance were made, based on the identified effects.

1.3 Thesis Organisation

The research is presented in seven chapters of which Chapters 3 to 6 are the main technical chapters. Chapter 2 describes the state of the art in IM and Chapter 7 presents the main contributions to knowledge.

Chapter 2 of this thesis gives an overview over the state of the art in µ-IM. It provides the technical background knowledge upon which the technical Chapters 3 to 6 were based and has three subsections. The first section gives a short overview of micro tool making technologies. In the second section the µ-IM process is analysed and special process variants are presented and critically analysed. The third section of this chapter describes the specific focus of this research and the main concepts that have been investigated.

In Chapter 3 the cavity pressure behaviour during the injection moulding cycle was investigated systematically by employing a specially designed process and condition monitoring experimental setup. Different process settings were analysed by applying a design of experiments approach and subsequently part quality was assessed. A pressure sensor mounted inside a tool cavity was employed to analyse maximum cavity pressure, pressure increase rate during filling and pressure work. The influence of four µ-IM parameters, melt temperature, mould temperature, injection speed and packing pressure on these three pressure-related process parameters was investigated. A design of experiment study was conducted by moulding a test part, a micro fluidic component, in three different polymer materials, PP, ABS and PC.

Chapter 4 investigates the effect of air traps and evacuation in micro cavities and their effects on the part quality. An advanced condition monitoring system, including sensors for measuring air flow out of the cavity, was utilised. A design of experiments study was conducted to investigate the melt flow filling behaviour of the cavity. A novel experimental setup was designed and implemented to monitor maximum air flow and air flow work by employing a Micro Electro Mechanical Systems (MEMS) gas sensor mounted inside the mould. The influence of four µ-IM parameters, melt temperature,

mould temperature, injection speed, and resistance to air evacuation, on two air flow-related output parameters was investigated. Conclusions were made about the effects of process parameters on cavity air evacuation and the influence of air evacuation on the part flow length.

Chapter 5 reports an experimental study that investigates part demoulding behaviour in μ-IM with a focus on the effects of pressure and temperature on the demoulding forces. In particular, the demoulding characteristics of a test part was studied as a function of four process parameters, melt temperature, mould temperature, holding pressure and injection speed, employing the design of experiment approach. Also, the results obtained using different combinations of process parameters were analysed to identify the best processing conditions in regards to demoulding behaviour of micro parts.

Chapter 6 reports a pilot application of the μSL technology to produce mould inserts for μ-IM. The moulding performance of μSL inserts as a function of tool geometry in combination with the effects of some process factors was investigated. Condition monitoring techniques were applied to provide information for process optimisation.

2 LITERATURE REVIEW

This Chapter presents a review of the state of the art in micro tooling and the micro replication process. The first section gives an overview of established micro tool making technologies. Then, prototype and rapid tooling technologies for µ-IM are reviewed together with various characteristics associated with their use. The third section presents the main characteristics and fundamental principles of µ-IM that is followed by an analysis of factors influencing the performance of the µ-IM process. The last section concludes the review with a summary of open research questions that are addressed in this research.

2.1 Micro Technology and Micro Tooling

It is more than 50 years ago, that miniaturisation and its potential was highlighted by Richard Feynman at the American Physical Society Meeting in Pasadena in 1959 (Feynman 1959, 1983; Senturia 1994). At that time nothing was done in this field and Feynman was the first to recognise and discuss the immense scientific and economic potential of miniaturised components and products. In his presentation he addressed the manufacture of multiple polymer components from a master tool as a possible replication technology, which could be considered the first reference to polymer micro replication in the literature. However, the idea of miniaturisation emerged long before, the driving force being the creation of more precise and smaller watches. Nicoud reported that back in 1929 J. Le Coultre held the record for the smallest caliber watch, 4.8 mm by 14 mm by 3.4 mm in size (Nicoud 1995). At the same time, extreme complexity was reached with astronomical watches, showing the movement of planets

and consisting of 213 parts of which many were of micro scale (Nicoud 1995). Still, these products were single-unit productions based on skilled work of individuals. As Feynman foresaw, initially the semiconductor and microcomputer industry drove the development in the field of micro technologies. Taking into account that silicon was the most commonly used material by the semiconductor industry, many “silicon” based processes and technologies were developed and reached a high level of maturity. These advances resulted in micro system technologies such as MEMS (Micro Electro Mechanical Systems), MMT (Micro Machine Technology) and MST (Micro System Technology) (Kussul et al. 1996).

In 2004, the European Network of Excellence for Multi Material Micro Manufacture (4M NoE) was created to address the requirements of developing micro manufacturing capabilities for a wider range of materials and also to broaden the field of their applications. Dimov described in 2005 that “the 20th century could be seen as the silicon based microelectronics revolution, whereas the 21st century would be looking forward to the adaptation of micro and nano technologies (MNT) for a much wider range of materials and applications” (Dimov 2005). To succeed in miniaturising products in the field of micro fluidics, micro optics and micro sensors, it was identified that manufacturing capabilities for serial production of parts should be created. The industrial community of the 4M NoE envisaged the most significant market opportunities to be in the following sectors:

- Medical / Surgical
- Automotive and transport
- Biotechnology

- Consumer Products
- Information and Communication
- Energy / chemical
- Scientific / academic
- Pharmaceutical

The requirements for low cost and mass production are predominant for the successful development of micro and nano products (Dimov et al. 2006). Replication processes such as micro injection moulding (µ-IM) and the related mould making technologies have the potential of fulfilling these requirements and hence are considered to be key technologies for the commercialisation of such products.

There are many technological advances in the area of micro fabrication (Alting et al. 2003). The increasing demand for product miniaturisation and the wide range of functions that micro parts have to fulfil led to the development of complex process chains for micro tool making. In particular, the need for length scale integration in micro products often requires the combination of different structuring technologies (Bigot et al. 2009). Processes with high removal rates have limitations in terms of achievable feature sizes, surface roughness and accuracy while others are capable of machining features at micro and sub-micron scales but with much lower through put. (Azcarate et al. 2006). Tosello et al. coined the term “hybrid tooling” when the capabilities of two or more processes have to be combined in a sequence (Tosello et al. 2007).

The following section provides a brief overview of micro tool making technologies which have been developed in recent years.

2.1.1 Micro milling

The micro milling process is the result of “down scaling” the established milling technology. Recent developments in computer numerical controls (CNC), high speed spindles and new materials for cutting tools have enabled the machining of micro features. The milling process is determined by a mechanical interaction of the tool with the work piece. The cutter, which needs to be significantly harder than the work piece, is following a determined machine path and is removing surplus material. The minimum achievable feature size is limited by the size of the commercially available sintered end mill tools, which is currently around 30 µm. Because of the high wear of these small cutting tools their lifetime is limited and therefore the volume of material which can be removed economically (Popov et al. 2006) is also limited. Another important factor for micro milling is the micro milling machine itself. For ultra-precision milling, machines with high spindle speeds and advanced CNC controllers for 3D machine path generation are required. Thermal expansion of both the work piece and the tool can compromise the quality and often leads to cutting tool breakage (Gandarias et al. 2006). For that reason, a temperature-controlled environment is crucial for the micro milling process.

2.1.2 Micro electrical discharge machining (µEDM) and µEDM milling

Micro electrical discharge machining (µEDM) and µEDM milling are technologies commonly used for the structuring of micro mould inserts. These techniques offer an

alternative way for making mould inserts out of high temperature resistant metals or alloys, for example tungsten carbide. A high frequency pulsing current is applied between the cathode work piece and the anodic electrode. The work piece is submerged into a dielectric fluid to avoid shortcuts and unwanted sparks (Madou 2001). One alternative, the so called die sinking EDM, uses electrodes often with complex shapes representing the negative shape of the actual micro cavity. These electrodes then are periodically brought closer to the work piece and the current removes material. The electrodes have to be manufactured smaller than the dimensions of the cavity because a spark gap between the electrode and the work piece appears which enlarges the cavity. For micro cavities the calculation of the spark gap is particularly challenging (Pham et al. 2004).

A second alternative is the so called µEDM milling process. A rotating electrode follows a predefined machine path and removes material in a layer based process. This process is similar to micro milling but contrary to micro milling where the material is removed by mechanical forces the removal of the material is made by energetic effects. The µEDM electrodes are usually made from copper, graphite or tungsten carbide and the wear of the electrode during the process has to be taken into account (Bigot et al. 2005; Pham et al. 2007a, b).

A third alternative is the so called wire EDM process. A wire is used to cut the work piece. Wire diameters can go down to 20 µm and good surface roughness down to Ra=0.07 µm can be achieved (Cao et al. 2006; Rees et al. 2008; Yang et al. 2010). Quality and feature size are limited by the wire diameter and wire vibration (Uhlmann et al. 2005).

2.1.3 Laser ablation

Laser ablation has been used for many micro related industrial processes in recent years (Campanelli et al. 2007). Laser ablation is a non-contact removal method, therefore no mechanical forces are applied to the work piece. This has some advantages in terms of clamping the work piece or the accuracy of the stages used to move the work piece. The fact that nowadays laser sources have become relatively cheap and different types of laser sources are available and can be integrated into CNC machines, means there is a wide range of options available for tool and micro tool manufacturing. Different types of laser sources with different wavelengths, pulse duration and power can be used to achieve a wide range of removal rates, accuracy and feature sizes (Bralla 1999; Dobrev et al. 2006). This technology allows the fabrication of structures down to 3 µm with an aspect ratio up to a factor of 10 (Madou 2001; Rötting et al. 2002).

Furthermore, its integration into CNC machines means laser milling can machine complex 3D features with layer based on CAD / CAM approaches. Ultra-short pulse laser ablation offers a good response to many different types of materials; even transparent materials can be machined with lasers (Petkov et al. 2008).

2.1.4 Ion Beam Machining (IBM) and Focused Ion Beam Machining (FIB)

Ion Beam Machining (IBM) and Focused Ion Beam Machining (FIB) offer structuring capabilities in the sub micro meter range (Lalev et al. 2009). IBM / FIB systems produce a beam of charged gas ions, for example argon gas ions, which is accelerated in a high energy field and then directed onto the work piece. The ions of the beam spatter atoms out of the work piece. By controlling the direction and intensity

of the beam, 3D features can be milled employing direct write and layer based methods. Reversely, the beam can be used to deposit material as well.

Amorphous materials have a very good response to FIB spattering (Li et al. 2007; Quintana et al. 2010). Metals with their multi crystalline structure are not appropriate for sub-micron structuring due to the different orientation of their grains.

Table 2-1 summarises achievable feature sizes, tolerances and aspect ratios for different mould making technologies.

Technology	Typical feature size	Typical tolerances	Achievable Aspect ratio	Wall /surface roughness (Niggeman n et al. 1999)	Materials (Weber et al. 1996)	Removal Rate [$\mu m^3/s$]
Ion Beam LIGA	0.1 - 0.5 µm	0.02 – 0.5 µm	3			
FIB	0.01 - 1 µm	0.0005 - 0.02 µm	20		amorphou s	20-30
X-Ray LIGA	0.5 µm – 1 mm	0.02 – 0.5 µm	10-100	<20 nm	Copper, Nickel, Ni-alloys	
E-Beam LIGA	0.1 – 0.5 µm		1-2		Copper, Nickel, Ni-alloys	
UV Liga	2 – 500 µm		1-10		Copper, Nickel, Ni-alloys	
Laser (fs)	1 µm	< 1 µm	1-10	1 µ - 100 nm	Polymer, Ceramics, metals	13 000
Eximer Laser	6 µm	< 1 µm	1-10		Polymer, Ceramics, metals	40 000
Laser (ps)	4-6 µm	< 1 µm	10			100 000
Laser (ms)	50 µ	20 µm	20		Metals	
ECM	few micro meters	< 1 µm	8			
µEDM milling	10 – 25 µm	3 µm	10-100	0.3 – 1 µm	Conductiv e materials	25 000 000
Micro Milling	25 µm	2 µm	10-50	0.1 µm	Polymers Aluminium , Brass, Steel	10 400

Table 2-1 Overview of technologies used for micro mould insert fabrication (Table taken from Giboz and modified (Giboz et al. 2007))

2.2 Prototype and Rapid Tooling technologies for µ-IM

Rapid prototyping (RP) is a potential tooling technology for fabricating µ-IM moulds. The following sections present an overview of RP technologies for fabricating mould inserts and also discuss the main issues associated with their effective use for µ-IM, in

particular, the mechanical and thermodynamic loads that they have to withstand during IM cycles.

2.2.1 The manufacture and usage of RP mould inserts

Cost effective tool-making technologies used for producing moulding inserts with feature sizes down to a few microns are essential for creating reliable platforms for micro-manufacture. Generally, the mould tool materials investigated by researchers are those traditionally used for IM, such as various tooling grade steels; however alternative materials like engineering polymers, e.g. PEEK, have also been investigated (Griffiths et al. 2010; Harris et al. 2004; Jensen et al. 2004).

Recently, rapid tooling (RT) solutions that allow “soft” tools to be produced by layer-based manufacturing (LBM) have been identified as a cost effective alternative to conventional machining, especially for small batch production (Chua et al. 1999). By eliminating multiple steps necessary to produce a tool, machining of the injection mould directly by a LBM process could potentially reduce significantly the lead time and costs, and address specific requirements for manufacturing low volume quantity parts. Much research on RT has been conducted employing stereolithography (SL) to produce tools at the macro scale. However, there are some limitations such as the feature sizes, achievable tolerances and laser spot size that limit the application area of conventional SL systems. New micro-stereolithography (μSL) systems have been developed to increase the process resolution, and thus to be able to fabricate features in the micron range. These technology advances have been successfully demonstrated with the manufacture of micro gears and complex micro fluidic devices

(Maruo and Ikuta 2002; Yang et al. 2009; Zhang et al. 1999). However, no attempts were reported to have used the μSL technology to produce micro moulds.

The prototyping stage is crucial in the development of micro devices and currently various micro fabrication processes are utilised to fabricate polymer prototypes. Such prototypes are used successfully by researchers to explore and validate new design concepts and ideas. With the development of RT solutions for fabricating soft tools it will be possible to produce small batches of parts in the required material for product design validation studies and at the same time to optimise the process for their scale-up production.

The reduction of time to market was initially the strongest motivation and economical driving force in developing LBM processes. Also, the advantages that the technology offered in producing components with freeform surfaces were very important for broadening its application areas (Levy et al. 2003). RT has emerged as a viable alternative to conventional methods for prototyping tooling, in particular for casting and IM, and is considered as a natural evolution of the LBM technology (Rosochowski and Matuszak 2000). Similarly to macro scale applications of RT the main advantages of LBM methods for fabricating micro tools are lead time, cost and also, very importantly, the tools' behaviour is similar to conventional ones produced for high volume replication. Research into RT techniques has advanced this technology. It is gaining more importance in different application areas and now can be considered as a viable alternative to conventional machining (Chua et al. 1999). It has been demonstrated that ceramic and plastic mould inserts can be applied successfully for replicating components for micro-systems technology based applications and SL has advanced to the most established LBM technology.

SL systems use 3D CAD data to convert liquid plastic materials and composites into solid cross-sections in a layer by layer fashion, and thus to build accurate three-dimensional parts. The technology has been applied successfully to manufacture polymer moulds, however the advantages of the SL-based RT process can be negated by the low mechanical forces that the SL inserts can withstand and their low thermal conductivity.

2.2.2 Mechanical strength of RP mould inserts

There are two main types of forces acting on mould inserts during the IM cycle. The first relates to the pressure (P) inside the cavity due to the injected polymer, while the second is caused by the demoulding force (F^e) necessary to remove a part from a mould. F^e is a friction force that occurs between the insert and the moulded part and is a function of the static friction coefficient and the surface area that is in contact. The coefficient of static friction is dependent upon the surface roughness or step effects that are the result of building parts in layer by layer fashion. Hopkinson and Dickens (Hopkinson and Dickens 2000a) measured F^e, surface roughness and temperature cycles in an aluminium (Al) mould and a SL mould. They reported that the surface roughness of the tools did not change after moulding 50 parts, but an increase in cycle time resulted in higher F^e for both insert materials. Harris et al. (Harris et al. 2002) investigated the effects of such SL mould design variables as build layer thickness, draft angle and surface roughness on F^e. It was reported that higher surface roughness and an increased thickness of the build layer resulted in a higher F^e, and that an increase of the tool draft angles led to a lower F^e. However, the results were not the same for all the polymer materials moulded, the greatest F^e were experienced

when using PA, ABS, and PP. This difference was attributed to the varying physical characteristics such as shrinkage and thermal conductivity (*k*).

Hopkinson and Dickens (Hopkinson and Dickens 2000c) predicted the conditions under which tensile failure could occur in mould tools with SL inserts employing a finite element analysis (FEA) model and thus to estimate the rate of cooling and contraction of PP inside the mould. It was predicted that an increase of the cooling time would result in an increased contraction of the part and a higher F^e, and, therefore, as short a cooling period as possible should be used in order to prevent tool failures. Dickens and Hopkinson (Hopkinson and Dickens 2000b) applied the same FEA method to predict F^e and estimate temperature. Using a modified heat transfer model, the prediction of tool strength showed that the tool weakens exponentially 120 s after the injection stage, thus suggesting that ejection should occur as early as possible to avoid mould failures.

F^e can be reduced by using a mould release agent. Knitter et al. (Knitter et al. 2003) developed a SL-based tool-making process chain for low pressure IM of ceramic components. It was reported that the quality of the SL master was of decisive significance for the quality and reproducibility of the mouldings and that use of a release agent reduced F^e. Combining the thermal shrinkage and the stair-step profile, Colton et al. (Colton et al. 2001) modelled the mechanical forces and F^e applied on a SL mould during the injection cycle. The mould insert was estimated to fail once the stress exceeds the maximum flexural stress. The experiments carried out to determine the effect of process conditions on the mechanical properties of two different SL resins revealed that failures occurred in a ductile manner above the materials Glass Transition Temperature (T_g), and in a brittle manner below T_g.

2.2.3 Thermal properties of RP moulds

SL mould failures can occur not only due to acting forces, but excessive temperatures can also have a detrimental effect on tool life and, therefore, should be investigated, too. Tool failures are more likely due to temperature changes during the injection moulding cycle, and therefore longer cooling time are advantageous and can increase the life of the SL inserts and enable them to withstand more moulding cycles (Ribeiro Jr et al. 2004). For photo polymer materials *k* of the mould is a major factor that sets apart a SL insert from a traditional steel tool. The photosensitive resins used to fabricate SL inserts have a heat transfer rate a thousand times lower than that of their aluminium counterpart, e.g. *k* of a SL acrylic and epoxy resins is 0.2 W/m-K, while *k* of Al is 200 W/m-K (Harris et al. 2003a). Harris et al. (Harris et al. 2004) established the extent to which the differences in the *k* characteristics of SL inserts and conventional ones affect the tool replication capabilities. Investigating the temperature difference in SL and Al moulds it was reported that each had a consistent start temperature but the SL mould showed a sharp reduction of their peak temperature, which was attributed to various losses of thermal energy during the mould opening stage. Al inserts did not show such a characteristic. The *k* properties of the material led to very fast cooling of Al inserts, while this is opposite for SL inserts.

There are differences in the quality of the parts produced employing SL inserts. Attanasio, et al. (Attanasio et al. 2006) reported that due to low *k* and hence the low energy loss in SL cavities, the injected polymer remains at a low viscosity for longer compared with steel cavities, which facilitates their complete filling. An and Chen (An and Chen 2008) found that the use of SL moulds reduced the flow mark surface defects because the injected polymer had sufficient time to relax before solidifying. It

was suggested that part anomalies were due to differing degrees of crystallinity developing within parts due to their thermal history during moulding, in particular, the rate of polymer cooling from its molten state which is imposed by the inherent *k* properties of the insert material (Harris et al. 2003a). With a focus on the differing *k,* Harris et al. (Harris et al. 2003b) evaluated the shrinkage of mouldings from SL cavities compared with those from a conventional metal tool. The results showed that overlooking the mould expansion in SL tools would result in significant errors in determining absolute part shrinkage. In particular, the shrinkage of PA (a crystalline polymer) parts in SL cavities was twice higher than that in AL moulds; while for the same experimental conditions ABS (an amorphous polymer) demonstrated no such differences. Consequently, it was recommended that amorphous polymers should be used in preference to crystalline alternatives when using SL inserts. FEA of the IM process predicted distortions and deformations occurring in the SL cavities, and that the part quality could be significantly improved by using photopolymers with a higher *k* (Rajitha et al. 2001; Zhou and Li 2006).

2.3 Micro replication processes

The key to overcoming the bottleneck between master production and serial mass production of micro components is a cost effective and reliable replication technology. Several moulding technologies such as hot embossing, µ-IM, compressive injection moulding, reaction injection moulding and thermoforming are utilized to manufacture thermoplastic micro components (Heckele and Schomburg 2004). Other replication technologies for special applications such as two-component injection micro moulding, powder injection moulding, micro over moulding, micro assembly moulding, micro

extrusion or roll to roll processes could be cited as well. In this section hot embossing and µ-IM are described because they appear to be the most industrially viable processes. In the last part of this section some specific process variants and add-ons to the µ-IM process are presented.

2.3.1 Hot Embossing

Hot Embossing uses a semi-finished polymer sheet which comes into contact with a pre-heated micro structured mould in a vacuum chamber. On contact, the polymer melts and the hot embossing stamp presses the polymer down into the mould and fills its cavities. Subsequently, the mould insert and polymer shim are cooled down simultaneously. The processing parameters for hot embossing include a prescribed thermal cycle, compression force and compression speed. The main disadvantages of this process are the long thermal cycle time of up to 30 minutes and the fact that semi-finished polymer shims have to be used. Advantages of the process are in the replication of features with very high aspect ratio. An illustration of the hot embossing process is given in Figure 2-1.

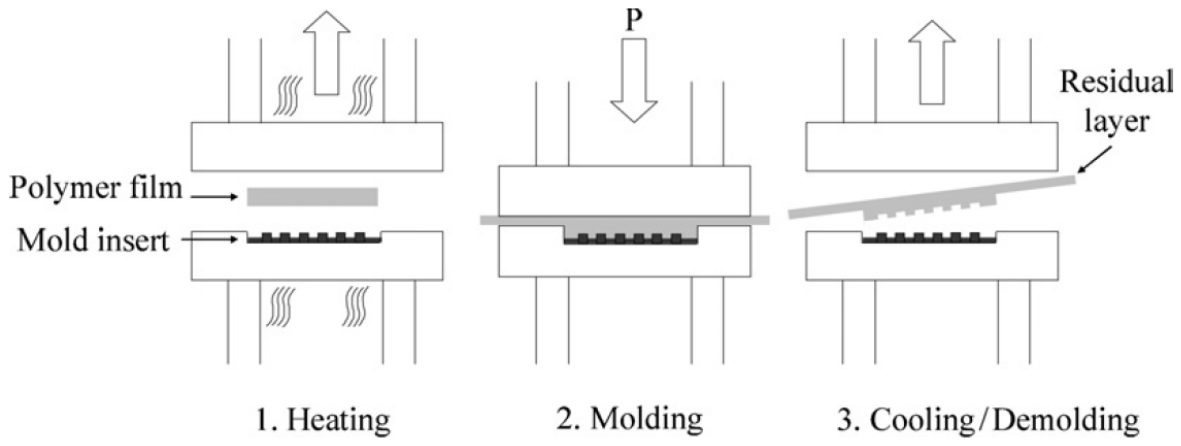

Figure 2-1 Scheme of the hot embossing process (Giboz et al. 2007)

2.3.2 Injection Moulding (IM)

IM is the most commonly used replication method for the mass-production of polymer parts. This process involves the melting of a polymer into plasticisation and injection of the molten polymer into a tool containing cavities with the negative shape of the part. Subsequently, the polymer is cooled in the mould and demoulded by opening the tool. For each type of polymer, different process conditions have to be chosen in order to produce good replicas. Whiteside et al. and Zhao et al. reported that the main influencing process parameters are (Whiteside et al. 2005a; Zhao et al. 2003a; Zhao et al. 2003b):

- Injection speed (V_i)
- Injection pressure (P_i)
- Temperature of the mould (T_m)
- Temperature of the barrel (T_b)
- Holding pressure (P_h)
- Holding pressure time (t_h)

The advantage of the IM process is that relatively short cycle times can be achieved, which makes this process very cost effective. Nevertheless, each part needs a tailor-made tool incorporating cavities, heating devices, cooling channels and a specific demoulding system. Hence, the costs for such moulds are not negligible and have to be taken into account. For this reason this process can only be considered for the production of larger numbers of polymer parts.

Heckele and Schomburg compared hot embossing and IM and concluded that hot embossing has advantages for the production of small to medium scale batches and for the production of polymer parts with very high aspect ratios and features in the nano meter scale. On the contrary, IM, although it is a less accurate process, has clear benefits when employed for mass production due to the short cycle time (Heckele and Schomburg 2004).

Figure 2-2 illustrates the concept of the injection moulding process and Figure 2-3 the IM process steps in chronological order.

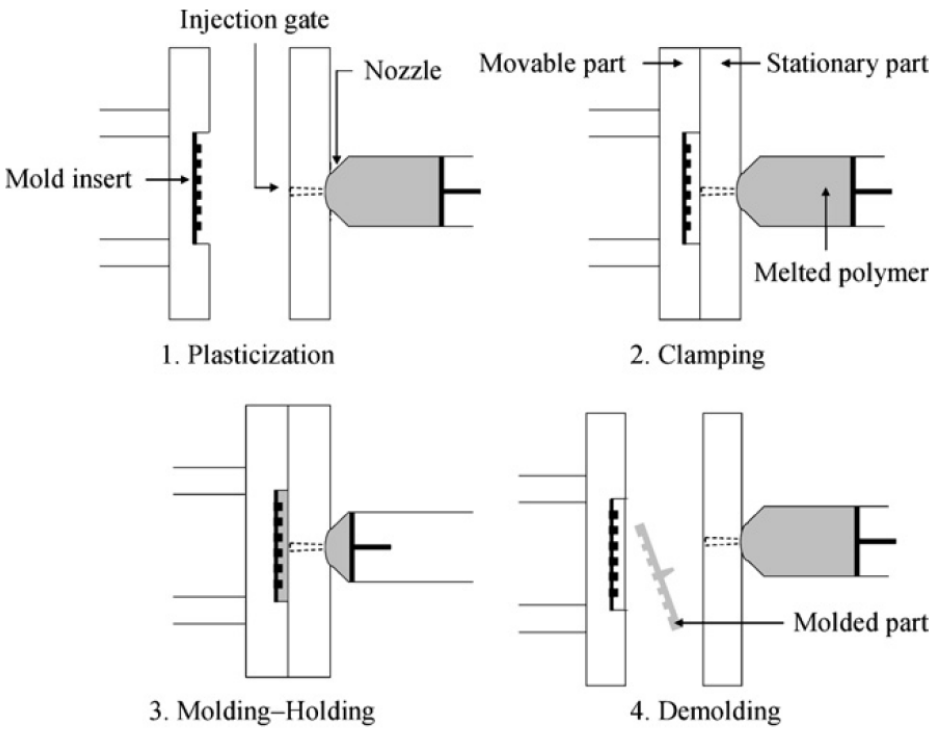

Figure 2-2 Scheme of the IM process (Giboz et al. 2007)

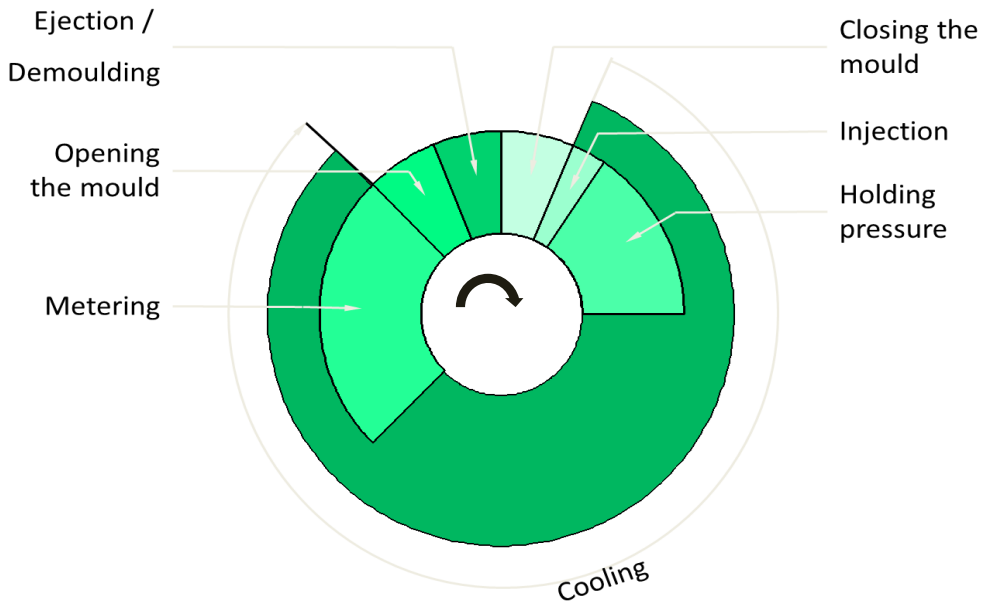

Figure 2-3 Chorographical cycle of the IM procedure

2.3.3 Micro injection moulding (µ-IM) process

The micro injection moulding process cannot simply be considered a downscaling of the injection moulding process (Griffiths et al. 2008a). Whilst acknowledging that there is a rich repository of polymer processing knowledge for IM, it is also important to recognise that due to scale effects such know-how cannot fully be employed directly to the µ-IM process, and also that some proven designs and processing strategies at macro scale should be carefully re-considered taking into account these scale effects (Fleischer and Kotschenreuther 2007). Martyn et al. and Griffiths et al. listed the technological differences of the µ-IM process in comparison with the conventional IM, which shows clearly that this truly is a new technology (Griffiths et al. 2008b; Martyn et al. 2002):

- Mould construction technology including micro cavities

- Application engineering
- Raw material variations
- Precision technology
- Nano rheology
- Process monitoring and measurement
- Product properties
- Modelling and simulation of the process
- Different set of process parameters in particular injection speed
- Different control systems

A general definition of the µ-IM process is that of the production of polymer parts with structure dimensions in the micro, sub-micron or nano meter scale range (Kemmann and Weber 2001). In addition, Yao and Kim suggested that components manufactured by µ-IM fall into one of the following two categories: Type 1 are parts with an overall size less than 1 mm, whereas Type 2 parts could have larger overall dimensions but incorporate features in the micro metre range, typically less than 200 µm (Yao and Kim 2004). Kukla et al. proposed that components produced by µ-IM could cover parts of any dimension but are limited to a mass of less than a few milligrams with tolerated feature sizes in the µm range (Kukla et al. 1998). Ruprecht et al. and Whitesite et al. summarised these definitions and in recent years the following has been accepted as a definition of µ-IM (Ruprecht et al. 2002; Whiteside et al. 2003):

- Part processing weight in the range of a few milligrams

- Parts where dimensions of processing features are in the micro meter range
- Parts exhibiting dimensional tolerances in the micro meter range but without dimensional limit

For an IM machine to perform at such a scale, two important factors have to be considered: the overall volume of polymer in the metering zone of the plastification unit and the control of the deliverable volume.

Also, the cycle of the µ-IM process is different from the IM cycle, particularly, if additional processes like variothermal mould heating and cavity evacuation are applied. The µ-IM cycle is illustrated in Figure 2-4.

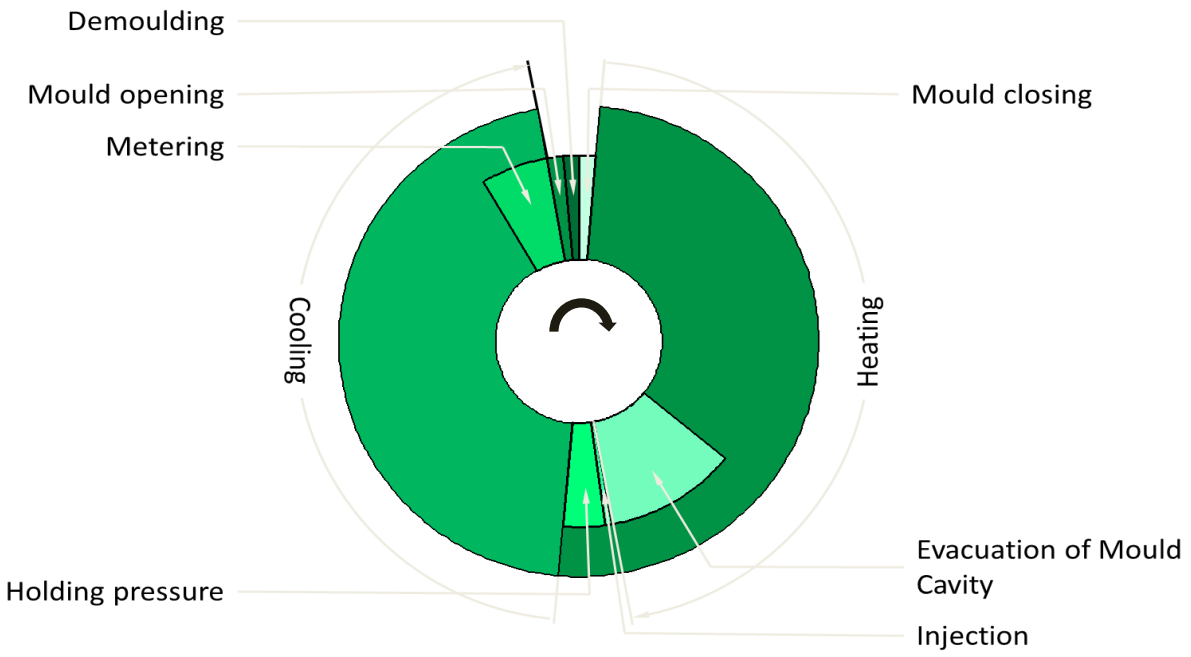

Figure 2-4 Schematic process steps of the µ-IM cycle

2.3.4 Micro injection moulding machine

The development of the µ-IM process goes back to the late 1980[s]. Back then, modified conventional IM machines were used (Piotter et al. 2002). The manufacturing of micro parts with these conventional machines led to a large amount of waste, because large runner systems had to be utilised in order to increase the volume on the metered polymer and thus to adapt the volume to the requirements of the machines. The actual micro part represented only a small fraction of the polymer which was used for each cycle. Moreover, the control of conventional IM machines using hydraulic power from central and sub distribution points was not accurate enough for the replication of polymer micro parts. Another consideration is that of accuracy of movement, for both the screw and the clamping device. Mould designs which require alignment tolerances of less than 10 µm have to use machines that can ensure that movements of clamping platens are within this positional and alignment accuracy. The same requirement applies to the linear and rotational precision of the machine screw, which could not be achieved with conventional servo hydraulic valves and concepts. A precise control of the metering volume requires the use of servo electric driven machines (Kelly et al. 2005). Another specific development is the identification of the switchover point from filling / injection pressure to holding pressure. Conventional IM machines use the injection pressure to identify the switchover point whereas µ-IM machines are generally using the position of the injection plunger to determine the switchover point (Zhao et al. 2003b). With this, a more precise control over the amount of polymer injected into the cavity can be realised.

Finally, the dimensions of the entire µ-IM machine can be much smaller than that of conventional machines because micro parts can be produced with much smaller tools.

The sizes of the critical injection unit parts such as barrel, screw, nozzle and clamping unit can be miniaturised to the requirements of the replication of micro parts. Therefore, specific µ-IM machines were developed to address these demands and to reduce waste, energy consumption and the degradation of the polymer (Michaeli et al. 2004b).

To address the demands for micro replication, two main concepts of µ-IM machines have been developed:

1. The first concept is aiming at the adaptation of the conventional barrel screw system to smaller diameters. Typically the screw diameter is less than 20 mm but limited to approx. 12 mm because of the size of a conventional polymer pellet which needs to fit into the screw channel (Michaeli et al. 2004b). Also the pellet weight can be a limiting factor. For example a single pellet of PMMA polymer weights 24 mg which exceeds for example the part weight of micro gears for watches (0.8 mg) by a factor of thirty.

2. The second concept is to separate units for plastification and homogenisation, metering, locking and injection of the polymer. One unit is used for the plastification, the other for the injection. For the plastification unit two different concepts are proposed so far. The first concept uses a plunger / piston and a hot cylinder, the second uses a conventional small screw and a barrel (Michaeli et al. 2004b; Piotter et al. 2002). The concept which uses two plungers, one for metering and the other for injection, is illustrated in Figure 2-5. The second concept with the screw and an injection plunger can be seen in Figure 2-6. A screw generally provides a more homogenous plastification than a plunger. The melted polymer is moved into the injection chamber where a plunger

pushes the material into the mould micro cavity. The small diameter of the plunger provides a better control over the amount of injected polymer than the conventional concept with the screw.

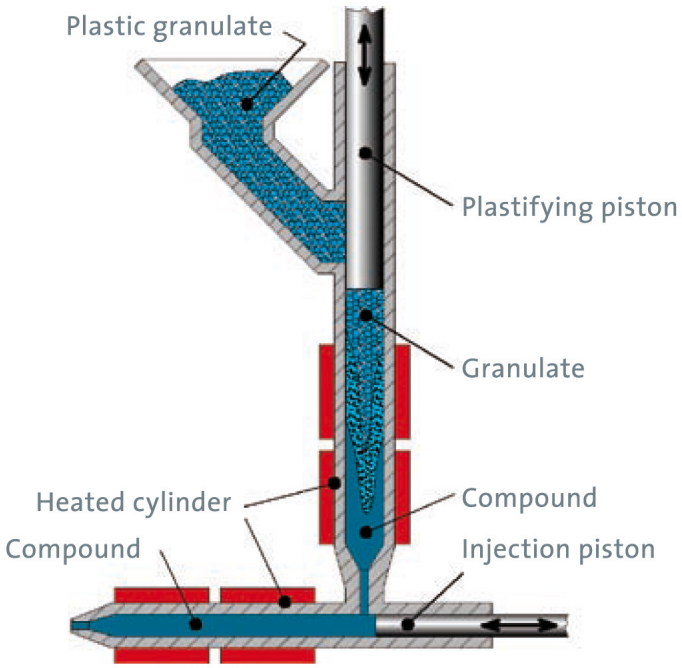

Figure 2-5 µ-IM concept with metering and injection plunger (DESMA 2008)

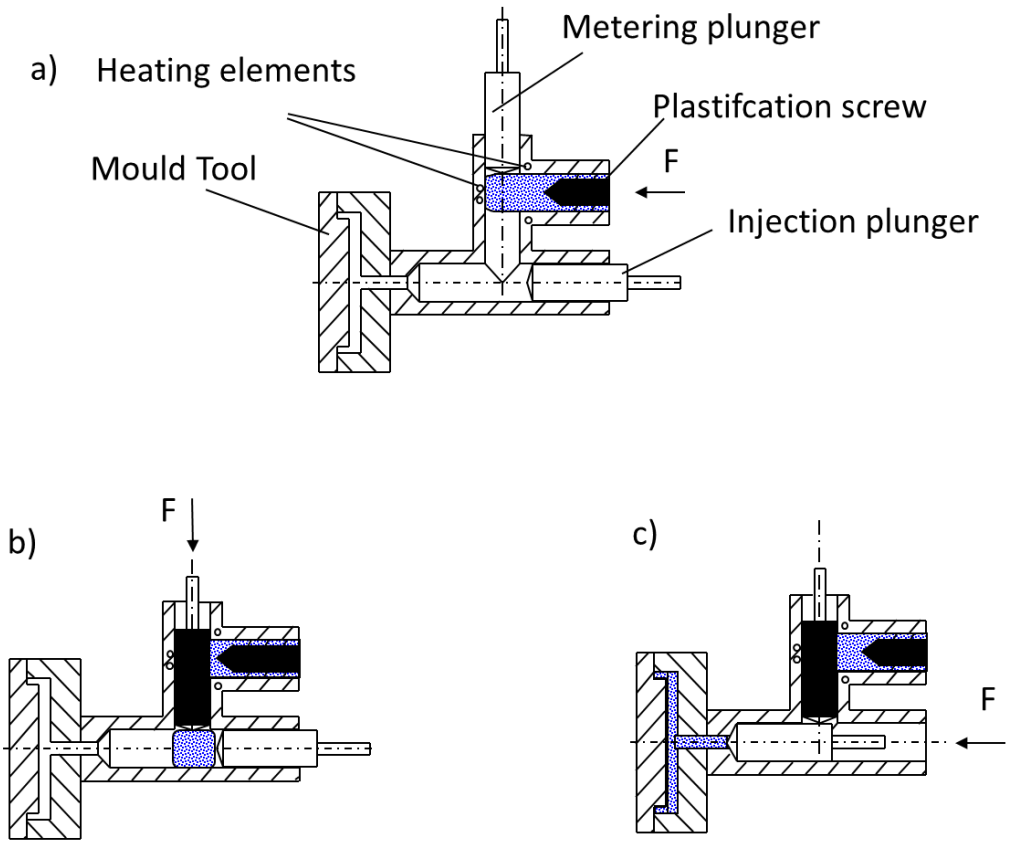

Figure 2-6 Concept and functional principal of µ-IM metering and injection system incorporating a screw and an injection plunger in particular of the Battenfeld Microsystems 50

Table 2-2 provides an overview of commercially available µ-IM machines and their injection capacities. The number of commercially available micro injection systems shows clearly that µ-IM has become an important technology for micro manufacture.

Manufacturer	Model	Clamping Force [kN]	Injection Pressure [bar]	Injection Volume [cm^3]	Diameter Screw or piston [mm]	Injection Speed [mm s^{-1}]
Lawton	Sesame Nanomolder	13.6	3500	0.082	10	1200
APM	SM-5EJ	50	2450	1	14	800
Battenfeld	Microsystem 50	56	2500	1.1	14	760
Nissei	AU3	30	-	3.1	14	-
Babyplast	Babyplast 6/10	62.5	2650	4	10	-
Sodick	TR05EH	49	1970	4.5	14	300
Rondoll	High Force 5	50	1600	4.5	20	-
Boy	12/AM 129-11	129	2450	4.5	12	-
Toshiba	EC5-01.A	50	2000	6	14	150
Fanuc	Roboshot S2000-I 5A	50	2000	6	14	300
Sumimoto	SE7M	69	1960	6.2	14	300
Milacron	Si-B17 A	147	2452	6.2	14	-
MCP	12/90 HSE	90	1728	7	16	100
Nissei	EP5 Real Mini	49	1960	8	16	250
Toshiba	NP7	69	2270	10	16	180
Desma	Formica Plat 1K	10	3000	150	6	500

Table 2-2 Commercially available µ-IM machines (Table taken from Bibber and modified (Bibber 2004))

The plastification and injection concept illustrated in Figure 2-6 addresses most needs of µ-IM. For all investigations in this thesis a Battenfeld Microsystem 50 was utilised. The design of this machine reflects all requirements of µ-IM as stated previously. The IM process of the Battenfeld Microsystem 50 consists of the following process steps:

1. Polymer pellets are plasticised by the fixed extruder screw and fed into the metering chamber of the injection unit (Figure 2-6 a).

2. The shut-off valve closes in order to avoid back flow of polymer from the metering chamber .

3. The pre-defined volume of polymer in the metering chamber of the plunger and in the dosage barrel delivers the shot volume into the injection barrel (Figure 2-6 b).

4. The injection plunger presses the polymer melt into the mould cavity (Figure 2-6 c).

5. Once the injection plunger movement is complete a holding pressure may be applied to the melt until the gate is frozen (sealing point). This can be achieved by a pressure / force controlled forward movement of the injection plunger.

The Battenfeld Microsystem 50 used for all experiments in this thesis is equipped with an additional air purity control chamber, which is not normally associated with an IM machine. This ensures a cleanroom environment around the IM unit and facilitates operational conditions for micro fabrication. The most important parameters for the Battenfeld Microsystem 50 µ-IM machine are listed in Table 2-3.

Clamp unit specifications		Injection unit specifications	
Clamp force	50 kN	International size designation	3
Opening force	10 kN	Extruder screw	14 mm
Max mould size	196 x 156 mm	Injection piston diameter	5 mm
Min mould height	100 mm	Specific injection pressure limited to	2500 bar
Opening stroke	200 mm	Theoretical shot volume	1.1 cm^3
Max daylight	300 mm	Nozzle stroke manual	165 mm
Ejector force	1.2 kN	Max screw speed	300 rpm
Ejector stroke	30 mm	Screw torque	54 Nm
Dry cycle rate	40 mm	Injection rate into air	25 cm^3/s

Table 2-3 Main technical characteristics of the Battenfeld Microsystem 50 µ-IM machine

2.3.5 Compression Injection Moulding

In this process, the mould has not reached its final closing state when the polymer injection is made. The mould is closed after the injection of the polymer melt into the cavity in a controlled manner to apply constant pressure during the packaging phase.

In conventional IM the pressure inside the mould is not uniform. In fact, the pressure decreases with the flow length of the polymer in the cavity. This reduces the ability to fill micro cavities in areas far from the runner and leads to strong orientation of the polymer macro molecules. By applying compression injection moulding, the pressure inside the mould is nearly uniform and relatively high over the surface area, which leads to a better surface replication, in particular when filling micro structures with high aspect ratio. This technology can be advantageous when moving from micro to nano replication because the reduction of the internal stress and sinking marks together with

a higher filling factor and aspect ratio lead to more accurate replication. Figure 2-7 illustrates the concept of the injection and compression stage in the compression injection moulding process.

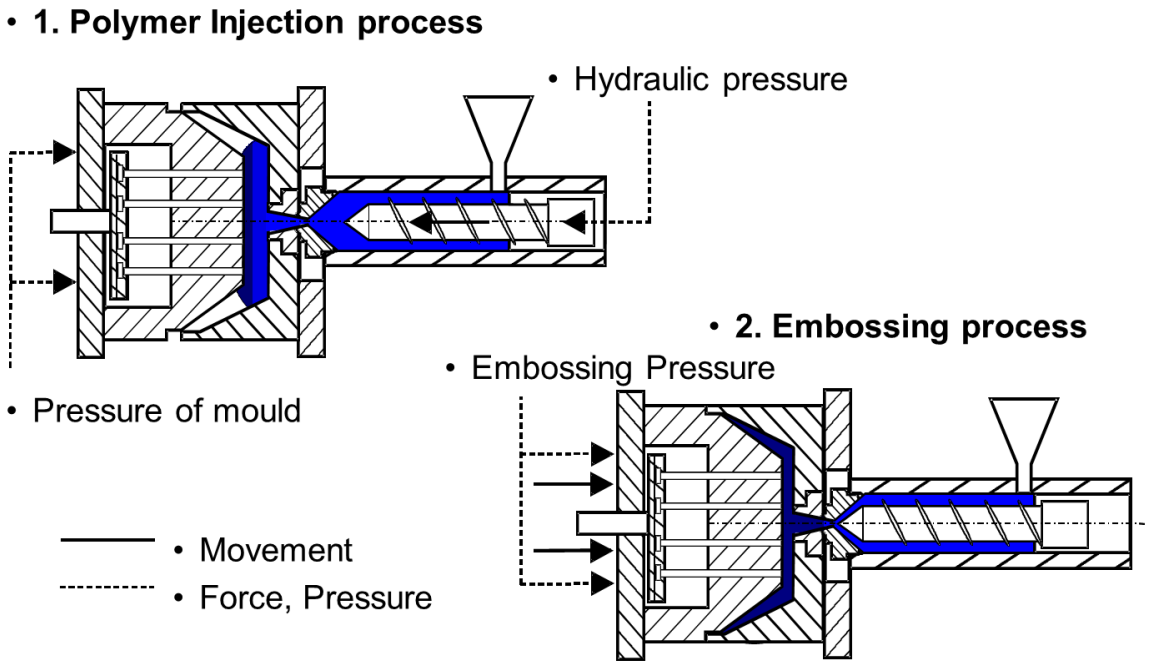

Figure 2-7 Concept of compression injection moulding

2.3.6 Mould Heating

Conventional IM mould tools usually require cooling to dissipate the heat from the polymer melts. Due to the large volume of macroscopic polymer parts, the volume of the steel mould is not sufficient to dissipate the heat. Without cooling, the mould would heat up with every cycle and cycle times could get significantly longer or even become impossible.

In µ-IM the volume of the polymer parts is rather small and the heat quantity which needs to be transferred is small as well. For that reason moulds for µ-IM very often

require heating instead of cooling and, therefore, electrical heating systems are often applied. The rapid cooling of polymer melts for micro parts is linked to the high contact area and the low volume to surface area ratio (Whiteside et al. 2005a). This results in an increase of the viscosity and impedes the filling of micro cavities.

It is well known, that the viscosity of polymer melts highly correlates with the shear rate and the temperature. This indicates that higher mould temperatures will allow a better filling of micro features. Hansen and Theilade summarised the findings of many authors who reported, that better filling of micro cavities, especially with high aspect ratio, was achieved with higher mould temperature (Hansen and Theilade 2005). Figure 2-8 and Figure 2-9 provide evidences, that small features or higher aspect ratio features can be replicated more accurately by using higher mould temperatures which could be close to the glass transition temperature (T_g) of a given polymer.

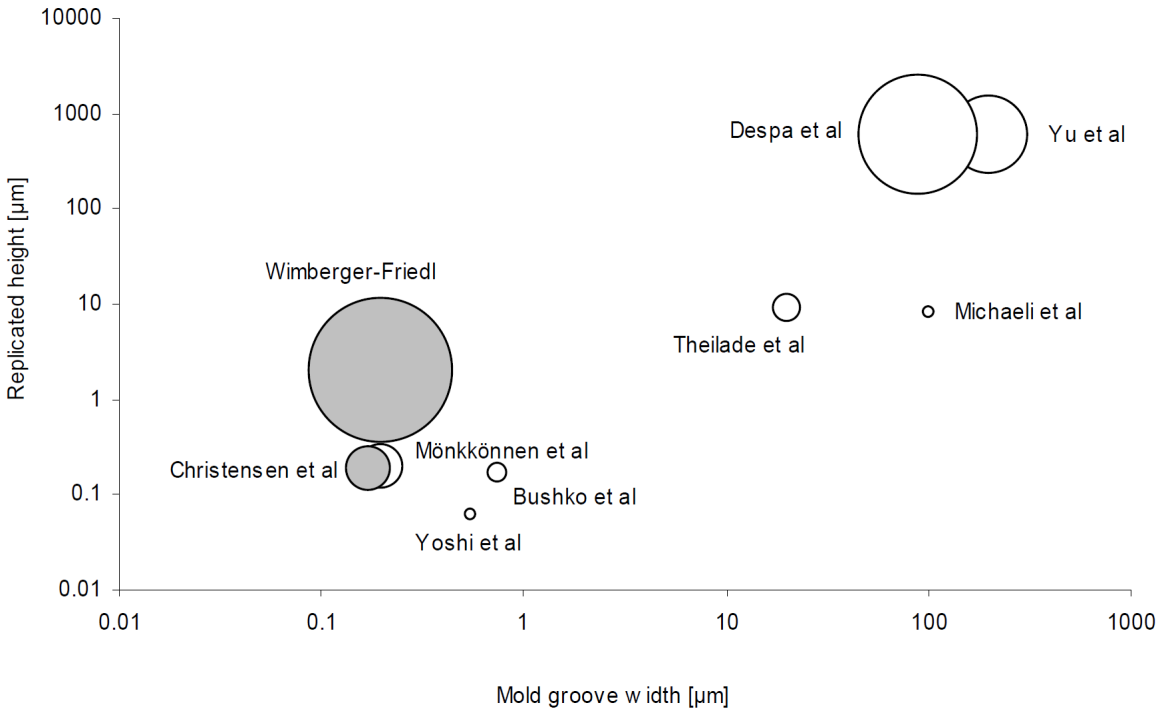

Figure 2-8 Replicated surface feature dimensions. Bubble size indicates replicated aspect ratio; shaded bubble indicates that elevated mould temperature was applied. Image taken from (Hansen and Theilade 2005)

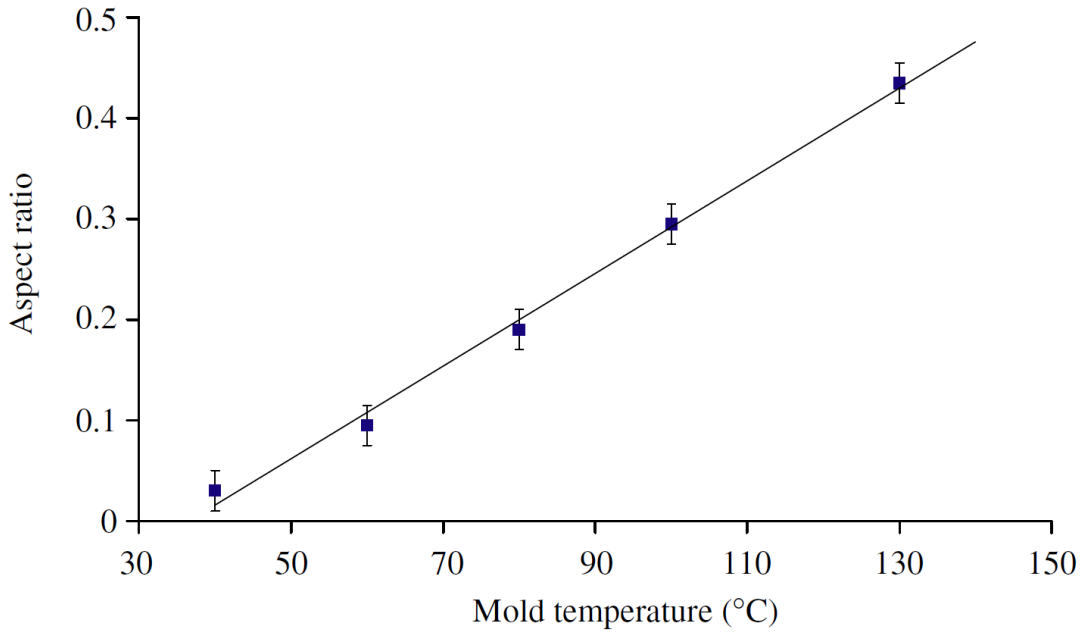

Figure 2-9 Achievable aspect ratio in respect to mould temperature, taken from (Giboz et al. 2007)

Table 2-4 gives an overview of typical mould temperatures for polymers commonly used in µ-IM. Note that the chosen mould temperature for µ-IM is much higher than the mould temperature recommended by the manufacturer.

Material		µ-IM mould temperature [ºC]	Conventional mould temperature [ºC]	Reference
HDPE	Semi crystalline	125-150	30-60	(Despa et al. 1999; Tseng et al. 2005; Yao and Kim 2002; Yuan et al. 2003)
PBT	Semi crystalline	120	80	(Debowki et al. 2003)
POM	Semi crystalline	90	70-90	(Huang et al. 2005)
PP	Semi crystalline	160	30-60	(McFarland et al. 2005)
ABS	Amorphous	120	30-60	(Huang et al. 2005)
PC	Amorphous	60-140	90-110	(Su 2004)
PS	Amorphous	170	140	(McFarland et al. 2004; McFarland et al. 2005)

Table 2-4 Mould temperatures used in µ-IM versus conventional IM for common polymers

On the other hand, high mould temperatures are increasing the cycle time (Despa et al. 1999) and could even, if the mould temperature was too high, produce a defect moulding. For this reason the variothermal process was developed which is described in the next section.

2.3.7 Variothermal process in injection moulding

For the replication of high aspect ratio and high definition nanostructured surfaces, the variothermal process or rapid thermal cycling has been developed. It is used with both IM and compression injection moulding. The variothermal process uses additional external and internal heating systems in order to reduce the heat transfer between the polymer melt and the tool surface during the injection stage. Different external and internal heating systems have been developed and tested and reasonable cycle times

have been achieved using variothermal control (Scholz 2007a). Especially through external heating systems it is possible to heat only the skin of the mould and thus high heating and cooling rates can be achieved in the IM process (Michaeli et al. 2008; Scholz 2007b). *Figure 2-10* shows the effect of the heat transfer reduction on the filling factor. Much better replication of pyramids with a base length of 40 µm has been realised with higher mould temperatures by applying an external induction heating system into the open mould cavities (Scholz 2007a).

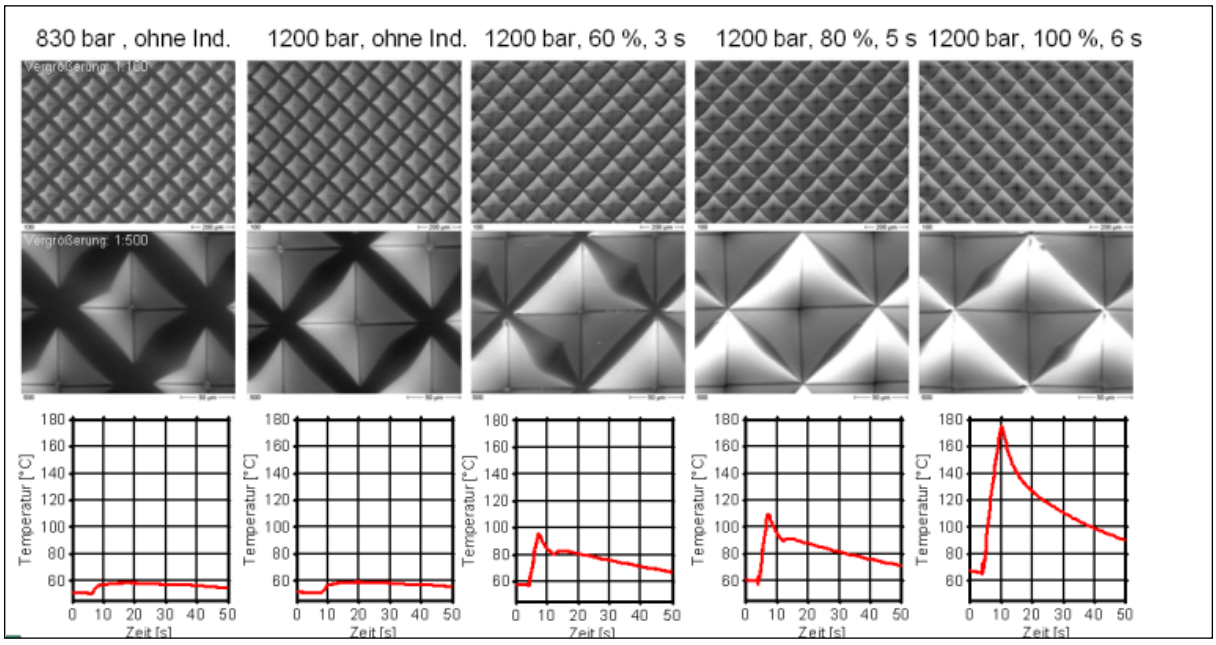

Figure 2-10 Heating and cooling rates achievable with external inductive heating systems for the variatherm process (Scholz 2007a)

The concept of using an external inductive heating device to heat rapidly and thus to reduce the cycle time is illustrated in Figure 2-11. With this setup, heating and cooling rates of 80 K/s could be achieved (Scholz 2007a, b).

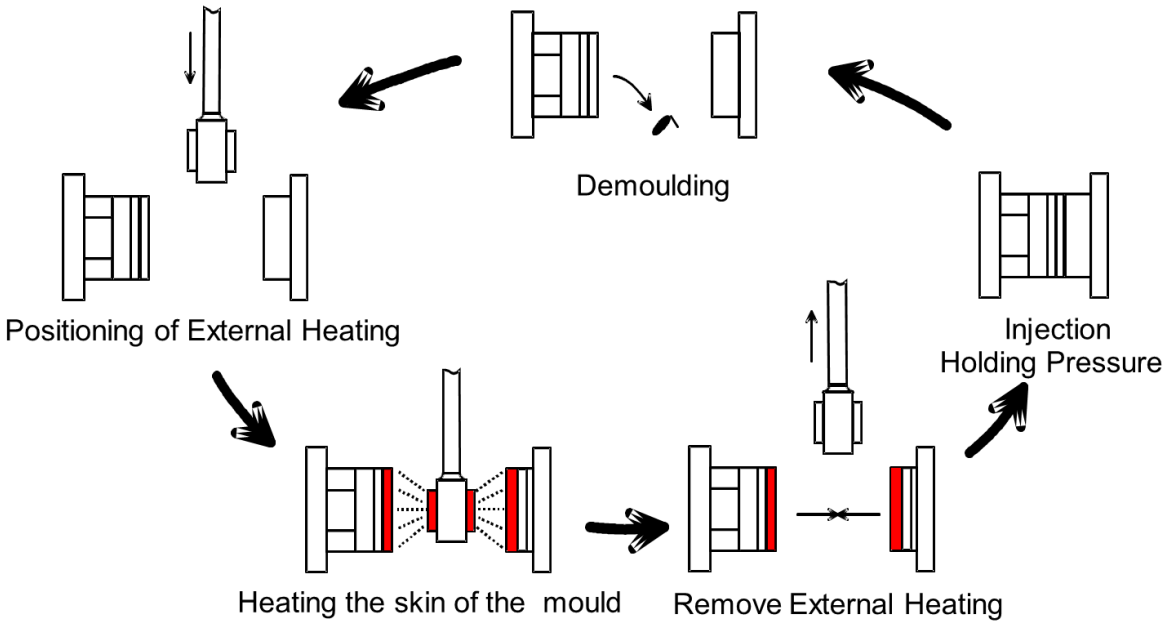

Figure 2-11 Process steps for the concept of dynamic tool tempering utilising external inductive heating system (Scholz 2007b)

The feasibility studies conducted on the replication of structures in the sub micro meter range clearly show the advantages of this variothermal process.

Figure 2-12 a shows a nickel mould which was structured using FIB milling. Figure 2-12 b and c show the difference in the replication quality, using normal IM and IM with variothermal process control. With variothermal process control, the structure with an aspect ratio of 2:1 was completely replicated, especially the features at the top, which are in a range of 50 nm.

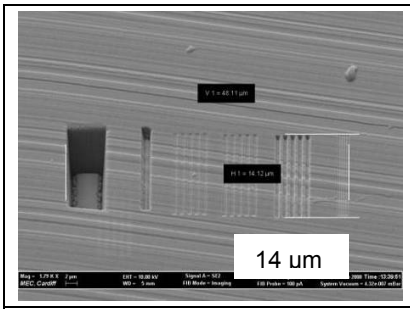	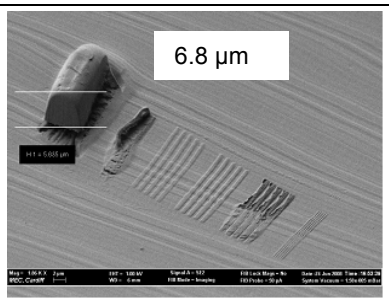	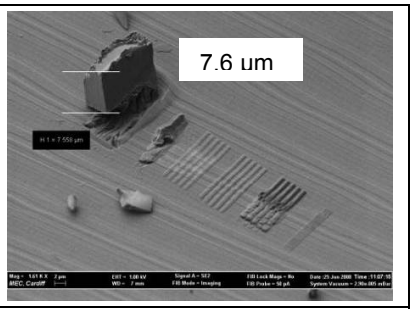
a) Nickel mould insert with micro and nano structures produced using Focused Ion Beam technology (FIB)	b) Replication results in PMMA using conventional injection moulding techniques (not completely filled high aspect ratio structures plus demoulding problems)	c) Replication results using variothermal process control (completely filled high aspect ratio structures but the demoulding problems still remain)

Figure 2-12 Feasibility study on filling nano features utilising variothermal IM. The height of the cube is approximately 8 µm (Scholz 2007b).

The above mentioned examples clearly demonstrate the advantages of the hybrid process even if Figure 2-12 c shows that demoulding issues still remain, mainly for high aspect ratio features.

2.3.8 Polymers used for micro injection moulding

In µ-IM, the small dimensions of the parts and the overall small volume of injected polymer melt affect the selection of polymers to be used in µ-IM. One of the main requirements is that the polymer should feature a viscosity low enough to allow the polymer melt to fill micro cavities. For µ-IM LCP, COC, PC, PA, POM, PBT, PEI, PPE and PSU materials have been investigated (Bourdon and Schneider 2002; Chang et al. 1996; Kao and Shih 2006; Kemmann and Weber 2001; Kim and Kang 2003; Lee 1997; Luo et al. 2007; Madou 2001; Madou et al. 2001; Mönkkönen et al. 2002; Saito et al. 2002; Shen and Wu 2002; Shen et al. 2002; Su 2004; Yoshii and Kuramoto

1994; Yoshii et al. 1996; Zhao et al. 2005; Zhao et al. 2003b; Zhao and Macosko 2002).

Mönkkönen et al. (Mönkkönen et al. 2002) found that different polymers have different responses to flow directions in small spaces, and also Yao and Kim (Yao and Kim 2004) concluded that previously used materials have to be researched again because of the complexity of the melt flow in micro cavities. In particular, the high injection speed in µ-IM leads to high shear rates. In this research three materials commonly used in IM, Polypropylene (PP), Acrylonitrile Butadiene Styrene (ABS) and Polycarbonate (PC), were selected to conduct the planned experiments.

2.4 Factors influencing the µ-IM performance

From the reported studies it is clear that the main factors affecting the µ-IM process and the cavity pressure behaviour are T_b, T_m, V_i and P_h.(Whiteside et al. 2005b). Many researchers have investigated the effects of these factors. It was reported that an increase of T_m and V_i led to improvements of the process performance (Yoshii and Kuramoto 1994) and longer flow length (Tosello et al. 2010), while T_m was of major importance for achieving better replication results (Wimberger-Friedl 2001). Considering the relationship between V_i and pressure in the cavity (P^c), generally, conventional part thicknesses result in an increase of P^c with the increase of V_i. However, the relationship between V_i and P^c was investigated and it was found that P^c was lower at higher values of V_i (Yao and Kim 2004). The results from the literature review indicate that high process parameters can be used to overcome the short freezing time of polymer melts when filling micro cavities. However, it should be noted that such settings may also lead to some negative effects. Therefore, it is important to

consider such factors in conjunction with other known process settings that affect the μ-IM performance.

2.4.1 μ-IM process / product control by pressure monitoring

To achieve a consistent replication quality a proven method is to monitor the influence of the varying factors in the IM process. T_m and P^c are two such factors that can have a direct impact on dimensional stability. Especially, to minimise the residual stress, their changes throughout the cavities are important. At the same time it should be noted that a uniform distribution of P^c is difficult to achieve because of the complexity of the mould geometry and flow resistance due to varying wall thicknesses and flow lengths.

It is essential to understand the relationship between pressure in the cavity and the melt flow rate (Clavería et al. 2005). By investigating the thermo mechanical history, the cavity pressure profile and its repeatability, it was shown that the process factors could influence the quality of the moulded parts, particularly, their dimensions, dimensional stability, mechanical behaviour, and surface quality (Kazmer and Barkan 1997). In particular, by measuring P^c, it is possible to monitor the overall behaviour of the IM process, and it is recognised as a critical process variable (Orzechowski et al. 1998). Subsequently, by monitoring the pressure in the cavity as an input signal, it is possible to vary some process settings in order to alter *T* and *P* of the polymer flow, and thus to achieve consistent replication and uniform product quality (Kazmer and Barkan 1997). The relationship between part quality and P^c has been investigated by researchers (Hellmeyer et al. 1977; Homes and Kabus 2001; Kuek and Angstadt 2007; Michaeli et al. 2004a; Michaeli and Schreiber 2009; Schnerr et al. 1998; Stahl

and Koch 2005). The results showed that an insufficient P^c could result in an unfilled part. In particular, a high melt resistance and a restricted flow path could lead to a premature solidification of the polymer melt. One proposed solution to reduce the solidified layer and also the part residual stress while maintaining a lower P_i was to increase the T_m above the polymer glass transition temperature (T_g) during the filling stage (Su 2004).

By using a numerical method for predicting residual stress, shrinkage and warpage it was found that stress profiles exist across the part thickness due to polymer regions freezing under high or low P^c *(Zheng et al. 1999)*. In particular, if the part thickness is below 2 mm, the ratio between the frozen skin layer and the molten core rises, leaving less material to pack out the part. For IM of thin parts, P_h is the most influential factor, especially, when considering the part warpage (Huang and Tai 2001). A T_m based system for P_c control was proposed and it was demonstrated that cavity pressure during the cooling stage could be controlled effectively by varying the polymer *T (Gao et al. 1996)*. Studies of part dimensional accuracy and especially the relationship between T_m and P^c using piezoelectric transducers and data collection techniques showed that the two strongly affect part shrinkage. Specifically, a higher cavity *P* and T_m, led to less shrinkage (Kurt et al. 2009). Surface waviness was found on polymer optical lenses manufactured by IM, and it was mostly influenced by T_b, and to a lesser extent by P_h and P_i. Also, it was suggested that surface waviness of lenses could be improved with a higher T_b, P_i, and P_h (Tsai et al. 2009). It was also reported that V_i and P_i were the most important parameters affecting part quality during the filling stage (Michaeli et al. 2004a). An increase of V_i can lead to an increase of maximum pressure (P_{max}), however such an increase can further result in over-packing followed by a residual cavity pressure before mould opening. Therefore, P_h and holding time (t_h)

during the holding stage have a significant effect on the resulting part quality (Huang 2007). In addition, a higher pressure in the cavity can result in an increase of the force required to demould parts. By reducing P_h, a reduction in the ejection force (E_f) was observed (Pontes et al. 2005).

The main requirement for achieving an optimum moulding quality would be a precise switching from the filling stage to the packing stage (Collins 1999). If the switching is incorrect the following conditions can be observed:

Switchover is occurring too late. This causes an over-packing, characterised by a peak *P* during the compression stage, and results in an increase of part weight, stress and E_f.

Switchover is occurring too early. This can lead to under packing characterised by a *P* drop during the compression stage and result in continuous part filling during the holding stage, and ultimately in reduced part weight and dimensions as well as sink marks.

In conventional IM, the factors affecting the switchover control are injection time (t_i), screw position, hydraulic pressure, and nozzle pressure. Inconsistent filling-to-packing switchover settings can significantly affect the cavity pressure profile. Thus, these profiles can be used to identify the compression and holding stage switching points, and monitoring P^c can provide accurate and valuable information about the injection, compression and holding stages of the process. In µ-IM, with cavity filling in the order of a few tens of milliseconds, the switchover can be challenging to monitor as for example in thin wall moulding, it was reported that V_i and P^c parameter settings for thin walled IM produced an insignificant volumetric filling point, and made the switchover point unrecognisable (Huang 2007).

2.4.2 Air flow behaviour in micro cavities

One of the most important conditions for consistent replication in µ-IM is the evacuation of air or gas from the cavity. Inadequate air evacuation (E_a) in the mould can result in air pockets trapped against the cavity walls and/or between converging flow fronts. This can cause problems such as burn marks and short shots (N.N. 1965). In particular, burning conditions can arise from air subjected to an adiabatic temperature change, the extreme of which is when *P* and *T* are high enough to cause the air to ignite and burn the polymer. In addition, incompletely filled parts, commonly known as short shots, can be caused by air that failed to evacuate and remained trapped in an unfilled area of the cavity. Such trapped air can resist the melt flow and lead to an excessive cavity pressure being required to fill the cavity completely. Thus, adequate E_a is required to improve part quality and also to prevent tool damage.

One important design solution for reducing air traps is venting or, often used in µ-IM, active venting. Different alternative solutions have been proposed in the literature (Despa et al. 1999; Gornik 2004; Heckele and Schomburg 2004; Liou and Chen 2006; Ruprecht et al. 2002). Ideally, vents are present at the mould split lines, however, it is often required to position them in areas of converging flow fronts and last-to-fill flow fronts of the cavity. When designing vent systems for macro-scale components it is necessary to consider the relationship between *T* and *P* in cavities. This is required in order to prevent the filling of vent gaps that can result in an excess polymer on the moulded part and further processing steps for flash removal (Su 2004). In particular, the permissible width of the vent gaps which prevents the melt from entering depends, primarily on the time between the first contact of the melt has with the vent area and the rise in *P* (Menges and Mohren 1993). The critical gap width for polymer materials

range from 15 to 30 µm, and typically a vent can be about 25 µm deep and several mm wide (Crawford 1990). For µ-IM such vent sizes could be comparable with some of the functional features of the moulded micro-parts, and thus it will be difficult or even impossible to prevent their filling by the melt flow due to the relatively high process settings applied in µ-IM.

In addition to changing vent dimensions, the air flow rate ($\dot{Q}$) at the vent exit can be considered. Traditionally, a reduction in the machine clamp force, and the use of a suitable V_i profile can change $\dot{Q}$ and allow more time for E_a. However, the high accuracy of the moulds and the high V_i requirements in µ-IM mean that the applicability of existing methodologies and solutions for venting should be re-considered. Taking this into account one solution suggested was to apply a vacuum at the vent exit (Yokoi et al. 2002). The trade-offs in selecting an appropriate position for the vents as far away as possible from the optimised location of the gate require extensive experimentation mostly on a trial and error basis (Roopesh et al. 1999). Therefore, each potential solution should be considered taking into account all relevant aspects of the moulding process.

The performance of the µ-IM process is highly dependent on E_a as an important pre-requisite for the production of quality parts and also for prolonging the tool life.

2.4.2.1 Venting and Vacuum

When a polymer is injected in a cavity the incoming melt has to displace the resident air. Ideally, the resident air evacuates by finding the easiest way to escape from the cavity as the melt front progresses beyond the runner and the gate. For parts with

different thicknesses the non-uniform, diverging or converging behaviour of the polymer and air flows make the positioning of injection gates and E_a vents an important design consideration, particularly for controlling the *P* levels during the filling stage of the process (Phelan 1997). Shen et al. (Shen et al. 2008) investigated the µ-IM process for the fabrication of micro-lens arrays and concluded that the melt front had been filling the thicker section of the cavity first before filling the microstructures. Also, it was observed that the remaining air in the microstructures, if not evacuated, resulted in incompletely filled parts.

The air trapped within the cavity influences the thermal interactions between the polymer melt and the mould. During the cooling cycle heat conduction takes place between the polymer surface and the mould. If there is an air gap present, the polymer surface reheats because the heat transfer is restricted. As a consequence polymers can exceed their critical temperatures, and also the air gap can lead to cooling variations that can result in part warpage (Bendada et al. 2004). Currently, changes to the processing conditions triggered by altering the injection locations and V_i profiles are used to prevent air traps. However, taking into account the relatively short injection time frames in the range of 100 ms in µ-IM, E_a becomes a key consideration in the mould design (Zauner 2006).

Venting is one of the methods for achieving E_a. Ideally, the primary vent is present at the parting plane or split line of the mould faces but in spite of this non-uniform filling patterns, hesitation effects and insufficient gaps between the split lines can result in trapped air. In such cases secondary vents are introduced to facilitate E_a. To improve the efficiency of the vents, the exit *P* can be modified by applying a vacuum or negative *P* to the vent exits. Yokoi et al. (Yokoi et al. 2006) investigated transcription

fidelity (TR) using ultra-high speed injection moulding and found that there was a correlation between TR and V_i, flow patterns and vent conditions. The use of a vacuum pump to facilitate E_a did not lead to noticeable improvements of replication results in comparison to those achieved employing conventional vents. However, the vacuum pump increased the average TR. For moulding diffractive optics with 0.5 to 1 µm gratings, Kalima et al. (Kalima et al. 2007) considered E_a as a process factor and a vacuum pump was used to remove any trapped air from the mould. The study concluded that the existence of a vacuum improved the filling for all studied materials. However, trapped air was still present inside the cavities and possibly contributed to the incomplete filling of some of the structures even when the vacuum unit was employed. Sha et al. (Sha et al. 2007b) investigated the importance of E_a as a control parameter in micro cavities. The results showed some improvements in part filling and surface quality, however E_a could also lead to a decrease of the surface temperature in micro channels caused by the removal of warm air from the cavity. Therefore, for polymers that are sensitive to T_m settings the melt fill decreases when a vacuum is applied. Liou and Chen (Liou and Chen 2006) used a continuous vacuum in a mould cavity and runner to keep the pressure under 1e-4 MPa before filling, thus to reduce the influence of temperature variations.

In conclusion, it can be stated that the use of vents and vacuum to remove air traps can have both positive and negative effects on the µ-IM process. The specific process requirements suggest that in order to achieve an adequate E_a it is necessary to consider all relevant tool design and process factors.

2.4.2.2 Weld lines

Another area where ineffective E_a can have a detrimental effect on part quality is the formation of weld lines. Weld lines are usually formed when two or more flow fronts meet and converge during the part filling stage. They are unavoidable when either the flow fronts separate and re-converge or the melts come from more than one gate. Such lines can result in a mechanical weakness, visual defects or incompletely filled cavities.

Weld line strength is generally influenced by *T* at which the weld line is formed. As soon as the melt enters the cavity it begins to cool and *T* may not be sufficient for the two melt fronts to bond perfectly together when they meet. Also, residual stresses can occur due to flow fronts having different *T*. It was shown that aberrations in molecular orientation due to differing viscosity of two melt fronts can cause bad entanglements when they meet and thus lead to the formation of weak weld lines. Additionally, a compatibilizer that results in finer polymer morphology was found to increase the weld line strength (Dairanieh et al. 1996; Kim et al. 1997). Debondue et al. (Debondue et al. 2004) identified a direct relationship between the molecular diffusion, in particular different entanglement densities, and fracture mechanisms of weld lines that were influenced not only by the material and processing parameters but also by the mould surface roughness and E_a capability.

To avoid varying *T*, and thus the occurrence of differential shrinkage during solidification, Michaeli and Ziegmann (Michaeli and Ziegmann 2003) adopted a variothermal heating of cavities before injecting, and then cooling down before de-moulding to prevent the formation of weld lines. Liu et al. (Liu et al. 2000) used different geometric shapes as flow obstacles to investigate weld line formation and

strength. From the set of process parameters investigated in this experimental study T_b and T_m were found to be the principle factors affecting weld line formation and their properties. Wu and Liang (Wu and Liang 2005) reported that weld line formation could be reduced by applying higher settings for V_i, T_b and T_m while T_b was found to be the most influential factor. Tosello et al. (Tosello et al. 2010) used weld lines as flow markers to investigate the filling performance in µ-IM, and the results showed that T_b and V_i were the most influential parameters.

Currently, in most cases the trial and error approach is used to identify process settings that can be applied to control weld line formation. However, with the need for higher *T* and V_i in µ-IM, it should be noted that such settings also intensify the occurrence of adiabatic conditions, localised air temperature increases, in the mould, and hence the requirements for and an increase in the rate of E_a.

2.4.2.3 Adiabatic processes

The specific process conditions in µ-IM suggests that the development of appropriate E_a solutions will require all relevant tool design and moulding process factors to be re-considered in a new context. Air traps within converging flow fronts or against cavity walls can lead to problems such as burn marks and surface defects. Burning conditions can arise due to air being subjected to an adiabatic temperature change, the extreme of which is when the air pressure is sufficiently high to ignite the air and burn the plastic, i.e. causing polymer degradation.

Considering the polymer flow in a mould, the specific volume (*V*) of polymers varies with *P* and *T*. In particular, *V* increases with the decrease of *P* and the increase of *T.* The functional dependence between the polymer volume and *T* and *P* can be

represented with pressure - volume - temperature (*PVT*) data that represents material compressibility of melt flows (Binet et al. 2005; Chang et al. 1996). If the total amount of heat in a given *V* of trapped air is held constant, then when the air is compressed, its *T* rises. This is called adiabatic heating, and the *T* increase attained when work is performed on the system is called adiabatic temperature. The *T* increase of the air during compression tends to increase *P* to compensate the decrease in *V*, and therefore, *P* during adiabatic compression rises faster while *V* diminishes.

The ideal gas law describes the relationship between *P*, *V*, the number of moles (*n*), and *T* of an ideal gas. The state equation of a hypothetical ideal gas reflects the fact that a given number of its atoms occupy the same *V*, and that *V* changes are inverse to *P* change, and linear to *T* changes. Thus, the state of a given amount of gas is determined by its *P*, *V* and *T*. Their functional dependence can be expressed analytically as follows:

$$P \cdot V = n \cdot R \cdot T \qquad (2.1)$$

where *R* is the value of universal gas constant. For an adiabatic process *T* can be defined as follows:

$$T_2 = T_1 \cdot \left(\frac{V_1}{V_2} \right)^{y-1} \qquad (2.2)$$

and *P* as:

$$P_2 = P_1 \cdot \left(\frac{V_1}{V_2} \right)^{y} \qquad (2.3)$$

where T_1, P_1 and V_1 are the initial state values and T_2, P_2 and V_2 are the final state values. y is a constant that depends on the type of gas used, and is related to the degrees of freedom of the gas molecules. For a diatomic gas such as nitrogen and oxygen, the main components of air, y is about 7/5, however y is not constant as heat capacity changes with changes in V and P. However, it is reasonable to assume a constant y when there are only small changes in the states.

Potentially, adiabatic conditions can cause combustion within the mould cavity. The diesel effect or diesel cycle are adiabatic effects in injection moulding of polymers (Giboz et al. 2007). The diesel cycle includes the following stages:

1. Injection of the polymer compresses the resident air in the cavity.
2. The volume of air experiences an adiabatic temperature increase.
3. The air ignites.
4. The air expands adiabatically.

The diesel reaction occurs when an explosive mixture of gas and processed material is formed during compression. Such a mixture results in a material volatility, which entails chemical reactions leading to the formation of a volatile gas or vapour that can etch the tool material (McGraw-Hill 2003). In particular, the theoretical or stoichiometric amount of air is the minimum amount of air that will provide sufficient oxygen for the ignition of all combustible chemical elements. In most combustion applications, air provides the necessary oxygen. In combustion calculations, air is considered to contain 21% oxygen and 79% nitrogen. With such idealisation the molar ratio of nitrogen to oxygen is 3.76 in combustion air. Also, the nitrogen present in air is considered inert; however, the air can be ignited due to the additional gases released

from the heating up of the polymer melt. Data obtained with a gas chromatograph device can be used to determine the composition of the gaseous products of the combustion (Morgan 1999).

In μ-IM the *T* settings can exceed those used in conventional IM. In particular, high T_b can improve the polymer flow while high T_m leads to a more uniform distribution of residual stresses in moulded parts (Young 2005). However, high *T* and V_i settings can also result in uneven melt fronts, gas traps and burning of the moulded polymers (Griffiths et al. 2007). Increasing T_b, T_m and V_i improves the polymer melt filling of micro cavities, though in some cases the part edge definition can be compromised. One explanation for this could be that the expanding residual air was not vented completely and hindered the melt flow (Sha et al. 2007a). Liou and Chen observed residual cavities of air in sub-micron structures with high-aspect ratios (Liou and Chen 2006). The cavities were filled by gas produced at high *P*, and this can be regarded as being created by the gasification of the polymer caused by its excessive *T* increase. This phenomenon was exhibited in all cases where T_m was 160 ºC or above and was more serious at higher T_m. At high V_i, a system for visualization analysis established that the gas bubbles generated in unstable asymmetric melt fountain flows expanded and collapsed in contact with the tool cavity walls, causing defects such as flow marks and silver streaks (Yokoi et al. 2006). Yuan et al. (Yuan et al. 2003) identified that during injection when trapped air was compressed *T* could increase and as a result could thermally degrade the polymer. Ruprecht et al. (Ruprecht et al. 2002) used E_a to prevent the burning of plastic caused by the diesel effect. While Ebnesajjad identified that adiabatic compression during polymer processing can raise *T* significantly, to about 800 ºC, which can degrade the plastic and may produce a by-product that will corrode the tool material (Ebnesajjad 2003).

2.4.3 Demoulding forces

Micro moulded components have a high surface to volume ratio (SV_R) and as a result µ-IM is characterised by higher cooling rates. Thus, the possibility of producing micro polymer parts with higher residual stresses increases (Haberstroh and Brandt 2002). An important stage in µ-IM process which can further affect the mechanical properties of the produced components is part demoulding. During the solidification process of the moulding cycle, the polymer melt shrinks onto the mould cavity walls and features. The part-mould forces that develop at this stage have to be overcome for subsequent part ejection from tool cavities. To avoid damage when breaking the bond between the polymer and the cavity, the stress applied for part ejection should not exceed the tensile yield stress of the material (Navabpour et al. 2006). Part-mould forces are the result of an interaction between the polymer and the mould cavities. In particular, they result from the contact pressures that are mainly due to the effect of shrinkage of the moulded material and the part and mould materials' coefficients of friction (Menges and Mohren 1993). Thus, the factors that influence the demoulding behaviour of tool cavities have to be studied carefully to avoid any detrimental effects on parts and features and/or introducing further residual stresses to the moulded components through plastic deformations.

The demoulding stage can lead to a variety of defects to the produced parts. These include stress marks, deformation, fracture and stretching of the polymer structures (Heyderman et al. 2000). An ejector system to remove the parts from the cavity is a key component of any tool and is essentially used to overcome the part-mould friction forces without introducing defects to the part. Potentially, ejector pins can cause high local stresses and strains that can lead to part deformation and damage. Previous

studies have shown that part deformation is affected by the number of pins and their positions within the cavity (Kwak et al. 2003). The lower mechanical strength and higher SV_R of micro parts makes them particularly susceptible to damage during demoulding. Therefore, it is necessary to investigate the effects of different factors on F^e and thus to identify processing windows for reducing them.

2.4.3.1 Factors affecting the demoulding behaviour

In polymer IM, predicting the adhesion forces between the part and the tool is a complex task due to its dependence on part geometry and processing parameters such as T and P used during the moulding. Studies have shown that the demoulding force (F^e) is influenced by the specific interactions between a given part and tool, in particular the contact pressure, area of contact and coefficient of friction (Menges and Mohren 1993).

As reported previously, to fill completely all part features, the polymer injected in the cavity requires optimum P_h and t_h. Otherwise, short shots or unpacked polymer volumes may result in voids and sinks that retreat from the tool surface and thus reduce F^e. Any warpage in moulded parts can have a major effect on product performance, and the processing P has a significant effect on the warpage of parts (Gui et al. 2008). However, an optimum processing window exists and if it is exceeded, the applied P can result in an increase of the demoulding stress (An and Chen 2007). Studies focused on the demoulding of micro-structures have shown that F^e increases as P increases. In addition, the optimum processing window is also defined by a critical temperature range (T_{cr}) at which F^e for a given array of micro structures is at its minimum level (Fu et al. 2008). Any variation of F^e may be explained

by some variations in the actual part T at ejection. To maintain T at a given level is critical for achieving the targeted effect by the applied pressure in µ-IM. In particular, an increase of T_b results in a better filling and replication of micro features, while the use of the correct mould T_m can prevent early solidification (Griffiths et al. 2008a; Griffiths et al. 2008b; Sha et al. 2007b). Pontes et al designed an instrumented mould to assess the effects of the processing variables on F^e. The experimental results indicated that T at the surface of the mould had a substantial influence on F^e. In particular, F^e had decreased when surface T increased, and thus an increase of T_m resulted in a reduction of F^e. Additionally, it was found that F^e changed inversely with respect to P_h. Especially, a lower P_h resulted in a lower part-mould contact pressure (Pontes and Pouzada 2004).

De Grave et al proposed a setup design for investigating the demoulding of polymer microstructured parts with a particular focus on the demoulding angle (De Grave et al. 2007). The part-mould contact area and the complete fill of surface irregularities that are dependent on surface finish characteristics are an important demoulding consideration. Studies on the influence of surface quality on F^e reported that an optimum surface roughness existed in minimising F^e *(Sasaki et al. 2000)*. In particular, F^e was found to increase with the increase of the tool surface roughness but also a similar effect was observed with highly polished surfaces. Another investigation of mould surface roughness effects at nanometer level on F^e, especially when moulding lenses and CDs, reported that they depended on the polymer material used (Pouzada et al. 2006).

The number of ejector pins used affects the part-mould forces, too. More specifically, an increase in the number of ejector pins can result in a reduced stress distribution in

moulded parts (Kwak et al. 2003). A critical issue when moulding high aspect ratio microstructures is the ejectors' position and the use of ejector cores of the same shape as the part, and thus to achieve a uniform distribution of the force (Hopkinson and Dickens 1999).

Two friction coefficients, static (μ_s) and sliding or kinetic (μ_k), are also important factors determining part demoulding forces. Previous research studies on µ-IM demoulding behaviour found out that there were instances in which the friction effects could be difficult to explain. In particular, Sasaki et al. showed that injection P did not affect F^e (Sasaki et al. 2000). However, Pontes et al. and Griffiths et al. reported that P_h and T of the cavity were substantially affecting F^e, especially the results showed F^e to increase when lower holding P and T were applied (Griffiths et al. 2008a; Pontes et al. 2005). Worgull et al. investigated the friction during the demoulding of microstructures replicated by hot embossing. It was found that μ_s had decreased when T was reduced. In contrast to this, μ_k was much less influenced by T (Worgull et al. 2006).

A study of F^e with regards to applied mould surface treatments showed that the efficiency of the coatings depend on the polymer used, its shrinkage nature, and the roughness of the coated surface (Charmeau et al. 2008). Griffiths et al. reported defects on PC and ABS moulded parts due to demoulding (Figure 2-13) and showed that it was possible to optimise the process with regard to F^e for each of the investigated polymers. However, it was apparent that there was no unique selection of process parameters that could be considered optimum for these polymers (Griffiths et al. 2009).

Considering the combined effects of high SV_R and high aspect ratio micro features in µ-IM, it is not difficult to conclude that they present challenges in decreasing part-

mould forces. Especially, this is very important for maintaining optimum mechanical and structural stability during demoulding, and thus to produce quality parts and also potentially to increase tool life.

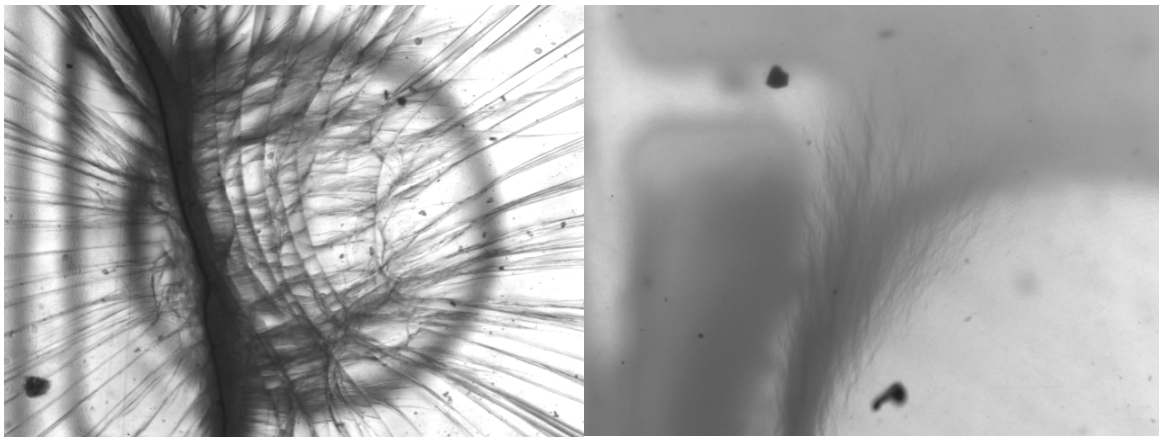

Figure 2-13 Part defects (micro cracks) caused by demoulding forces for PC (a) and ABS (b) (Griffiths et al. 2009).

2.5 Summary

The first section of this chapter reviewed the available micro manufacturing processes. Its focus was on non-silicon based micro and nano tool making technologies, and presented an analysis of their capabilities. The necessity of replication processes for scale up manufacture of polymer micro parts was also discussed.

Next, the recent developments in rapid tooling for µ-IM, especially the tool making capabilities of µSL technology, were discussed as a new manufacturing route for fabricating mould inserts that can be applied for producing small batches of polymer parts. Open research issues in utilising this rapid tooling technology were identified. It was shown that it is necessary to identify the effective processing window for moulding

small batches of parts employing μSL mould inserts, and also to study their wear mechanism in order to understand their limitations.

In the third section, an overview on the state of the art in IM was presented with a special focus on μ-IM, in particular the development of dedicated μ-IM machines, special process variations and add-ons. Then, in the follow up section the key factors affecting the process performance were examined and open research issues associated with the effective use of the μ-IM technology that need addressing were discussed. The literature review further highlighted the advantages of cavity pressure monitoring in macro scale injection moulding and how it can be effectively applied for process optimisation.

In addition, the effects of air trapped in the micro mould cavities on the μ-IM process were discussed as a mayor hindrance for an error free replication of polymer micro parts. However, these effects have not yet been properly studied and therefore it is necessary to investigate systematically the influence of trapped air on the filling behaviour of polymer micro parts.

Finally, the research in part demoulding was reviewed as an important stage in the μ-IM cycles that can lead to part damage if ejection forces exceed a particular threshold. To minimise this process uncertainty it is necessary to study the influence of processing parameters on demoulding forces, and thus to find processing windows for moulding parts with minimum residual stresses.

3 PROCESS FACTORS INFLUENCE ON CAVITY PRESSURE BEHAVIOUR IN MICRO INJECTION MOULDING

3.1 Motivation

Process monitoring is of crucial importance when analysing the effects of different parameter settings in µ-IM on the process and also in assessing its performance. As discussed in Section 2.4 factors related to cavity pressure can provide valuable information about the process dynamics and also about the filling behaviour of different polymer melts. For that reason online pressure monitoring techniques should be used to investigate process dynamics and thus to identify optimum process parameters for low pressure µ-IM. In this chapter an approach based on in-process cavity pressure monitoring is proposed for identifying the optimum processing window for moulding a typical Type B polymer micro part and thus to investigate the main parameter settings affecting the process (Whiteside et al. 2003). In particular, a pressure sensor mounted inside a tool cavity was employed to analyse maximum cavity pressure, pressure increase rate during filling and pressure work. The influence of four µ-IM parameters - T_b, T_m, V_i and P_h - on these three pressure-related process parameters was investigated. A design of experiment study was conducted by moulding a test part, a micro fluidic component, in three different polymer materials, PP, ABS and PC.

3.2 Experimental setup

3.2.1 Test Part design

The design of a 15mm x 20mm x 1mm micro fluidics platform was used to analyse *P* in the cavity during the production of micro parts in this study (Figure 3-1 a). In particular, the system design includes features commonly found in micro fluidics components such as reservoirs, channels and waste compartments. The pin dimensions are 500 µm in diameter and 600 µm in height, and the cross section of the main channels vary between 50 and 200 µm. The overall design also includes a draft angle of 2-3º on the side walls. Table 3-1 shows some part design characteristics and compares two designs, one with the micro features and the other one without them. In particular, surface to volume ratio (SV_R) is 15.7% higher for the design that includes micro features. Higher SV_R means that a higher heat transfer should be expected, thus challenging the capability of the process to avoid premature freezing and achieve complete filling / replication. The increase of SV_R by 15.7% can be considered as critical for a successful replication of the micro features.

Design properties	Design with micro features	Design without features
Volume	310 mm^3	337 mm^3
Surface area	833 mm^2	762 mm^2
SV_R	2.68	2.26

Table 3-1 Design characteristics of the polymer micro part which was chosen for the experimental cavity pressure study

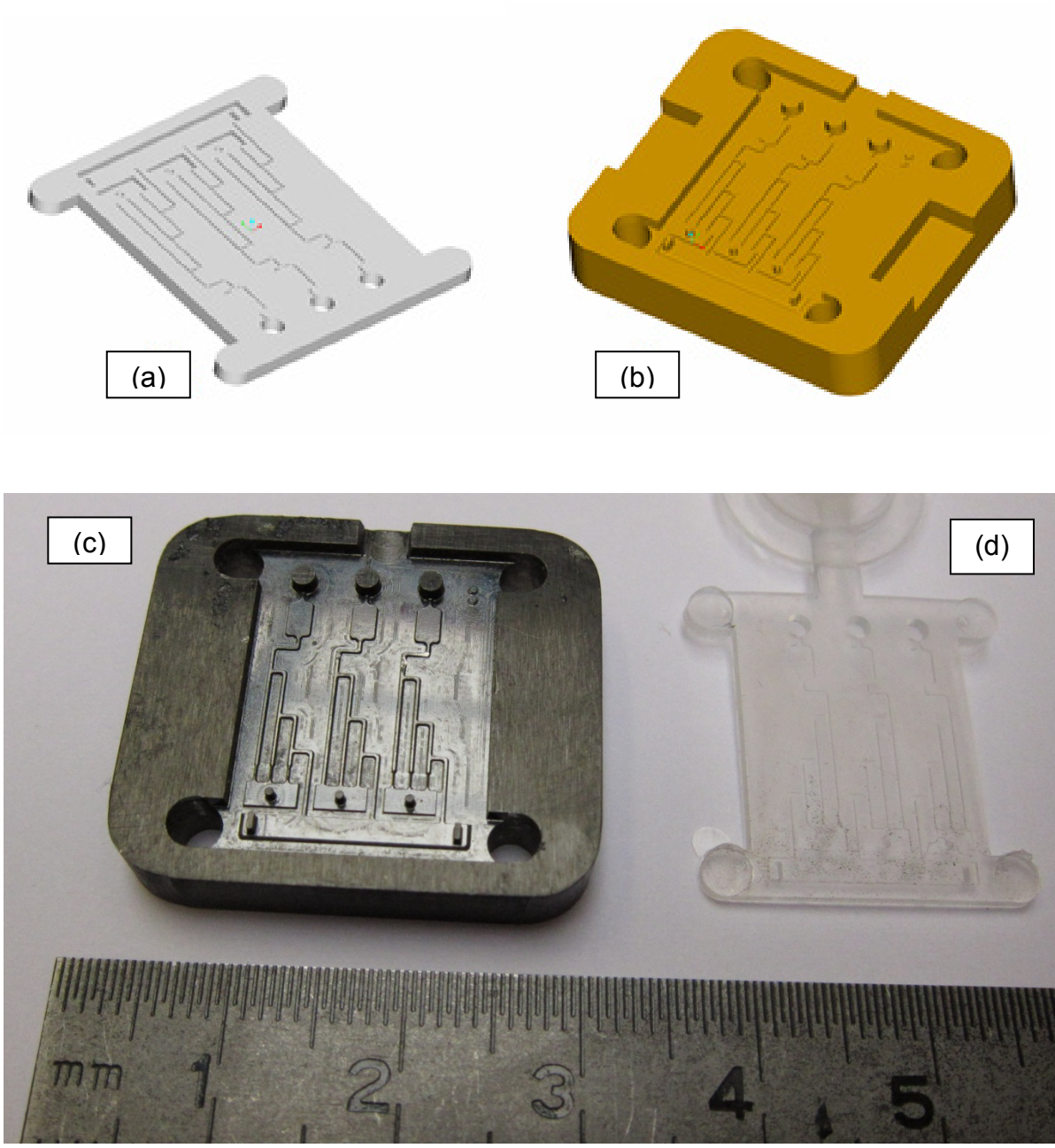

Figure 3-1 a) CAD model of Micro fluidics test part design and b) mould insert. The final mould steel insert (c) and a replicated PP polymer part (d)

3.2.2 Mould Manufacture

The tool used to perform the experiments was manufactured in standard mould steel using conventional milling except for the cavity faces that were machined employing micro-cutters. The overall size of the mould insert was 25 x 28 x 5 mm^3 with four 3 mm holes for ejectors (Figure 3-1 b). To reduce *P* and *T* influences on the gating, a single open gate design was used. The gate is the same depth as the cross-sectional thickness of the part, thus reducing the flow resistance and premature freeze-off of the gate. The tool halves were assembled to a primary mould tool and then inspected for parallelism and shut off of the mating faces.

The part design is made up of many features that could determine the mould accuracy. The focus of the research is on the manufacture and replication of micro features, therefore the assessment would be based on the results obtained for the 50 µm width channel features as shown in Figure 3-2. To determine the influence of the process factors on part replication, the dimensions of the tool and the mouldings are compared, and also the parts' weight.

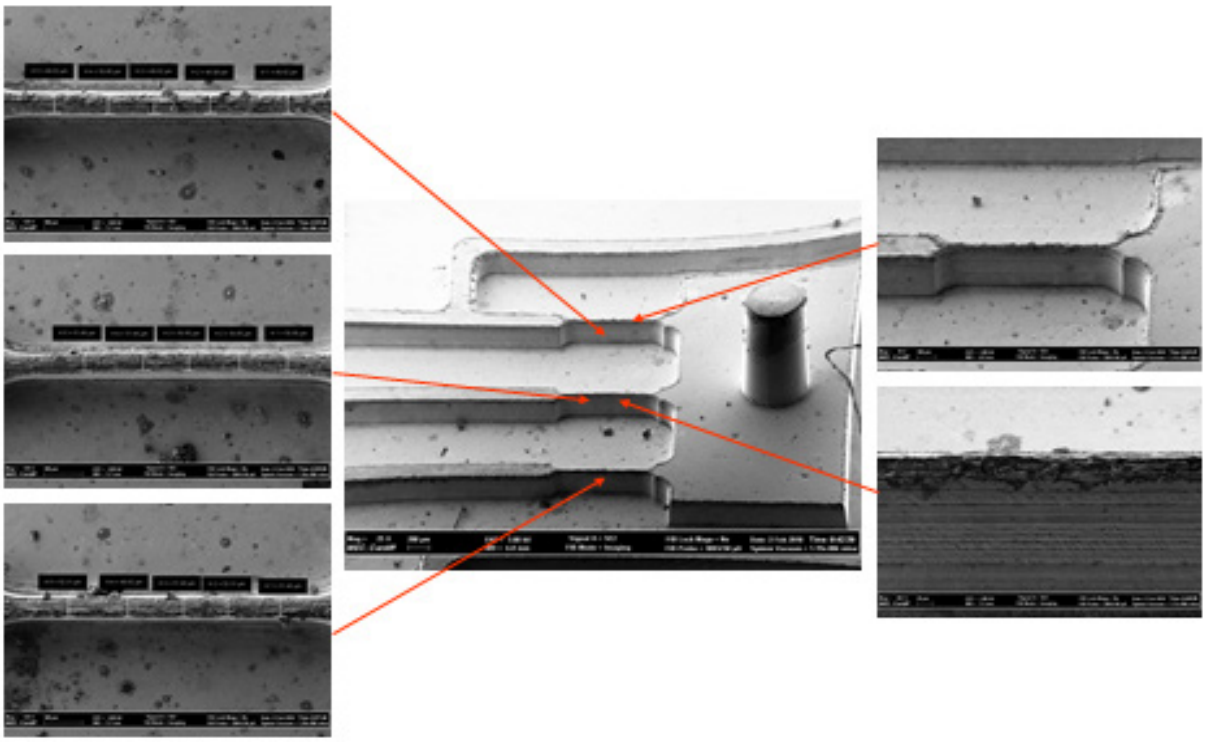

Figure 3-2 SEM Image of injection moulding tool with micro features. The height of the ribs is 200 µm and the minimum width is 50 µm.

3.2.3 Test materials

Three commonly used materials in IM, Polypropylene (PP), Acrylonitrile Butadiene Styrene (ABS) and Polycarbonate (PC), were selected to conduct the planned experiments. Their properties are provided in Table 3-2. Each polymer went through desiccant drying and dehumidifying cycles before the trials to remove any surface or absorbed moisture. The machine used to perform the µ-IM tests was a Battenfeld Microsystem 50.

Material	Sabic 56M10	DOW Magnum 8434	SABIC Lexan HPS1
Category	Polypropylene (PP)	Acrylonitrile butadiene styrene (ABS)	Polycarbonate (PC)
Structure	Semi-Crystalline	Amorphous	Amorphous
n	0.3747	0.2777	0.100
τ [Pa]	1.06E+04	7.68E+04	9.31E+05
D1[Pa-s]	1.19E+12	1.70E+14	6.89E+10
D2 [K]	263.15	373.15	417.15
D3 [K]	0	0	0
A1	23.8250	33.6060	26.1310
A2T [K]	51.6	51.6	51.6
Moldflow viscosity index*	VI(240)0087	VI(240)0166	VI(300)0163
Transition temperature [ºC]	150	90	155
Ejection temp [ºC]	80	85	125
Specific heat [J/kg-C]	2750	2032	2000
Thermal conductivity [W/m-C]	0.18	0.152	0.26
Elastic modulus [MPa]	1340	2240	2280
Poisson ratio	0.39	0.39	0.41
Shear modulus [MPa]	481	805	804
Coefficient of thermal expansion 1/C (E-05)	9.05	8.0	7.3

*Table 3-2 Polymer materials properties. Note: * - the number in the brackets refers to the material melt temperature [°C] while the other four digits signify its viscosity [Pa s] measured at a shear rate of 1000 [1/s] The numbers are provided by Moldflow material database.*

3.2.4 Condition monitoring

Condition monitoring techniques are used in μ-IM to quantify natural variations that can occur within moulding cycles, and thus to identify interdependences between the resulting part quality and the various tool, material and process factors. In this study, *P*

variations in the cavity area were recorded using a Dynisco PCI piezoelectric force transducer. A National Instruments cDAQ-9172 USB data acquisition unit was utilised to analyse sensor output signals employing the National Instruments Labview 8 software. Using an indirect *P* measurement method, the Battenfeld Microsystem 50 machine was modified to accommodate the force transducer behind the 5 mm injection pin. When the transducer is subjected to a mechanical load, this results in an electrical tension that is converted into a proportional voltage using a Kistler charge amplifier. The technical specifications of the transducer and amplifier used in this experimental study were:

- *transducer:* measuring range from 0 to 10,000 N and force sensitivity (E_f) of 4.2 pC / N;
- *amplifier:* measuring range up to 5000 pC and output range from 0 to 10V.

Ultimately, the output signal was monitored employing a National Instruments NI 9205 16-bit module.

The pressure sensitivity (E_p), of the setup can be expressed as follows:

$$E_p = \frac{d^2 \cdot \pi \cdot 0.1}{4} E_f \tag{3.1}$$

Thus, *P* in MPa can be calculated as follows:

$$P = \frac{Output(v) \times 500(pC)}{E_p} \div 10 \tag{3.2}$$

In this study the effects of the process parameters were analysed by using a condition monitoring experimental setup that enabled the assessment of P_{max}, P_{work} and P_{rate}.

3.2.5 Cavity pressure curve and pressure parameters definition

The IM cycle can be split into three consecutive stages: filling, packing, and cooling. During the polymer filling stage the cavity pressure rises during the volumetric filling of the cavity. At the second stage *P* continues to rise rapidly until it reaches the packing pressure level which is then maintained during the packing stage until the gate is frozen. Finally, the cooling stage covers the time until the end of cycle. Condition monitoring of injection *P* in µ-IM can be used to quantify the process factors' influence on cavity *P*. *P* varies over time (*t*), and by integrating a piezoelectric force transducer into the injection piston it is possible to identify the following conditions (Collins 1999) as depicted in Figure 3-3:

- The start of the injection cycle.
- Volumetric filling of the cavity.
- The second stage compression pressure and P_{max}.
- A reduction in *P* due to polymer solidification and gate sealing.
- An eventual drop to atmospheric pressure, due to the tool opening and part removal from the cavity.

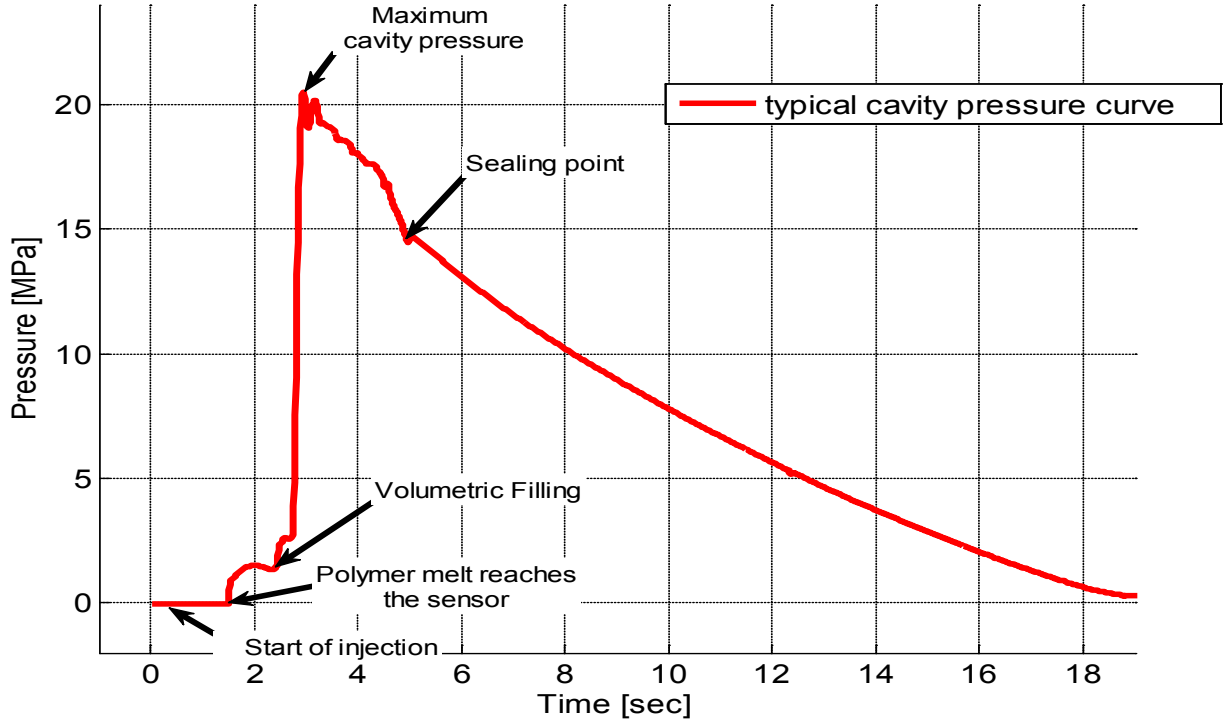

Figure 3-3 Typical cavity pressure curve over time for indirect pressure cavity measurement

This investigation focuses on the filling stage of the µ-IM process as shown in Figure 3-4. Due to the large amount of condition monitoring data that can be recorded it is often necessary to reduce it by pre-processing. In this way it will be easier to construct the profiles for further analysis. In this research, the Matlab software tool was employed to calculate the key values, while a *t* series function provided the key variables as outlined below to determine the cavity pressure conditions.

P_{max} is measured to obtain the peak *P* value that the tool can experience. This is the maximum that the cavity P reaches at t_{max}.

$$P_{max} = P_{cavity}(t_{max}) = max\left(P_{cavity}(t)\right) \qquad (3.3)$$

The pressure work (P_{work}) is determined by *P* over *t* during the filling stage. Especially, it is the area that is defined by the maximum integral value of the interval that begins with the pressure at the start of the filling stage (P_{start}) and ending with P_{max}. Thus, the post P_{max} pressure is ignored because this region is strongly dependent on the material characteristics. Due to the fact, that the *P* curve is defined with discrete values, P_{work} is a sum starting with *P* at the start time (t_{start}) and ending with *P* at the time of P_{max}, t_{max}, multiplied with the time step of Δt. The time step Δt was chosen to be 0.01 [sec] represented by the sampling rate of the data acquisition system. Thus, the P_{work} value was calculated employing the following equation:

$$P_{work} = \left(\sum_{t=t_{start}}^{t_{max}} P_{cavity}(t) \right) \cdot \Delta t \qquad (3.4)$$

The pressure rate of change (P_{rate}) represents the average gradient of the cavity pressure curve during the compression stage of the process. It starts when the cavity pressure reaches 10% above the compression threshold level and the end point is determined to be at 10% below P_{max} of the pressure curve.

$$P_{rate} = \frac{0.9 \cdot P_{max} - 1.1 \cdot P_{start}}{t_{Slope\_end} - t_{Slope\_start}} \qquad (3.5)$$

where 1.1 and 0.9 are constants to reduce the gradient error for P_{start}, $1.1 \cdot P_{start} = P_{cavity}(t_{slope\_start})$, and P_{max}, $0.9 \cdot P_{max} = P_{cavity}(t_{slope\_end})$, respectively.

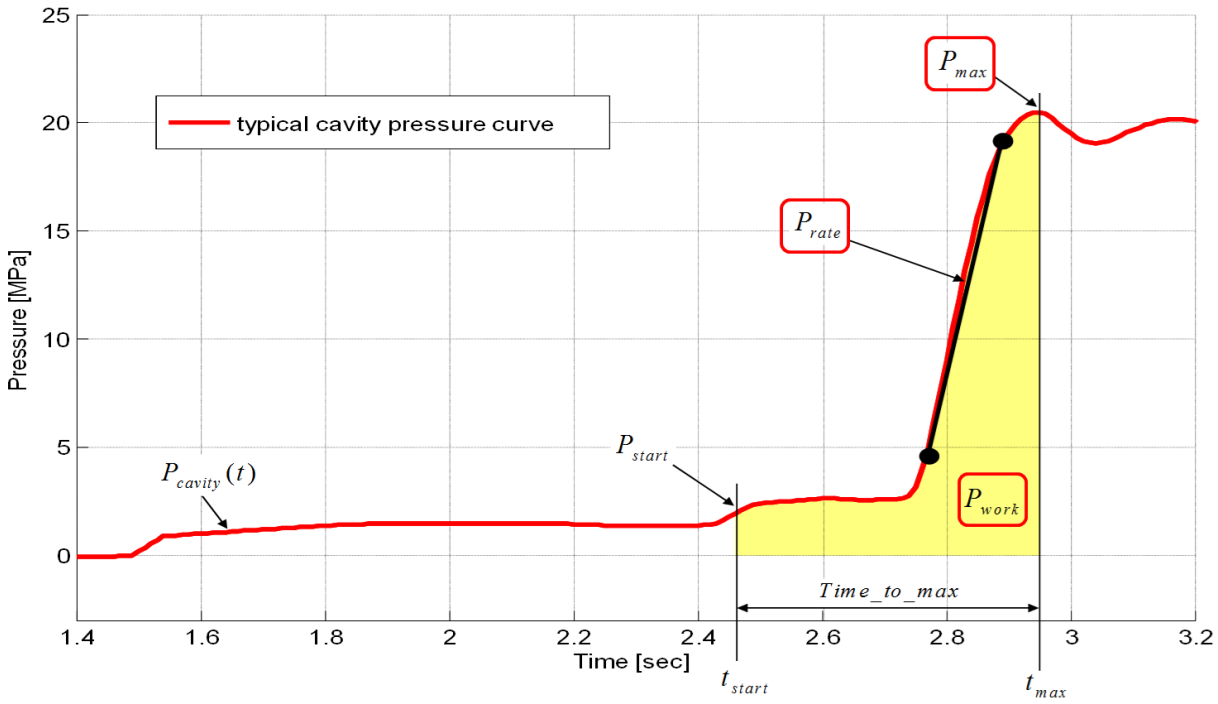

Figure 3-4 Filling stage of the cavity pressure curve. The characteristic variables P_{rate}, P_{max} and P_{work} are highlighted.

3.2.6 Design of experiments

To investigate the effects of the µ-IM process on part replication, this experimental research was focused on *P* during the filling stage of the process. The filling performance of micro cavities relies heavily on the *P* and *T* control during injection, therefore the effects of T_b, T_m, P_h and V_i were investigated in this study. Process parameters acquired by monitoring the cavity pressure maximum value and its integral over the cycle time were investigated by performing a one-factor-at-the-time analysis in µ-IM, i.e. the melt and mould temperature effects were evaluated separately (Whiteside et al. 2005a). However, a global approach to condition monitoring was implemented by carrying out a design of experiment (DOE) study. This approach allows all investigated process parameters to be taken into account simultaneously, and also to consider their main effects. Thus, it was possible to investigate

systematically the process and part related variables that influenced the part and process quality, respectively. In particular, process settings and part characteristics that affect product quality and cost can be identified in order to enable improvements of product manufacturability, quality, reliability and production throughputs (Park and Ahn 2004). Factorial design is frequently used in experiments involving several factors, and when it is necessary to study the factors' effects on various responses. Two different approaches can be distinguished when implementing DOE studies (Montgomery 2004a), full factorial design, widely used when it is necessary to investigate the joint effects of several factors on a response, and fractional factorial designs that are applied to reduce experimental efforts in large DOE studies, mostly for screening purposes. In this research, the full-factorial design was applied for each investigated material. Given that four factors at two levels were considered, a Taguchi L16 Orthogonal Array (OA) was selected as presented in Table 3-3. The two levels of control for P_h and V_i were the same for all materials, while the levels for T_b and T_m were different (Table 3-4).

The melt temperature was controlled through T_b, and was within a recommended processing window. Two levels, maximum and minimum temperatures, were used for each of the polymers. In µ-IM the polymer solidification time is much shorter than that in conventional moulding and, therefore, the processing requires heated tools. Therefore, T_m is raised to keep the bulk temperature of the polymer high enough to facilitate the melt flow during the filling stage. The T_m settings used in this research were the minimum and maximum temperatures within the recommended range for each material.

V_i has two main effects. It can help polymers to fill the cavities before the melt flow solidifies but also it can increase the shear rate of the polymer which results in shear heating. The two levels of V_i used in this research were chosen by taking into account the capabilities of the Battenfeld Microsystem 50, for which the maximum injection speed is 946.4 mm/s over a stroke distance of 84 mm. The two levels of P_h during which the cavity pressure is maintained were controlled using the Microsystem 50 P_h on and off functions. The holding pressure time (t_h) was set at 10 seconds.

Given that three different materials are considered, three L16 OAs were defined. In addition, ten trials were performed for each combination of controlled parameters in these three OAs. Thus, in total 10 x 16 x 3 = 480 experimental trials were carried out. The response variables considered are P_{max} , P_{work} and P_{rate}.

RUN	Factors			
	T_b	T_m	P_h	V_i
1	1	1	1	1
2	1	1	1	2
3	1	1	2	1
4	1	1	2	2
5	1	2	1	1
6	1	2	1	2
7	1	2	2	1
8	1	2	2	2
9	2	1	1	1
10	2	1	1	2
11	2	1	2	1
12	2	1	2	2
13	2	2	1	1
14	2	2	1	2
15	2	2	2	1
$16 = 2^4$	2	2	2	2

Table 3-3 Taguchi L16 Orthogonal Array design for process parameter variation of T_b, T_m, P_h and V_i

RUN	Factors											
	PP	ABS	PC	PP	ABS	PC	PP	ABS	PC	PP	ABS	PC
	T_b [ºC]			T_m [ºC]			P_h			V_i [mm/s]		
1	210	210	250	10	30	70	Off			200		
2	210	210	250	10	30	70	Off			800		
3	210	210	250	10	30	70	On			200		
4	210	210	250	10	30	70	On			800		
5	210	210	250	70	90	130	Off			200		
6	210	210	250	70	90	130	Off			800		
7	210	210	250	70	90	130	On			200		
8	210	210	250	70	90	130	On			800		
9	270	270	310	10	30	70	Off			200		
10	270	270	310	10	30	70	Off			800		
11	270	270	310	10	30	70	On			200		
12	270	270	310	10	30	70	On			800		
13	270	270	310	70	90	130	Off			200		
14	270	270	310	70	90	130	Off			800		
15	270	270	310	70	90	130	On			200		
16	270	270	310	70	90	130	On			800		

Table 3-4 Process parameter which have been calculated for three different materials PP, ABS and PC based on Taguchi Orthogonal Array

3.3 Analysis of the results

3.3.1 Average cavity pressure

In this study, L16 OAs were employed to ensure that the experimental results were representative of the considered processing windows for the three selected materials. For each trial, the effects on P_{max} , P_{work} and P_{rate} were investigated, and then based on the 480 trials conducted, the mean values were calculated for each of the three OAs as shown in Figure 3-5.

The quantitative P_{max} data from the experiments identified that the highest recorded P_{max} was for PC, 48 MPa, while the lowest was for ABS, 7.29 MPa. The normal distribution of the recorded P_{max} for the three materials showed wide variations of the experimental results. In particular, Figure 3-5 depicts that PC has the highest average cavity pressure, 29.24 MPa, followed by PP, 16.78 MPa, and ABS, 13.01 MPa. At the same time, PC has the lowest probability density, $pd(x)$, and a high standard deviation (σ) of 8.63 compared to 1.61 for PP. This result indicates that the process factors have a greater influence on the P_{max} for PC than for ABS and PP.

The P_{work} normal distribution results are similar to those for P_{max}. The highest recorded P_{work} was for PC, 1267.8 MPa s, and the lowest was for ABS, 15.6 MPa s. Figure 5 shows a wide variation of the results; in particular the highest average P was for PC at 633.7 MPa s, followed by PP, 200.1 MPa s, and ABS, 130.3 MPa s. And, like P_{max} PC has the lowest $pd(x)$, and σ of 303.6 compared with 77.8 for PP. Again, this result shows that the process factors have a greater influence on P_{work} for PC than for the other two.

The P_{rate} distributions differ to those recorded for P_{max} and P_{work}. The experiments show that the highest recorded P_{work} was for PC, 1.88 MPa/s, while the lowest was for PC, 0.05 MPa/s. Also, Figure 3-5 depicts that the highest average P change is for PP, 0.54 MPa/s, followed by ABS, 0.50 MPa/s, and PC, 0.37 MPa/s. $pd(x)$ of the three materials is similar while σ for the three materials is between 0.30 and 0.35.

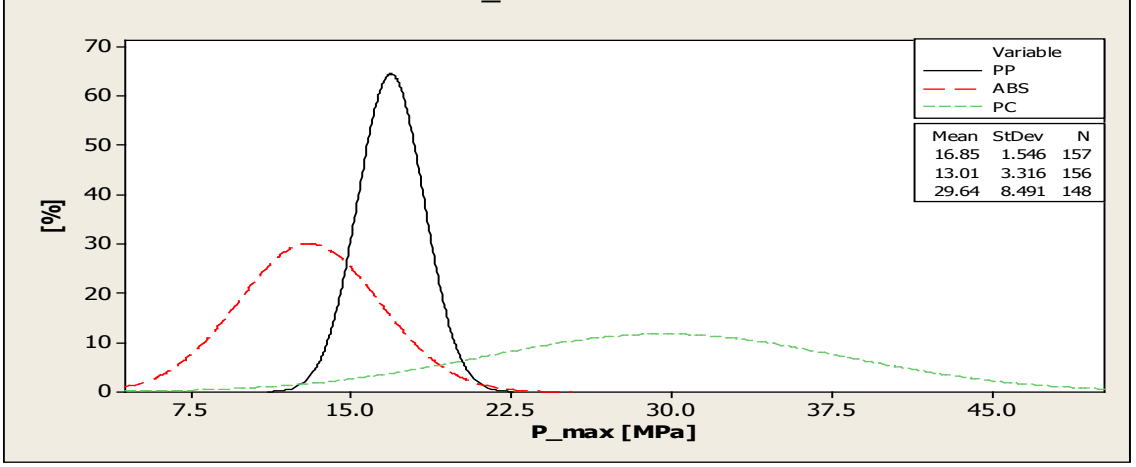

Normal distribution of P_{max} results

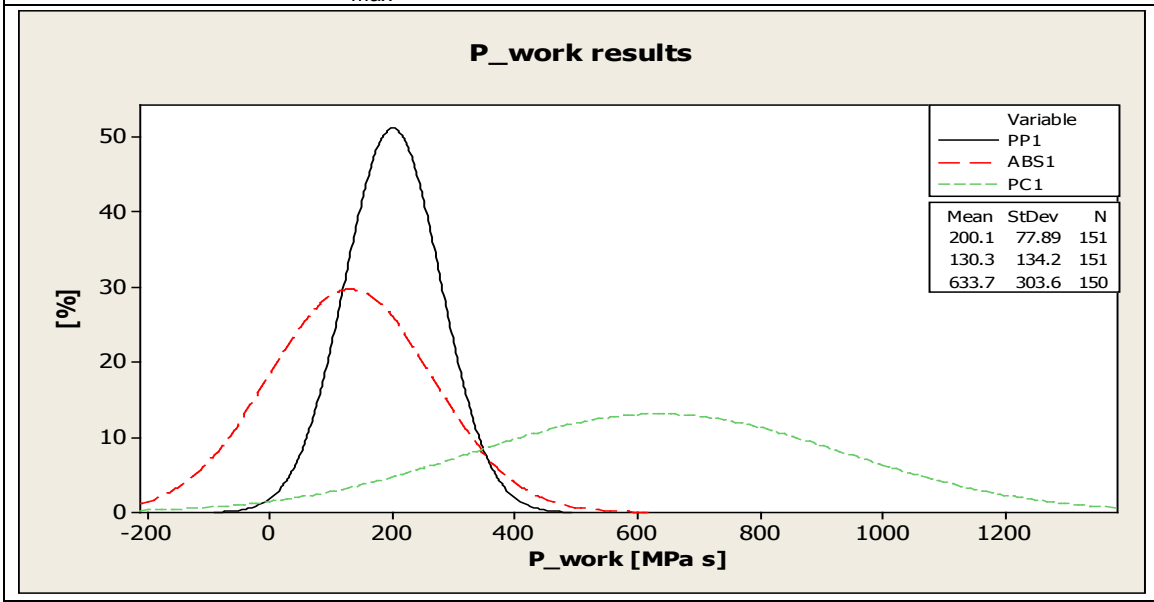

Normal distribution of P_{work} results

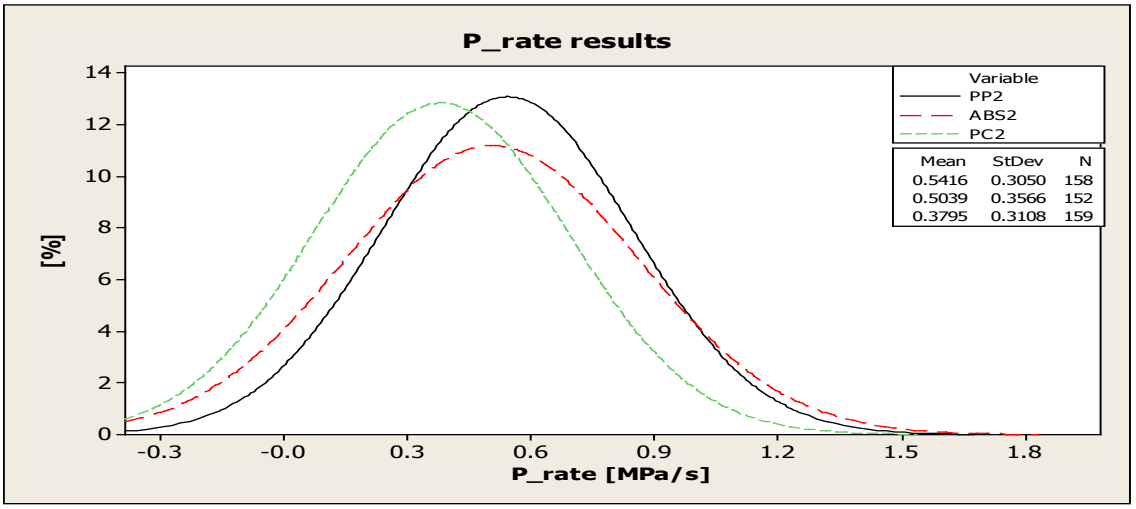

Normal distribution of P_{rate} results

Figure 3-5 Normal distribution of P_{max} P_{work} and P_{rate} results

3.3.2 Process parameters' effects on cavity pressure factors

Based on the experimental results, an analysis of variance (ANOVA) was performed in order to assess the contribution of each processing parameter to the resulting $P_{max,}$ P_{work} and P_{rate}. Table 3-5, Table 3-6 and Table 3-7 and Figure 3-6, Figure 3-8, and Figure 3-9 show the response of each parameter and the main effects plot for each, respectively.

From the P_{max} analysis, it is immediately apparent that there is no selection of parameter levels that can be considered optimum for each type of polymer investigated in this research. The results show that *T* is ranked as the most important factor for the three materials, in particular T_m was the most important for PP, while T_b for ABS and PC. Indeed, the increase of T_b led to a decrease of P_{max} for ABS and PC by 32% and 41%, respectively, and it had no effect on PP (see Figure 3-6). This observation highlights the influence that melt solidification has on flow resistance and resulting *P* increase and it is supported by the different viscosity characteristics of the three polymers (see Figure 3-7). A comparison between the respective viscosity curves shows that the melt temperature of PP has a very limited effect on the viscosity (i.e. the viscosity curve at 210°C is very close to the curve at 270°C). On the other hand, the viscosity differences between the two melt temperatures for ABS and PC (210°C / 270°C and 250°C / 310°C, respectively) is much bigger, leading to a larger influence of T_b on pressure for these two polymers.

Looking at the P_{work} results, it is also evident that optimum unique parameter settings cannot be identified for the three polymers investigated in this research. The results show that V_i is the most important factor, being ranked first for ABS and PC and second for PP. In all cases the increase of V_i results in a P_{work} reduction in the range

from 26 to 79%. Additionally, an increase of T_m results in an increase of P_{work} for all materials.

Regarding P_{rate}, it was observed that the influence of the parameter levels were similar for all three polymers investigated in this research. The results show that an increase of T_B and V_i generally led to an increase of P_{rate}, whilst for T_m and P_h the opposite was observed. For all materials, T_m was identified as the factor with the highest overall influence; in particular an increase of T_m resulted in a reduction of P_{rate} in the range from 44 to 57%. Thus, by increasing T_m the polymer viscosity is maintained longer resulting in an increase in the filling rate.

Materials	Level	T_b	T_m	P_h	V_i
PP	1	16.77 [MPa]	17.89 [MPa]	17.41 [MPa]	17.06 [MPa]
	2	16.89 [MPa]	15.76 [MPa]	16.25 [MPa]	16.59 [MPa]
Delta		0.12	2.13	1.17	0.47
Difference [%]		0.71	11.90	6.66	2.75
Rank		4	1	2	3
ABS	1	15.56 [MPa]	12.30 [MPa]	12.96 [MPa]	12.98 [MPa]
	2	10.44 [MPa]	13.69 [MPa]	13.03 [MPa]	13.01 [MPa]
Delta		5.12	1.39	0.07	0.03
Difference [%]		32.90	10.15	0.53	0.23
Rank		1	2	3	4
PC	1	37.19 [MPa]	29.53 [MPa]	28.90 [MPa]	27.52 [MPa]
	2	21.70 [MPa]	29.37 [MPa]	29.99 [MPa]	31.38 [MPa]
Delta		15.49	0.16	1.09	3.86
Difference [%]		41.65	0.54	3.63	12.30
Rank		1	4	3	2

Table 3-5 Response table for P_{max}

Materials	Level	T_b	T_m	P_h	V_i
PP	1	199.6 [MPa s]	154.3 [MPa s]	208.5 [MPa s]	229.8 [MPa s]
	2	199.3 [MPa s]	244.5 [MPa s]	190.4 [MPa s]	169.1 [MPa s]
Delta		0.3	90.2	18.1	60.7
Difference [%]		0.15	36.89	8.68	26.41
Rank		4	1	3	2
ABS	1	132.4 [MPa s]	125.7 [MPa s]	77.0 [MPa s]	221.7 [MPa s]
	2	134.7 [MPa s]	141.3 [MPa s]	190.1[MPa s]	45.3 [MPa s]
Delta		2.3	15.6	113.1	176.4
Difference [%]		1.70	11.04	59.49	79.56
Rank		4	3	2	1
PC	1	656 [MPa s]	540 [MPa s]	586.8 [MPa s]	877.4 [MPa s]
	2	602.8 [MPa s]	718.8 [MPa s]	672 [MPa s]	381.4 [MPa s]
Delta		53.2	179.2	85.2	496
Difference [%]		8.10	24.87	12.67	56.53
Rank		4	2	3	1

Table 3-6 Response table for P_{work}

Materials	Level	T_b	T_m	P_h	V_i
PP	1	0.54 [MPa /s]	0.75 [MPa /s]	0.58 [MPa /s]	0.54 [MPa /s]
	2	0.53 [MPa /s]	0.32 [MPa /s]	0.49 [MPa /s]	0.54 [MPa /s]
Delta		0.01	0.43	0.08	0.001
Difference [%]		1.85	57.33	15.51	0
Rank		3	1	2	4
ABS	1	0.45 [MPa /s]	0.66 [MPa /s]	0.51 [MPa /s]	0.39 [MPa /s]
	2	0.57 [MPa /s]	0.36 [MPa /s]	0.51 [MPa /s]	0.63 [MPa /s]
Delta		0.11	0.29	0.005	0.23
Difference [%]		21.05	45.45	0	38.09
Rank		3	1	4	2
PC	1	0.35 [MPa /s]	0.49 [MPa /s]	0.45 [MPa /s]	0.36 [MPa /s]
	2	0.41 [MPa /s]	0.27 [MPa /s]	0.32 [MPa /s]	0.40 [MPa /s]
Delta		0.06	0.22	0.13	0.04
Difference [%]		14.63	44.89	28.88	10
Rank		3	1	2	4

Table 3-7 Response table for P_{rate}

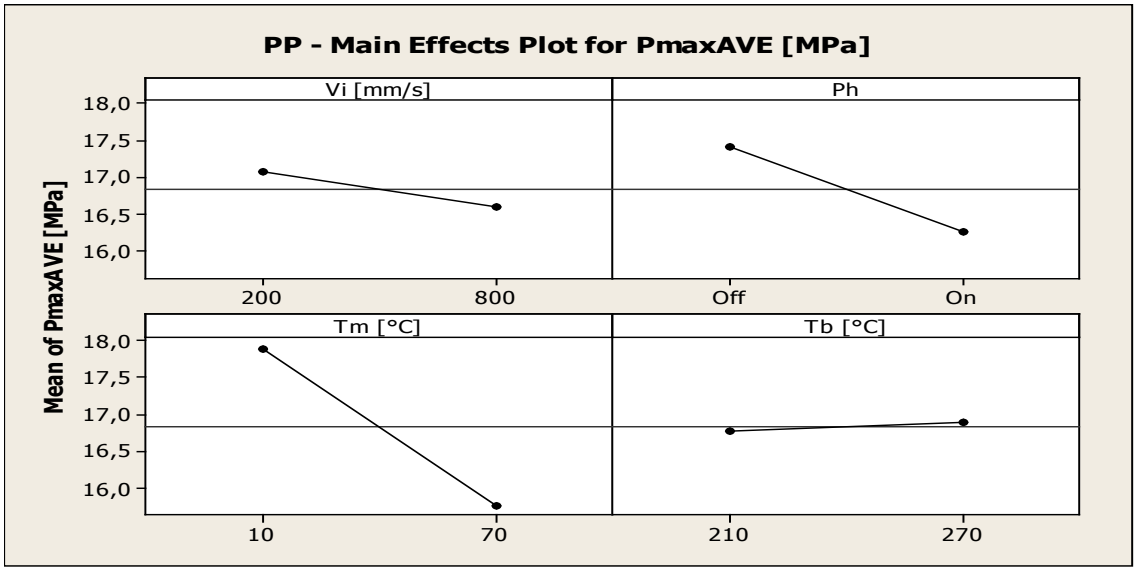

PP main effect plot

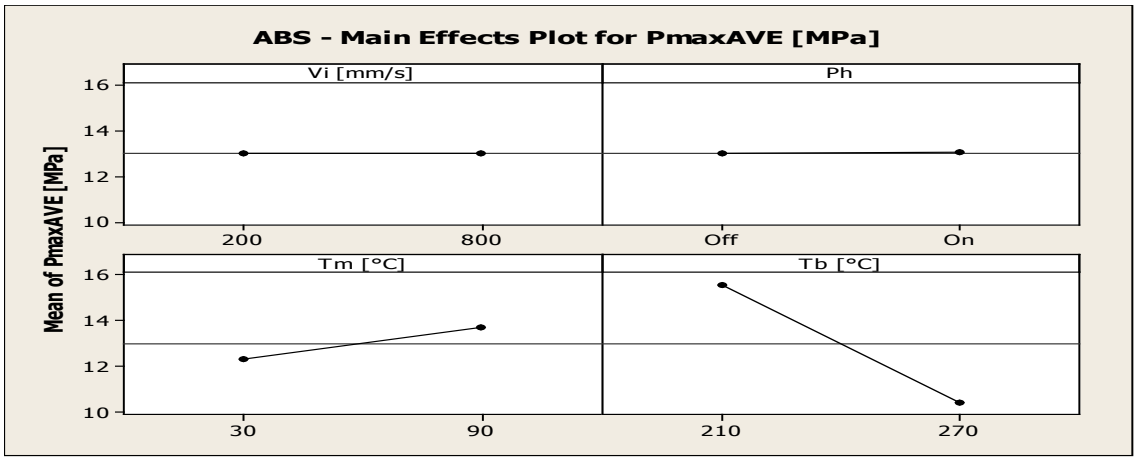

ABS main effect plot

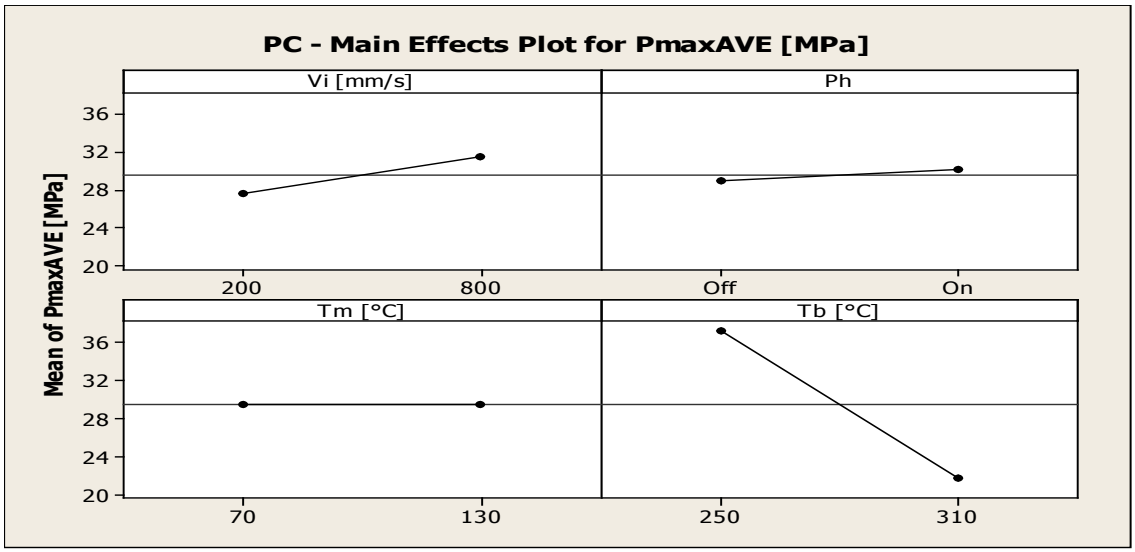

PC main effect plot

Figure 3-6 Main effects plot of average P_{max} for PP, ABS and PC

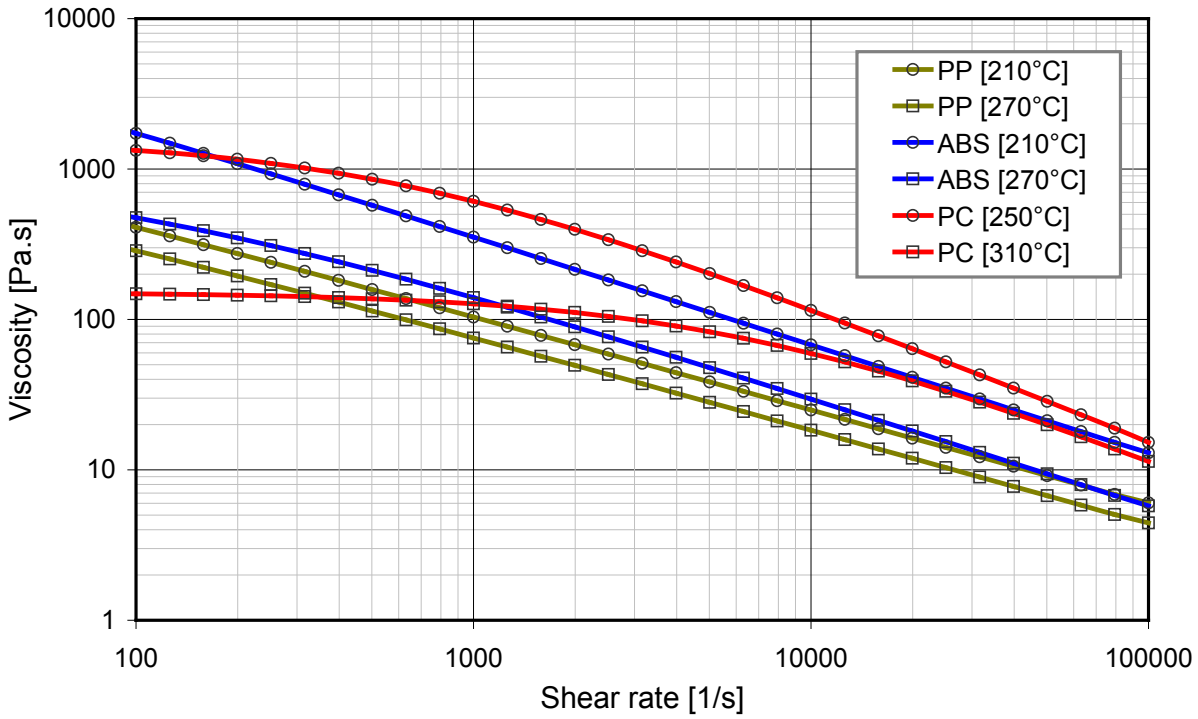

Figure 3-7 Viscosity characteristics of the three polymers PC, PP and ABS

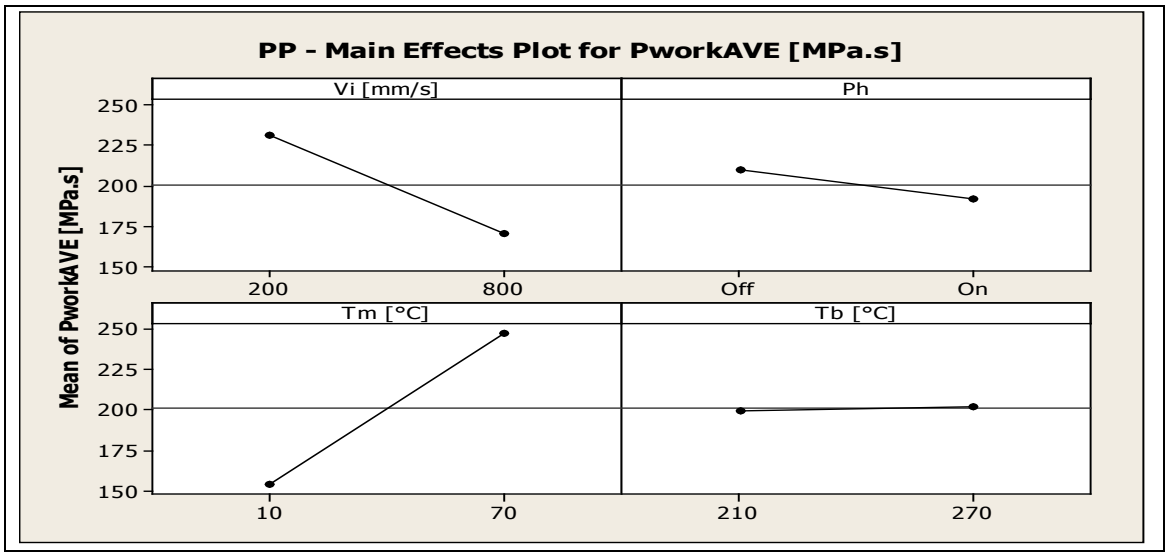

PP main effect plot

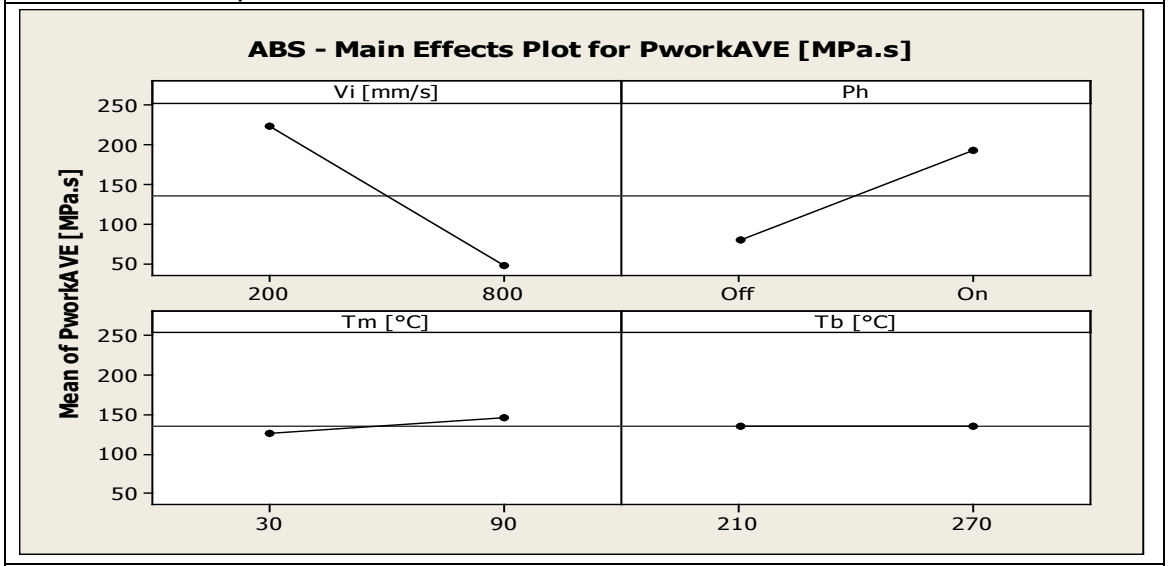

ABS main effect plot

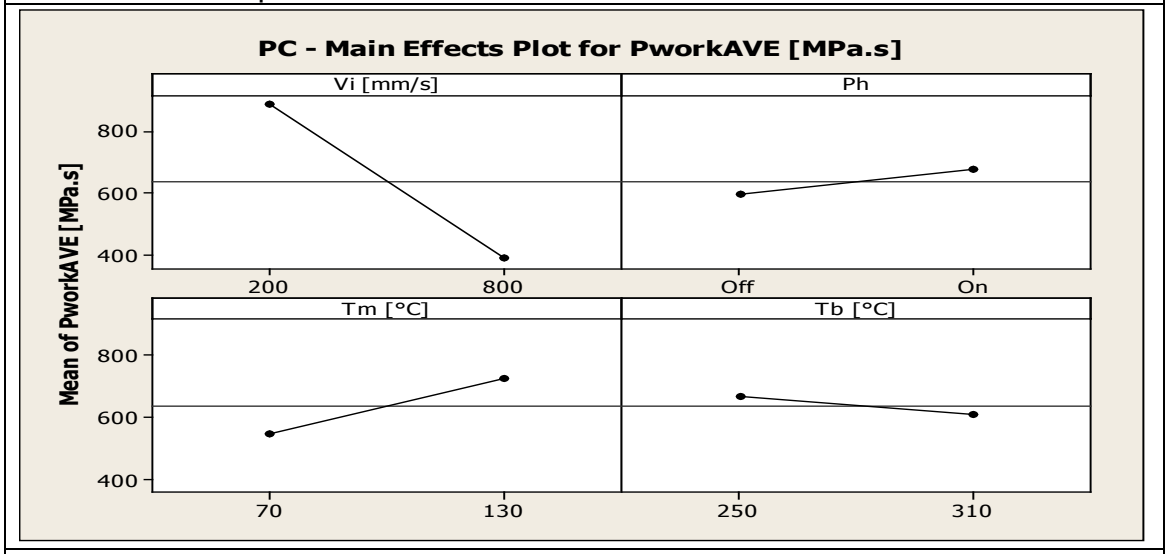

PC main effect plot

Figure 3-8 Main effects plot of average P_{work} for PP, ABS and PC

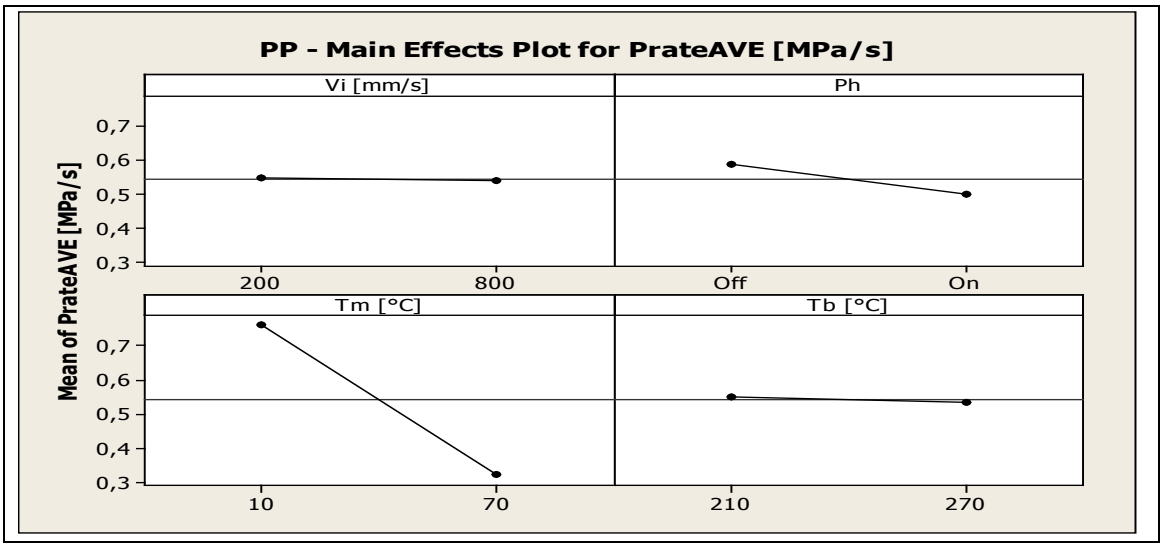

PP main effect plot

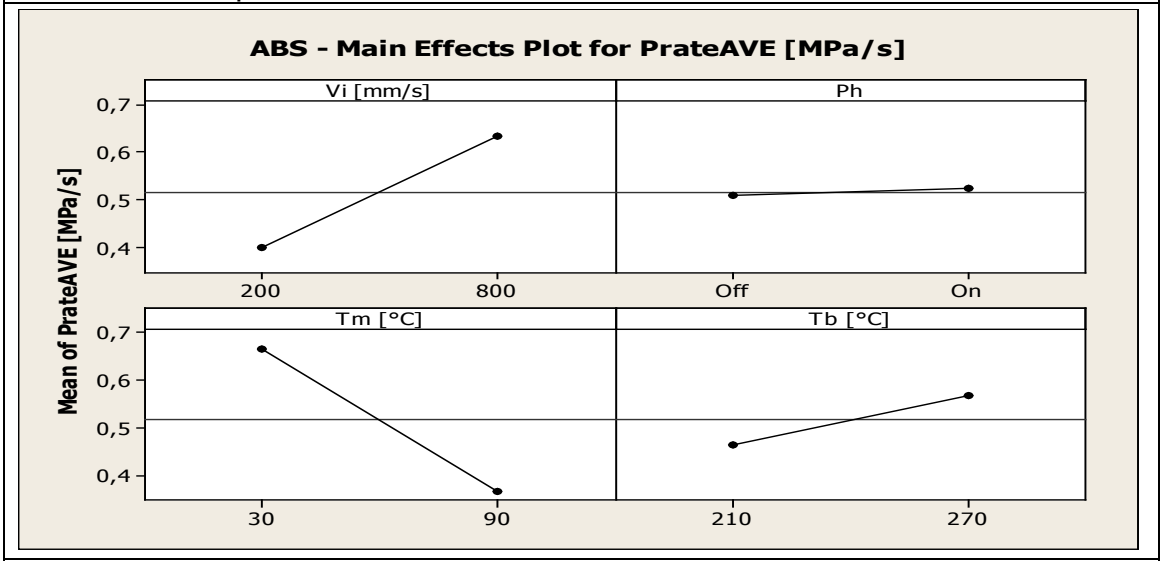

ABS main effect plot

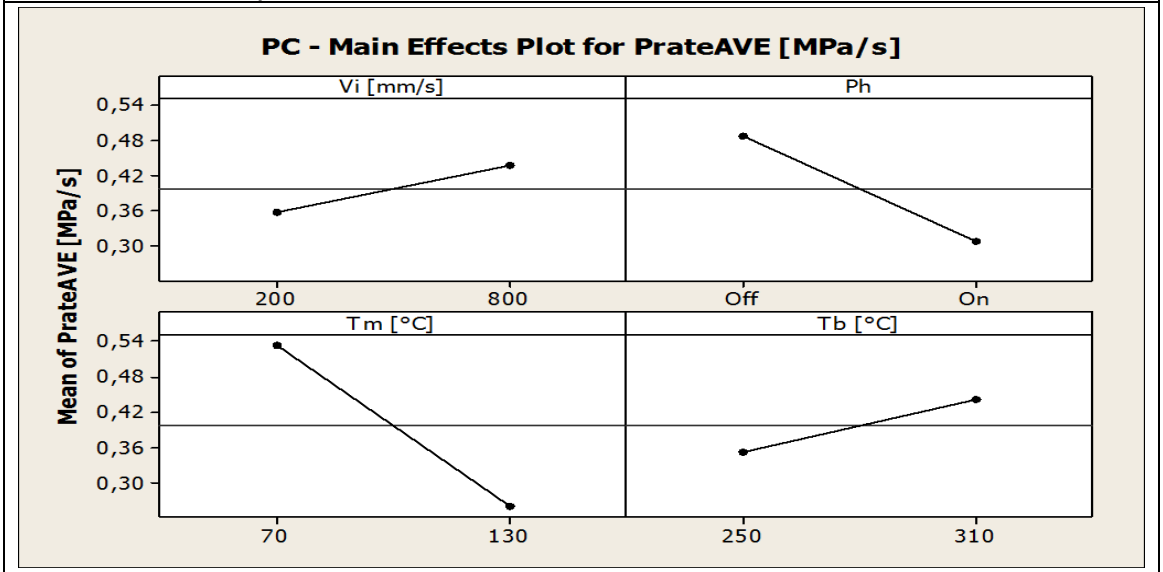

PC main effect plot

Figure 3-9 Main effects plot of average P_{rate} for PP, ABS and PC

3.4 Conclusion

This chapter reports an experimental approach for studying the effects of pressure conditions in micro cavities when replicating parts in three different polymers. To measure the pressure state of a polymer inside the mould cavity a condition monitoring system was designed and implemented. Then, by employing a design of experiment approach the moulding performance was studied. In particular, the effects that four process factors, T_b, T_m, P_h and V_i have on three cavity pressure related factors (P_{max}, P_{work}, P_{rate}) were investigated.

The main conclusions based on the obtained results are:

- It is possible to assess cavity pressure conditions during part filling by employing a specially designed condition monitoring setup. It was shown that P_{max}, P_{work} and P_{rate} were dependent on both materials and processing conditions.

- The mean value of P_{max}, P_{work} and P_{rate} were analysed, and the results identify a clear relationship between P_{max} and P_{work}. It was shown that the mean values for each material were similar in terms of their distribution over the considered pressure range. PC had the broadest P_{max} and P_{work} distributions while PP the narrowest, thus indicating that PC is affected more by the process factors. The P_{rate} distributions were comparable for all three materials, which showed that the process factors led to a similar rate of pressure change in the range from P_{start} to P_{max}.

- The process parameters' effects on P suggest that in the context of P_{max}, P_{work} and P_{rate} there is no unique selection of parameter levels that can be considered

optimum for the three polymers investigated in this research. Temperature can be considered the most influential parameter for $P_{max,}$ while V_i for P_{work}, and for both an increase in the parameter setting results in a decrease of the *P* related factor.

- T_m dominates as the most influential parameter for P_{rate}. It can also be concluded that the parameters influence is similar for all materials, in particular for all materials an increase of T_B and V_i generally increases P_{rate}, while an increase of T_m and P_h leads to a decrease of P_{rate}.

- By predicting the processing parameters' effects, it was shown that for PC there was a clear interdependence between P_{rate} and P_{work}. In particular, the suggested settings for achieving low P_{work} were the same as those for high P_{rate} and vice versa. Thus, it can be concluded that if P_{rate} is higher the P_{work} will be lower.

4 CAVITY AIR FLOW BEHAVIOUR DURING FILLING IN MICRO INJECTION MOULDING

4.1 Motivation

As described in Chapter 3, the monitoring of cavity pressure in µ-IM can be of crucial importance in understanding the effects of different parameter settings on the process, especially on its performance and consistency with regards to part quality. Quality factors related to mould cavity air evacuation can provide valuable information about the process dynamics and also about the filling of a cavity by a polymer melt. In this chapter, a novel experimental setup is proposed to monitor maximum air flow and air flow work by employing a MEMS gas sensor mounted inside the mould. The influence of four µ-IM parameters, melt temperature (T_b), mould temperature(T_m), injection speed (V_i), and resistance to air evacuation (E_a^R), on these two air flow-related output parameters is investigated by carrying out a design of experiment study. In particular, by measuring the flow length in a specially designed test cavity the effects of process settings and air flow-related characteristic numbers are analysed in order to identify the most influential process parameters with regards to filling behaviour.

4.2 Experimental setup

4.2.1 Test Part design

The test part design used in this study to analyse E_a in a cavity during IM was a 5 mm x 21 mm x 250 µm micro fluidics platform (Figure 4-1). The design includes seven

micro channels with cross sections of 100 x 100 μm^2 and 14 mm in length. The part surface area is 226.5 mm^2 and the volume is 18.7 mm^3.

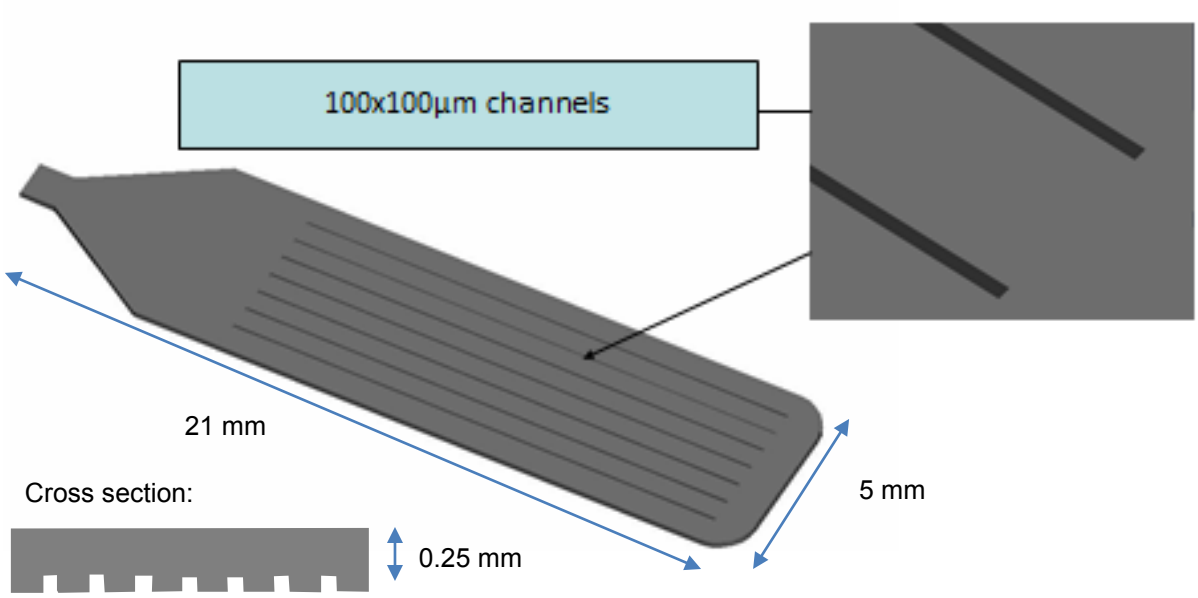

Figure 4-1 Test part design: seven ribs (100 µm x 100 µm) separate the flow front into eight independent "fingers"

4.2.2 Test materials

ABS was selected to conduct the planned experiments. Its properties are provided in Table 4-1. The polymer went through desiccant drying and dehumidifying cycles before the trials to remove any surface or absorbed moisture. The machine used to perform the micro injection moulding trials was a Battenfeld Microsystem 50.

Material	Magnum 8434
Category	Acrylonitrile butadiene styrene (ABS)
Structure	Amorphous
N	0.2777
τ [Pa]	7.68E+04
D1[Pa-s]	1.70E+14
D2 [K]	373.15
D3 [K]	0
A1	33.6060
A2T [K]	51.6
Moldflow viscosity index (*)	VI(240)0166
Transition temperature [ºC]	90
Ejection temp [ºC]	85
Specific heat [J/kg-C]	2032
Thermal conductivity [W/m-C]	0.152

*Table 4-1 Polymer material properties. Note: * the number in the brackets refers to the material melt temperature [°C] while the other four digits signify its viscosity [Pa s] measured at a shear rate of 1000 [1/s].*

4.2.3 Mould Manufacture

The tool used to perform the experiments used a Hasco K-standard modular system of machined and drilled plates. The plates are made out of standard tool steel. However, the standard system was modified to integrate an air flow transducer. The tool halves were assembled and then inspected for parallelism and shut off of the mating faces. Any gap between these faces is considered as a primary vent for E_a during polymer injection. The surface mapping of the K-Standard cavity block performed with an interferometric white light profiling microscope revealed a R_a roughness value of 8.6 µm, which with two mating plates would provide an air gap of up to 17.2 µm (Figure 4-2). The measurement was taken at the WLI measurement point which is marked in Figure 4-3 Therefore, to control the amount of E_a from the cavity through such a primary vent, a circular channel was machined to accommodate a 4 mm diameter O-

ring (46 mm inside diameter). The O-ring surrounds the cavity and seals the shut off faces, and thus restricts E_a through the primary vent.

The 3 mm diameter half round runner, gate and micro part cavity, as shown in Figure 4-3, are machined on the moving half of the mould by micro-milling. At the end of the flow path, as far as possible from the gate, a secondary vent, 1 mm x 5 mm x 200 µm, was machined on the cavity face. This vent led to a 1 mm diameter air relief orifice, through which E_a from the cavity was channelled to a sealed air flow transducer. This experimental setup allowed the influence of air evacuation on the part flow length in µ-IM to be investigated, especially the filling of micro parts and the $\dot{Q}$ variations of E_a.

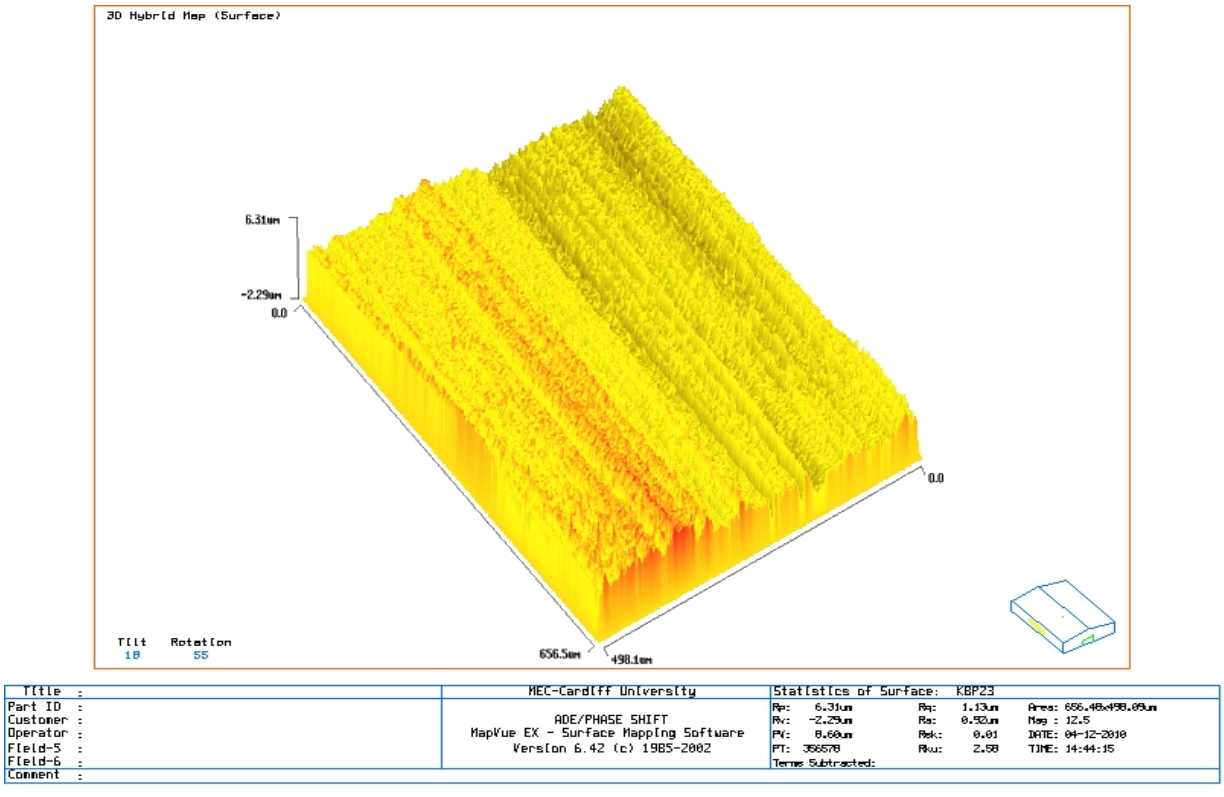

Figure 4-2 Surface map of the mould shut off face image taken by white light interferometry

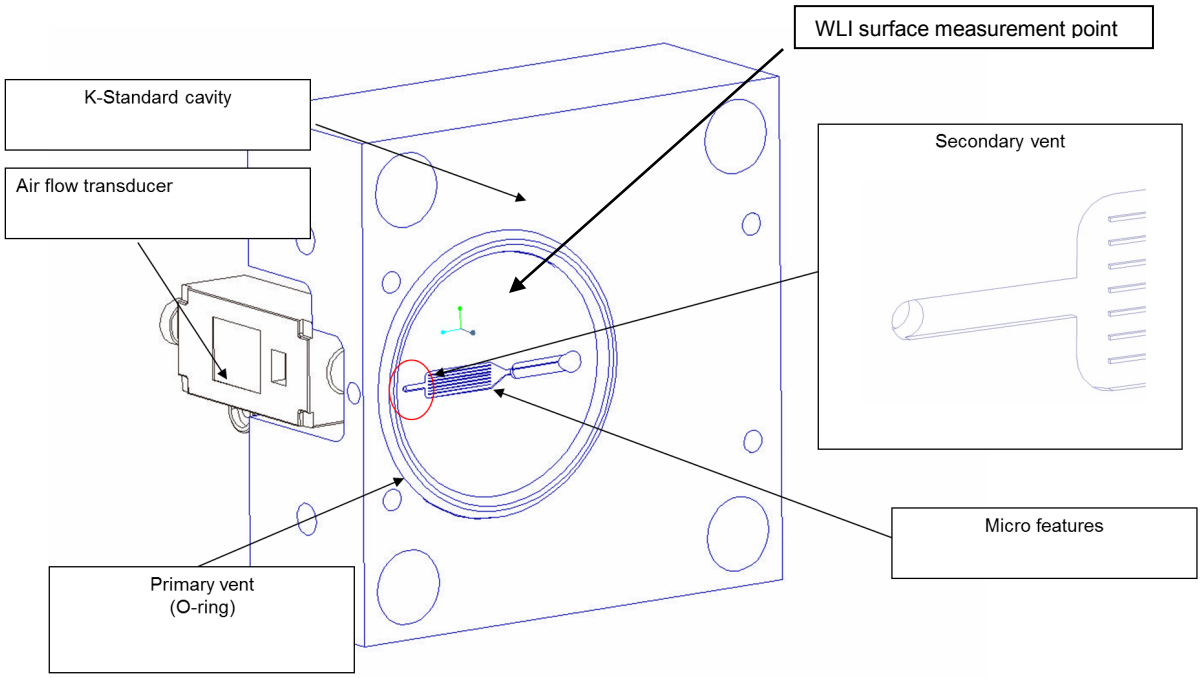

Figure 4-3 Experimental setup and tool design for the study of the air flow behaviour

4.2.4 Condition monitoring

Condition monitoring techniques are used in µ-IM to quantify natural variations that can occur during moulding cycles, and thus to identify interdependences between the resulting part quality and various tool, material and process factors. In this study, airflow rate ($\dot{Q}$) variations in the cavity area were investigated using an air flow transducer, Omron D6F-01A1-110, as shown in Figure 4-4. This supersensitive gas flow sensor based on a proprietary MEMS technology was used to measure accurately low $\dot{Q}$ over a wider range of *T*. In particular, the extreme sensitivity of this sensor is achieved with thermopiles that can be used to measure *T* or radiant energy, and then to convert them into an electric signal (McGraw-Hill 2003). Inside each sensor there is a highly sensitive MEMS flow chip with dimensions 1.55 x 1.55 x 0.4 mm^3. The chip has two thermopiles on the either side of a heater element used to measure the

deviations in heat symmetry caused by the passing gas flow. A thin layer of insulating film protects the chip from direct exposure to the gas. When there is no $\dot{Q}$ present, the *T* distribution around the heater is uniform and the differential voltage of the two thermopiles is zero volts. When $\dot{Q}$ is present, the side of the flow sensor facing the source of the airflow cools and the opposite side warms, thus unsettling the *T* equilibrium as presented in Figure 4-5. The difference in *T* appears as a differential voltage between the two thermopiles, thus allowing $\dot{Q}$ to be calculated.

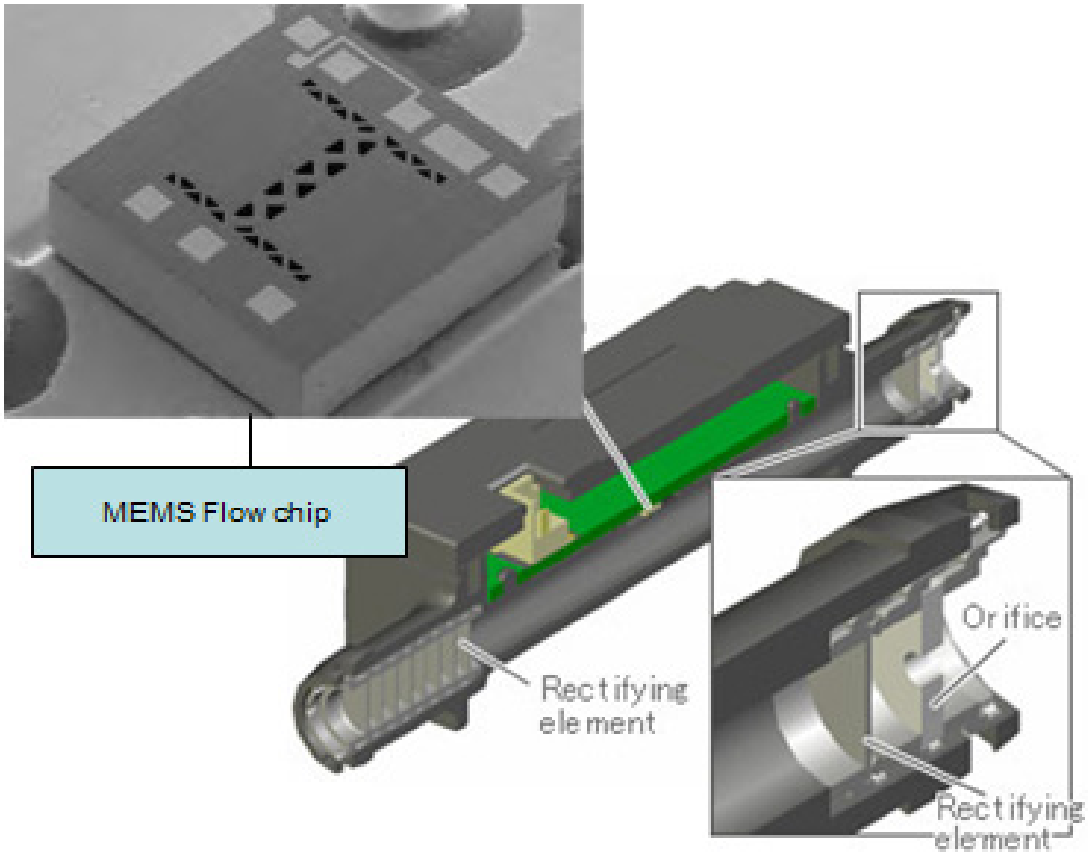

Figure 4-4 Components and cross section of the air flow transducer

A National Instruments cDAQ-9172 USB data acquisition unit was utilised to analyse sensor output signals on a computer employing the National Instruments Labview 8

software. When the gas sensor is subjected to $\dot{Q}$, this results in an electrical output. Ultimately, the output signal is monitored employing a National Instruments NI 9205 16-bit module. In this study the effects of the process parameters were analysed by using this condition monitoring experimental setup, allowing the maximum flow rate, $\dot{Q}_{\max}$ [ml/s] to be measured, and thus to calculate the integral of Q [ml]. $\dot{Q}_{\max}$ is monitored in order to determine the peak $\dot{Q}$ value that the gas sensor has experienced. This value is the maximum of $\dot{Q}$ over t where $t_{\max}$ represents the time when $\dot{Q}$ in the cavity reaches its maximum.

$$\dot{Q}_{max} = \dot{Q}(t_{max}) = max\left(\dot{Q}(t)\right) \qquad (4.1)$$

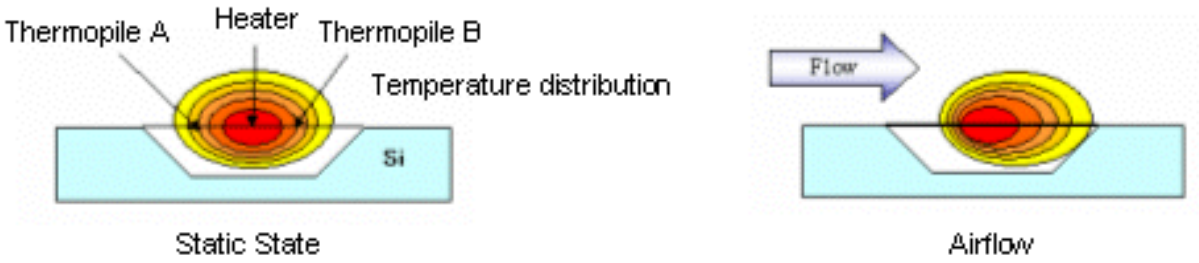

Figure 4-5 Thermopile and functional principal of air flow transducer

The total air flow over time, Q, determines $\dot{Q}$ over the whole duration of the filling stage and is the integral of $\dot{Q}$. Due to the fact, that the $\dot{Q}$ curve, Figure 4-6, is defined by the measured discrete values, Q is the sum of $\dot{Q}$ from the start of the filling stage, t_{start}, until its completion, t_{end}, multiplied by a time step of Δt. The chosen time step Δt is 1 ms and is determined by the sampling rate of the data acquisition system. Thus, Q is calculated employing the following equation:

$$Q = \left(\sum_{t=t_{start}}^{t_{end}} \dot{Q}(t) \right) \cdot \Delta t \qquad (4.2)$$

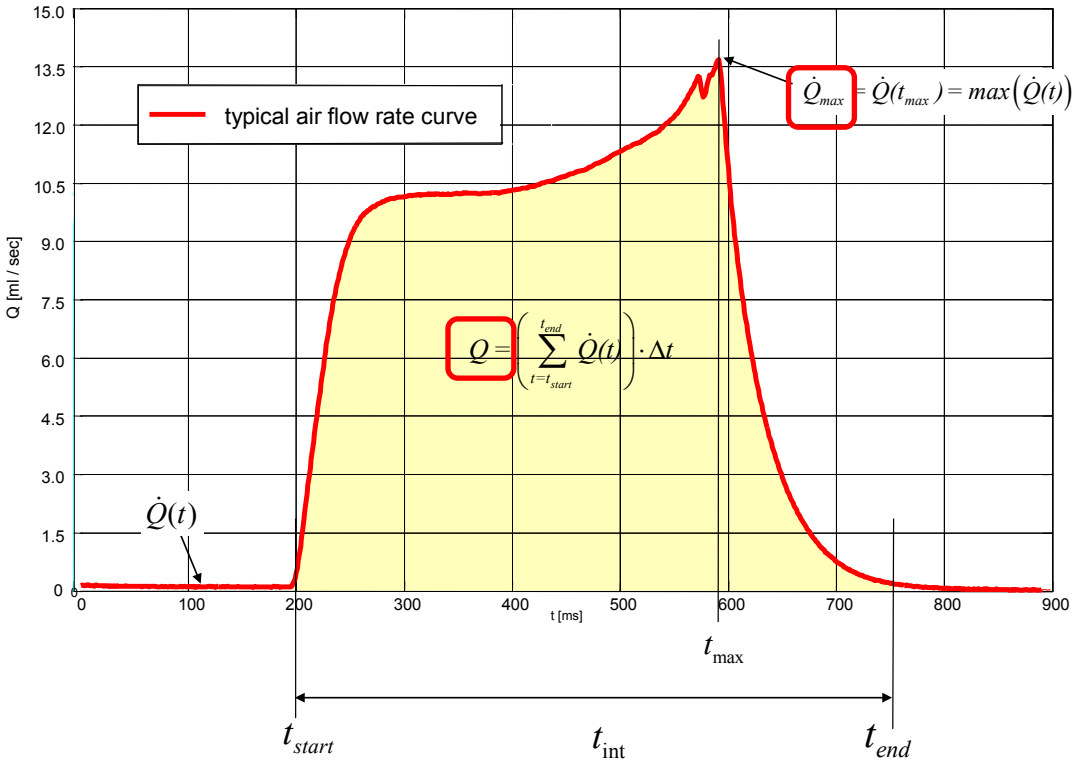

Figure 4-6 Typical for the air flow measurement during the µ-IM cycle

4.2.5 Design of experiments

To investigate the effects of the µ-IM process on part replication this experimental research was focused on $\dot{Q}$ of E_a, and the part flow length. The replication performance of micro cavities is highly dependent on the *P* and *T* control during injection, and therefore the effects of T_b, T_m, and V_i have been investigated in this study. Additionally, the resistance to air evacuation (E_a^R) from the cavity is an important aspect that can affect the process performance, and therefore an O-ring was incorporated into the tool design. As four factors at two levels were considered, a Taguchi L16 orthogonal array (OA) was selected as shown in Table 4-2.

The melt temperature was controlled through T_b and was within the recommended processing window of the material manufacturer. Two levels, maximum and minimum temperatures, were used for the polymer. In μ-IM the polymer solidification time is much shorter than that in conventional moulding and therefore it is necessary to heat the cavities. In this way, T_m can be raised to keep *T* of the polymer bulk sufficiently high and thus to facilitate melt flow during the filling stage. The T_m settings used in this research were the two extremes, the minimum and the maximum values, within the recommended range for the material.

V_i has two main effects. It can help polymers to fill the cavities before the melt flow solidifies but it can also increase the shear rate of the polymer which results in shear heating. The two levels of V_i selected in this research were chosen by taking into account the capabilities of the Battenfeld Microsystem 50, for which the maximum injection speed is 946.4 mm/s over a stroke distance of 84 mm. The two levels of E_a^R were investigated with the help of the O-ring, in particular, the low setting is a tool without the O-ring, and the high setting is the tool with it (high restriction of air evacuation through the split line / primary vent which results in a high E_a^R).

For each combination of controlled parameters for the selected L16 OAs, as presented in Table 4-3, ten runs were performed and in total 10 x 16 = 160 experimental trials were carried out. The response variables considered are $\dot{Q}_{max}$, *Q* and part flow length.

RUN	Factors			
	T_b	T_m	E_a^R	V_i
1	1	1	1	1
2	1	1	1	2
3	1	1	2	1
4	1	1	2	2
5	1	2	1	1
6	1	2	1	2
7	1	2	2	1
8	1	2	2	2
9	2	1	1	1
10	2	1	1	2
11	2	1	2	1
12	2	1	2	2
13	2	2	1	1
14	2	2	1	2
15	2	2	2	1
$16 = 2^4$	2	2	2	2

Table 4-2 Taguchi L16 Orthogonal Array Design for airflow DOE study

RUN	Factors			
	T_b	T_m	E_a^R	V_i
	[°C]	[°C]	-	[mm/s]
1	210	30	Off	200
2	210	30	Off	800
3	210	30	On	200
4	210	30	On	800
5	210	90	Off	200
6	210	90	Off	800
7	210	90	On	200
8	210	90	On	800
9	270	30	Off	200
10	270	30	Off	800
11	270	30	On	200
12	270	30	On	800
13	270	90	Off	200
14	270	90	Off	800
15	270	90	On	200
$16 = 2^4$	270	90	On	800

Table 4-3 L16 Taguchi Orthogonal Array for process parameter variation during the DOE airflow investigation

4.3 Analysis of the results

4.3.1 Average $\dot{Q}_{max}$, Q and Flow length

In this study, a L16 OA was employed to ensure that the experimental results were representative of the considered processing windows for the selected material. For each trial, the effects of the selected combinations of process parameters/factors on $\dot{Q}_{max}$, Q and flow length were investigated and then, based on the 160 trials conducted, the mean values were calculated for each of the sixteen different processing conditions.

The quantitative $\dot{Q}_{max}$ data obtained through the experiments identified that the highest recorded $\dot{Q}_{max}$ was 40.5 ml/s, and the lowest 13.8 ml/s. The normal distribution of the recorded $\dot{Q}_{max}$ shows some variation of the experimental results. In particular, Figure 4-7 depicts that the average $\dot{Q}_{max}$ is 26.23 ml/s while the standard deviation (σ) was 11.12 ml/s. This result indicates that the process factors have a significant influence on $\dot{Q}_{max}$.

For the conducted trials the highest recorded Q was 5.2 ml, while the lowest was 3.6 ml. Figure 4-7 shows a wide variation of the results; the average Q is 4.4 ml with σ = 0.61 ml. These results suggest again that the process factors have a significant influence on Q.

Regarding the flow length measurements, it was observed that they varied, too. The deviations in length for each combination of controlled parameters for each of the 16 experimental settings are given in Figure 4-8 . The flow front is characterised by eight

individual streams resulting from the polymer flow splitting into the micro channels of the test part design. In order to determine the influence of the process factors on the part dimensions, the highest and lowest flow stream lengths were considered and measured for each part. The flow length measurements identify that the highest flow length stream was 18.99 mm, while the lowest was 7.66 mm. Figure 4-7 shows that the mean values of high and low flow lengths are 13.27 and 11.7 mm respectively, while σ is 2.6 mm for both. As it was the case with Q, these results show that the process factors also have a significant influence on flow length, and that the variation in flow length for each part (experimental run) has a similar overall distribution. Figure 4-9 shows the overall variation of the flow front for two experiments.

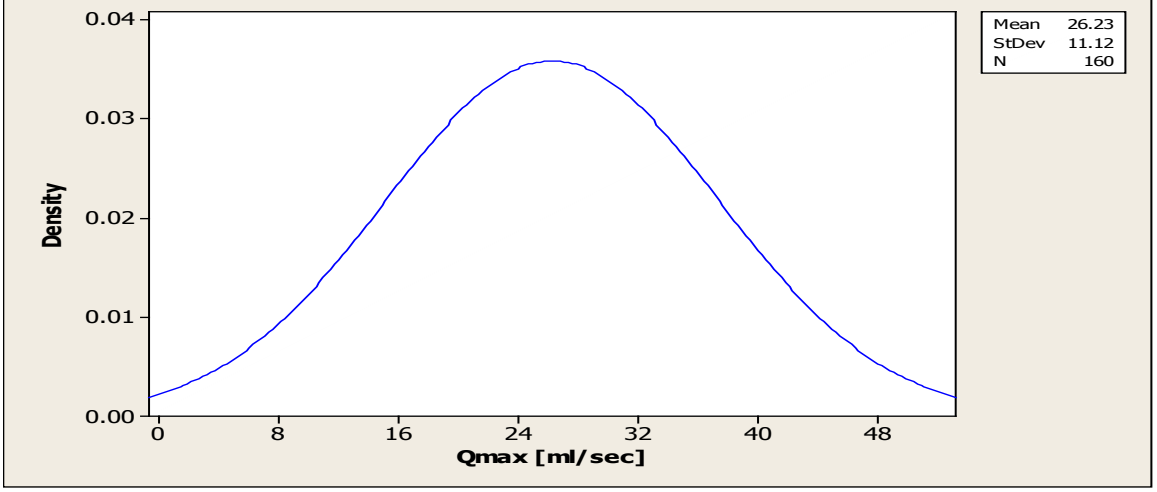

Diagram of $\dot{Q}_{max}$ results

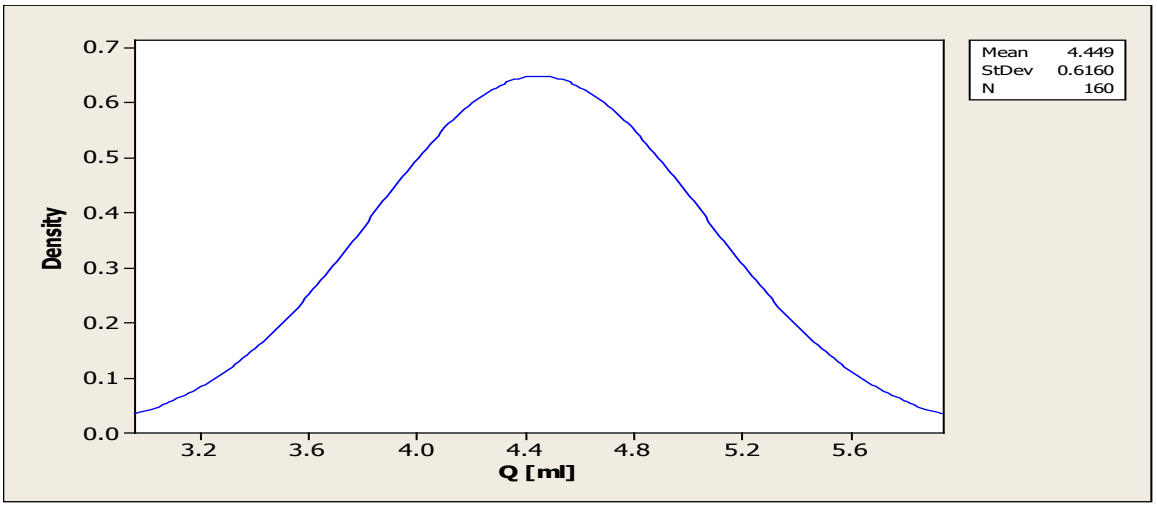

Diagram of *Q* results

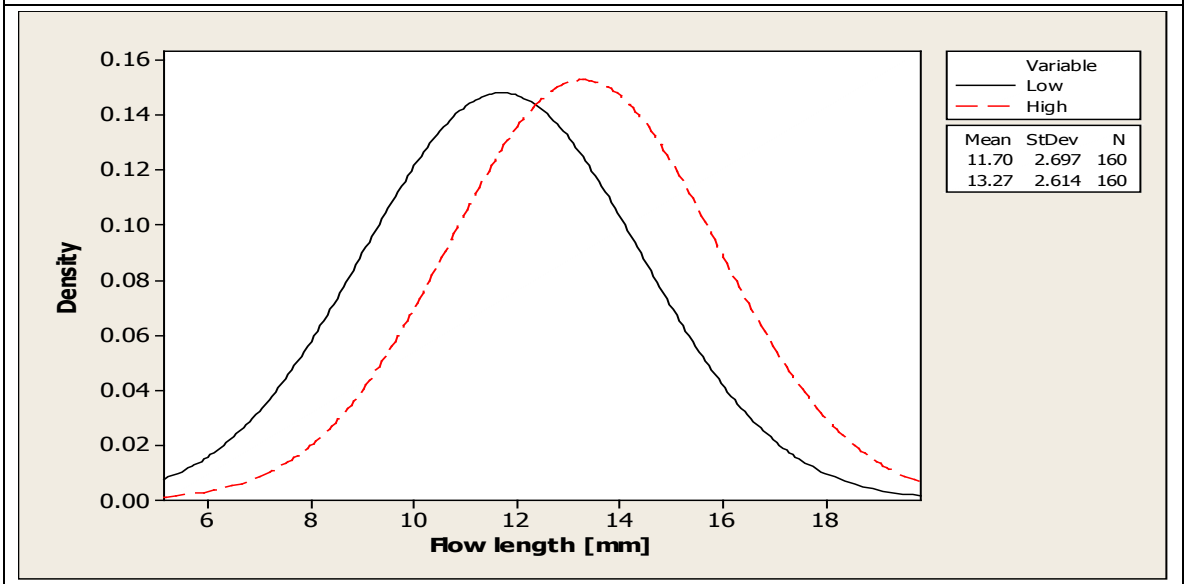

Diagram of Flow length results

Figure 4-7 Diagram of $\dot{Q}_{max}$, Q and Flow length results

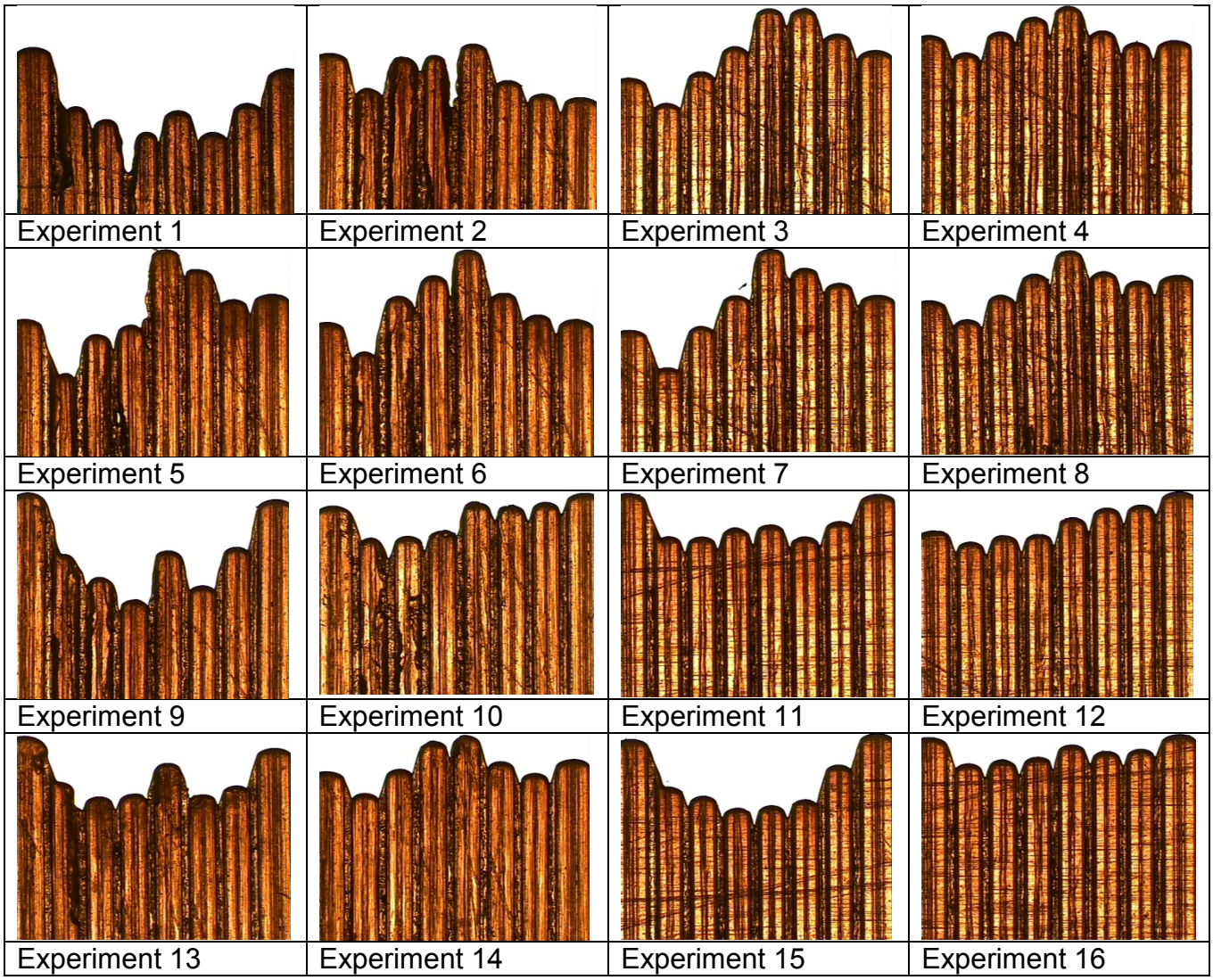

Figure 4-8 Variation in the part flow length

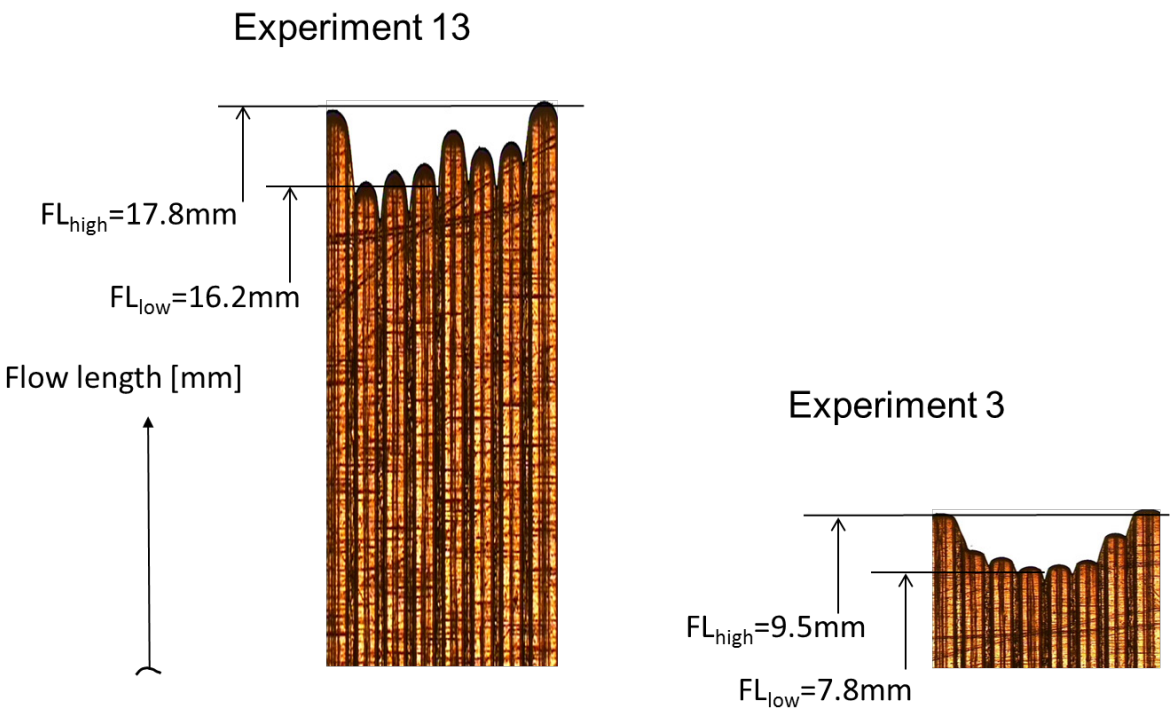

Figure 4-9 Variation in the flow front length for experiment number 13 and 3

4.3.2 Interval plots of $\dot{Q}_{max}$, Q and flow length

In this study, an L16 OA was employed, and for each combination of controlled parameters ten runs were carried out and thus ten measurements of $\dot{Q}_{max}$, Q and flow length were obtained. The mean value plots including confidence intervals are provided in Figure 4-10.

The interval plots for $\dot{Q}_{max}$ identified that there is a difference, in particular for experiments 1 to 16, where there is a significant variation between each consecutive experiment (Figure 4-10). These differences can be explained by the variations in V_i, with a low V_i resulting in a low $\dot{Q}_{max}$ while a high V_i leads to a high $\dot{Q}_{max}$. The confidence intervals are consistent for all experiments.

The interval plots for Q in Figure 4-10 show that the variations in the experimental results are almost identical to those for $\dot{Q}_{max}$. In particular, the variations for experiments 1 to 16 are similar. Also, these variations can be explained with different settings for V_i. However, there are some differences, in particular low V_i results in high Q while low V_i leads to low Q. Again, the confidence intervals are consistent for all experiments.

Finally, the analysis of the interval plots for the flow length data presented in Figure 4-10 shows again variations in the obtained results. In particular, for both high and low flow length measurements E_a^R was the most influential factor, with the high level of E_a^R resulting in a lower overall flow length. Generally, high V_i led to a further reduction of the flow length. In addition, the confidence intervals for the flow length results show a wider variance than those for the mean $\dot{Q}_{max}$ and Q results.

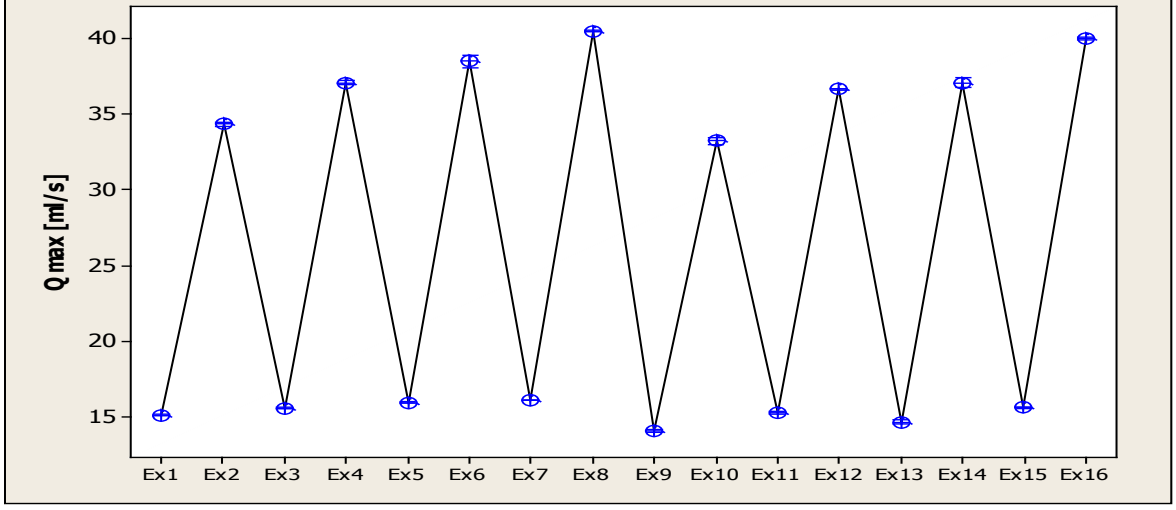

Interval plot of $\dot{Q}_{max}$ results

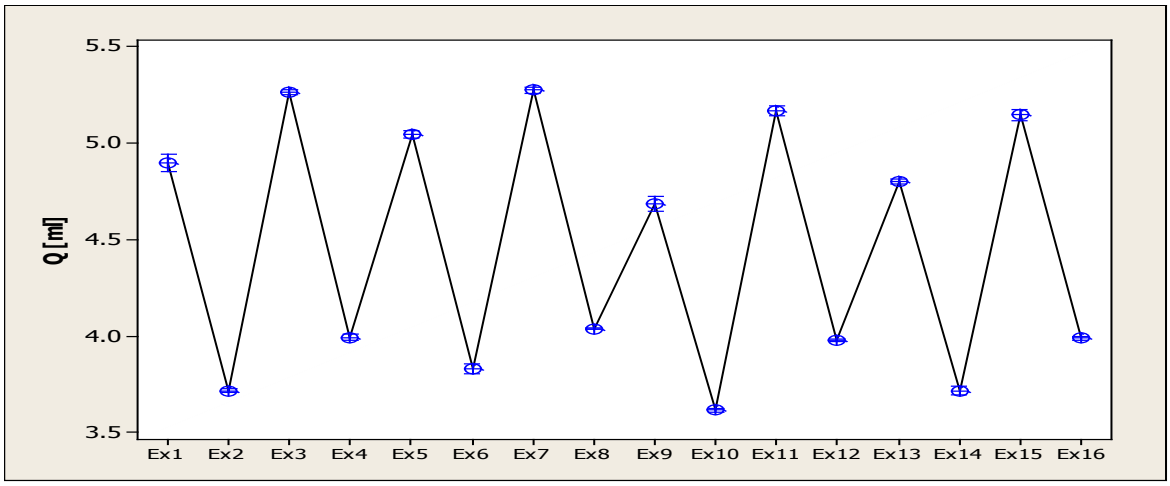

Interval plot of Q results

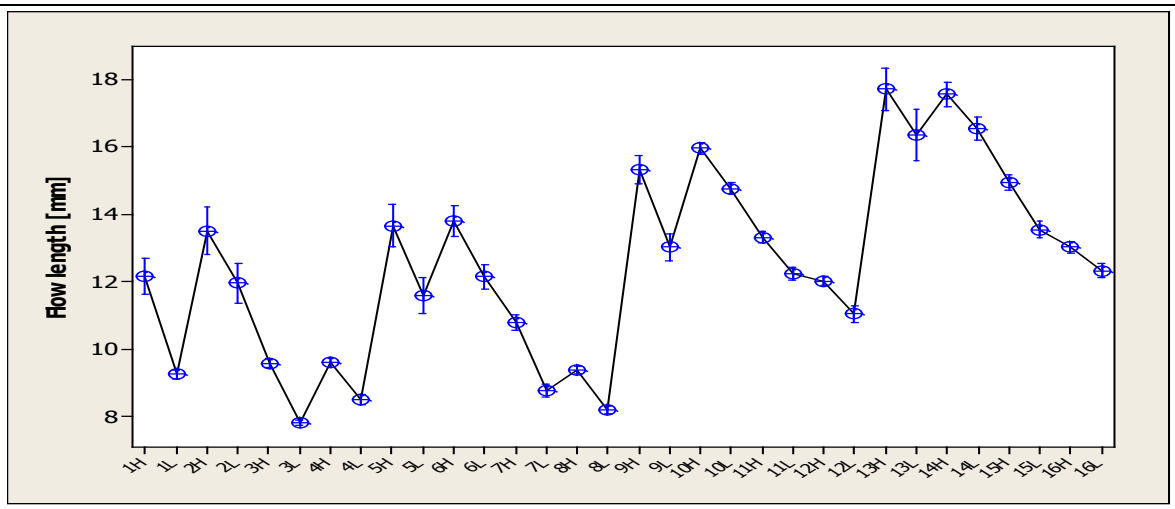

Interval plot of flow length results

Figure 4-10 Interval plot of $\dot{Q}_{max}$, Q and flow length process parameters' effects on $\dot{Q}_{max}$, Q and flow length

Based on the experimental results, an analysis of variance (ANOVA) was performed in order to assess the contribution of each processing parameter to the resulting flow length, $\dot{Q}_{max}$ and Q. Table 4-4, Figure 4-11 and Figure 4-12 show the response of each parameter and the plots of main effects, respectively.

From the $\dot{Q}_{max}$ analysis it is immediately apparent that V_i has a strong influence on the process, and the parameter levels of T_b, T_m and E_a^R cannot be considered as having an overall influence on the process. The results in Table 4-4 show that V_i is ranked as the most important factor, in particular an increase of V_i led to an increase of $\dot{Q}_{max}$ by 143.2%. This indicates that the increase of V_i and the consequent increase in the speed of the melt flow entering the cavity contributed to an increase in the rate of E_a and hence an increase of $\dot{Q}$ through the MEMS flow sensor.

Looking at the Q results, it is immediately apparent that V_i can be considered as having the highest influence on the process. The results show that V_i is ranked first among the controlled factors, in particular an increase of V_i led to a decrease of Q by 23.2%. E_a^R is ranked the second as the O-ring sealing resulted in an increase of Q by 7.2%. Regarding the temperature factors, the levels set have no statistical importance on Q (Table 4-4). Due to the enclosed volume of air in the cavity, singling out V_i as the main factor affecting E_a is an important observation. In particular, the low level of $\dot{Q}_{max}$ when increasing V_i shows that less air was going through the MEMS flow sensor. This suggests that more air was evacuated through the primary split line vent. This is confirmed by the increase of Q when the cavity is sealed with the O-ring (E_a^R) as shown in Figure 4-11.

The part flow length for all experiments is characterised by an uneven flow front and in this research the highest and lowest flow length measurements are considered for each part. It was observed that the influence of the selected parameter levels was similar for both high and low measurements, as can be seen in Figure 10. Also, the results show that an increase of T_B and T_m has led to an increase of the flow length, while for E_a^R the opposite has been observed. Considering the significance of different controlled factors, V_i was ranked as having the lowest statistical importance, while T_b was identified as the factor with the highest influence (Table 4-4). E_a^R being ranked second is of a particular interest because this parameter is not directly linked to the polymer viscosity, and thus flow mobility. The sealing of the cavity with the O-ring resulted in a decrease of the flow length by 22%, which indicates that by restricting the venting through the primary split line the resident air prevents the polymer from filling the cavity. Such a conclusion is supported by the identified relationship between V_i and E_a. V_i is ranked the most important factor for $\dot{Q}_{max}$ and Q and as the least important one for flow length. This illustrates that regardless of the speed of the polymer entering the cavity the displaced air will evacuate through either the primary or secondary vents, or both. However, if E_a is restricted, the resident air can reduce the polymer flow length as demonstrated by E_a^R in the conducted experiments.

The ANOVA analysis of the variation in flow length shows that V_i has the greatest statistical importance while T_m the least as shown in Table 4-4. Additionally, by analysing the main effects' plot for flow length variations in Figure 4-12 it can be seen that in all cases the high level settings of all controlled factors resulted in a reduction of the flow length variations. However, different influences depending on the considered factors can be observed.

As far as µ-IM process factors are concerned, T_b, T_m and V_i, high parameter settings not only prevent an early solidification of the melt flow, i.e. promote high flow length, but also improve the evenness of the flow front (lower flow front variation). In particular, mould temperature has the least statistical significance, especially if compared with the other factors. With respect to air evacuation, the presence of the O-ring, i.e. resistance to air evacuation hampers the optimal filling and decreases flow length, but also improves filling stability, i.e. decreases flow length variation. This effect suggests that venting by using the split line of the mould leads to varying results and thus a less repeatable process. Therefore, such a venting is not suitable for the precision moulding of polymer micro components. Hence, secondary air vents coupled with vacuum technology are recommended design features to improve process performance and product quality in µ-IM.

$\dot{Q}_{max}$				
Factors	T_b	T_m	$E_a{}^R$	V_i
	[°C]	[°C]	-	[mm/s]
Level 1	26.64	25.16	25.36	15.28
Level 2	25.81	27.29	27.09	37.17
Delta	0.83	2.13	1.73	21.89
Rank	4	2	3	1
Q				
Level 1	4.50	4.41	4.29	5.03
Level 2	4.38	4.48	4.60	3.86
Delta	0.12	0.06	0.31	1.17
Rank	3	4	2	1
Flow length (low)				
Level 1	9.77	11.07	13.20	11.57
Level 2	13.73	12.43	10.29	11.92
Delta	3.96	1.35	2.90	0.35
Rank	1	3	2	4
Flow length (high)				
Level 1	11.56	12.68	14.97	13.44
Level 2	14.98	13.86	11.58	13.11
Delta	3.42	1.18	3.39	0.33
Rank	1	3	2	4
Flow length variation				
Level 1	1.85	1.63	1.86	1.90
Level 2	1.29	1.51	1.28	1.24
Delta	0.56	0.12	0.58	0.66
Rank	3	4	2	1

Table 4-4 Response table for means for the flow length variation

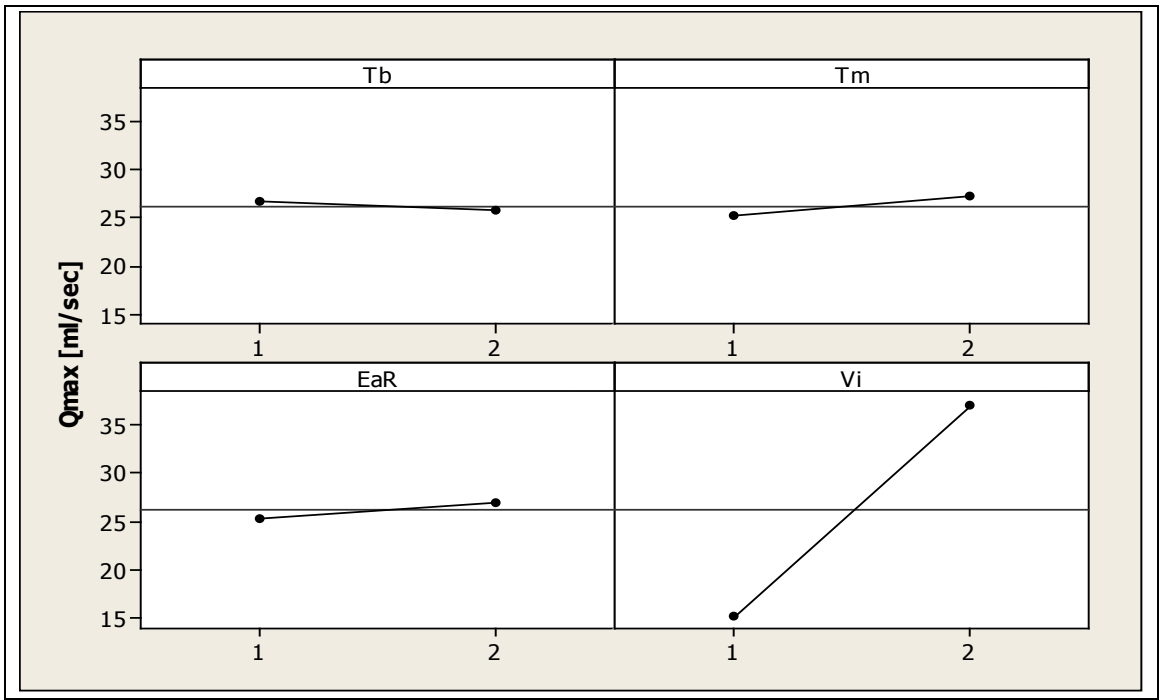

Main effects' plot of $\dot{Q}_{max}$

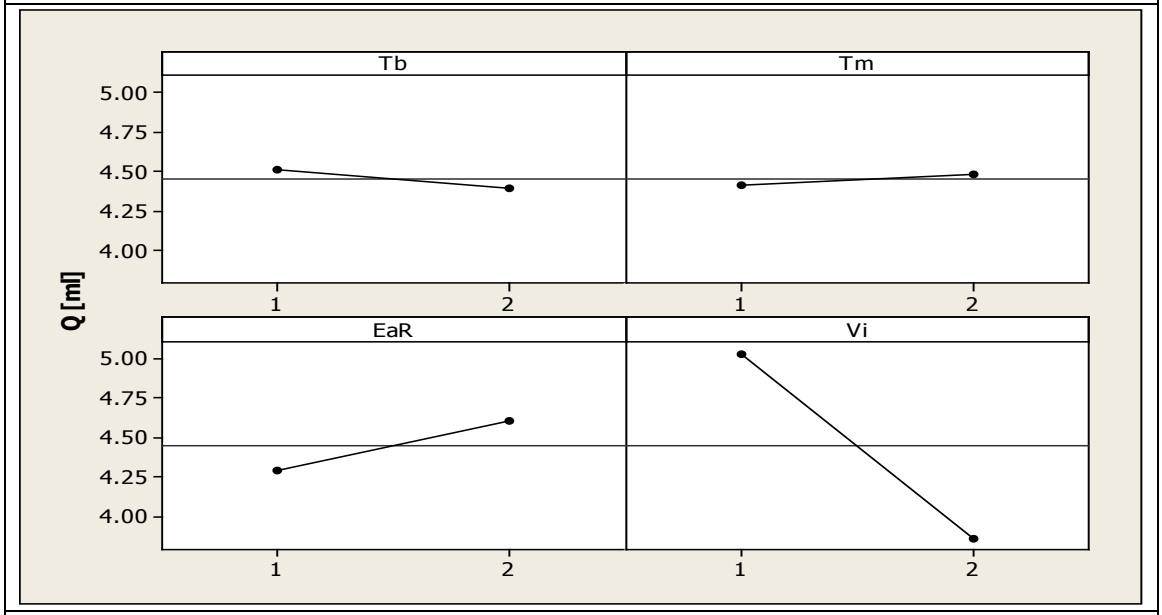

Main effects' plot of Q

Figure 4-11 Main effects' plots of $\dot{Q}_{max}$ and Q

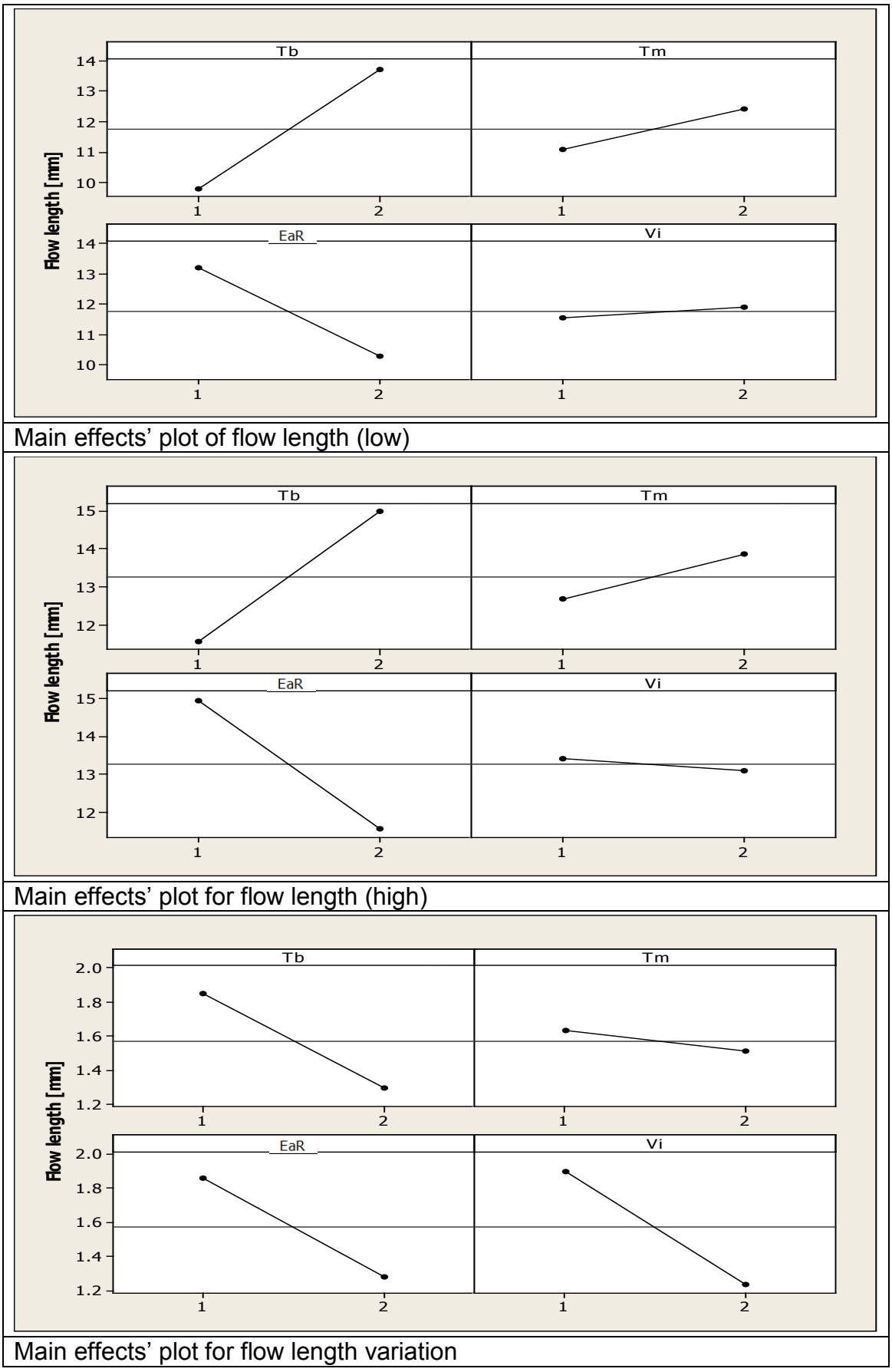

Main effects' plot of flow length (low)

Main effects' plot for flow length (high)

Main effects' plot for flow length variation

Figure 4-12 Main effects' plots for the flow length

4.4 Conclusion

This chapter reports an experimental study on the effects of air evacuation conditions in micro cavities when replicating polymer parts. To analyse the air flow state during the filling stage, a condition monitoring system was designed and integrated into the mould cavity. Then, by employing a design of experiment approach, the moulding performance was investigated, especially the effects of four process factors, T_b, T_m, E_a^R and V_i, on flow lengths of micro features and air flow rates. The main conclusions made based on the obtained results are:

- It is possible to assess air evacuation (E_a) conditions during part filling by employing a specially designed condition monitoring setup. It was shown that maximum air flow ($\dot{Q}_{max}$), and air flow over time (Q) were dependent on the processing conditions.

- The data recorded for $\dot{Q}_{max}$ and Q shows a normal distribution of the experimental results. This indicates that the considered process factors have a significant influence on $\dot{Q}_{max}$ and Q. Regarding the flow length results it was observed that the part length was not uniform. In particular, the average of high and low flow lengths shows that the process factors have a significant effect on the flow length, and that the variations in the flow length for all parts have a similar distribution.

- The interval plots of the recorded $\dot{Q}_{max}$ and Q data have shown that low V_i results in low $\dot{Q}_{max}$ and high Q. The interval plots of the flow length data has identified that an increased resistance to air evacuation (E_a^R) results in a lower overall flow length.

- The parameters' effects on E_a suggest that in context to $\dot{Q}_{max}$ and Q, V_i can be considered as the most influential parameter. In particular, an increase of V_i led to an increase of $\dot{Q}_{max}$. This suggests that the increase in the speed of the polymer entering the cavity contributes to an increase in the rate of E_a. However, an increase of V_i led to a decrease of Q. This suggests that an increase of V_i results in an increased amount of E_a through the split line and not the secondary vent.

- The ANOVA analysis of the part flow length results show that an increase of T_b and T_m leads to an increase of the flow length, while for E_a^R the opposite is observed. The increase of E_a^R results in a decrease in the flow length. This indicates that a restricted venting through the primary split line results in un-evacuated resident air, which prevents the polymer from filling the cavity. This conclusion is supported by the identified dependences between V_i and $\dot{Q}_{max}$ and Q.

- The analysis of the flow length variations shows that V_i has the greatest statistical importance while T_m the least. Also, based on this analysis it can be concluded that in all cases the high level settings of all controlled factors resulted in a reduction of the flow length variations. In addition, the high settings of T and V_i can prevent an early solidification of the melt flow and thus improve the evenness of the flow front.

By understanding the effects of V_i and E_a^R on $\dot{Q}_{max}$, Q, and the part flow length and its variations it will be possible to improve the performance of the µ-IM process. The study showed clearly that the high process settings that are required in µ-IM, together with the limited venting through the primary split line, due to the high accuracy and surface quality of mould tools used, has a significant impact on the filling performance. In the extreme this inability to vent the resident air could lead to air traps, air compression

and diesel effects, and ultimately part and mould failures. Thus, to improve the μ-IM process performance it is necessary to incorporate in micro mould tools secondary vents and vacuum methods for E_a^R.

5 INFLUENCE OF INJECTION AND CAVITY PRESSURE ON THE DEMOULDING FORCE IN MICRO INJECTION MOULDING

5.1 Motivation

In this chapter an experimental study is reported that investigates part demoulding behaviour in µ-IM with a focus on the effects of pressure and temperature on the demoulding forces. Especially, to investigate the demoulding behaviour of polymer micro parts and identify important process parameter a DOE study was conducted. The demoulding characteristics of a representative microfluidics part was studied as a function of four process parameters, melt temperature (T_b), mould temperature (T_m), holding pressure (P_h) and injection speed (V_i). In addition, the results obtained using different combinations of process parameters were analysed to identify the best processing conditions in regards to the demoulding behaviour of micro parts.

5.2 Experimental setup

5.2.1 Part design and tool manufacture

The part design chosen for this study is a micro fluidics platform used in disposable smart diagnostic chips (Figure 5-1). The test design which was chosen for the experiments comprises a typical microfluidic channel system for biosensors for the detection of diseases. The overall dimensions of the polymer chip are 10 mm in diameter and thickness of 1 mm. The chip functional structure includes features

commonly found in micro fluidic components such as reservoirs and channels. The main channels are 50 µm wide and 80 µm deep as shown in Figure 5-3. The insert for the µ-IM tool as depicted in Figure 5-2 was manufactured in steel and produced using conventional turning except for the cavity face that was machined by micro milling. To eject the part a hole is drilled and reamed at the centre of the insert. The bore accommodates a single 2 mm pin positioned at the centre of the part. A draft angle of 1 degree was applied to each of the features. The insert was assembled to a primary mould tool and then inspected for parallelism and shut off of the mating faces.

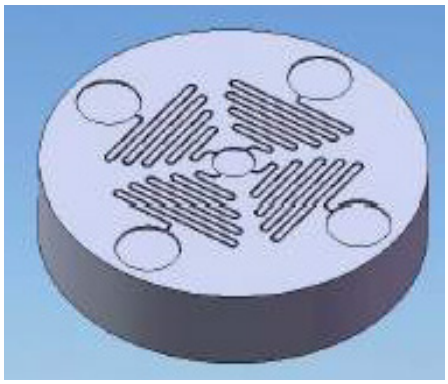

Figure 5-1 Microfluidic part with channels 50 µm in width and 80 µm deep

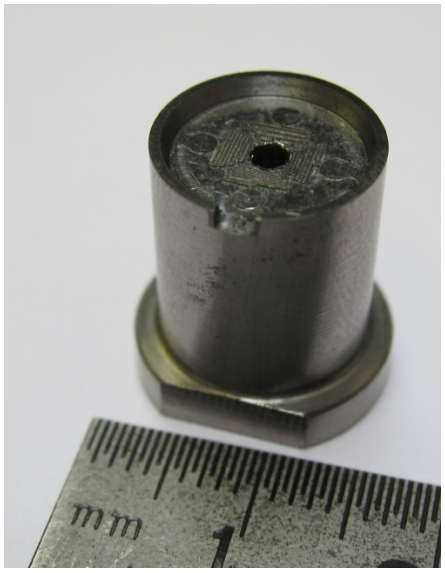

Figure 5-2 Steel mould insert incorporating test structures for microfluidic part and central bore hole for 2 mm ejector pin

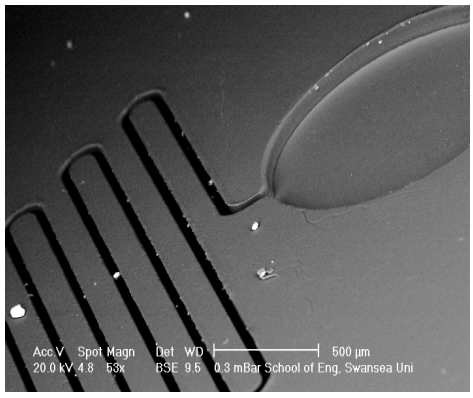

Figure 5-3 SEM image of microfluidic polymer test part with micro channel features

5.2.2 Test material

The material used in this research is Topas COC 5013. Topas® is the trade name for Topas Advanced Polymers' cyclic olefin copolymers (COC). COC resins are suitable for the production of transparent mouldings with applications in optical data storage and optics, e.g. lenses, sensors and other industrial products. The special performance characteristics of this material are: low density, birefringence and water absorption, high transparency, rigidity, strength and hardness. Also, due to its good bio and blood compatibility, COC finds applications in pharmaceutical packaging, medical devices and diagnostic disposable systems. In particular, the 5013 grade is characterised by high flowability and excellent optical properties and is recommended for optical lenses and storage media, applications where low birefringence and high moulding accuracy are essential. In the context of this research COC was chosen as the test material, because it is a commonly used material for microfluidic applications (Blanco 2004; Blattert et al. 2005; Chen et al. 2010; Jena et al. 2011). The machine used to perform the micro injection moulding tests was a Battenfeld Microsystem 50.

5.2.3 Pressure and force measurements

In this study, variations in injection pressure (P^i), cavity pressure (P^c) and demoulding force (F^e) during the µ-IM process were assessed. P^i was measured indirectly using a Dynisco PCI 4011 piezoelectric force transducer behind the injection pin and P^c was measured using a Kistler 9211B sensor positioned behind the ejector pin as shown in Figure 5-4**.** The Kistler miniature force sensor measures F^e by means of the ejector pin and allows the actual mould P^c to be calculated. To carry out these measurements, the tool was modified to accommodate the measuring ejector pin at the centre of the

microfluidic insert. Behind the pin the transducer was positioned on the ejector plate sub assembly as presented in Figure 5-4. When the ejector assembly moves forward the part is removed from the cavity and the transducer is subjected to a mechanical load that generates an electric potential. For both sensors the electric charge is then converted using an ICAM Type 5073A Industrial Charge Amplifier. The amplifier is used to set the sensitivity and range of the sensor, and then converts the piezoelectric charge signal from the sensors into an output voltage proportional to the mechanical input force. The output signals are monitored with a National Instruments NI 9205 16-bit module. The measurement and output ranges of the charge amplifier are 0 to 10,000 pC and 0 to 10 V, respectively. With the injection and ejector pins acting on the transducer, the resulting P and F^e from the measured output voltages can be calculated. The sensor output signals are then downloaded into a computer using a National Instruments cDAQ-9172 USB data acquisition unit and the measured values were accessed through the National Instruments Labview 8 software.

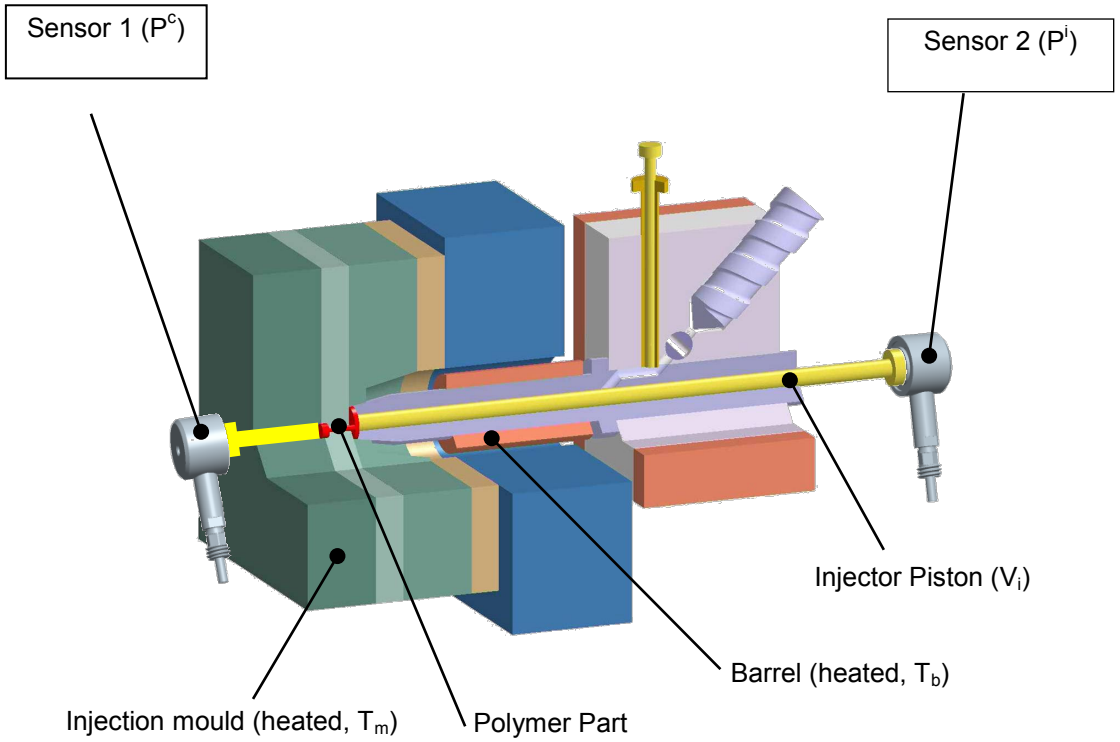

Figure 5-4 Cavity (P^c) and injection (P^i) pressure measurement positions

The IM cycle can be split into three consecutive stages: filling, packing, and cooling. During the polymer filling stage the cavity pressure rises during the volumetric filling of the cavity. At the second stage P continues to rise rapidly until it reaches the packing pressure level which is then maintained during the packing stage. This process continues until the gate is frozen. Finally, the cooling stage covers the time until the end of cycle. Condition monitoring in µ-IM can be utilised to quantify the process factors' influence on P^c and P^i. P varies over time (t), and by integrating a piezoelectric force transducer behind the injection piston it is possible to record P^i curves over time (Collins 1999). Using such curves, it is possible to identify the following conditions as depicted in Figure 5-5:

- The start of the injection cycle.

- Volumetric filling of the cavity.
- The second stage compression pressure and P_{max}.
- A reduction in P due to polymer solidification and gate sealing.
- An eventual drop to atmospheric pressure, due to the tool opening and part removal from the cavity.

In this research a second pressure transducer was integrated behind the ejector pin and a cavity pressure curve P^c was indirectly measured during each injection moulding cycle.

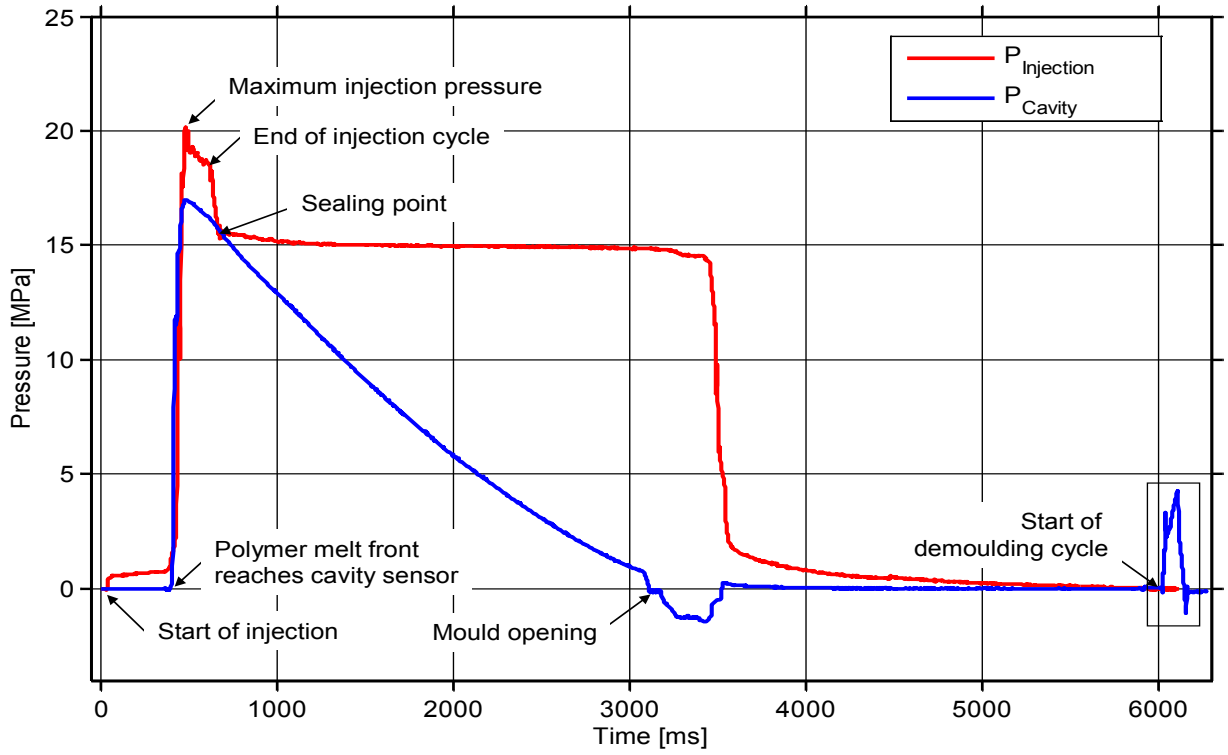

Figure 5-5 μ-IM injection and cavity pressure curves

The investigation reported in this research focuses on the filling stage and the demoulding stage of the μ-IM process as shown in Figure 5-5 and Figure 5-6. Due to the large amount of condition monitoring data that can be recorded it is often necessary to reduce it by employing pre-processing techniques. In this way it is easier to construct the profiles for further analysis. In particular, the software Matlab™ was utilised in this research to calculate key values, while a t series function provides the key variables as outlined below to determine the P conditions.

P^{i}_{max} and P^{c}_{max} are measured to obtain the peak P value that the tool can experience. This is the maximum value that the cavity P reaches.

$$P^{c}{}_{max} = P^{c}(t_{max}) = max\left(P^{c}(t)\right) \tag{5.1}$$

Accordingly P^i was calculated

$$P^i{}_{max} = P^i(t_{max}) = max\left(P^i(t)\right) \tag{5.2}$$

The pressure work (P^i_{work} and P^c_{work}) is determined by P over t during the filling stage. It is represented by the area defined by the integral value of the interval that begins with P at the start of the filling stage (P_{start}) and ends with the "zero" P at the beginning of the mould opening. Due to the fact, that the P curve is defined with discrete values, corresponding to the selected sampling rate of the data acquisition system, P_{work} is the sum starting with P at the start time (t_{start}) and ending with P at the time of the opening of the mould ($t_{mould\_opening}$), multiplied by the time step of Δt. The time step Δt was chosen to be 0.001 sec representing the sampling rate of the data acquisition system. Thus, the P^i_{work} value was calculated employing the following equation:

$$P^i{}_{work} = \left(\sum_{t=t_{start}}^{t_{mould\_opening}} P^i(t) \right) \cdot \Delta t \tag{5.3}$$

Respectively, the same is done for the P^c_{work} :

$$P^c{}_{work} = \left(\sum_{t=t_{start}}^{t_{mould\_opening}} P^c(t) \right) \cdot \Delta t \tag{5.4}$$

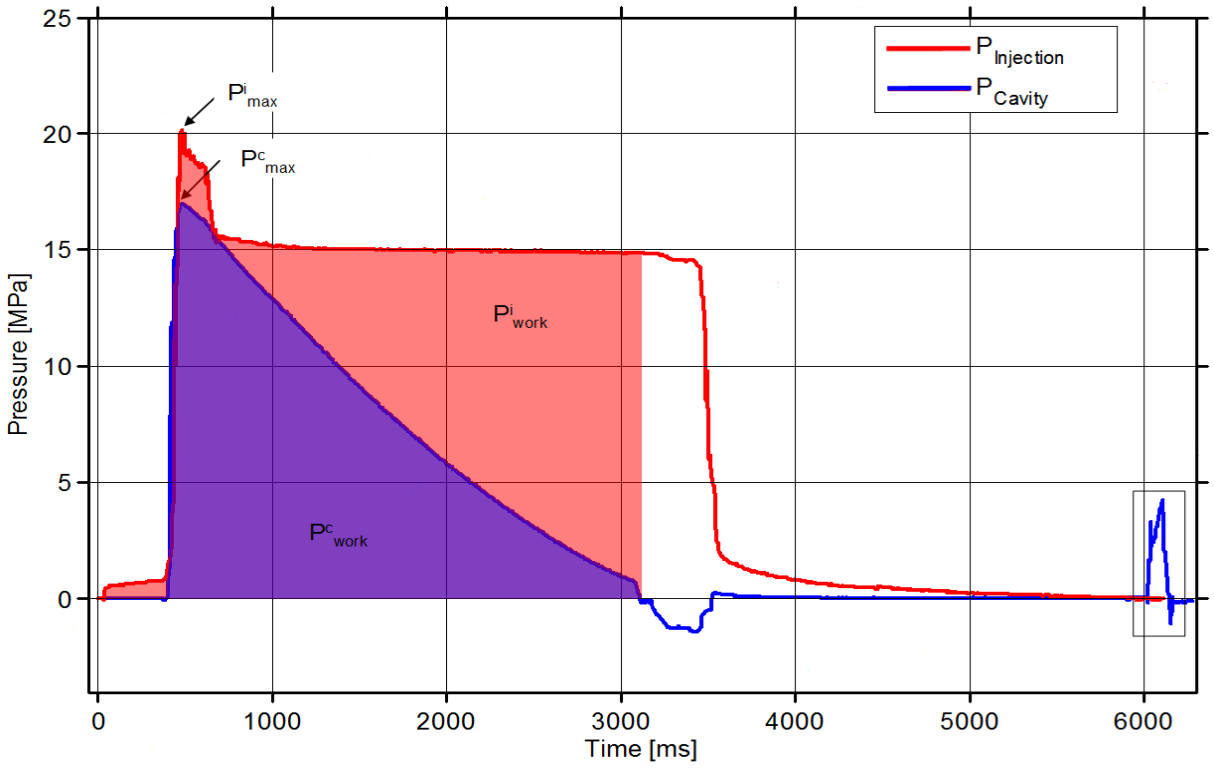

Figure 5-6 Characteristic numbers for the pressure curves

5.2.5 F^e curves

The focus of this chapter is on the demoulding forces in µ-IM. To acquire the necessary information about F^e, a P sensor positioned behind the ejector pin was utilised to measure the demoulding force. In particular, the P data obtained during the demoulding stage (see Figure 5-5), is used to calculate F^e as follows:

$$F^e(t) = P^c(t) \cdot \frac{4}{d^2 \pi} \qquad (5.5)$$

Where $d = 2mm$ is the diameter of the injection pin in the centre. The result is shown in Figure 5-7. In this investigation the focus is on the maximum ejection force (F^e_{max}) that parts can experience, which is calculated as follows:

$$F^e{}_{max} = F^e(t^e{}_{max}) = max\left(F^e(t)\right) \tag{5.6}$$

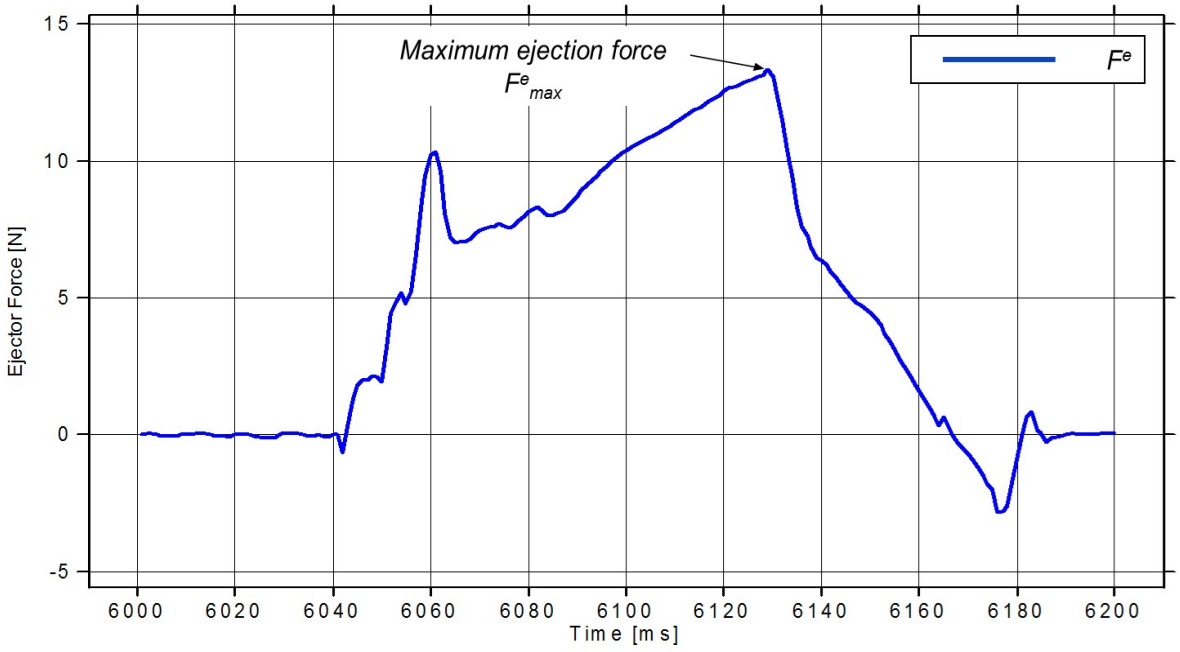

Figure 5-7 Typical curve for the ejector force over time

5.2.6 Design of experiments

The Taguchi DOE method was used to plan experiments with the objective of acquiring data in a controlled way, obtaining information about the behaviour of the µ-IM process and identifying the significant factors affecting the process. Especially, by using the DOE signal-to-noise ratio (S/N), which is the ratio between the strength of a signal and the strength of the associated noise, it is possible to identify the process parameters that reduce variability by minimizing the effects of uncontrollable noise factors (Park et al. 2005). In this research the nominal is the best quality characteristic S/N ratio that is used to identify those control factors that reduce variability and is defined as:

$$S/N = 10 \cdot \log_{10}\left(\frac{\overline{y}^2}{s^2}\right) \tag{5.7}$$

where *y* is the signal and *s* is the noise.

To investigate how part demoulding affects process performance, this experimental research was focused on P^i, P^c and F^e during the μ-IM process. The filling performance of micro cavities relies heavily on the P and T control during injection, and therefore the effects of T_b, T_m, P_h and V_i were investigated. Given that four factors at two levels were considered for the selected material, a Taguchi L16 orthogonal array (OA) was selected (Table 5-1).

The melt temperature was controlled through T_b and was within a recommended maximum and minimum processing window for the COC polymer. In μ-IM the polymer solidification time is much shorter than that in conventional IM and therefore the processing requires heated tools. The T_m has to be raised to keep the bulk temperature of the polymer sufficiently high and thus to facilitate the melt flow during the filling stage. The T_m settings used in this research were the minimum and maximum temperature range for COC.

V_i has two main effects. It can help polymers to fill the cavities before the melt flow solidifies but also it can increase the shear rate of the polymer which results in shear heating. The two levels of V_i selected in this research were chosen by taking into account the capabilities of the Battenfeld Microsystem 50. Especially, the system is equipped with an injection piston (5 mm diameter), for which the maximum injection speed is 946.4 mm/s over a stroke distance of 84 mm. The two levels of P_h during which the P is maintained were controlled using the Microsystem 50 P_h on and off functions. The holding pressure time (t_h) was set at 10 seconds.

Using the L16 OA defined in this way a total of ten trials were performed for each combination of controlled parameters. Thus, a total of 160 experimental trials were carried out. The response variables considered were F^e_{max}, P^i_{max}, P^i_{work}, P^c_{max} and P^c_{work}.

RUN	Factors			
	COC			
	T_b [ºC]	T_m [ºC]	P_h	V_i [mm/s]
1	240	70	Off	200
2	240	70	Off	800
3	240	70	On	200
4	240	70	On	800
5	240	130	Off	200
6	240	130	Off	800
7	240	130	On	200
8	240	130	On	800
9	300	70	Off	200
10	300	70	Off	800
11	300	70	On	200
12	300	70	On	800
13	300	130	Off	200
14	300	130	Off	800
15	300	130	On	200
16	300	130	On	800

Table 5-1 Taguchi L16 Orthogonal Array Design for the process parameters which have been varied during the demoulding force DOE experimental study

5.3 Results

5.3.1 Average P and F^e

In this study, an L16 OA was employed to ensure that the experimental results were representative of the considered processing window. For each trial, the effects of the selected process factors on F^e and P were investigated and the mean values were

calculated. The mean value of F^e_{max} for the 160 trials was 21.5 N with σ=3.4 N while the highest and lowest F^e_{max} for all experiments were 26.3 N and 8.7 N, respectively. For P_{work} the two sensors have different results, the mean of P^c_{work} and P^i_{work} were 23036 MPa·ms (σ=10807) and 67742 MPa·ms (σ=29998), respectively. The two sensors measuring P_{max} also gave different results; the mean of P^c_{max} was 16.0 MPa (σ=2.2) while the mean of P^i_{max} was 20.6 MPa (σ=1.4). The normal distribution curves for P_{work} and P_{max} can be seen in Figure 5-8. The average P results for both P_{work} and P_{max} showed that P^i was higher than P^c. This shows that for monitoring P the position of the sensor is critical.

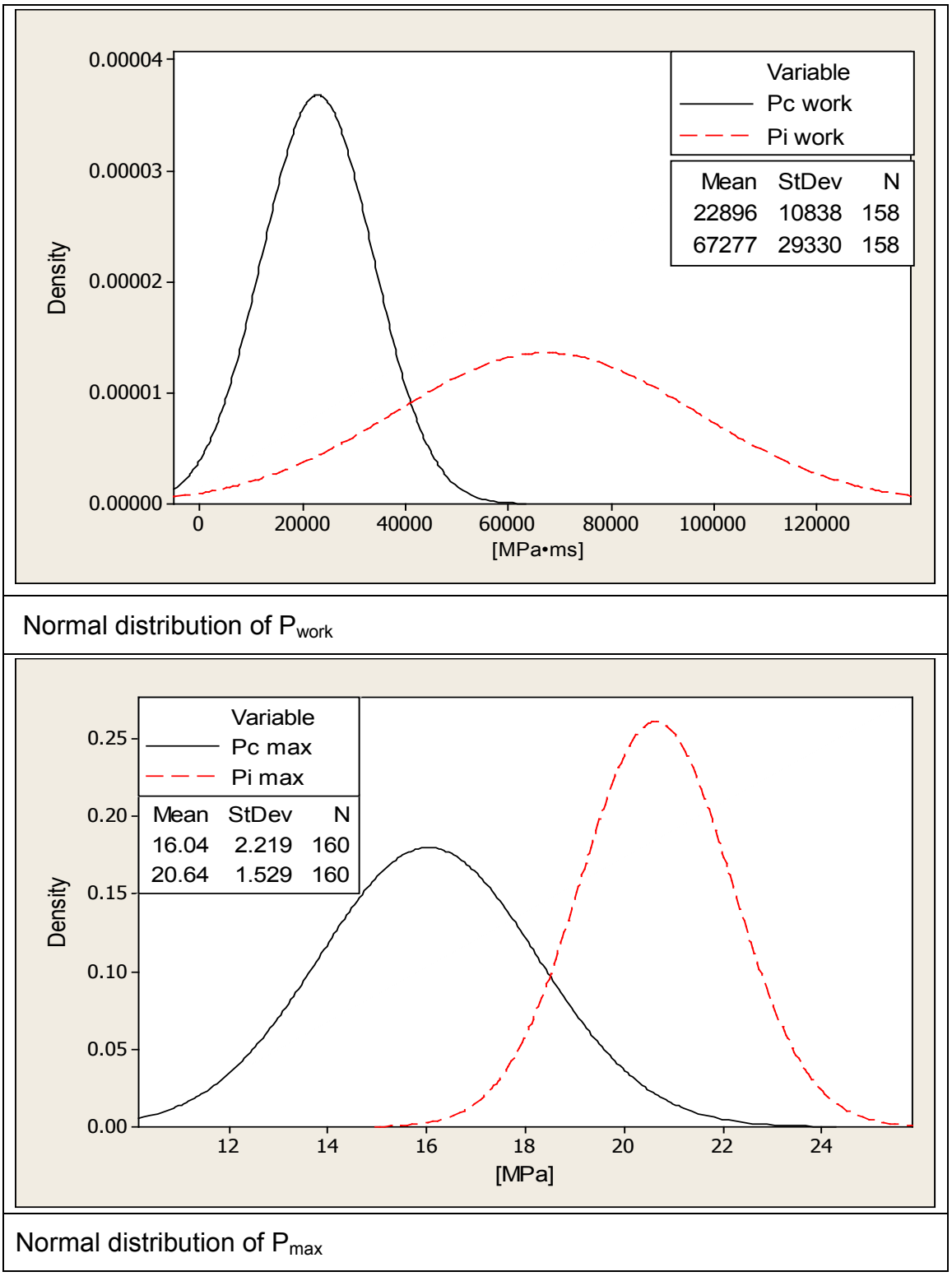

Figure 5-8 Normal distribution of P results

5.3.2 Interval plots for F^e, P_{max} and P_{work}

In this study, a L16 OA was employed, and for each combination of controlled parameters ten runs were carried out and thus ten measurements of F^e_{max}, P_{max}, P_{work} and moulded parts were obtained. The mean value plots for each experiment are provided in Figure 5-9 (P_{work} and P_{max} results), Figure 5-10 (P_{work} and F^e_{max} results) and Figure 5-11 (P_{max} and F^e_{max} results). The results show that the factors and their respective levels have a varying influence on the process. Two clear trends were identified based on the experiments carried out.

The two sensors monitoring P did not show the same readings during the carried out trials. It can easily be seen that the acquired data from these two sensors fall within different ranges; for both P_{work} and P_{max} the P^i sensor readings are higher than those for the cavity sensor in all cases (see Figure 5-9). The higher P could be due to polymer solidification at the gate and runner, which causes a build-up of P behind the injection pin. In contrast, P^c is not susceptible to any further filling pressure due to gate and runner freeze.

The interval plots for F^e_{max}, P_{max} and P_{work} identified that there is a difference in the results for experiments 1 to 16 (Figure 5-10 and Figure 5-11). Especially, there is a significant variation between some of the experiments. In particular, experiments 4, 8, 12 and 16 result in a higher reading. The variation in F^e_{max} can be explained with some changes in process conditions due to P_h and V_i, where their high settings result in a higher F^e_{max}. Additionally, a high V_i with high P_h leads to the four highest F^e_{max} measurements. Like F^e_{max} the P^i_{work} variations are also due to P_h and V_i, where the high settings result in the four highest P^i_{work} measurements (Figure 5-10). The high

results for P^{c}_{work} can also be explained with the variations in P_h and its interaction with V_i, where the high settings result in high P^{c}_{work}.

The main reason for the P^{i}_{max} variations can be associated with changes in process conditions due to P_h where the high settings result in high P^{i}_{max}. Additionally, a high V_i with high P_h leads to the four highest P_{work} measurements. While, for P^{c}_{max} the influence of P_h is less obvious. The variation is much smaller, which suggests that P_h observed during the injection stage is higher due to the freezing off at the gate, which leads to losses of P_h applied to the part in the runner system.

However, the high V_i and P_h (experiments 4,8,12, and 16) result in the highest peaks for both P_{max} and F^{e}_{max} as depicted in Figure 5-11. The histogram of P^{i}_{max} and F^{e}_{max} experimental results shows that there is an additional peak that does not follow the observed trend for F^{e}_{max}. This deviation is due to the increase of V_i to 800 [mm/s] without P_h. So this shows that for P^{i}_{max}, the sensor detects variations in V_i that do not affect the F^{e}_{max} measurements.

A stronger correlation between the P_{work} and F^{e}_{max} results can be observed, while between the P_{max} and F^{e}_{max} results it is relatively weak. This observation suggests that integral results are more representative of the actual dynamics of the process, i.e. the P_{work} results describe more accurately the state of the polymer during the injection, cavity filling and packing stages. However, these considerations are based on the qualitative comparison of the histograms presented in Figure 5-10 and Figure 5-11. Hence, further data analysis was carried out in order to rank the correlation between the different P related parameters with F^{e}_{max} by performing a quantitative analysis. Due to the different scales of the four P related parameters, P^{c}_{work}, P^{i}_{work}, P^{c}_{max} , P^{i}_{max} and F^{e}_{max}, they were normalised as follows:

$$Y_j = \frac{X_{i,j} - \frac{\sum_{i=1}^{160} X_{i,j}}{160}}{MAX(X_{1,j},...,X_{160,j}) - MIN(X_{1,j},...,X_{160,j})} \qquad (5.7)$$

where: Y_j is the normalised value of the j output; j denotes one of the five outputs, P^c_{work}, P^i_{work}, P^c_{max}, P^i_{max} and F^e_{max}; i is the trial number, 1 to 160.

By using these normalised values the plots of F^e_{max} as a function of all four P related parameters are shown in Figure 5-12. A higher coefficient of determination (R^2) denotes a better linear fit of the data. Especially, P^c_{work} and P^i_{work} have higher R^2 coefficients, 0.1833 and 0.4489, respectively, compared to P^c_{max} and P^i_{max}. This reveals a stronger correlation between the F^e_{max} and P_{work} results. All regression plots show positive trends, which means that at a higher P a higher F^e_{max} should be expected.

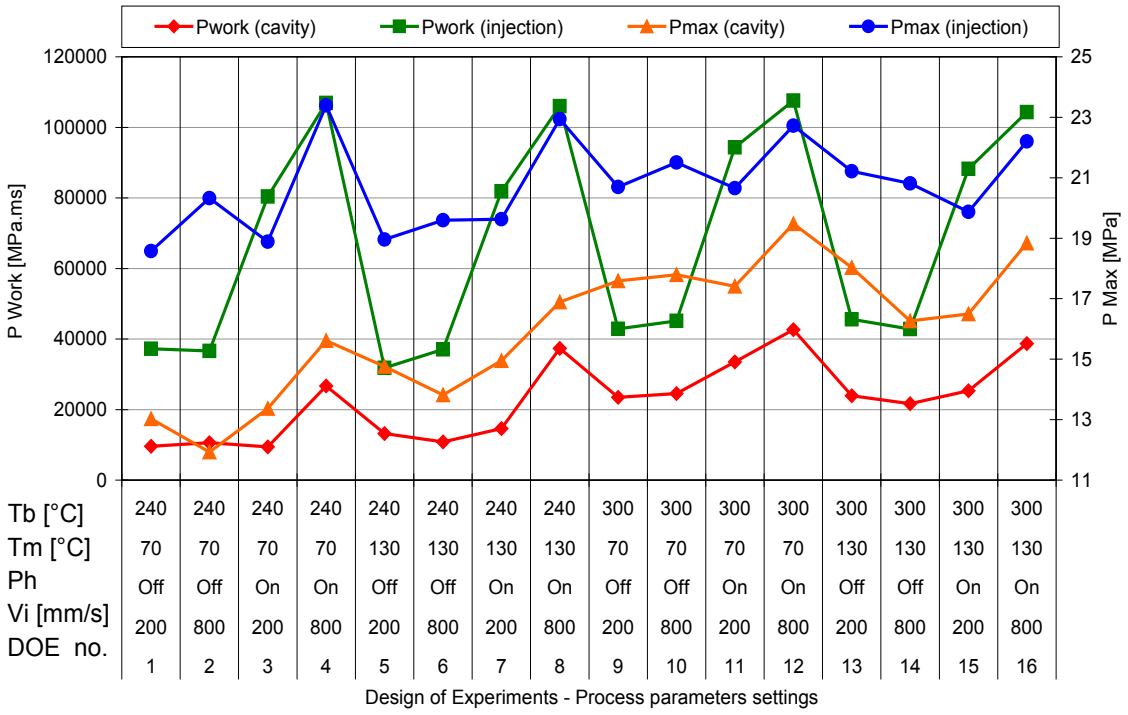

Figure 5-9 Result plot of P_{work} and P_{max} (plotted points represent the average values of the 10 trials for each setting)

Result plot of P^{i}_{work} and F^{e}_{max}

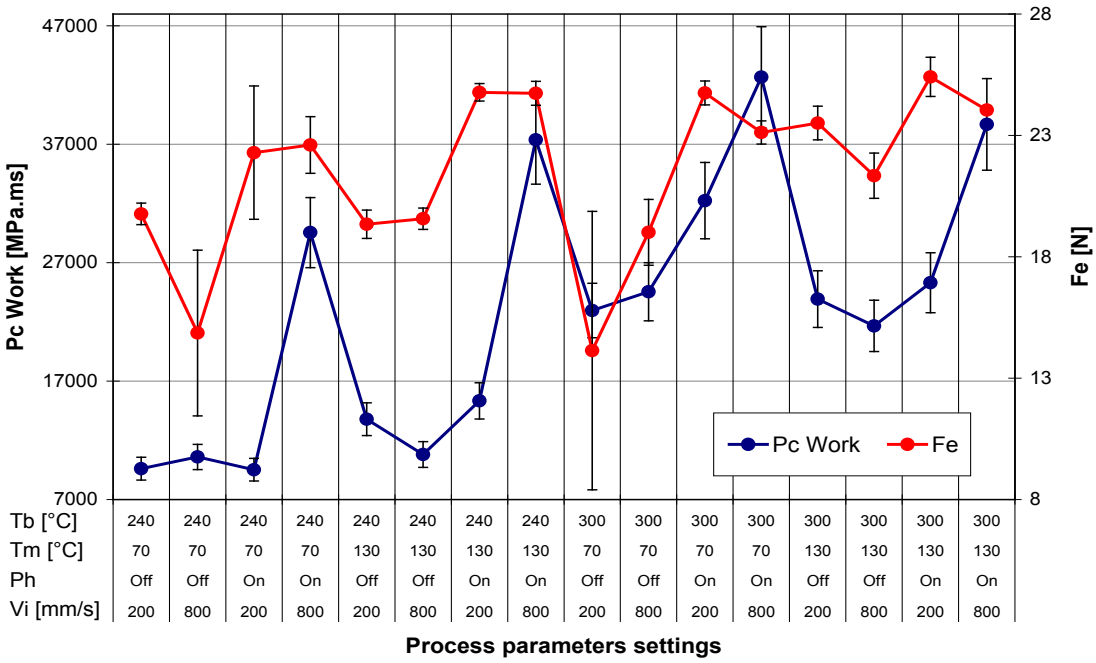

Result plot of P^{c}_{work} and F^{e}_{max}

Figure 5-10 Plot of P_{work} and F^{e}_{max} experimental results (the plotted points represent the average values of the 10 trails at each setting while the error bars represent the 1σ standard deviation)

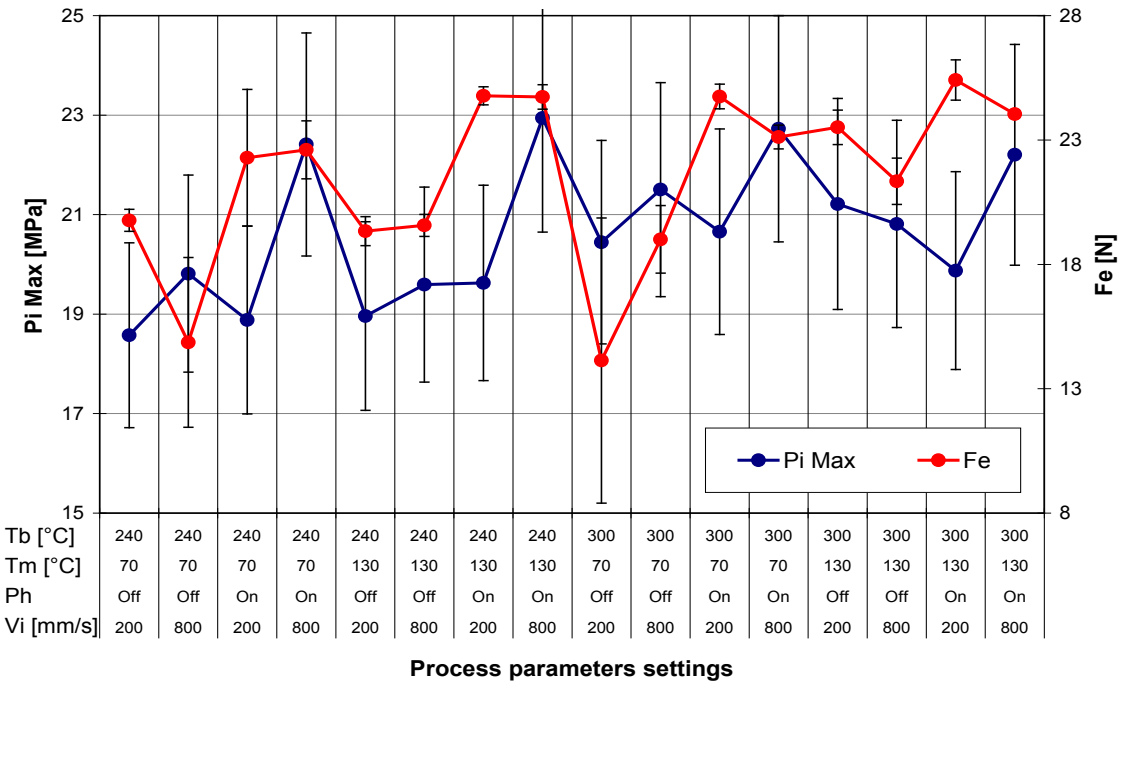

Result plot of P^{i}_{max} and F^{e}_{max}

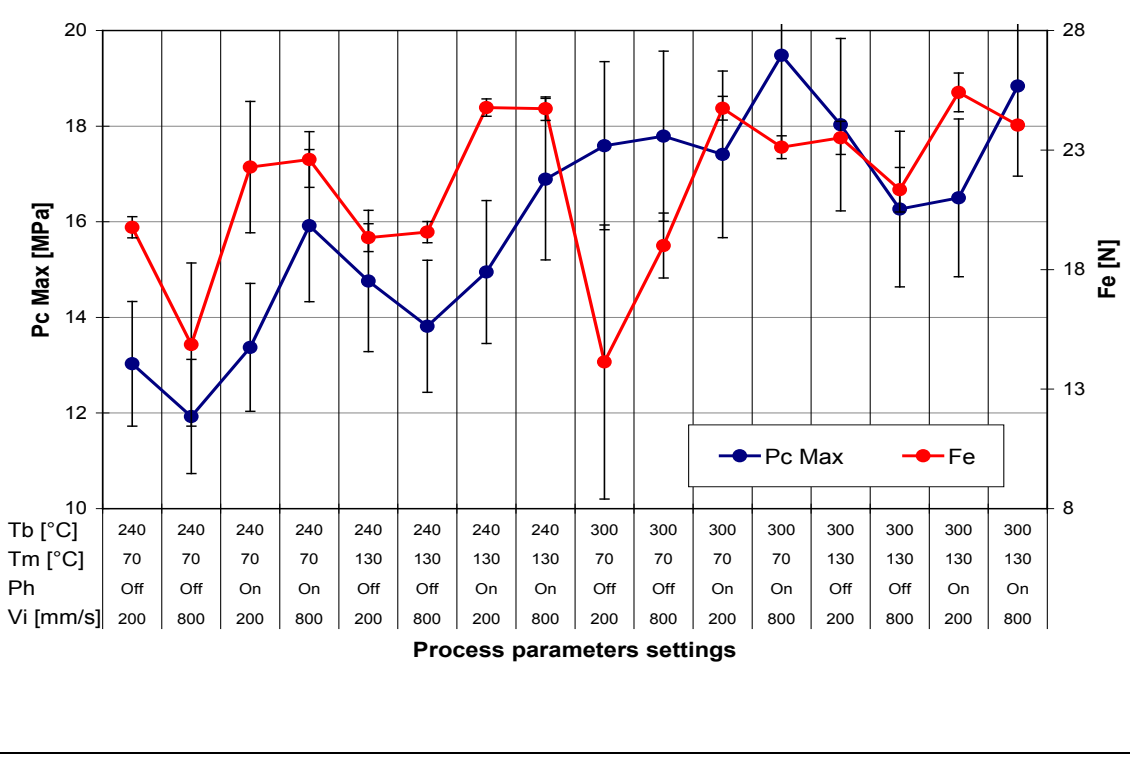

Result plot of P^{c}_{max} and F^{e}_{max}

Figure 5-11 Plot of P_{max} and F^{e}_{max} experimental results (the plotted points represent the average values of the 10 trails at each setting while the error bars represent the 1σ standard deviation)

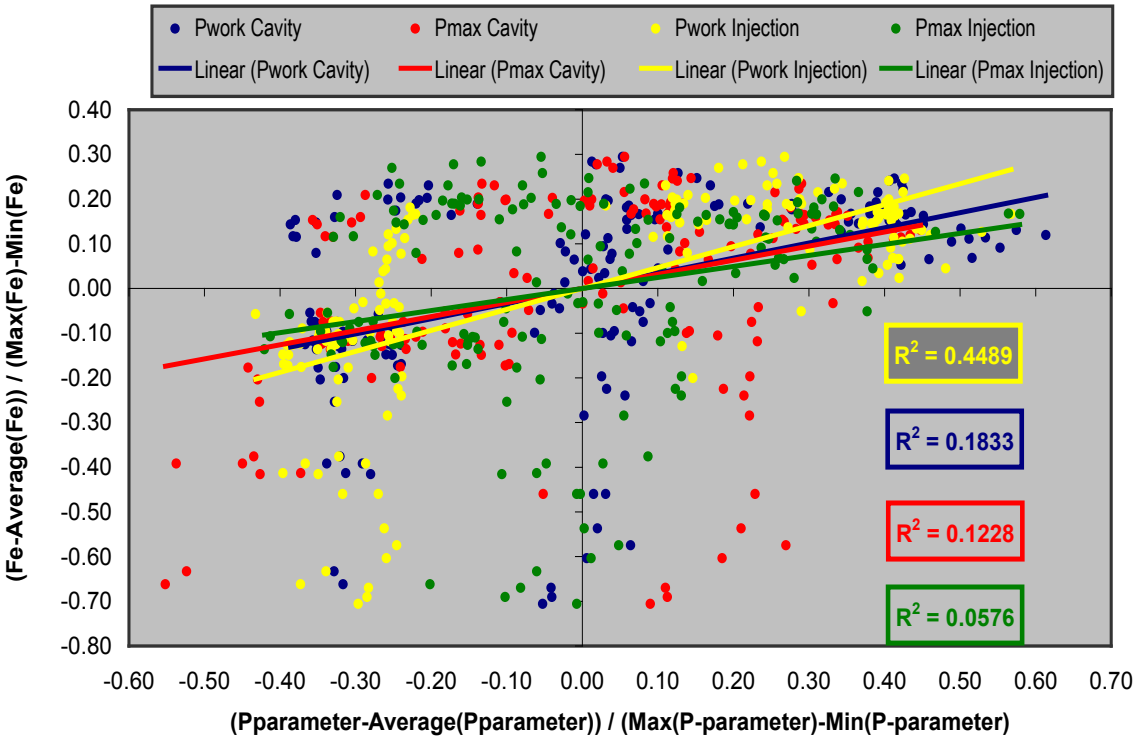

Figure 5-12 Correlation plots between the four pressure-related parameters, P^{c}_{work}, P^{i}_{work}, P^{c}_{max}, P^{i}_{max}, and F^{e}_{max}

5.3.3 Parameters' contribution to optimum performance

Based on the experimental results, ANOVA was performed in order to assess the contribution of each processing parameter to the resulting F^{e} and P behaviour. Table 5-2 shows the rank importance and percentage contribution of each parameter, and also include ranks based on σ statistics, which compare the relative magnitude of effects, where the σ statistic is the highest minus the lowest average for each factor. For each response there is also a S/N rank importance and S/N σ. The Nominal was considered the best S/N ratio, and was used to identify those control factors that were reducing the variability. At the same time higher S/N values were indicative of process parameter settings that were resistant to variation due to noise factors.

The results for F^e_{max} show that P_h has the highest contribution, 20.9%, and an increase in the parameter setting results in an increase of F^e_{max}. At the same time V_i provides the lowest contribution, 2.7%. Also, it can be seen that T_m is ranked second with an influence of 12%. Both T_m and P_h have higher S/N σ, which indicate process parameter settings that minimise the effects of the noise. Thus, T_m and P_h are identified as critical control factors that make the process resistant to variation due to noise factors.

For P_{max} both P^i_{max} and P^c_{max} sensors are not completely in agreement. For P^c_{max} T_b is by far the most contributory factor (19.2%), while for P^i_{max} it is ranked second in importance at 5% after V_i at 8%. For both, T_b and V_i, an increase of their settings results in an increase of P. However, it is worth noting that V_i has the lowest ranked S/N for both P^i_{max} and P^c_{max}. Thus, this indicates that any changes of V_i have a lesser effect on P_{max} than that of the high S/N σ of T_b for P^i_{max} and T_m for P^c_{max}. Both sensors are in agreement that T_m is the process factor with the lowest influence on P^i_{max} and P^c_{max} with a contribution of between 2.7 and 0.1%.

For P_{work} again both sensors are not in agreement. However, it is clear that like P^c_{max} T_b is by far the highest contributing factor (41.1%) for P^c_{work}, where an increase in the parameter setting results in a P increase. Furthermore, like P_{max} T_m is the lowest contributing factor, with an influence of approximately 2.7 to 2.3% for the P^c_{work} and P^i_{work} sensors, respectively. For P^i_{work} the highest contributing factor is P_h (58.2%) and also it has the highest overall contribution, while for P^c_{work} it is the second highest ranked factor. From S/N it can be seen that both sensors are in agreement that V_i is the most important factor.

F^e_{max} response				
Factor	T_b [ºC]	T_m [ºC]	P_h [+/-]	V_i [mm/s]
Level 1	20.99	20.07	18.94	21.75
Level 2	21.91	22.84	23.97	21.16
Δ	0.92	2.77	5.03	0.59
Rank importance	3	2	**1**	4
% influence	4.1	12.1	20.9	2.7
S/N Rank importance	4	1	2	3
S/N δ	0.69	9.57	7.21	1.47

P_{max} response								
Factor	T_b [ºC]		T_m [ºC]		P_h [+/-]		V_i [mm/s]	
Sensor	P^c_{max}	P^i_{max}	P^c_{max}	P^i_{max}	P^c_{max}	P^i_{max}	P^c_{max}	P^i_{max}
Level 1, MPa	14.33	20.10	15.82	20.63	15.4	20.12	15.71	19.78
Level 2, MPa	17.74	21.18	16.26	20.67	16.67	21.17	16.37	21.5
Δ	3.41	1.08	1.27	1.05	1.27	1.05	0.66	1.72
Rank importance	**1**	2	4	4	2	3	3	**1**
% influence	19.22	5.09	2.70	0.19	7.61	4.95	4.03	8
S/N Rank importance	2	**1**	**1**	3	3	2	4	4
S/N δ	1.81	4.12	3.3	2.14	0.41	2.79	0.08	1.77

P_{work} response								
Factor	T_b [ºC]		T_m [ºC]		P_h [+/-]		V_i [mm/s]	
Sensor	P^c_{work}	P^i_{work}	P^c_{work}	P^i_{work}	P^c_{work}	P^i_{work}	P^c_{work}	P^i_{work}
Level 1 MPa ms	17072	64469	22713	68521	17239	39903	19088	62541
Level 2 MPa ms	29001	71017	23360	66964	28833	95583	26984	72945
Δ	11929	6548	647	1557	11594	55680	7896	10404
Rank importance	**1**	3	4	4	2	**1**	3	2
% influence	41.13	9.22	2.76	2.32	40.21	58.25	29.26	14.26
S/N Rank importance	3	2	2	4	4	3	**1**	**1**
S/N δ	3.03	3.14	3.97	0.02	2.11	2.28	6.39	4.83

Table 5-2 Response table for F^e_{max}, P_{max} and P_{work}

The main effect plot for F^e_{max} (see Figure 5-13) shows that F^e_{max} depends mainly upon the presence of P_h and that also F^e_{max} increases with the increase of T_m. The packing pressure produces a compressive internal stress that can only be released after ejection, and makes part demoulding more difficult. This effect is coupled with the

influence of high T_m that facilitates the polymer-tool surface replication, and thus creates conditions for mechanical interlocking at texture/topography level between polymer and metal surfaces, leading to an increase of F^e_{max}. Conversely, the effects of T_b and V_i appear very limited. Hence, these two parameters can be considered as not having a significant effect on F^e_{max}.

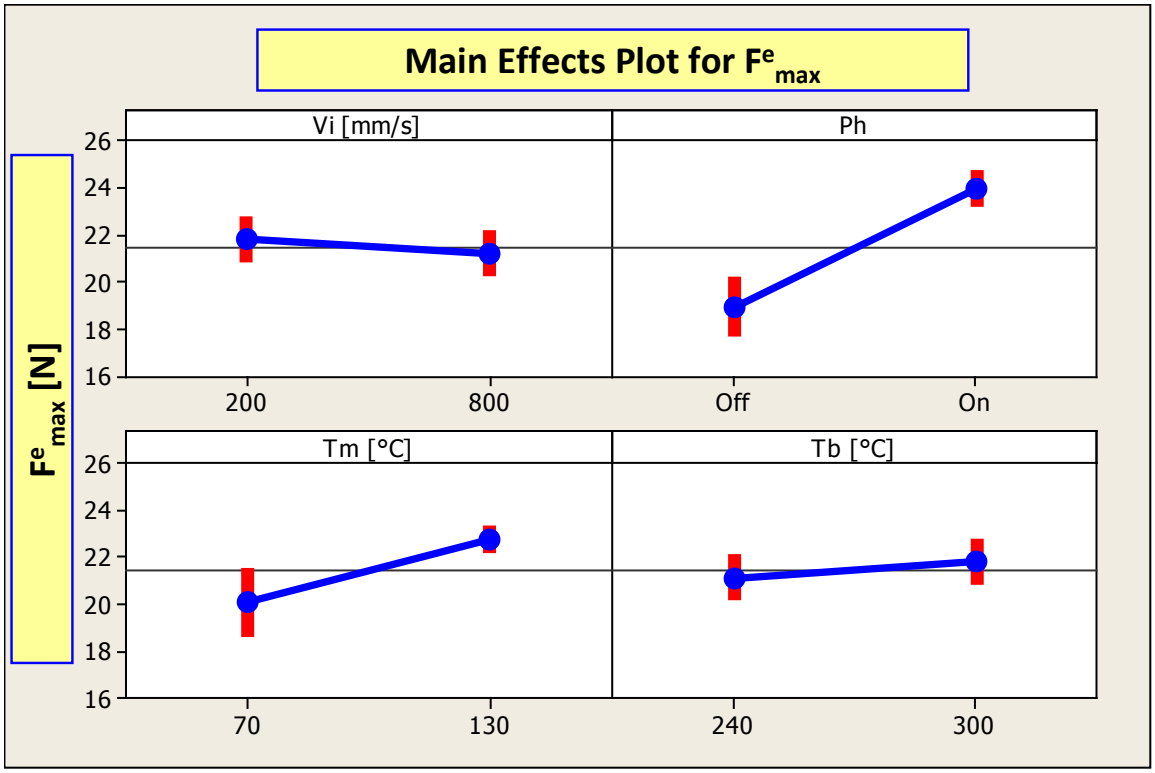

Figure 5-13 Main effects' plots of F^e_{max} (error bars represent the average 1σ standard deviation of the considered effects; F^e_{max} σ ranges from 0.6 to 1.4 N)

The main effect plots (see Figure 5-14 and Figure 5-15) for the four P related process parameters depict their effects on the process behaviour. As expected, an increase of Vi leads to an increase of P, but the registered increase is lower in the cavity than during injection. This is due to melt compressibility in the injection chamber before the

melt passes through the nozzle and enters the cavity. Melt compressibility causes a lower melt speed in the cavity than in the injection chamber, and therefore a lower P increase is observed in the cavity, both for Pmax and for Pwork. Furthermore, the effect of Tm on melt viscosity and thus on P is negligible and within the process uncertainty. Conversely, melt viscosity is obviously affected by T_b where a higher T_b means lower viscosity and therefore a lower polymer P drop during injection, which explains the fact that a higher P_{max} and P_{work} are measured by the sensors. The presence of P_h means a higher integral value both in the injection phase and in the cavity filling phase because P is applied and maintained for a longer time, as shown in Figure 5-7.

Finally, the robustness of the micro moulding process was also monitored. The repeatability of all five outputs of the experiments, P^c_{work}, P^i_{work}, P^c_{max}, P^i_{max} and F^e_{max}, was evaluated, and overall a low experimental standard deviation was observed: more than 95% of the experiments had a coefficient of variation (COV=standard deviation/average [%]), lower than 10%, and more than 70% of the experiments had a COV < 5%.

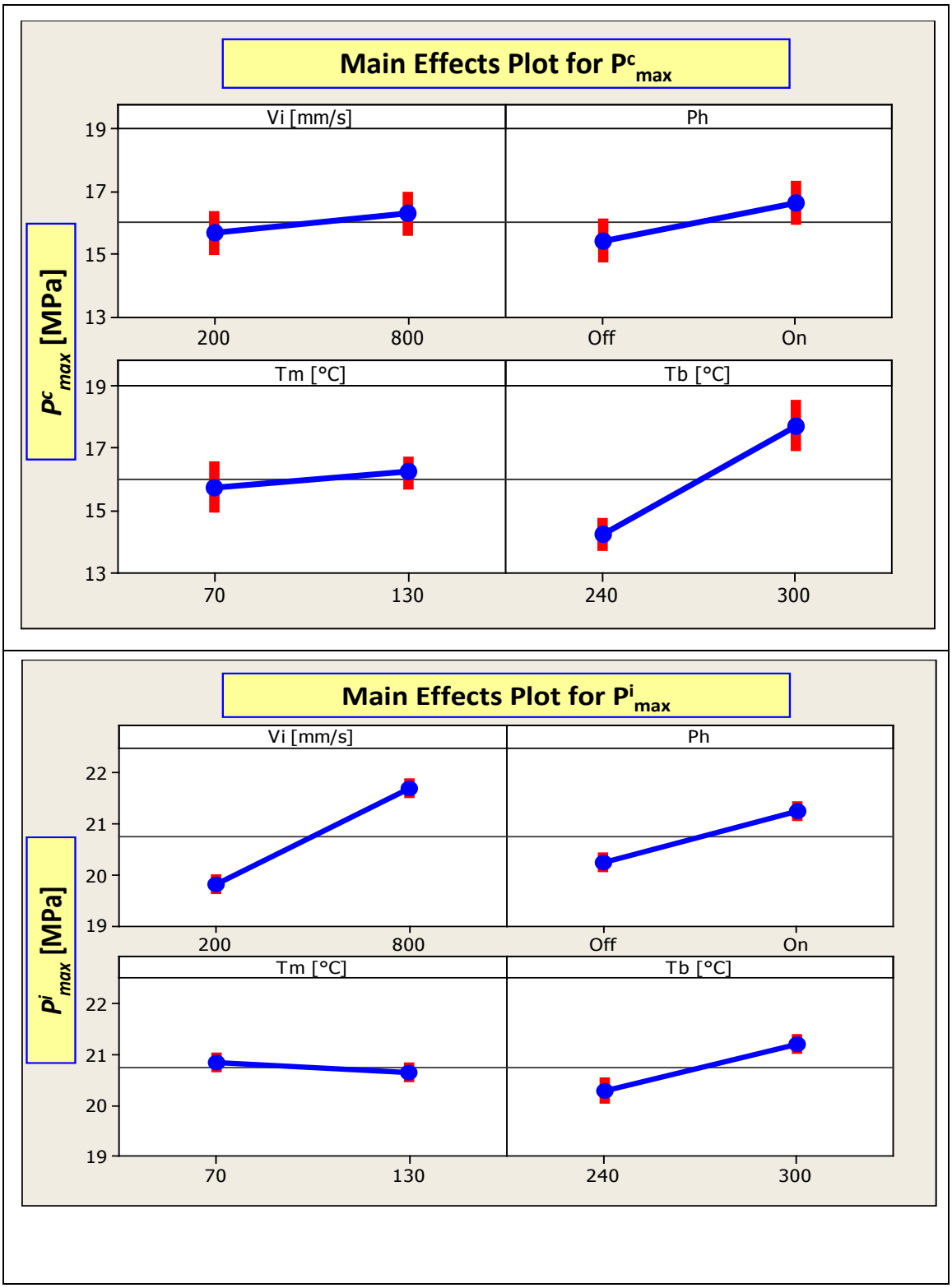

Figure 5-14 Main effects' plots of P_{max} (error bars represent the average 1σ standard deviation of the considered effects; the standard deviations of P^{c}_{max} and P^{i}_{max} were from 0.40 to 0.60 MPa and 0.37 to 0.53 MPa, respectively)

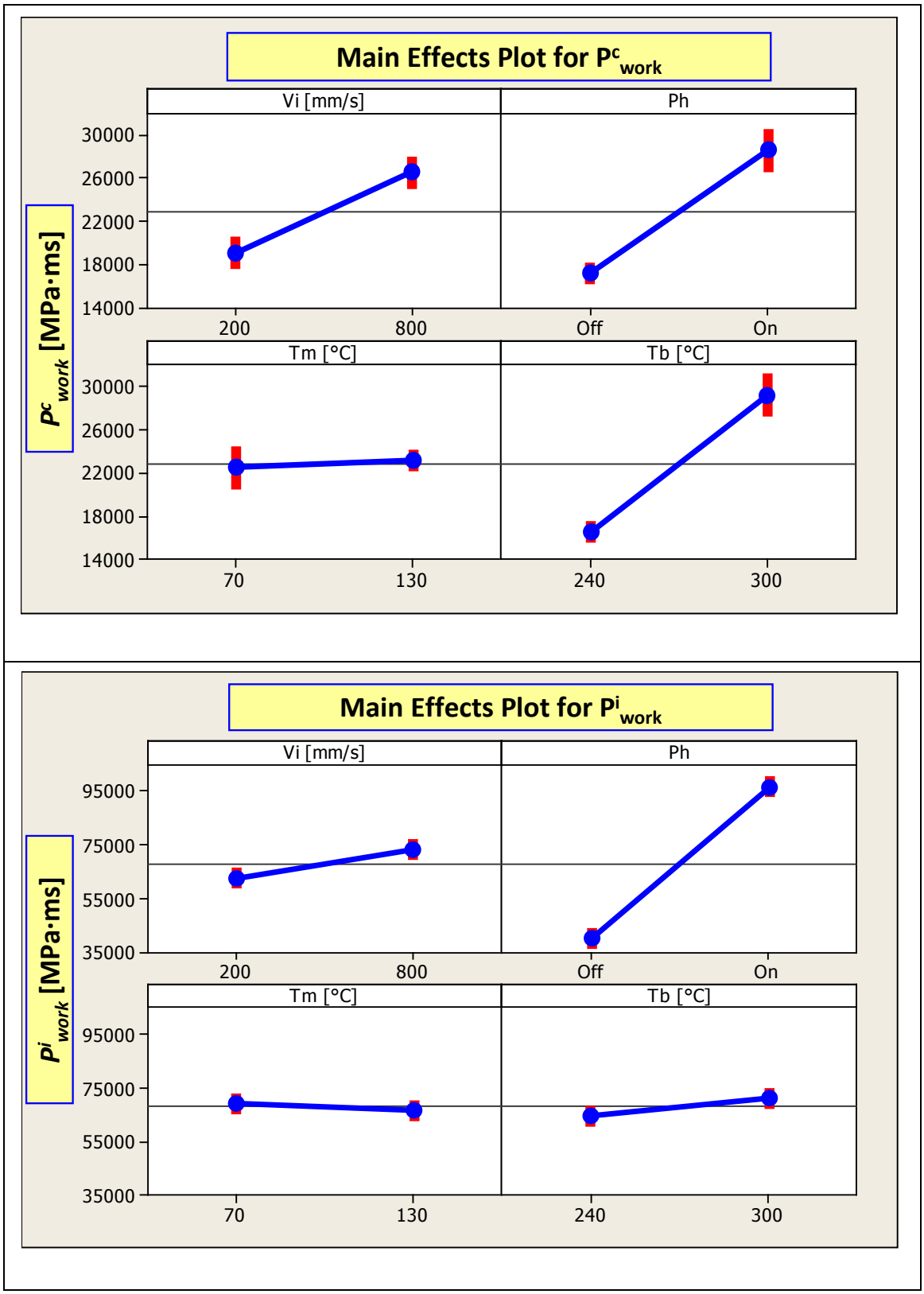

Figure 5-15 Main effects' plots of P_{work} (error bars represent the average 1σ standard deviation of the considered effect; the standard deviations of P^{c}_{work} and P^{i}_{work} were from 1000 to 2000 MPa•ms and 1500 to 3500 MPa•ms, respectively)

5.3.4 Factor Interaction analysis

In this research, an analysis of variance (ANOVA) was applied to investigate and model the relationship between response variables and one or more predictor variables, and thus to identify the level of interactions between them. A two-way ANOVA P-value test was performed to study the factors' interactions with respect to F^e and P. The results are provided in Table 5-3. Low P-values indicate high interactions between the factors. The interaction results are also represented as pareto charts in Figure 5-16, Figure 5-17 and Figure 5-19. The pareto charts were used to highlight graphically, as a percentage and a cumulative function any factor interactions with respect to F^e and P (Montgomery 2004b). In the charts the x-axis represents the interaction source, while the y-axis is the frequency in % of interaction occurrences.

By analysing the results in Table 5-3 it is immediately apparent that P_h and V_i interactions are very high for F^e_{max}, P^c_{work}, P^i_{work} and P^i_{max}. While for P^c_{max} the interactions between T_b and T_m are also high. It is possible to see in Table 5-3 that only the interactions between T_m and V_i are consistently low for F^e_{max}, and P^i_{work}. At the same time the pareto analysis shows that 80% of the interactions are caused by 20% of the investigated factors. Especially, P_h and V_i dominate as interaction sources for F^e_{max}, P^c_{work} and P^i_{work}. The cumulative function shows similar trends for all measurements except for F^e_{max} where the P_h, V_i interactions dominate with 55% of the total interactions, and all the rest are less than 15%. It can be seen for P_{max} that there is no dominant interaction as no interaction exceeds 32%. Also, the cumulative function for P^i_{max} is close to linear, which indicates again that the influence is spread over the all six interactions.

The fact that P_{max} for both 'injection' and 'cavity' are affected by the presence of a holding phase can be explained with the interaction plot in Figure 5-18. In fact, as far as the experiments at low V_i are concerned, the presence of P_h does not affect the P_{max} results; and the P_{max} results are approximately at the same level for both injection speeds when P_h is not applied. On the contrary, at high V_i and when P_h is set to 'On', a certain delay at the switchover point is observed, which results in a sharper P rise towards the end of the injection phase, i.e. near 100% injected volume, resulting in high P_{max} both for injection and cavity.

Interaction	P-value				
	F^e_{max}	P^c_{work}	P^I_{work}	P^c_{max}	P^I_{max}
T_m V_i	**0.992**	0.951	**0.963**	0.828	0.686
T_m P_h	0.888	**0.995**	0.871	0.872	**0.964**
T_b V_i	0.801	0.642	0.882	**0.945**	0.389
T_b T_m	0.785	0.446	0.935	0.121	0.651
T_b P_h	0.747	0.97	0.678	0.329	0.302
P_h, V_i	0.016	0.045	0.002	0.169	0.027

Table 5-3 Two-way ANOVA P-test interaction results

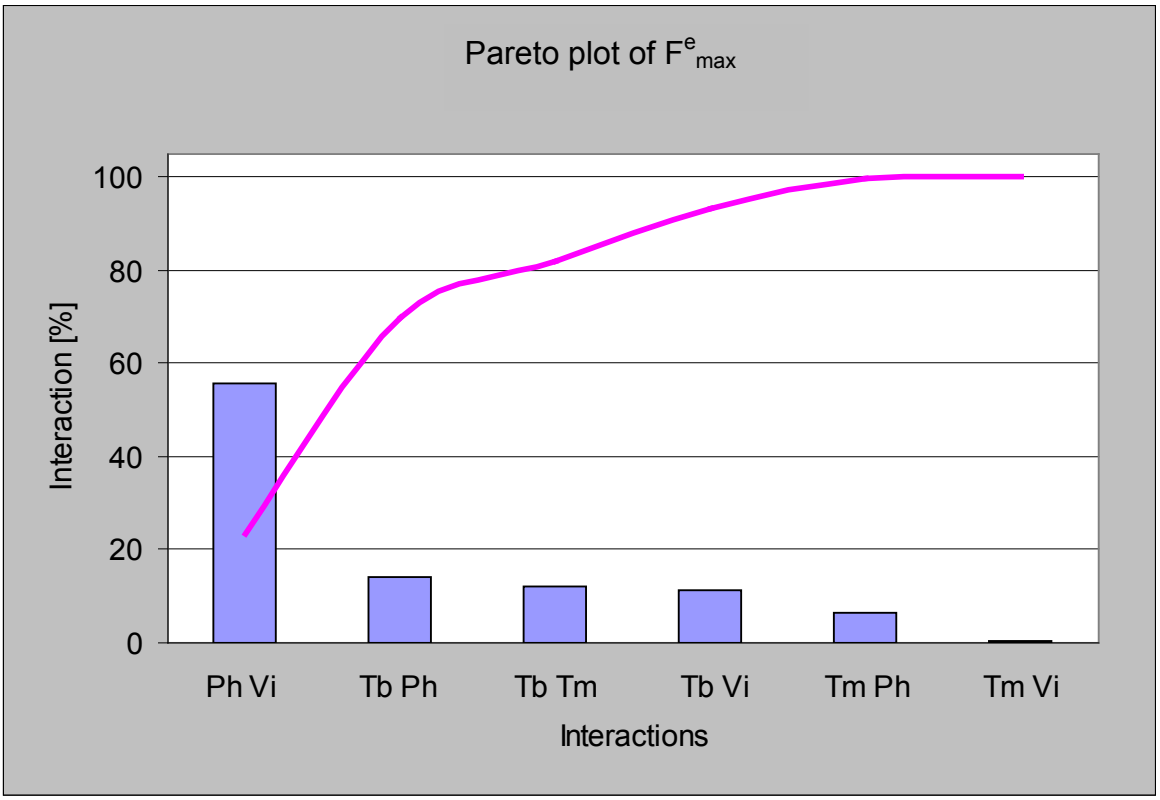

Figure 5-16 Pareto plot of F^e_{max} interactions

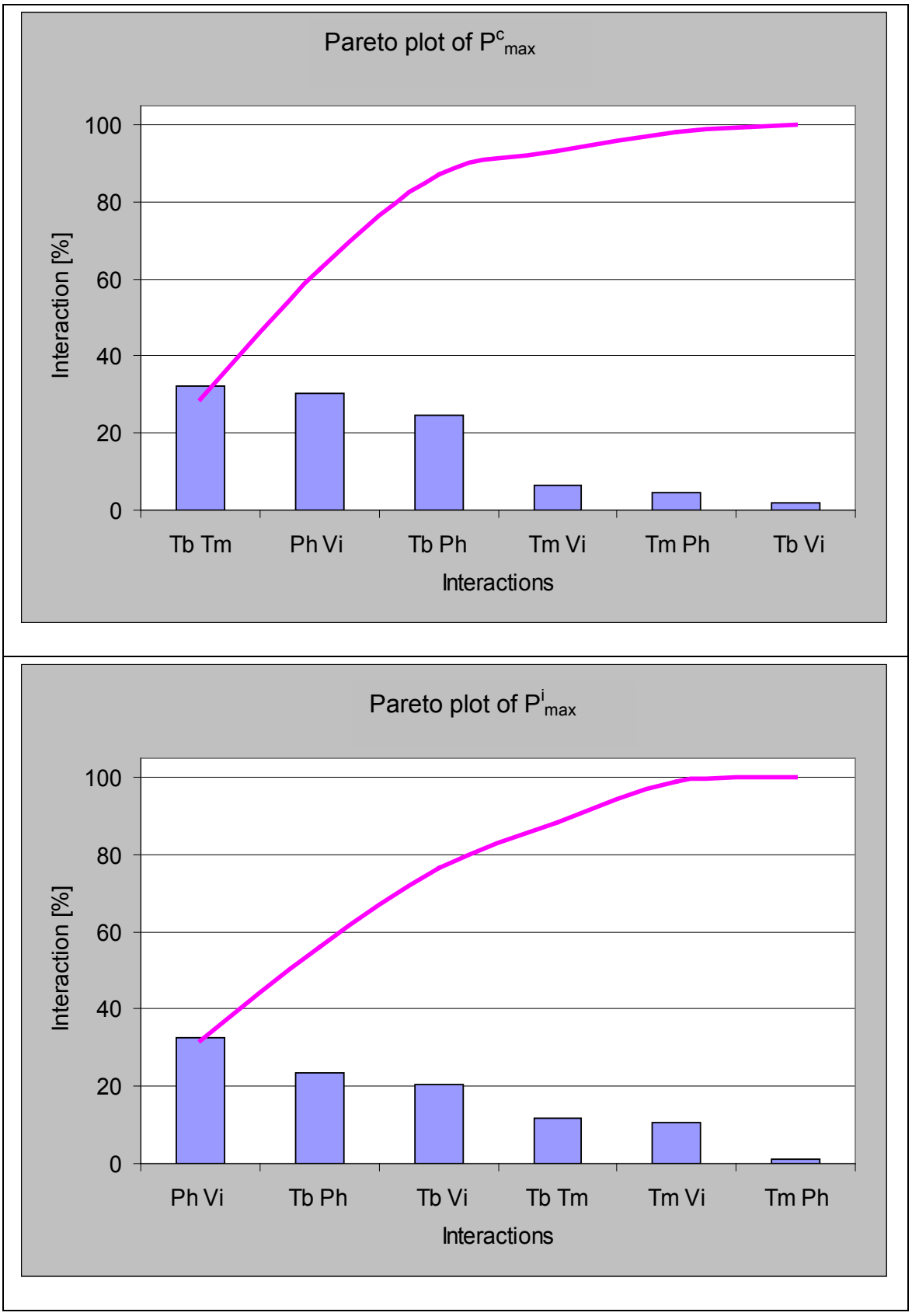

Figure 5-17 Pareto plot of P_{max} interactions

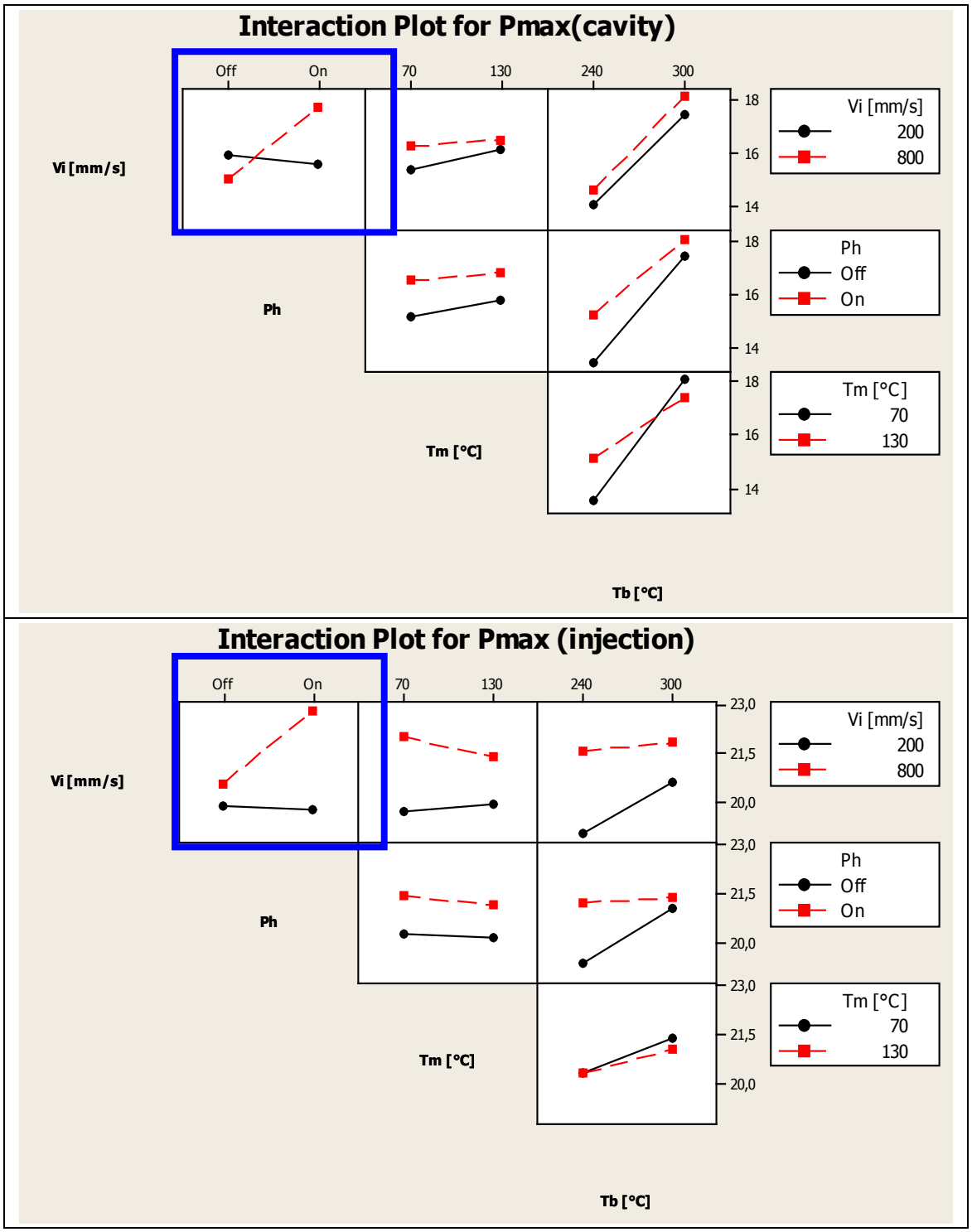

Figure 5-18 The effects of V_i , P_h and T_m interactions on P_{max}

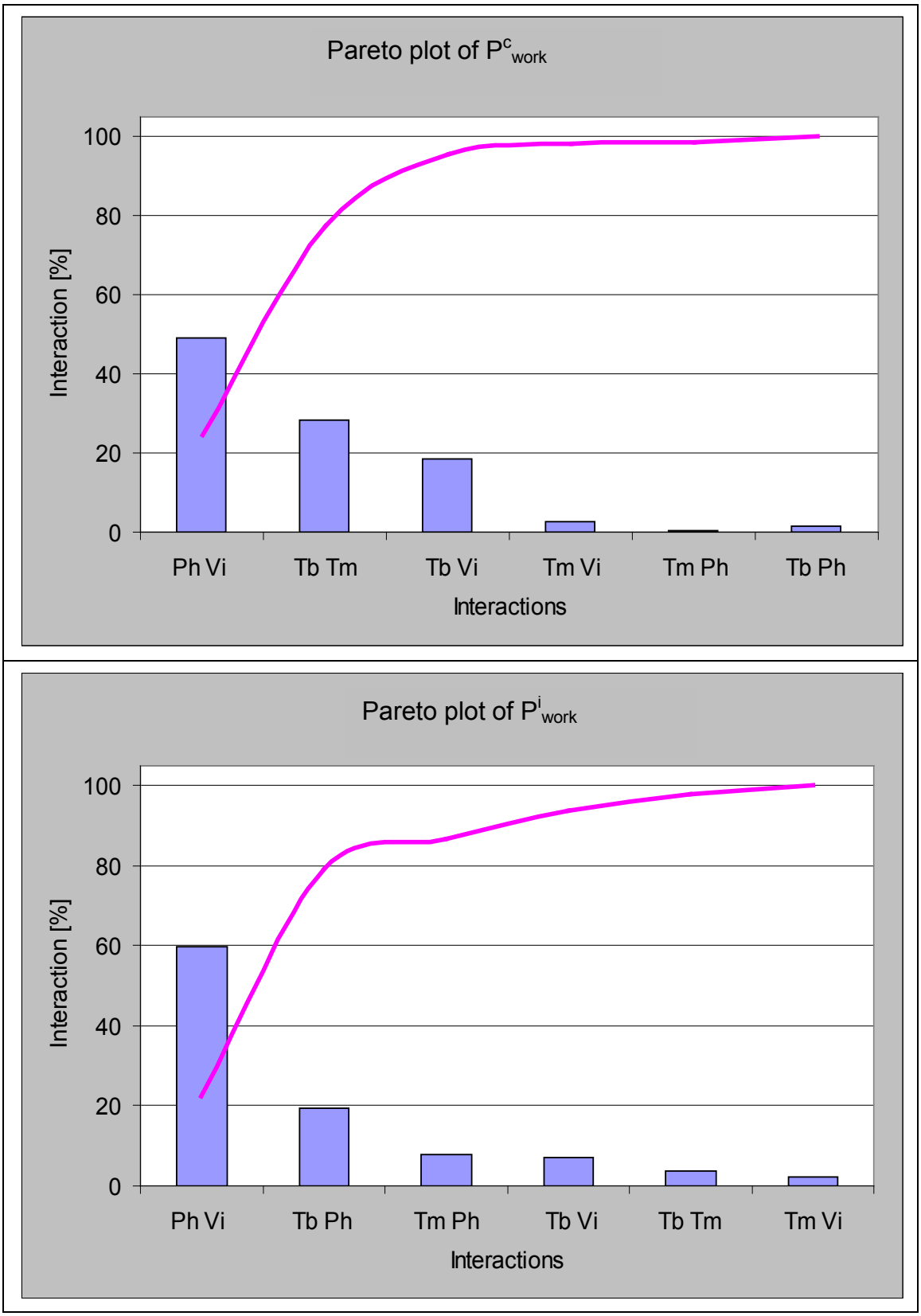

Figure 5-19 Pareto plot of P_{work} interactions

5.3.5 Optimum parameters levels

The average of the F^e_{max}, P_{max} and P_{work} results was calculated based on the 10 trials conducted for each combination of control parameters in the OA. The optimum parameter levels for the investigated polymer were determined by employing the Taguchi parameter design method (Montgomery 2004a). By applying this method it was possible to identify theoretically the best set of µ-IM parameters in respect to F^e and P within the investigated processing window. For F^e the value of a given parameter was considered to be the best of the selected two levels, if its corresponding average F^e_{max} was the lowest. For P_{max} and P_{work} this was not strictly true, however in this research it was assumed that a lower P would be better. The theoretical best set of processing parameters is provided in Table 5-4. From this analysis, it was immediately apparent that the low settings of the process parameter levels resulted in the lowest values for F^e_{max}, P_{max} and P_{work}. The only factors that did not comply with this observation were the V_i setting for F^e_{max} and T_m for P^i_{work}, where their high settings led to theoretically lower values. However, for both F^e_{max} and P^i_{work}, the respective V_i and T_m settings were not unique and, as was shown in the previous section, they had the lowest response of the four factors. Conversely, the main effect plots combined with the process repeatability (see Figure 5-15) showed that the effect of T_m had a similar standard deviation, and therefore could be ignored.

Resulting	Factor levels for the theoretical low F^e_{max}, P_{max} and P_{work}				Mean Predicted values
	T_b [ºC]	T_m [ºC]	P_h	V_i [mm/s]	
F^e_{max}	1	1	1	2	16.79 [N]
P^c_{max}	1	1	1	1	13.14 [MPa]
P^i_{max}	1	1	1	1	18.70 [MPa]
P^c_{work}	1	1	1	1	7003 [MPa·ms]
P^i_{work}	1	2	1	1	30647[MPa·ms]

Table 5-4 The theoretical best set of processing parameters

5.4 Conclusion

Chapter 5 reports an experimental study on the effects of injection and cavity pressures and demoulding conditions in micro cavities when replicating polymer parts. A condition monitoring system was designed and implemented to measure the pressure state of a polymer inside the mould cavity, and also the force required to eject a part. Then, by using the design of experiments approach the pressure work, maximum pressure and maximum demoulding force were studied as a function of the four process factors, T_b, T_m, P_h and V_i. The main conclusions made based on the obtained results are:

- A condition monitoring setup was designed and implemented to measure injection and cavity pressures during part filling, and applied forces during demoulding. It was shown that P_{max}, P_{work} and F^e_{max} were dependent on the processing conditions, and by monitoring P the demoulding force behaviour was analysed.

- The mean values of P_{max} and P_{work} were analysed by using two sensors. Their readings were within different ranges, which shows the importance of sensor

position for monitoring P. Also, it was observed that in all cases the mean P^i results were higher than those of P^c.

- The study showed that there was a direct correlation between the pressure and the demoulding force. The interval plots for F^e_{max}, P_{max} and P_{work} pointed to significant variations between the trials. These variations can be explained with the use of two different settings for P_h and V_i, where the high ones resulted in an increase of P and F^e_{max}. The P^i_{work} response was the closest to the F^e_{max} response, and it could be used to estimate the force required to eject parts from the mould. This was confirmed with the conducted correlation study over the whole set of experiments. The analysis of variance showed that the interactions between P_h and V_i had a dominant effect on F^e_{max}, P^c_{work} and P^i. While for P^c_{max}, interactions between T_b and T_m had the highest influence

- There was a direct correlation between the process factors and the demoulding force, and it was possible to identify those that had a significant effect on the demoulding behaviour. In particular, the P^i_{max} variations can be attributed mostly to P_h as the high settings resulted in high P. Experimental results showed that there were additional peaks when high settings were applied for V_i. These deviations did not correlate to the F^e_{max} variations and did not influence the F^e_{max} measurement results. For P^c_{max} the influence of P_h was less obvious and was less correlated to the applied demoulding forces.

- The effects of process settings on P and F^e_{max} suggested that T_b was the highest contributing factor for P^c_{max} and P^c_{work}, while P_h was the highest for F^e_{max} and P^i_{work}. The main contributing factor for P^i_{max} was V_i. For each of these factors an increase of their settings resulted in an increase of P. It was also

observed that based on the S/N ratios the main control factors were the temperature settings, T_b and T_m, for P^i_{max} and P^c_{max} , respectively, and V_i for P^c_{work} and P^i_{work}.

- With respect to F^e_{max} and P it was immediately apparent that the low settings of control factors resulted in their lowest results. However, there were two factors that did not comply with this; in particular the high settings of V_i and T_m led to theoretically lower values for F^e_{max} and P^i_{work}, respectively. In practice, the influence of these factors was found to have a standard deviation of the same order of magnitude, and therefore their effects should be considered limited from the processing perspective.

- The strong effect of P_h indicates that an effective holding phase is necessary to ensure complete filling, to compensate for polymer shrinkage during cooling, reduce warpage and provide dimensional stability. In setting the holding pressure the trade-offs with the demoulding force should be considered to avoid part deformation and damage.

6 PROTOTYPE TOOLING FOR PRODUCING SMALL SERIES OF POLYMER MICRO PARTS

6.1 Motivation

Any changes of design, which are usually needed during product development, lead to design iterations and increase the development costs. The use of layer-based manufacturing technologies to produce three-dimensional functional models and concept prototypes can minimise these design iterations. However, due to the limited set of materials available for layer-based manufacturing it is not possible to produce the final parts in one process step by rapid prototyping. More often it is required, to produced parts by the final process and the final polymer material in order to carry out the necessary functional tests, especially for producing polymer micro-components. Therefore, it is necessary to develop rapid tooling process chains, e.g. for low-pressure IM, that can be used to fabricate small batches of functional micro-components in the required material. In this Chapter, the moulding performance of µSL inserts is investigated as a function of tool geometry and process settings.

6.2 Experimental setup

6.2.1 Test Part design

The design used to analyse the capabilities of layer based manufacture (LBM) inserts for moulding micro parts is a 15 mm x 20 mm x 1 mm micro fluidics platform (Figure

6-1). The mould inserts which have been utilised have an identical design to those reported in Chapter 3. As described, the system design includes features commonly found in micro fluidics components such as reservoirs, channels and waste compartments. The pin dimensions are 500 µm in diameter and 600 µm in height, and the cross section of the main channels is 200 x 100 µm. The overall part volume is 3.10 mm^3 while its surface area is 8.33 mm^2 and the design includes a 2-3º draft angle.

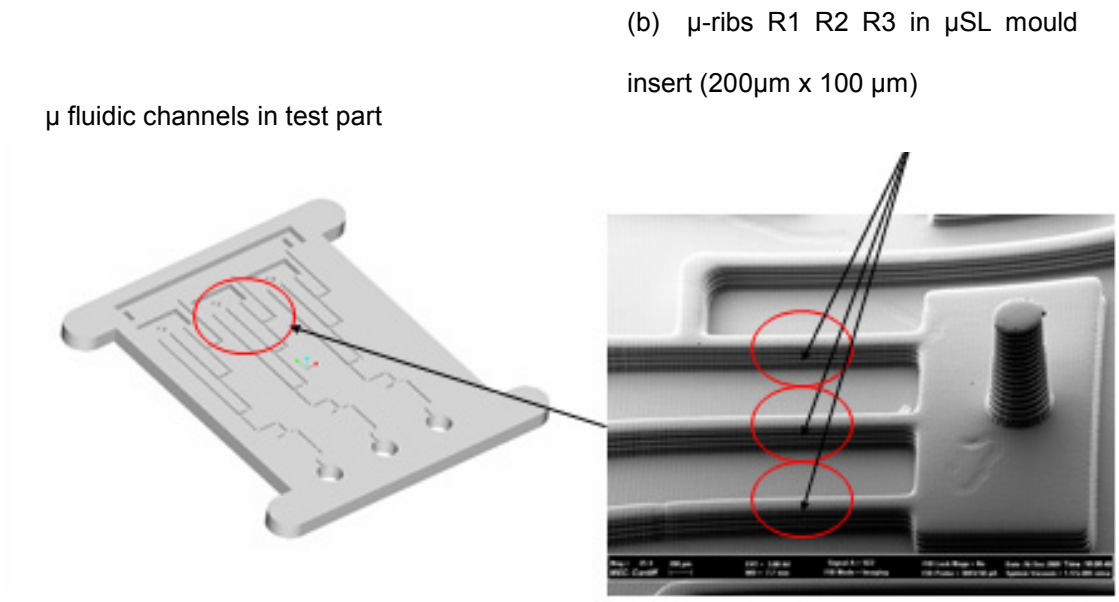

Figure 6-1 Part and mould designs: (a). Micro fluidic part design; (b) micro features of µSL mould insert

6.2.2 µSL layer-based manufacturing process

µSL of 3D structures is based on light induced solidification of a liquid photopolymer in a layer-by-layer fashion. A light source is focused onto the photopolymer surface using a laser or a mask to draw a cross section of the part. The light hardens the photopolymer where exposed. The part is then covered with a new layer of

photopolymer and the process is repeated until the part structure is completed. The selected Rapid Micro Fabrication (RMF) system, Envisiontec Perfactory (Table 6-1), works in a projection mode. This is in contrast to direct write systems like stereolithography used to build 3D objects from a UV photosensitive liquid resin. The light is projected using a digital mirror technology, in particular a Digital Light Processor (DLP) projector with resolution of 1400 x 1024 pixels (SXGA+). A 3D model in STL data format is processed by the system software to generate a series of bitmaps. Each bitmap represents an individual layer of the part, and can be set to a thickness that is constant throughout the whole build between 25 and 150 µm depending on the material used. The bitmaps are sequentially projected onto the liquid resin using DLP and the light cures the liquid resin to produce solid parts. The resolution in X and Y can be altered from 16 µm to 60 µm in Perfactory Mini and from 43 µm to 136 µm in Perfactory Standard.

Build area (Lens dependant) *	84 x 63 x 230 mm in X, Y, and Z (f=60 mm lens) 44 x 33 x 230mm in X, Y, and Z (f=85 mm lens)
Resolution (Lens dependant)	30 x 30 µm in X-Y plane (f=85 mm lens) 16 x 16 µm in X-Y plane (f=85 mm lens)
Layer thickness* *	20 µm to 150 µm (material dependant)
Build time	The build speed is material and layer thickness dependant. It is constant through the build and up to 10 mm per hour.

*Table 6-1 Perfectory specifications * The largest build area cannot be reached when using the highest resolution settings. ** The machine specifications give a maximum layer thickness of 150 µm however this is dependent on the material and 20 µm has been achieved*

6.2.3 Mould manufacture

To investigate the capabilities of µSL moulds as viable prototype tools, the following three builds were considered

- µSL 1: 50 µm layer thickness throughout the build;
- µSL 2: 50 µm layer thickness up to 3.8 mm height and then 20 µm for the functional area;
- µSL 3. 20 µm layer thickness throughout the build;

In total, 15 µSL tools were manufactured, five builds for each process setting. The part design is made up of many features that can be used to determine the mould accuracy (Figure 6-1 a). The focus of this investigation is on the manufacture and replication of micro features, therefore, the assessment of tool-making capabilities of µSL is based on the 200 x 100 µm and 100 x 100 µm rib features (Figure 6-2). After studying the scanning electron microscope (SEM) images of the three µSL builds the following observations were made: For µSL 1, the layers' step effects resulted in small undercuts, overhangs, at each layer (Figure 6-3), and the resolution of the 100 x 100 µm channel features was relatively poor. Therefore, based on the SEM analysis only the 200 x 100 µm rib features were considered for µSL 1. For µSL 2 and 3 the functional area was identical. and therefore µSL 3 was excluded from the moulding experiments as the inserts were identical to µSL 2

µSL mould insert 1: 50 µm layer thickness	
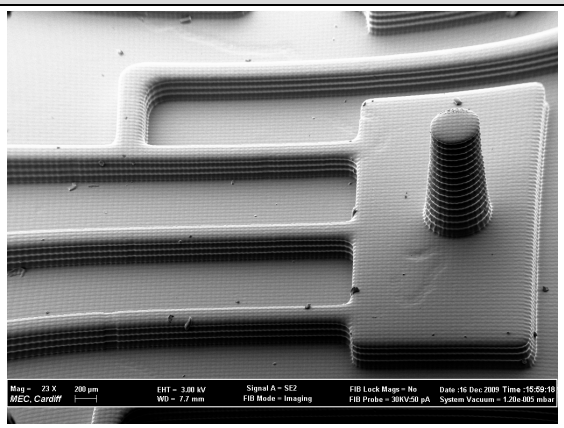	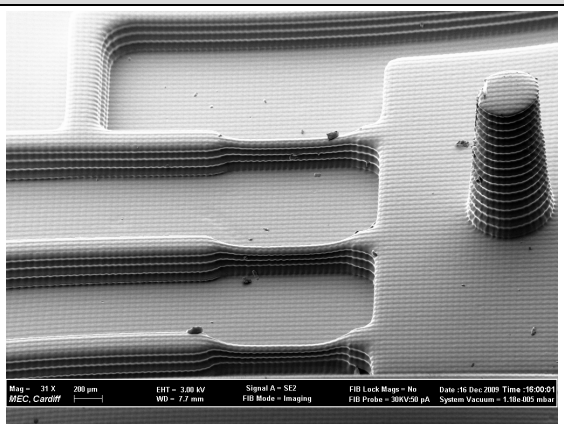
200 x 100 µm rib	100 x 100 µm rib
µSL mould insert 2: 20 µm layer thickness (functional area)	
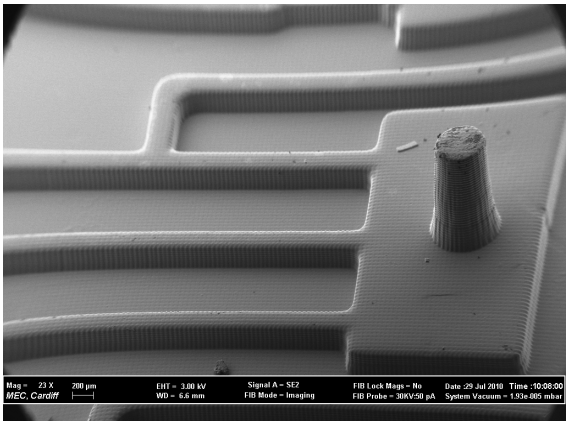	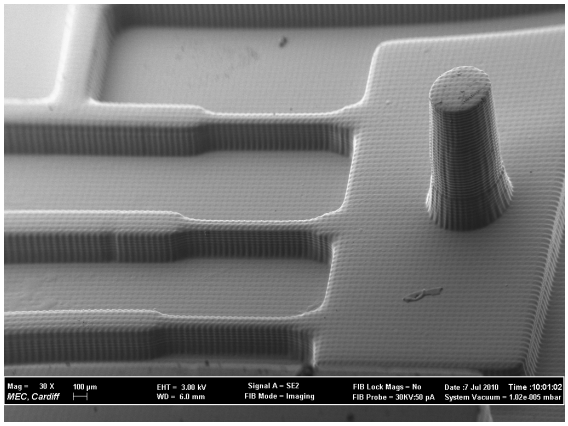
200 x 100 µm rib	100 x 100 µm rib

Figure 6-2 µSL mould inserts with microfluidics features

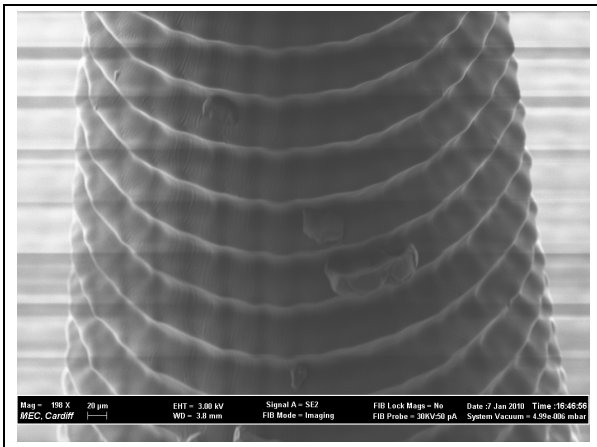	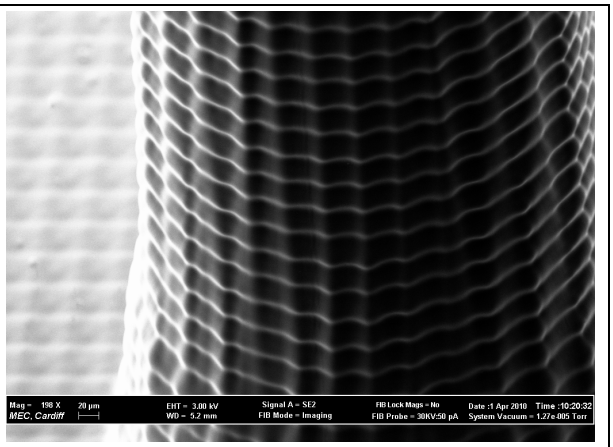
µSL 1: 50 µm layer thickness	µSL 2: 20 µm layer thickness

Figure 6-3 Builds with different layer thickness and reduced amount of undercuts by utilising 20 µm layer thickness

6.2.4 µSL insert measurements

The quality of the µSL inserts is critical for performing successfully a subsequent polymer replication. To validate their replication capabilities for prototype tooling, the ribs R1, R2, and R3 in Figure 6-1 with nominal heights of 100 µm were selected. The ribs were inspected before and after the carried out experiments. To measure the height of the ribs and then the depth of the channels of the mouldings, a White Light Interferometer (WLI) was employed. This measurement technique was selected because WLI allows height measurement to be performed with nanometre accuracy up to several mm. The repeatability of the µSL process was also assessed by measuring the height of the channels. In particular, three ribs were inspected on each µSL insert by taking 5 measurements in different places, and thus in total 15 measurements were taken on each µSL insert. The measurements of rib heights and channel depths were taken following the recommendations in the ISO 5436-1985 standard (Standard 1985).

The mean results presented in Figure 6-4 show that the rib heights measured on each insert were not the same. In all cases the mean value was in the range from 93.75 to 91.06 µm while the standard deviation (σ) was in the range from 0.78 to 1.78. It should be stressed that this was expected because the model and its dimensions were not modified to off-set the shrinkage.

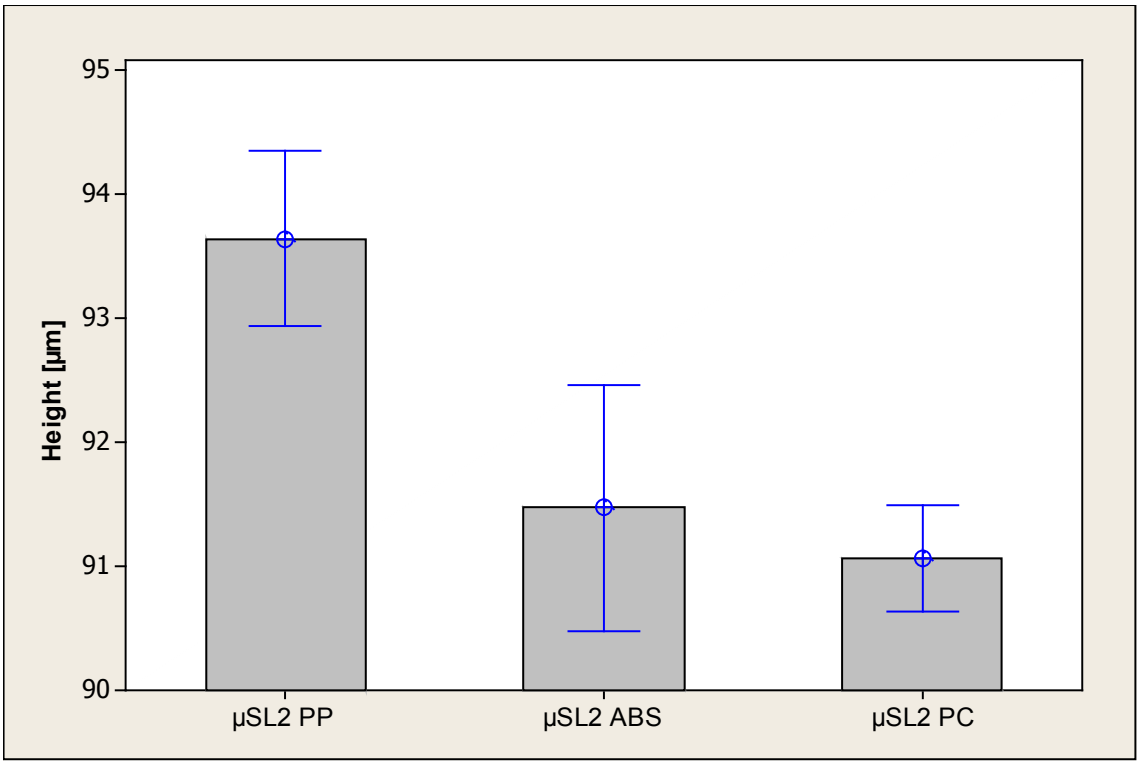

Figure 6-4 Height measurements of the µSL 2 inserts

6.2.5 Mould insert integration

Figure 6-5 shows the µSL mould insert. Its overall dimensions are 25 x 28 x 5 mm with four 3 mm holes for ejectors. The insert has identical outer dimensions and cavity dimension as the insert chosen in Chapter 3.

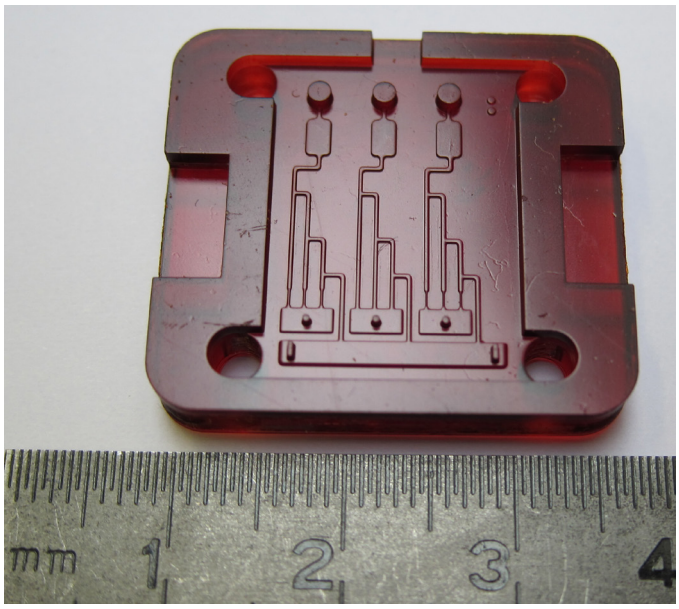

Figure 6-5 µSL mould insert

6.2.6 Test materials

To perform the planned experiments the same three materials (ABS, PC and PP) as investiagted in Chapter 3 were chosen. Therefore, the results of Chapter 3 could be utilised to identify the best processing window for low pressure injection moulding of these materials. The parameter sets for each material were used to perform replication trials on the machined µSL mould inserts. The material properties can be seen in Table 3-2.

6.3 Experimental setup for the µSL mould inserts

To assess the capabilities and the potential of the µSL inserts as viable prototype and short run manufacture tools, one polymer part was replicated with each set of µ-SL mould and material. By using the results of the ANOVA response characteristics from

Chapter 3 it was possible to select process settings from the investigated factors in order to achieve the required processing conditions for low pressure injection moulding. Thus, to ensure that the μSL inserts were subjected to the lowest possible *P*, the parameters' levels to attain the theoretical lowest setting of processing parameters with regards to P_{max} were selected. Table 6-2 describes the set of experiments that were conducted to validate the capabilities of the μSL inserts for moulding small batches of parts. The only change to the process settings used for the P20 steel inserts utilised in Chapter 3 is the cooling time. In particular, 15 seconds were added to compensate for the lower thermal conductivity of the μSL inserts.

Two sets of experiments were performed for each of the three materials. The first set was with the μSL 1 inserts (50 μm layer thickness) while the second with the μSL 2 inserts (20 μm layer for the functional area). Especially, one μSL insert was produced for each of the three tested materials and thus six inserts were produced for the two set of experiments. For each of the six tool inserts one part was moulded. The tool micro features were examined prior to and after the experiments, and the parts were also inspected to assess the replication accuracy.

Exp	Material	RT	Factor levels for the theoretical low P_{max}				*Mean Predicted P_{max} values (for the P20 steel mould)*
			T_b	T_m	P_h	V_i	
1	PP	1	210 ºC	70 ºC	ON	800 mm/s	14.88 [MPa]
2		2					
3	ABS	1	270 ºC	30 ºC	OFF	200 mm/s	9.69 [MPa]
4		2					
5	PC	1	310 ºC	70 ºC	OFF	200 mm/s	19.30 [MPa]
6		2					

Table 6-2 RT experiment settings with low P_{max}

6.4 Results

6.4.1 µSL inserts

The results from the inserts' inspections before and after the replications are presented in Figure 6-6 and Figure 6-7. Figure 6-6 shows that the two types of µSL inserts used did not behave in the same way. µSL 1 performed poorly particularly for ABS and PC, and this should not be regarded as an ability to identify an optimum process window for performing low pressure moulding. On the contrary, the results for µSL 2 show that such a window can be found and the µSL inserts can perform adequately. Looking at the differences between the two insert types it can be judged that the undercuts shown in Figure 6-3 have a detrimental effect on the replication capabilities of the µSL 1 inserts. Thus, by minimising the layer thickness of the µSL builds it is possible to improve the inserts' performance and extend the tool life.

ABS parts had a higher tendency to stick to the tool. ABS is a rubber modified glassy plastic made by the grafting of styrene polymers to Acrylonitrile Butadiene Copolymer rubber. It was observed that the ABS material delaminated during demoulding, which could be due to the polymer grafting to the µSL insert polymer (Griffiths et al. 2010).

Figure 6-7 depicts the resulting 200 x 100 µm ribs after moulding using µSL 2. The images show that the micro features were replicated relatively well for all three materials. It is also shown that larger high aspect ratio features, such as the microfluidic pin, are prone to damage during demoulding particularly for ABS and PC.

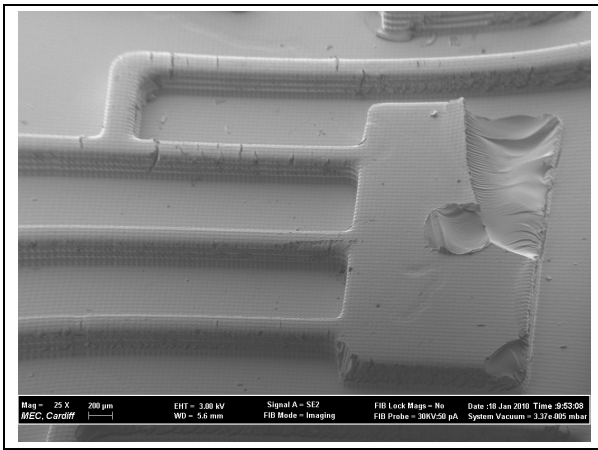

µSL 1 PP Low P_{max}

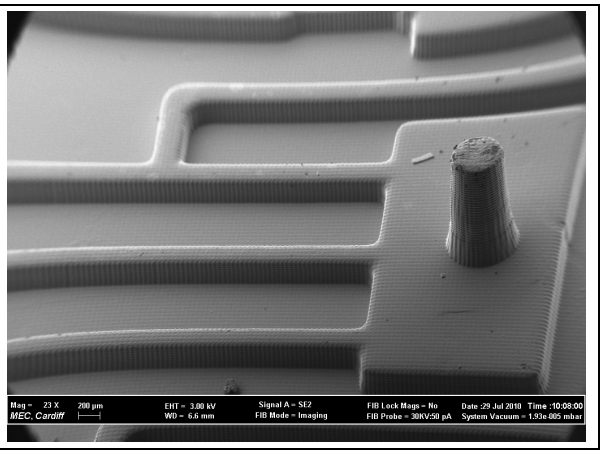

µSL 2 PP Low P_{max}

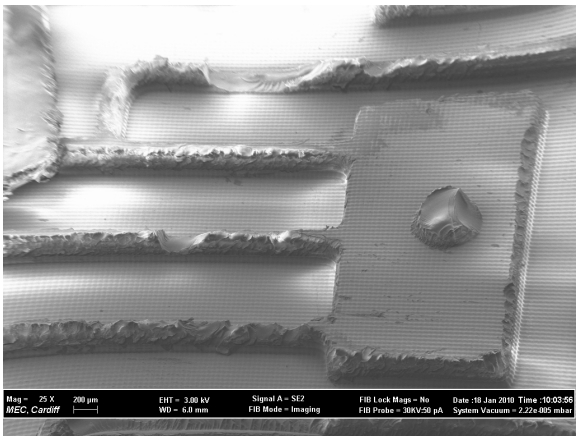

µSL 1 ABS Low P_{max}

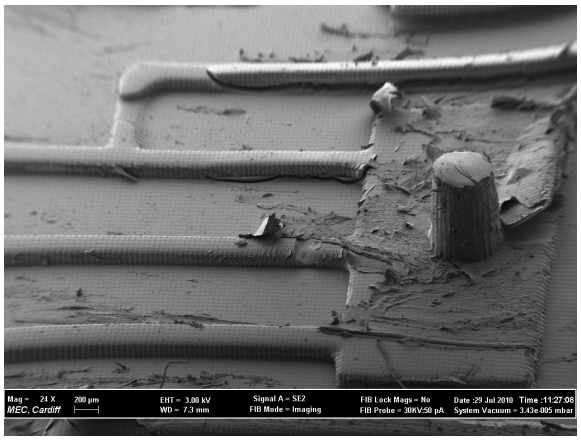

µSL 2 ABS Low P_{max}

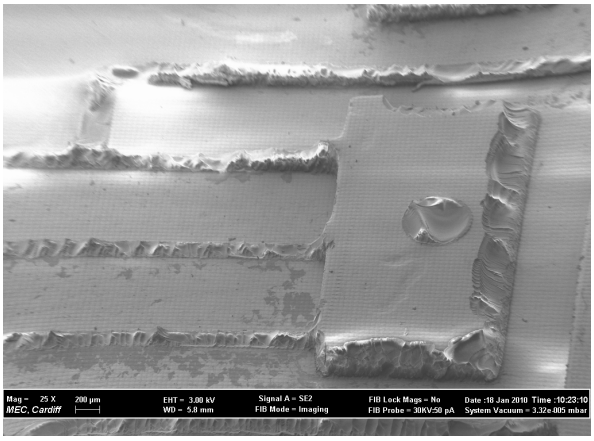

µSL 1 PC Low P_{max}

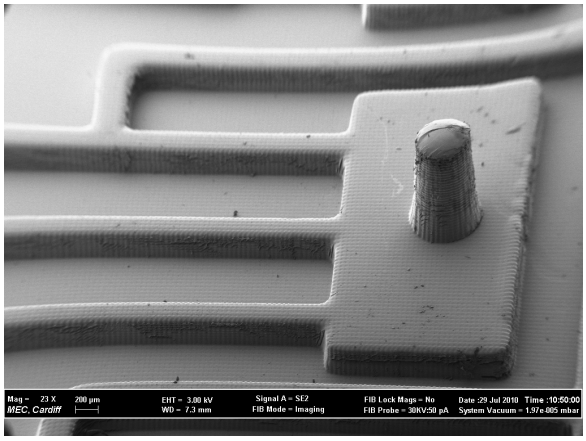

µSL 2 PC Low P_{max}

Figure 6-6 200 µm x 100 µm ribs replicated using the µSL 1 and 2 inserts

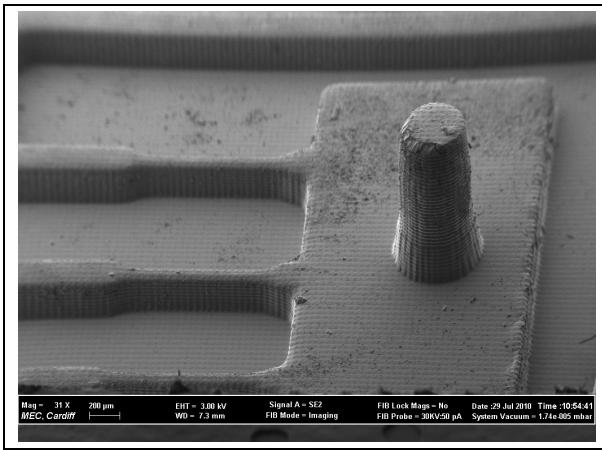

μSL 2 PP Low P_{max}

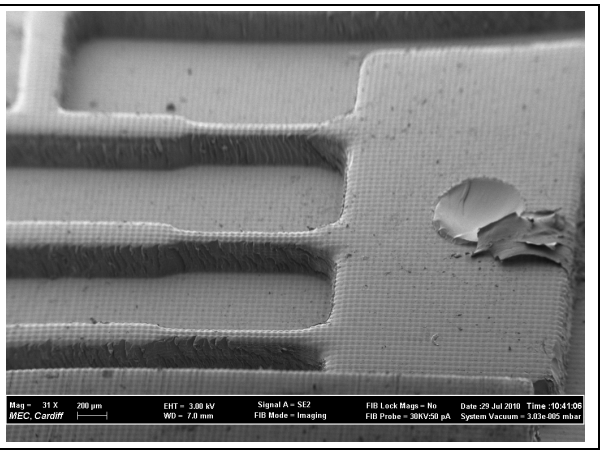

μSL 2 20 μm ABS Low P_{max}

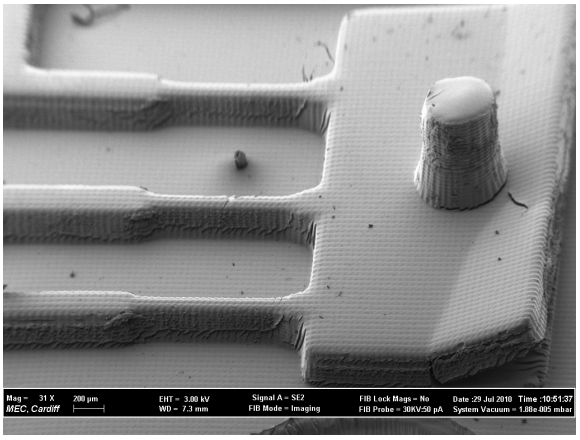

μSL 2 PC Low P_{max}

Figure 6-7 100 μm x 100 μm ribs after moulding using the μSL 2 inserts

6.4.2 Replication results

The μSL inserts were used to mould one polymer part per μSL mould insert and thus to assess the replication accuracy and repeatability of the process. As was already stated the moulding process was not successful when using the μSL 1 insert because of the poor tool performance in particular the undercuts of the mould. So the study is limited to the analysis of mouldings produced with the μSL 2 inserts. The three ribs, R1, R2 and R3 (Figure 6-1 b) of the inserts and their corresponding channels on each moulding were measured as illustrated in Figure 6-8. Five measurements of the three ribs and their corresponding channels C1, C2 and C3 were made for the tree different

materials, and thus in total 90 measurements were taken**.** Figure 6-9, Figure 6-10 and Figure 6-11 present the mean values and σ of the channels measured on the PP, ABS and PC mouldings, and their respective µSL 2 inserts.

The measurements made on the PP mouldings shows consistently that the depth of the channels is smaller (4.22 - 4.80 µm) on average than the height of their corresponding ribs on the µSL 2 insert. PP is a semi crystalline polymer structure and therefore experiences a higher shrinkage in comparison with amorphous polymers such as ABS and PC. At the same time, σ shows that the height and depth variations of the ribs and channels, respectively, are relatively low (0.26 - 0.27).

For the ABS mouldings, the C1 and C2 measurements show that the channels are deeper than the height of their corresponding ribs, R1 and R2, on the µSL 2 insert. A closer inspection suggests that this is due to defects on the channel surface. For the R3 rib and the C3 channel there is an average part shrinkage of 2.10%. The defects on the ABS mouldings and the µSL 2 insert used to replicate them, result in an increase of σ for the channels' depth and ribs' height.

The PC results show an average part shrinkage in the range of 0.28% to 0.47% for C1 and C3. For C2 the measurements show that the channels are 0.5% deeper than the height of their corresponding insert's rib. σ of the channel depths, in the range of 0.12 to 0.28, shows a low variation.

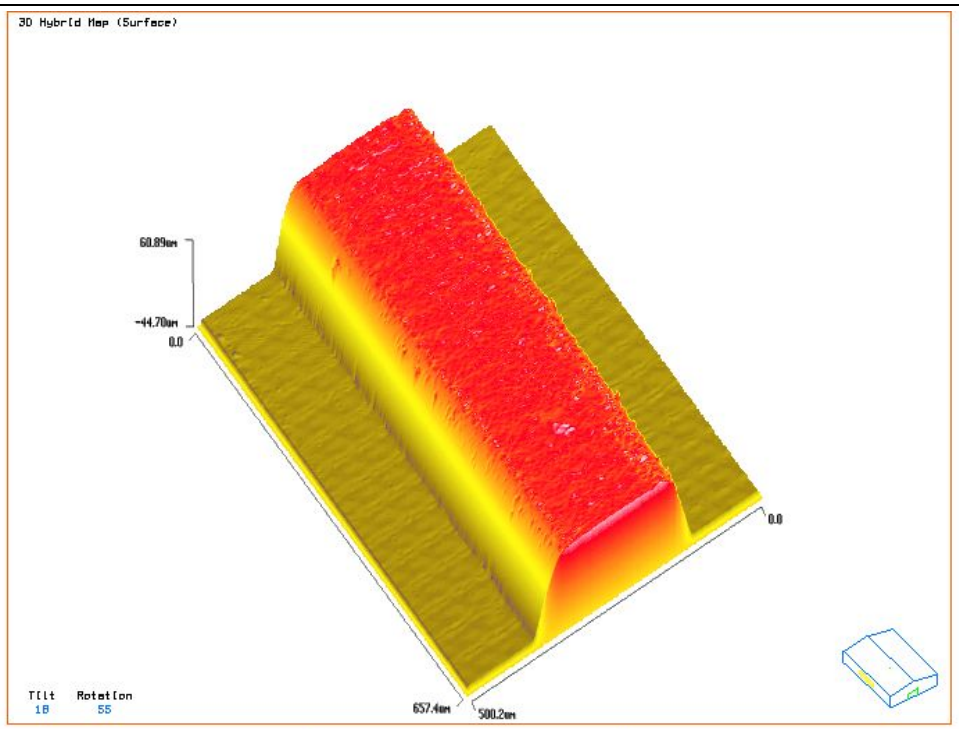

µSL 2 insert rib feature

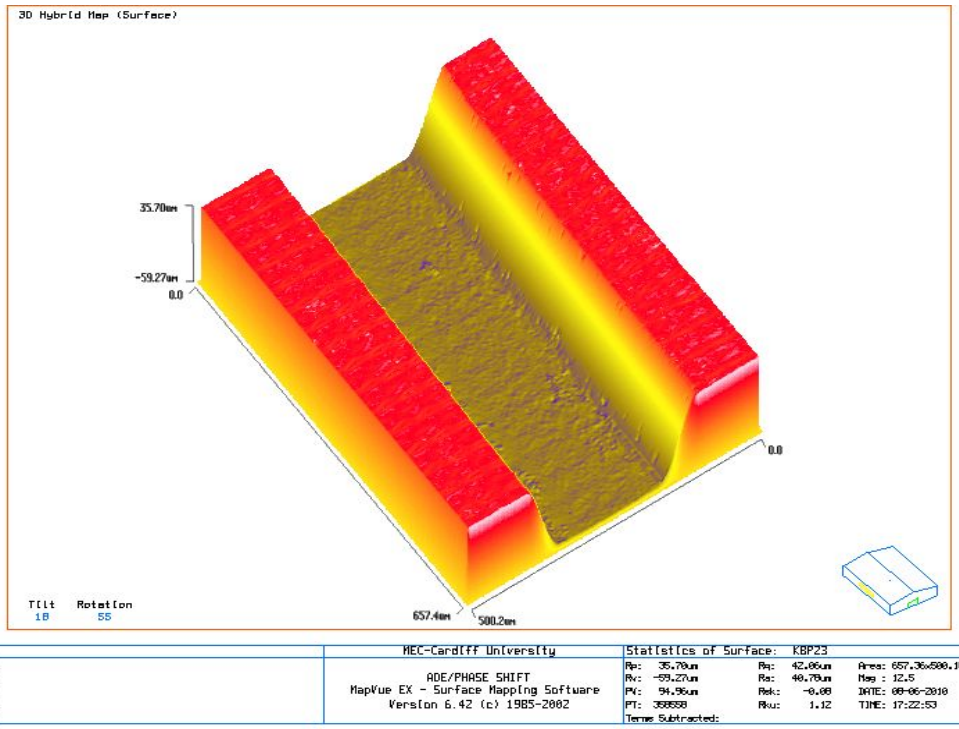

Replicated PP channel feature

Figure 6-8 Measurements of the 200 x 100 µm ribs and channels of the µSL 2 insert and PP mouldings, respectively (measurements taken by white light interferometer)

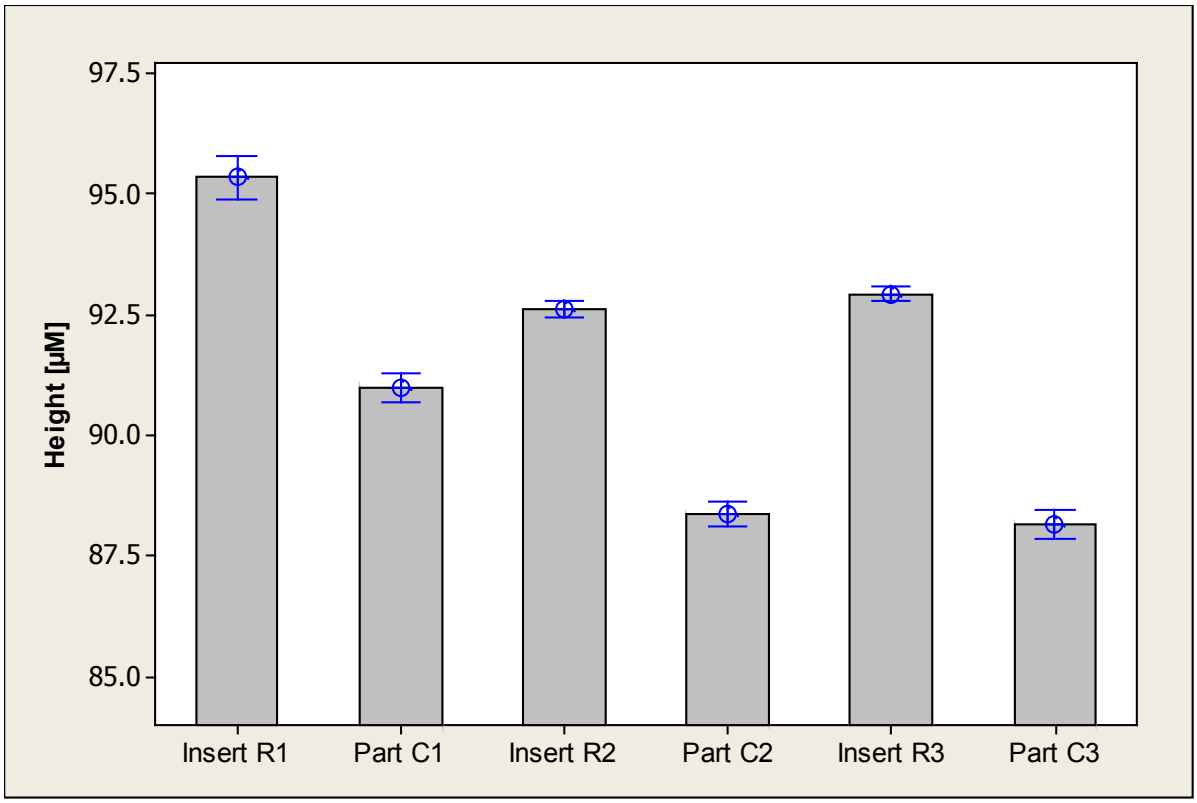

Figure 6-9 PP insert and part measurements

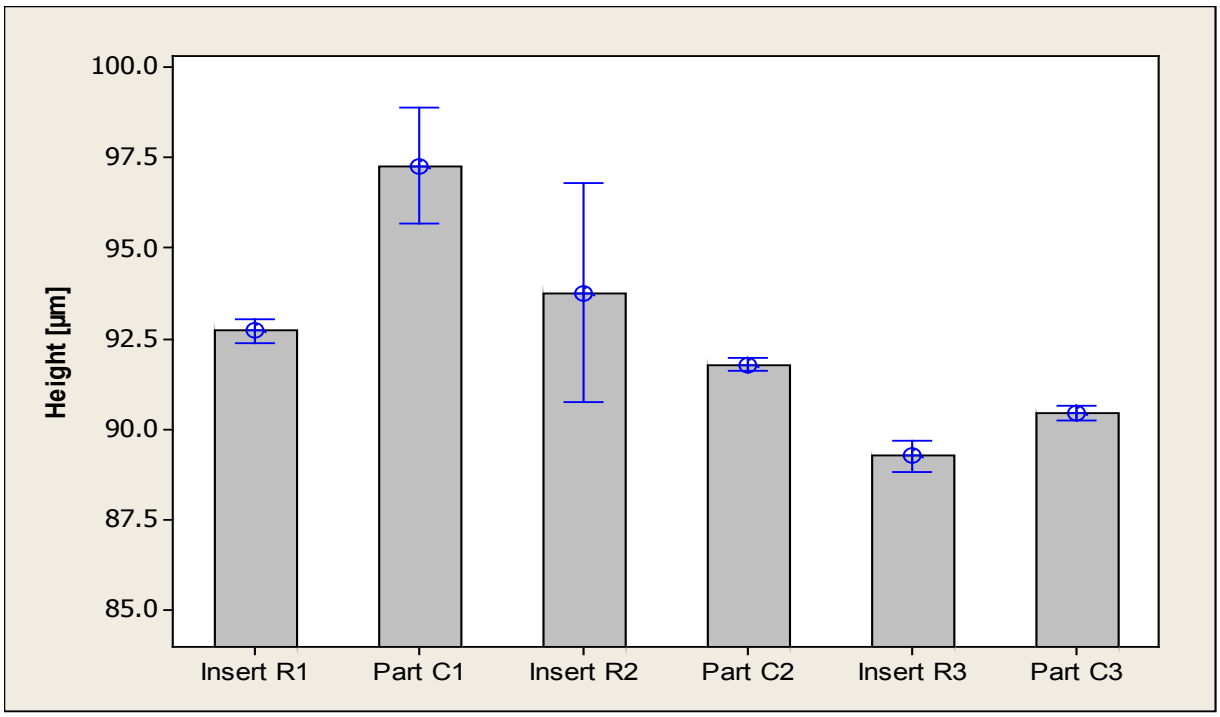

Figure 6-10 ABS insert and part measurements

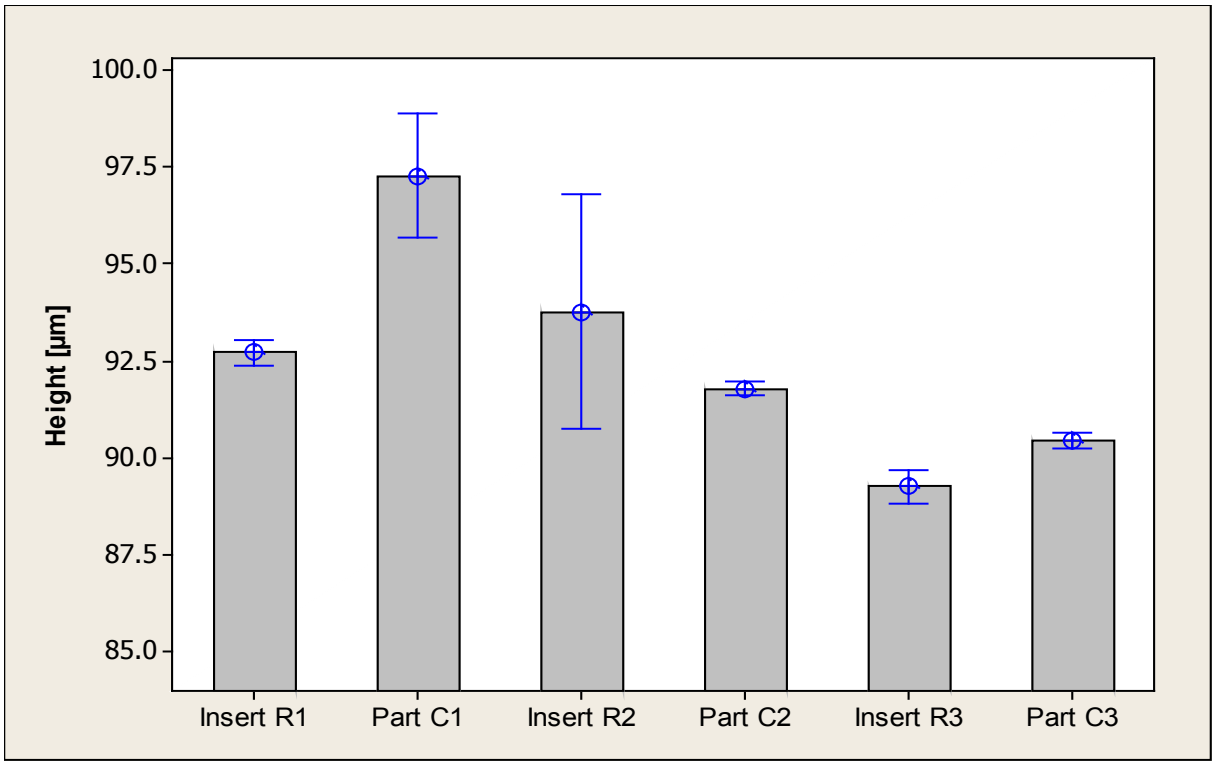

Figure 6-11 PC insert and part measurements

6.5 Conclusion

The chapter reports an experimental study that investigates the potential of using µSL polymer inserts in µ-IM to produce small batches of microfluidic parts with thermoplastic polymer materials. Prior to this study, optimum process parameters for low pressure injection moulding for the three materials ABS, PP and PC were found by using a steel mould insert (Chapter 3). The effects of the moulding process were assessed to judge the tool capabilities. The moulding performance was studied as a function of tool geometry in combination with process factors. The following conclusions can be made based on the obtained results:

- Advances in the µSL process have allowed the accurate manufacture of polymer moulds with features in the micrometre range. It has been

demonstrated that a process chain for rapid tooling can produce μSL inserts employing a fabrication process much faster and cheaper than some of the existing technologies. Also, the use of this layer-based manufacturing process offers high flexibility with regard to part complexity and their dimensions without any increase of the lead time.

- The use of μSL inserts demonstrated the feasibility of this manufacturing route for producing parts with fine details and relatively high aspect ratio structures. However, the two types of μSL inserts used in this study did not behave in the same way. In particular, the presence of significant undercuts at each layer in the builds was observed with a layer thickness of 50 μm. During demoulding these undercuts compromised severely the tool life. The reduction of layer thickness down to 20 μm reduced the resulting undercuts.

- Best replication results and minimum tool damage have been observed for the replication of PP polymer parts.

7 CONTRIBUTIONS, CONCLUSIONS AND FUTURE WORK

The first part of this chapter summarises the most important contributions to the existing knowledge in µ-IM and the main conclusions of the principal open research issues investigated in this thesis. The second part discusses briefly the implication of the results for future work.

7.1 Contributions

The overall aim of this thesis was to investigate systematically important fundamental factors affecting the µ-IM process, in particular, the mould cavity pressure behaviour during the filling and demoulding stage by utilising an advanced condition monitoring system. In order to meet this aim, four main open research issues were investigated:

- The cavity pressure behaviour during the filling stage of polymer micro parts;
- The cavity air flow behaviour in micro injection moulds;
- The demoulding forces applied on polymer micro parts;
- The use of micro stereo lithography (µSL) polymer mould inserts for µ-IM.

The main research findings and generic conclusions of this research and its contribution to the existing knowledge in µ-IM can be summarised as follows.

7.1.1 Cavity pressure behaviour

The use of integratied pressure sensors inside the cavities of injection moulds to assess cavity pressure, which has proven to be a valuable information in macroscopic injection moulding, has been successfully applied in µ-IM. By employing a specially designed condition monitoring setup it was possible to assess the cavity pressure conditions during part filling. It was shown that characteristic variables such as P_{max}, P_{work} and P_{rate} were dependent on both materials and processing conditions and, therefore, can be utilised do gain additional information about the IM cycle.

The process parameters' effects on P suggest that, in the context of P_{max}, P_{work} and P_{rate}, the optimum selection of parameter levels is material dependant and will be diffident for different materials. Temperature can be considered the most influential parameter for P_{max}, while V_i can be considered the most influential parameter for P_{work}, and for both an increase in the parameter setting results in a decrease of the P related factor.

The mould temperature T_m dominates as the most influential parameter for P_{rate}. Also, it can be concluded that the parameters influence is similar for all materials; in particular for all materials an increase of T_b and V_i generally increases P_{rate}, while an increase of T_m and P_h leads to a decrease of P_{rate}.

7.1.2 Air flow behaviour

It has been shown that it is possible to assess the air evacuation conditions during part filling by employing a specially designed sensor and condition monitoring setup. The condition monitoring results showed a strong correlation between key variables

representing the air flow out of micro cavities such as maximum air flow rate, overall air flow and processing parameters.

The carried out research showed that an increased resistance to air evacuation leads to a lower overall flow length of the moulded polymer parts. This indicates that mould evacuation systems, venting systems and optimised tool designs have a major influence on the complete filling of micro features or micro components.

In addition, a restricted venting through the primary split line results in un-evacuated resistant air pockets which prevent the polymer from filling the cavity. It is important to take this into account when designing micro injection moulds because high precision and small tolerances restricts the air evacuation through the primary split line to a minimum. Thus, dedicated venting channels (secondary vents) or active venting systems (vacuum methods) have to be considered.

It was shown that V_i was the most influential parameter in regards to E_a. In particular, an increase of V_i led to an increase of $\dot{Q}_{max}$. This suggests that an increase in the speed of the polymer entering the cavity contributes to an increase in the rate of E_a. However, an increase of V_i led to a decrease of Q which suggests an increased amount of E_a through the split line and not to the secondary vent.

By understanding the effects of V_i and E_a^R on $\dot{Q}_{max}$, Q and flow lengths it will be possible to improve the performance of the µ-IM process. In particular, the research showed clearly that high process settings required in µ-IM, together with the limited venting through the primary split line, have a significant impact on the filling performance. The extreme of this is the inability of the resistant air to vent, resulting in air traps, air compression and diesel effects and, ultimately, part failures.

7.1.3 Demoulding behaviour

It was shown, that the maximum demoulding forces of polymer micro parts were dependent on the process conditions / parameters. A direct correlation between the pressure inside the cavity and the demoulding forces at the end of the moulding cycle was observed. It was shown that high settings for P_h and V_i resulted in an increase of P and F^e_{max}.

The characteristic number P^i_{work} showed the highest correlation with F^e_{max} and hence could be used to estimate the maximum demoulding force during injection cycles. This was confirmed by the study conducted over the whole set of experiments.

Furthermore, a direct correlation between the process factors and demoulding forces was observed. In particular, it was noted that the holding pressure level P_h contributed most to the demoulding forces; a high P_h led to higher F^e_{max}. The effects of process settings on P and F^e_{max} suggested that T_b was the highest contributing factor for P^c_{max} and P^c_{work}, while P_h was for F^e_{max} and P^i_{work}.

The strong effect of P_h on F^e_{max} and P^i_{work} indicates that an effective holding pressure phase is necessary to ensure complete filling, compensate for the polymer shrinkage during cooling, reduce warpage and also to provide dimensional stability. At the same time the holding pressure also leads to large demoulding forces which could cause part deformation and damage during demoulding.

7.1.4 µSL moulds

Recent developments in µSL technologies did allow the accurate manufacture of polymer mould inserts with cavities in the micro meter range. Subsequently, it was

demonstrated in a new process chain for rapid tooling, that polymer micro parts can be successfully replicated in small batches utilising such µSL mould inserts.

The manufacturing of polymer mould inserts by applying a layer based additive technology, in particular µSL, is cheaper and faster than by using some other existing technologies and offers a high flexibility with regard to part complexity and dimensions without any increase of the lead time. However, the use of this layer-based technology inherently leads to the formation of some significant undercuts at each layer and they could compromise severely the tool life. It was shown that by reducing the layer thickness during the µSL build process down to 20 µm the amount of undercuts was significantly reduced and the tool life extended.

Ribs with dimensions of 200 µm x 100 µm and 100 µm x 100 µm were successfully replicated in PP and PC and thus the µSL technology could be considered a viable prototype tooling solution. The shrinkage observed during the moulding trials is significant and needs to be taken into consideration during the tool design and should be compensated for in the CAD models for the mould inserts. The highest amount of shrinkage was observed during the PP moulding trials.

7.2 Future Work

In Chapter 3 a condition monitoring system has shown its potential for the µ-IM process. Further research should be undertaken to directly use key numbers calculated from cavity pressure curves as input parameters for the control of the µ-IM process. This approach has been proven beneficial for macroscopic injection moulding and could help in µ-IM as well to control and predict part quality inline.

Currently, sensors with smaller dimensions for assessing the cavity pressure in micro injection moulds are under development. These sensors could allow the assessment of the pressure in even smaller µ-IM cavities and could be positioned at the bottom of micro channels. The analysis of the pressure drop at the end of small channels should be the focus of future research.

In Chapter 4 it was shown that venting through the primary split line is limited due to the high accuracy and surface quality of micro injection moulds and hence may lead to part failures. Future work in this area should focus on optimising secondary vents and active vacuum methods for E_a^R. more precise design rules should be developed and introduced to ensure air traps are not in the functional area of micro parts and therefore do not lead to part failures.

In Chapter 5 it has been observed, that the holding pressure is the factor with the highest influence on demoulding forces. Future research in this area is required to identify the optimum level and time of P_h to ensure complete filling and, at the same time, to avoid part damage at the demoulding stage.

In Chapter 6 a process chain for rapid tool making has been investigated. In this context the interactions between the µSL mould and the polymer micro part should be investigated in future research. In particular, a study investigating the maximum acceptable demoulding forces in relation to tool wear and tool life should be conducted. Furthermore, it should be investigated, how tool life could be maximised, too.

Recently, new materials such as bulk metallic glasses / amorphous metals for making micro injection moulds have been made commercially available. These materials have properties that are beneficial for some structuring processes such as focused ion

beam machining and can be used to design new tool making process chains for achieving function and length scale integration in new emerging products. These materials have a great potential and shall be investigated further as new manufacturing routes for fabricating micro and nano replication masters.

8 APPENDICES

8.1 Appendix Chapter 3

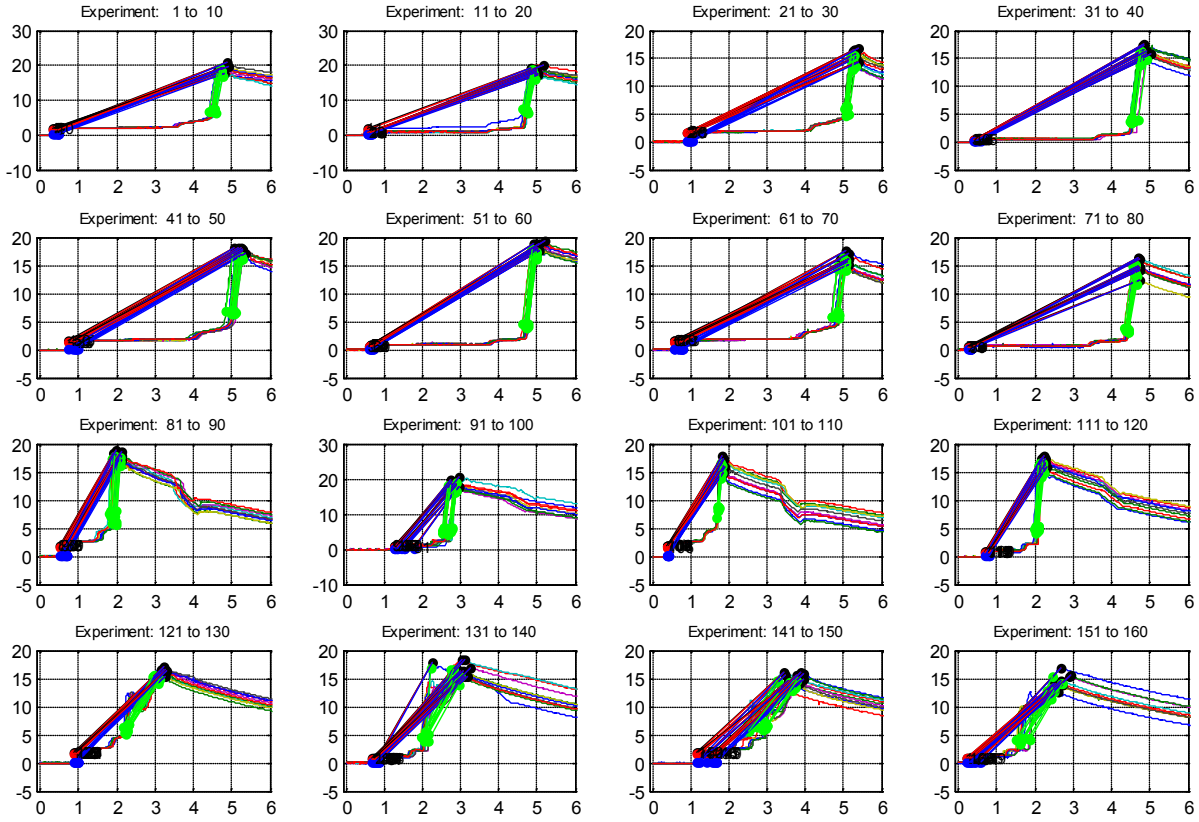

Figure 8-1 Cavity pressure curves for experiments utilising PP

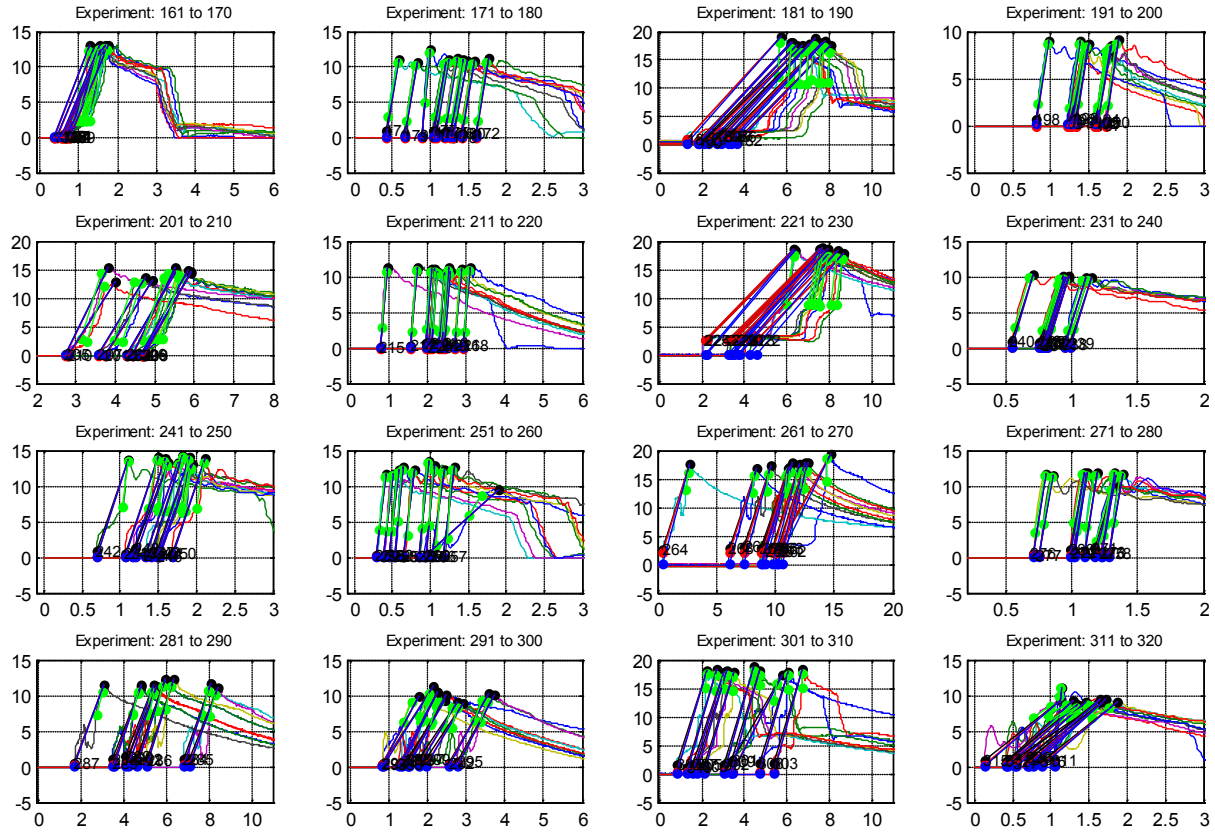

Figure 8-2 Cavity pressure curves for experiments utilising ABS

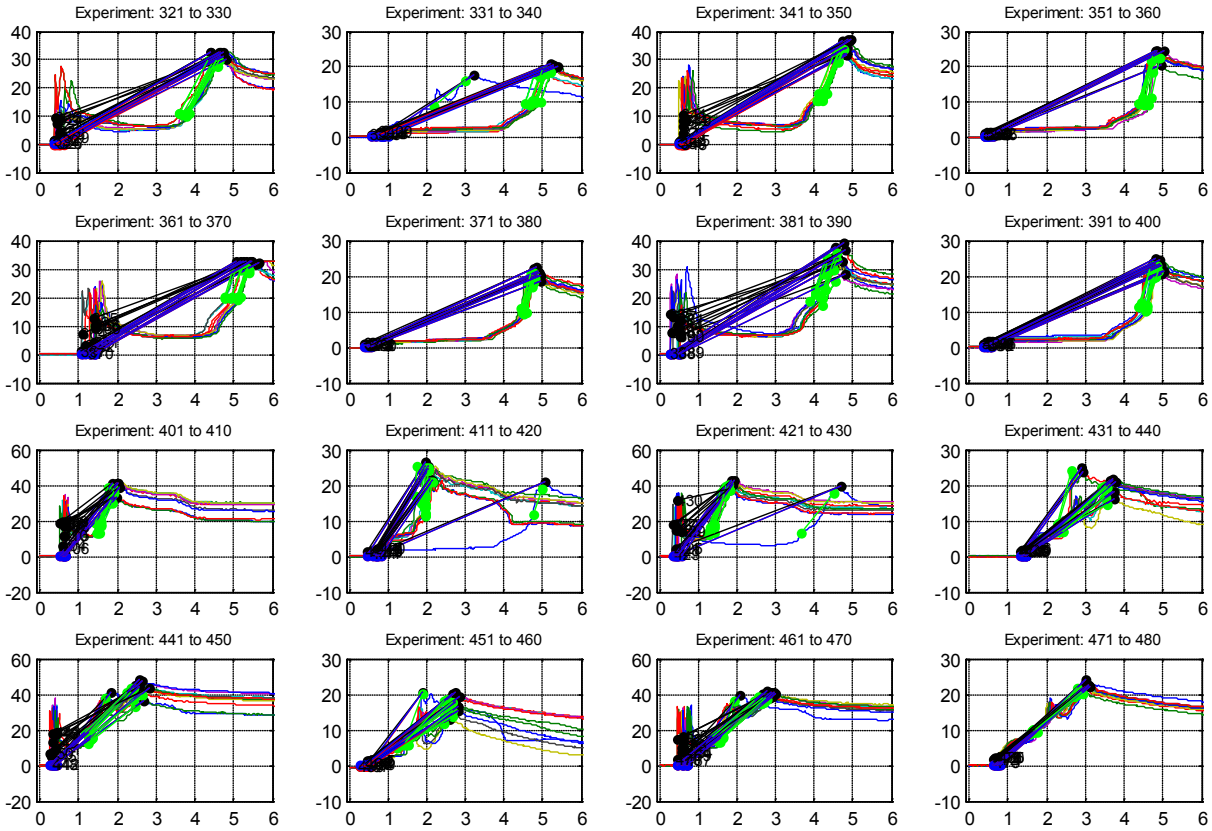

Figure 8-3 Cavity pressure curves for experiments utilising PC

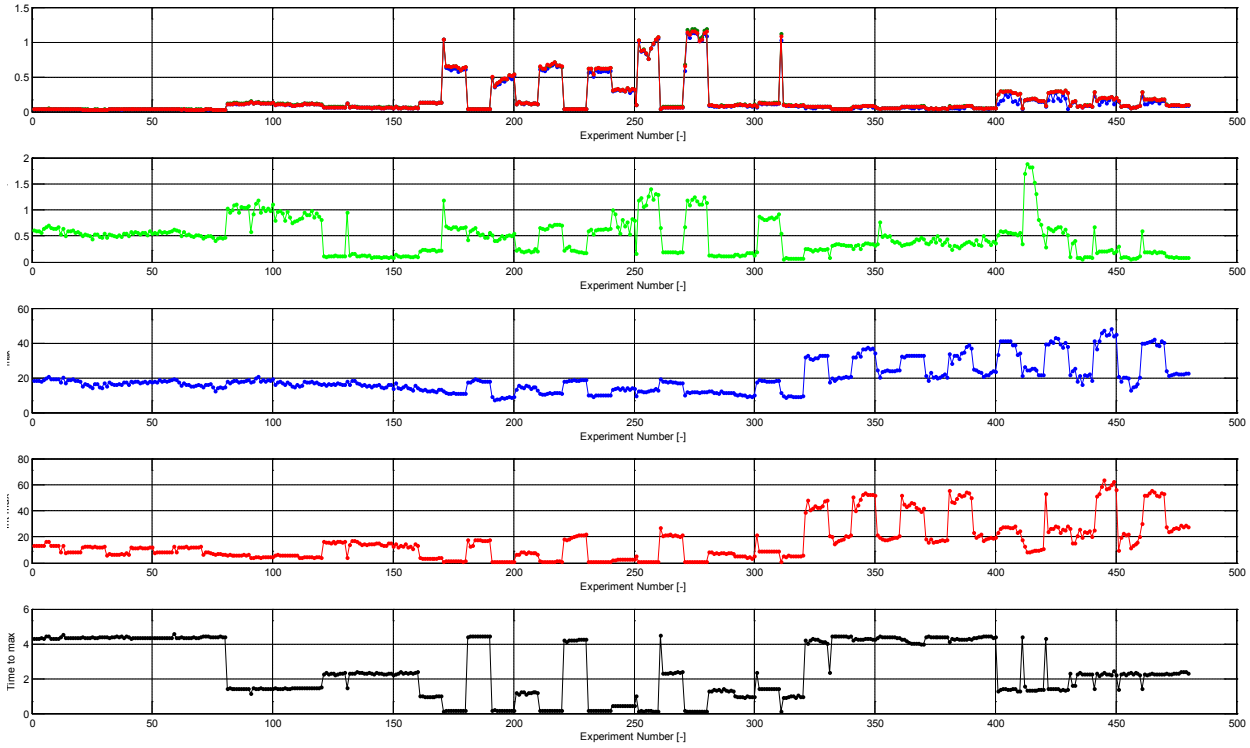

Figure 8-4 Distribution of all characteristic variables

8.2 Appendix Chapter 4

Key Numbers	Experiment:		1									
K_Start	0.219383	0.202967	0.2057	0.202967	0.2057	0.211167	0.213917	0.268667	0.222117	0.2276	0.224867	0.26045
Q_dot__max	15.20877	14.64205	15.0801	15.13212	15.0582	15.08557	15.23342	14.97332	15.13485	15.02533	15.12663	15.04998
Q_to_max	4.423269	4.622544	4.577699	4.59613	4.601364	4.613997	4.581707	4.533738	4.542729	4.613594	4.648788	4.612236
Q	4.988085	4.880756	4.800421	4.875633	4.805275	4.927961	4.935249	4.962577	4.95642	4.855516	4.89689	4.804114
Time_to_max	0.394	0.376	0.394	0.394	0.396	0.396	0.396	0.395	0.396	0.395	0.396	0.396
Gradient1	0.038044	0.038402	0.037752	0.037891	0.037506	0.037562	0.037928	0.037227	0.037658	0.037463	0.037631	0.037347
Gradient2	0.038601	0.038942	0.038274	0.038406	0.038026	0.038095	0.038468	0.037907	0.038219	0.038039	0.038199	0.038005
Gradient3	0.038093	0.03841	0.037767	0.037899	0.037521	0.03759	0.037963	0.037401	0.037714	0.037532	0.037694	0.0375
Gradient_slope	0.169837	0.185686	0.16552	0.168563	0.170703	0.172192	0.156228	0.175617	0.152803	0.172285	0.171136	0.172089
	Experiment:		2									
K_Start	0.233417	0.356617	0.340183	0.362083	0.27175	0.307333	0.362083	0.27995	0.31555	0.255317		
Q_dot__max	34.31615	34.10808	34.08618	34.42018	34.78432	34.43113	34.2395	34.35173	34.44483	34.4284		
Q_to_max	2.137356	2.205552	2.169424	2.111949	2.146188	2.022763	2.130736	2.208076	2.107961	2.277003		
Q	3.713625	3.707434	3.701118	3.715267	3.700733	3.734963	3.725605	3.732575	3.724705	3.733569		
Time_to_max	0.105	0.108	0.107	0.106	0.104	0.103	0.103	0.104	0.107	0.104		
Gradient1	0.324597	0.312514	0.315383	0.321303	0.331852	0.331299	0.328907	0.327613	0.318965	0.328587		
Gradient2	0.32682	0.315816	0.318562	0.324719	0.334465	0.334283	0.332422	0.330305	0.321914	0.331042		
Gradient3	0.324916	0.313964	0.316693	0.322832	0.332542	0.332341	0.330481	0.328382	0.320045	0.329119		
Gradient_slope	0.41883	0.423094	0.422304	0.427463	0.440086	0.438261	0.441496	0.434308	0.433044	0.436309		
	Experiment:		3									
K_Start	0.230917	0.219967	0.271983	0.241867	0.217233	0.288417	0.217233	0.2583	0.29115	0.2008	0.324	
Q_dot__max	15.55157	15.60085	15.54883	15.64465	15.61455	15.47765	15.57073	15.52967	15.53515	15.60633	15.55978	
Q_to_max	4.644224	4.79055	3.969198	4.315618	3.822866	4.185992	4.023453	4.542578	4.675427	4.650671	4.722459	
Q	5.232686	5.276775	5.263133	5.282848	5.256212	5.254605	5.256125	5.262802	5.252579	5.290919	5.266024	
Time_to_max	0.392	0.392	0.392	0.392	0.392	0.392	0.392	0.392	0.391	0.392	0.391	
Gradient1	0.039083	0.039237	0.038972	0.039293	0.039279	0.038748	0.039167	0.038958	0.038987	0.0393	0.038966	
Gradient2	0.039672	0.039798	0.039665	0.03991	0.039833	0.039484	0.039721	0.039616	0.039732	0.039812	0.039795	
Gradient3	0.039162	0.039288	0.039155	0.0394	0.039323	0.038974	0.039211	0.039106	0.03922	0.039302	0.039283	
Gradient_slope	0.158488	0.160617	0.165773	0.162501	0.162678	0.167655	0.167872	0.168675	0.167979	0.172433	0.170671	
	Experiment:		4									
K_Start	0.21425	0.233417	0.274483	0.233417	0.3265	0.2252	0.329233	0.216983	0.329233	0.318283		
Q_dot__max	37.1087	37.13335	37.19357	37.21548	37.17442	37.13608	37.17988	37.24012	36.5803	36.84862		
Q_to_max	2.200127	2.457452	2.52988	2.614026	2.602659	2.388416	2.667265	2.1546	2.680001	2.2425		
Q	4.014581	4.004944	4.005284	3.997391	3.990683	4	3.982908	4.009297	3.949466	4.00452		
Time_to_max	0.099	0.099	0.099	0.099	0.099	0.099	0.098	0.1	0.099	0.099		
Gradient1	0.372671	0.372727	0.37292	0.373556	0.372201	0.372837	0.376027	0.370231	0.366172	0.368993		
Gradient2	0.374835	0.375084	0.375693	0.375914	0.375499	0.375112	0.379387	0.372401	0.369498	0.372208		
Gradient3	0.372815	0.373064	0.373672	0.373894	0.373479	0.373092	0.377346	0.370401	0.367478	0.370188		
Gradient_slope	0.527143	0.529853	0.524108	0.523572	0.52381	0.531192	0.525476	0.519655	0.515716	0.521608		
	Experiment:		5									
K_Start	0.266983	0.291633	0.239617	0.223183	0.26425	0.26425	0.22865	0.234133	0.247817	0.212233	0.30805	
Q_dot__max	16.0914	16.02295	16.00105	15.9326	15.9463	15.93808	15.93535	15.98188	15.8094	15.80393	15.79572	
Q_to_max	4.427536	4.155923	4.224247	4.106073	4.325165	4.165533	4.259869	4.533456	4.398422	4.225194	4.00463	
Q	5.097458	5.076867	5.043141	5.019048	5.038683	5.025942	5.033328	5.027185	5.045519	5.052996	5.0364	
Time_to_max	0.371	0.369	0.368	0.369	0.369	0.369	0.37	0.371	0.372	0.373	0.372	
Gradient1	0.042653	0.042632	0.04283	0.042573	0.042499	0.042477	0.042451	0.042447	0.041832	0.041801	0.041634	
Gradient2	0.043373	0.043423	0.043481	0.043178	0.043215	0.043193	0.043069	0.043078	0.042498	0.04237	0.042462	
Gradient3	0.042834	0.042881	0.042938	0.042636	0.042673	0.042651	0.042528	0.042539	0.041961	0.041834	0.041924	
Gradient_slope	0.266408	0.265425	0.260774	0.261353	0.258721	0.258379	0.259131	0.254748	0.259879	0.257078	0.259177	
	Experiment:		6									
K_Start	0.20925	0.34615	0.201033	0.247583	0.34615	0.3571	0.274967	0.2558	0.318767	0.225683	0.280433	
Q_dot__max	39.38428	39.38155	38.94625	38.88875	38.03182	38.42058	38.22893	38.04277	37.93873	37.64853	37.50617	
Q_to_max	2.463527	1.960891	2.251061	2.107018	1.951114	2.235921	2.12837	2.15249	1.791441	2.234695	2.455818	
Q	3.889644	3.886221	3.858592	3.861606	3.790875	3.820263	3.814847	3.795915	3.785736	3.819066	3.809098	
Time_to_max	0.098	0.098	0.098	0.098	0.097	0.097	0.099	0.098	0.098	0.098	0.099	
Gradient1	0.399745	0.39832	0.395359	0.394298	0.388512	0.392407	0.383373	0.385581	0.383877	0.381866	0.376018	
Gradient2	0.40188	0.401853	0.397411	0.396824	0.392081	0.396088	0.386151	0.388191	0.38713	0.384169	0.37885	
Gradient3	0.39984	0.399812	0.39537	0.394783	0.390019	0.394027	0.384131	0.386151	0.385089	0.382128	0.37683	
Gradient_slope	0.671911	0.672632	0.668093	0.662184	0.662471	0.672386	0.658798	0.65851	0.659585	0.656699	0.652703	
	Experiment:		7									
K_Start	0.231633	0.253533	0.2289	0.269967	0.231633	0.245317	0.207	0.28365	0.253533	0.215217	0.28365	
Q_dot__max	15.99582	16.10258	16.11902	16.17377	16.07522	16.09985	16.06427	16.05878	16.05605	16.07795	16.09712	
Q_to_max	4.522684	4.466754	4.679154	4.703044	4.66374	4.757649	4.721957	4.767035	4.404694	4.490011	4.751563	
Q	5.233005	5.250272	5.257954	5.275451	5.285118	5.292168	5.28836	5.282583	5.286687	5.290359	5.279585	
Time_to_max	0.371	0.372	0.372	0.37	0.37	0.37	0.37	0.369	0.37	0.37	0.369	
Gradient1	0.042491	0.042605	0.042715	0.042983	0.04282	0.04285	0.042857	0.042751	0.04271	0.042872	0.042855	
Gradient2	0.043115	0.043287	0.043331	0.043713	0.043447	0.043513	0.043417	0.04352	0.043395	0.043454	0.043624	
Gradient3	0.042576	0.042749	0.042793	0.043172	0.042906	0.042973	0.042876	0.042978	0.042854	0.042913	0.043082	
Gradient_slope	0.273058	0.256484	0.263238	0.276444	0.289445	0.290281	0.290966	0.288761	0.289065	0.28547	0.288381	
	Experiment:		8									
K_Start	0.3327	0.357333	0.212233	0.234133	0.346383	0.3546	0.204017	0.225917	0.269733	0.357333	0.236867	0.236867
Q_dot__max	40.0854	40.288	40.39203	40.43037	40.47417	40.47143	40.46322	40.51523	40.47692	40.5563	40.55357	40.58368
Q_to_max	2.48736	2.049648	2.042995	2.031012	2.275447	2.126604	2.22278	2.137498	2.241433	2.518325	2.082039	2.456043
Q	4.031663	4.028254	4.03805	4.037404	4.045018	4.044683	4.038915	4.043328	4.047227	4.048571	4.05158	4.045973
Time_to_max	0.095	0.094	0.095	0.095	0.094	0.094	0.095	0.096	0.095	0.095	0.096	0.095
Gradient1	0.418449	0.424794	0.422945	0.423118	0.426891	0.426775	0.423781	0.41968	0.423234	0.423147	0.419966	0.424703
Gradient2	0.421952	0.428596	0.425179	0.425583	0.430576	0.430547	0.425929	0.422034	0.426073	0.426908	0.422433	0.427197
Gradient3	0.419846	0.426468	0.423074	0.423478	0.428449	0.42842	0.423823	0.41995	0.423968	0.424803	0.42035	0.425091
Gradient_slope	0.720647	0.740689	0.727187	0.736693	0.727263	0.732511	0.7446	0.732891	0.711085	0.72635	0.713823	0.721223

Q [ml]		
max(Q)	4.988085	ml
min(Q)	4.800421	ml
average(Q)	4.890741	ml
Q_dot_max [ml/sec]		
max(Q_dot	15.23342	ml/sec
min(Q_dot	14.64205	ml/sec
average(Q_	15.06253	ml/sec

	Experiment:		9														
K_Start	0.2397	0.215067	0.258867	0.2096	0.283517	0.261617	0.22055	0.256133	0.22055	0.201383	0.236967						
Q_dot__max	13.93685	13.94233	14.1504	14.2079	13.89305	13.89305	14.16957	14.0409	14.11755	14.10387	14.15315						
Q_to_max	4.185394	4.086423	4.375473	4.415516	4.131511	4.181525	4.279817	4.366184	4.331307	4.12384	4.455216						
Q	4.705176	4.679909	4.551934	4.6594	4.73038	4.678847	4.735054	4.693239	4.729468	4.682888	4.661829						
Time_to_max	0.391	0.391	0.389	0.389	0.39	0.388	0.391	0.39	0.391	0.388	0.391						
Gradient1	0.035031	0.035108	0.035711	0.035985	0.034896	0.035133	0.035675	0.035346	0.035542	0.035831	0.035591						
Gradient2	0.035644	0.035658	0.036376	0.036524	0.035623	0.035807	0.036239	0.036002	0.036106	0.03635	0.036197						
Gradient3	0.035133	0.035147	0.035862	0.03601	0.03511	0.035291	0.035728	0.035489	0.035595	0.035835	0.035686						
Gradient_slope	0.172744	0.164168	0.162165	0.161049	0.17227	0.171428	0.156337	0.148334	0.163925	0.177097	0.172842						
	Experiment:		**10**														
K_Start	0.280533	0.2778	0.302433	0.228517	0.225783	0.2641	0.31065	0.261367	0.313383	0.275067	0.283267						
Q_dot__max	33.79107	32.75618	33.57478	33.3804	32.9889	33.03543	32.98068	33.0765	32.99985	33.0683	33.32292						
Q_to_max	1.978754	1.875878	1.890501	1.951636	2.137693	2.005581	2.125913	1.793074	1.809183	2.328566	1.868733						
Q	3.643168	3.56832	3.624494	3.636077	3.601699	3.600971	3.60525	3.61671	3.612272	3.607399	3.638684						
Time_to_max	0.098	0.098	0.1	0.099	0.098	0.099	0.098	0.098	0.098	0.1	0.098						
Gradient1	0.341944	0.331412	0.332724	0.334868	0.334318	0.331024	0.333368	0.334848	0.333535	0.327932	0.337139						
Gradient2	0.344807	0.334247	0.335748	0.337176	0.336621	0.333691	0.336538	0.337515	0.336733	0.330683	0.34003						
Gradient3	0.342766	0.332206	0.333748	0.335156	0.334581	0.331671	0.334497	0.335474	0.334692	0.328683	0.337989						
Gradient_slope	0.473935	0.468527	0.465599	0.469471	0.47455	0.4634	0.471435	0.467269	0.476375	0.4659	0.468686						
	Experiment:		**11**														
K_Start	0.213767	0.221983	0.249367	0.254833	0.24115	0.282217	0.254833	0.30685	0.26305	0.312333	0.2302	0.21925					
Q_dot__max	14.94307	15.09912	15.069	15.12923	15.18125	15.17303	15.33183	15.32635	15.33457	15.35373	15.32635	15.351					
Q_to_max	4.555415	4.415068	4.474483	4.681506	4.804313	4.333665	4.701709	4.830833	4.552699	4.447398	4.714067	4.497563					
Q	5.121272	5.15726	5.157783	5.163836	5.110145	5.192432	5.202091	5.150902	5.193442	5.215594	5.207805	5.207906					
Time_to_max	0.393	0.393	0.393	0.393	0.393	0.394	0.393	0.393	0.393	0.393	0.394	0.394					
Gradient1	0.037479	0.037855	0.037709	0.037848	0.038016	0.037794	0.038364	0.038218	0.03835	0.038273	0.038315	0.038405					
Gradient2	0.038023	0.03842	0.038344	0.038497	0.038629	0.03851	0.039012	0.038998	0.039019	0.039068	0.038899	0.038962					
Gradient3	0.037514	0.037911	0.037835	0.037988	0.03812	0.038003	0.038503	0.038489	0.03851	0.038559	0.038392	0.038454					
Gradient_slope	0.164499	0.160632	0.15951	0.157202	0.155315	0.158567	0.1543	0.153145	0.151336	0.151574	0.154642	0.154942					
	Experiment:		**12**														
K_Start	0.342933	0.222467	0.211517	0.296383	0.227933	0.23615	0.2471	0.255317	0.244367	0.25805	0.3265						
Q_dot__max	36.44068	36.52282	36.5146	36.65423	36.61042	36.70625	36.7035	36.74457	36.82672	36.7172	36.73088						
Q_to_max	2.16087	2.138675	2.549092	1.916933	2.332982	2.084878	2.661697	2.132244	2.549396	2.064593	2.22793						
Q	3.975536	3.982244	3.965127	3.998547	3.987224	3.992072	3.962597	3.986709	3.97316	3.977882	3.973532						
Time_to_max	0.1	0.1	0.101	0.1	0.1	0.101	0.1	0.1	0.1	0.1	0.099						
Gradient1	0.360978	0.363004	0.359436	0.363579	0.363825	0.36109	0.364564	0.364893	0.365824	0.364592	0.367721						
Gradient2	0.364407	0.365228	0.361531	0.366542	0.366104	0.363428	0.367035	0.367446	0.368267	0.367172	0.371019						
Gradient3	0.362407	0.363228	0.35955	0.364542	0.364104	0.361448	0.365035	0.365446	0.366267	0.365172	0.368999						
Gradient_slope	0.492688	0.489449	0.490623	0.494456	0.495083	0.496794	0.497992	0.500388	0.499989	0.503069	0.50521						
	Experiment:		**13**														
K_Start	0.20435	0.231733	0.237217	0.256367	0.21805	0.259117	0.256367	0.21805	0.226267	0.267333	0.242683	0.242683					
Q_dot__max	14.35872	14.66262	14.43812	14.48192	14.36145	14.3724	14.67082	14.857	14.6982	14.9008	14.81318	14.69547					
Q_to_max	3.972418	3.911349	3.98623	4.027568	3.838718	3.943203	3.811537	4.040517	3.946195	3.926661	3.976264	3.949404					
Q	4.830222	4.826753	4.793574	4.799427	4.7739	4.817538	4.796564	4.784736	4.803518	4.814745	4.812237	4.809721					
Time_to_max	0.348	0.356	0.357	0.361	0.36	0.358	0.367	0.37	0.369	0.369	0.368	0.367					
Gradient1	0.040673	0.040536	0.039778	0.039406	0.039287	0.039423	0.039276	0.039565	0.039219	0.039657	0.039594	0.039381					
Gradient2	0.041261	0.041187	0.040443	0.040116	0.039893	0.040146	0.039975	0.040154	0.039833	0.040382	0.040253	0.040042					
Gradient3	0.040686	0.040625	0.039883	0.039562	0.039337	0.039588	0.03943	0.039614	0.039291	0.03984	0.03971	0.039497					
Gradient_slope	0.281245	0.282314	0.2839	0.272762	0.276838	0.276114	0.274013	0.276908	0.265337	0.249068	0.254614	0.250868					
	Experiment:		**14**														
K_Start	0.2265	0.2046	0.284	0.231967	0.300417	0.325067	0.2046	0.245667	0.2484	0.201867	0.234717						
Q_dot__max	37.98883	37.92313	37.66577	37.45497	37.21403	36.93752	36.83895	36.80063	36.53507	36.75408	36.65827						
Q_to_max	2.397882	2.550676	2.663733	2.440507	2.426632	2.660724	2.246825	2.343036	2.286457	2.265792	2.479674						
Q	3.764208	3.744934	3.723618	3.749807	3.720825	3.715473	3.705017	3.705162	3.674578	3.695977	3.697825						
Time_to_max	0.098	0.097	0.097	0.097	0.097	0.096	0.097	0.098	0.097	0.098	0.098						
Gradient1	0.38533	0.388851	0.385379	0.383742	0.380553	0.38138	0.377674	0.37301	0.374089	0.372982	0.371669						
Gradient2	0.387641	0.39096	0.388307	0.386134	0.38365	0.384766	0.379783	0.375517	0.37665	0.375042	0.374064						
Gradient3	0.3856	0.388898	0.386245	0.384072	0.381588	0.382682	0.377721	0.373476	0.374588	0.373001	0.372023						
Gradient_slope	0.667059	0.670388	0.663951	0.654405	0.650336	0.662241	0.647228	0.654109	0.662165	0.64856	0.653814						
	Experiment:		**15**														
K_Start	0.301867	0.211517	0.2252	0.21425	0.288167	0.216983	0.23615	0.2252	0.227933	0.222467	0.208767						
Q_dot__max	15.28577	15.4035	15.44182	15.55682	15.69917	15.66905	15.63073	15.64715	15.58967	15.64715	15.62798						
Q_to_max	4.421886	4.065454	4.271059	4.312789	4.583222	4.306771	4.513381	4.369431	3.987383	4.487035	4.770273						
Q	5.090056	5.088167	5.11065	5.142715	5.196791	5.160237	5.180937	5.179839	5.138649	5.180715	5.086231						
Time_to_max	0.368	0.37	0.37	0.37	0.372	0.37	0.37	0.37	0.37	0.37	0.37						
Gradient1	0.040717	0.041059	0.041126	0.041466	0.041427	0.041762	0.041607	0.041681	0.041518	0.041688	0.041674						
Gradient2	0.041537	0.041631	0.041735	0.042045	0.042202	0.042349	0.042245	0.04229	0.042134	0.04229	0.042238						
Gradient3	0.040994	0.041091	0.041194	0.041505	0.041664	0.041808	0.041705	0.041749	0.041594	0.041749	0.041697						
Gradient_slope	0.281601	0.285512	0.285825	0.289032	0.284197	0.283969	0.283589	0.27807	0.281231	0.27696	0.279178						
	Experiment:		**16**														
K_Start	0.340183	0.3484	0.219733	0.208767	0.233417	0.2827	0.2033	0.227933	0.3046	0.334717							
Q_dot__max	39.69045	39.74793	39.95602	40.00528	40.1367	40.05183	40.08468	40.1148	40.24622	40.05732							
Q_to_max	2.456779	2.380865	2.670343	2.398806	2.915766	2.721153	2.833545	2.847886	2.571856	2.854604							
Q	3.969076	3.997371	3.98084	4.016319	3.97341	3.991791	3.984019	3.984005	3.997943	4.006058							
Time_to_max	0.095	0.096	0.096	0.096	0.095	0.095	0.096	0.096	0.096	0.096							
Gradient1	0.414213	0.410412	0.41392	0.414547	0.420035	0.418622	0.415431	0.415488	0.416059	0.413777							
Gradient2	0.417794	0.414041	0.416209	0.416722	0.422492	0.421598	0.417549	0.417863	0.419231	0.417264							
Gradient3	0.415689	0.411958	0.414125	0.414638	0.420386	0.419493	0.415465	0.415779	0.417148	0.41518							
Gradient_slope	0.714867	0.682069	0.709315	0.688554	0.701614	0.702724	0.69821	0.701392	0.69583	0.68668							

Table 8-1 Complete table of characteristic variables

8.3 Appendix Chapter 5

8.3.1 Cavity pressure and demoulding force curves

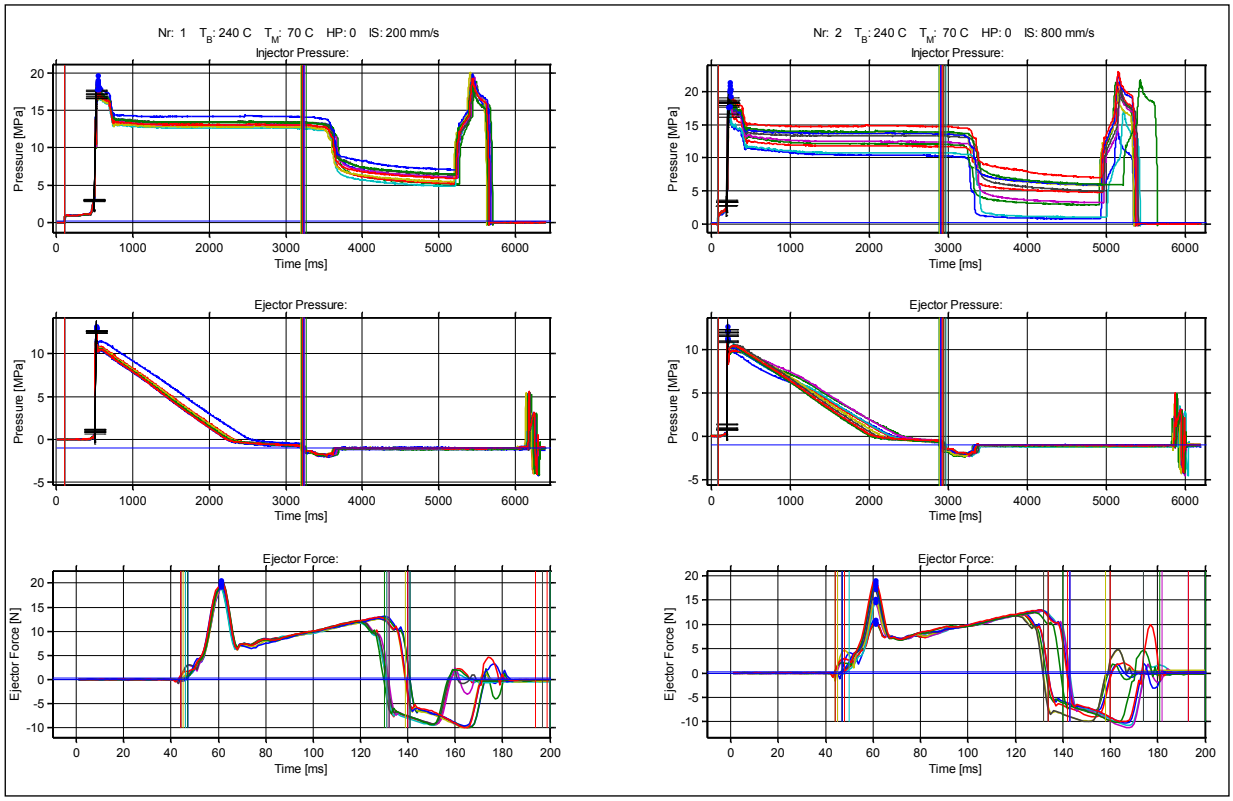

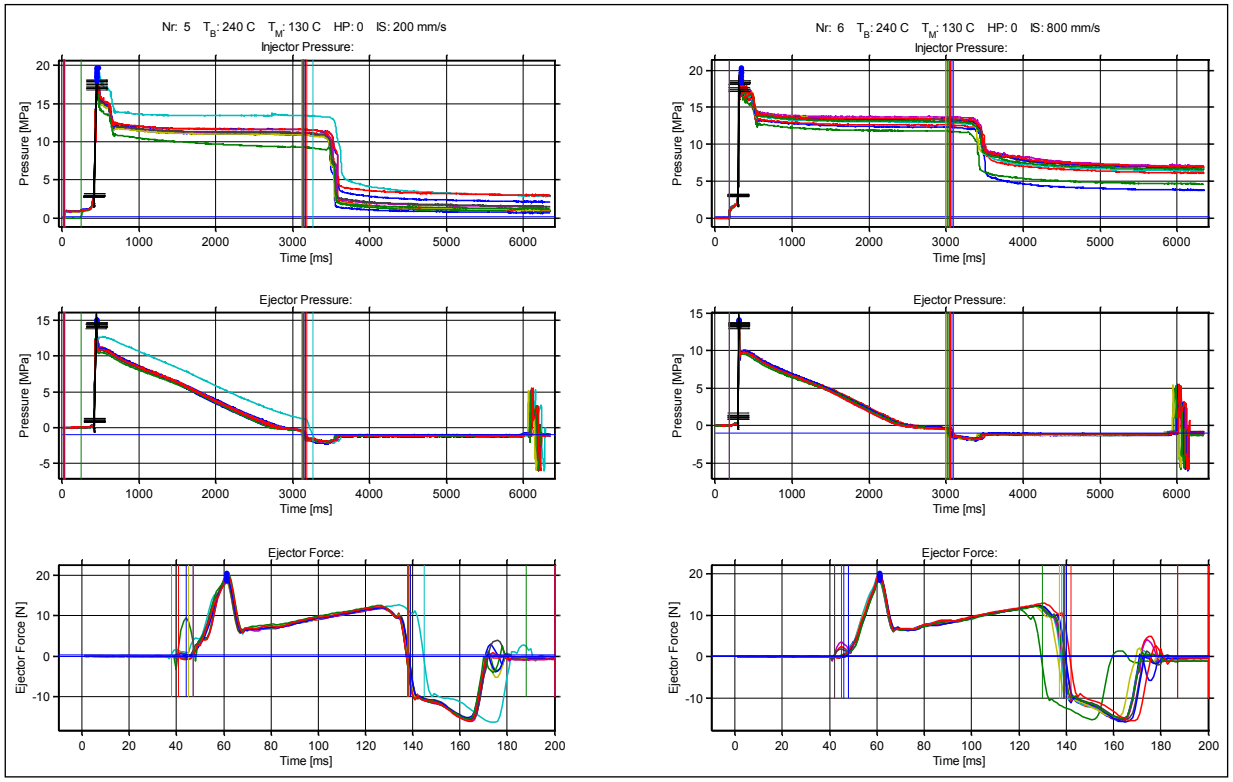

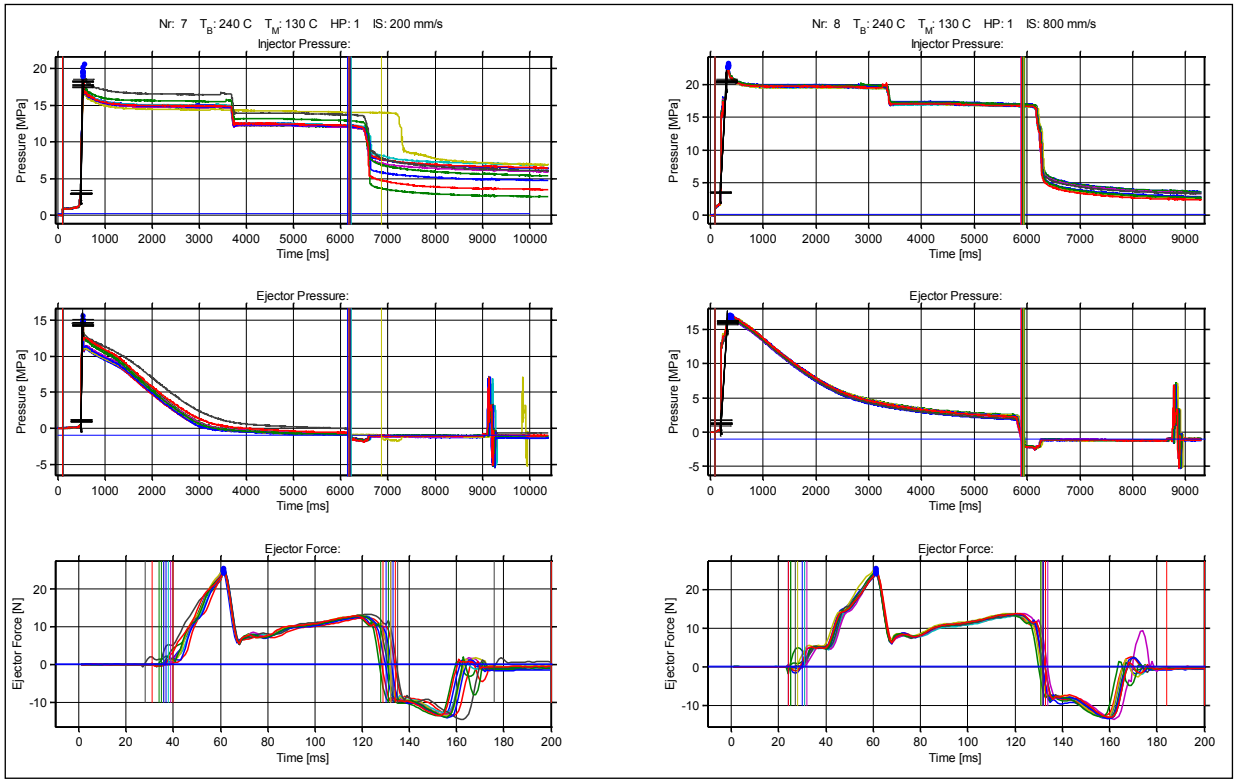
Nr: 7 T_B: 240 C T_M: 130 C HP: 1 IS: 200 mm/s
Injector Pressure:
Pressure [MPa]
Time [ms]
Ejector Pressure:
Pressure [MPa]
Time [ms]
Ejector Force:
Ejector Force [N]
Time [ms]
Nr: 8 T_B: 240 C T_M: 130 C HP: 1 IS: 800 mm/s
Injector Pressure:
Pressure [MPa]
Time [ms]
Ejector Pressure:
Pressure [MPa]
Time [ms]
Ejector Force:
Ejector Force [N]
Time [ms]

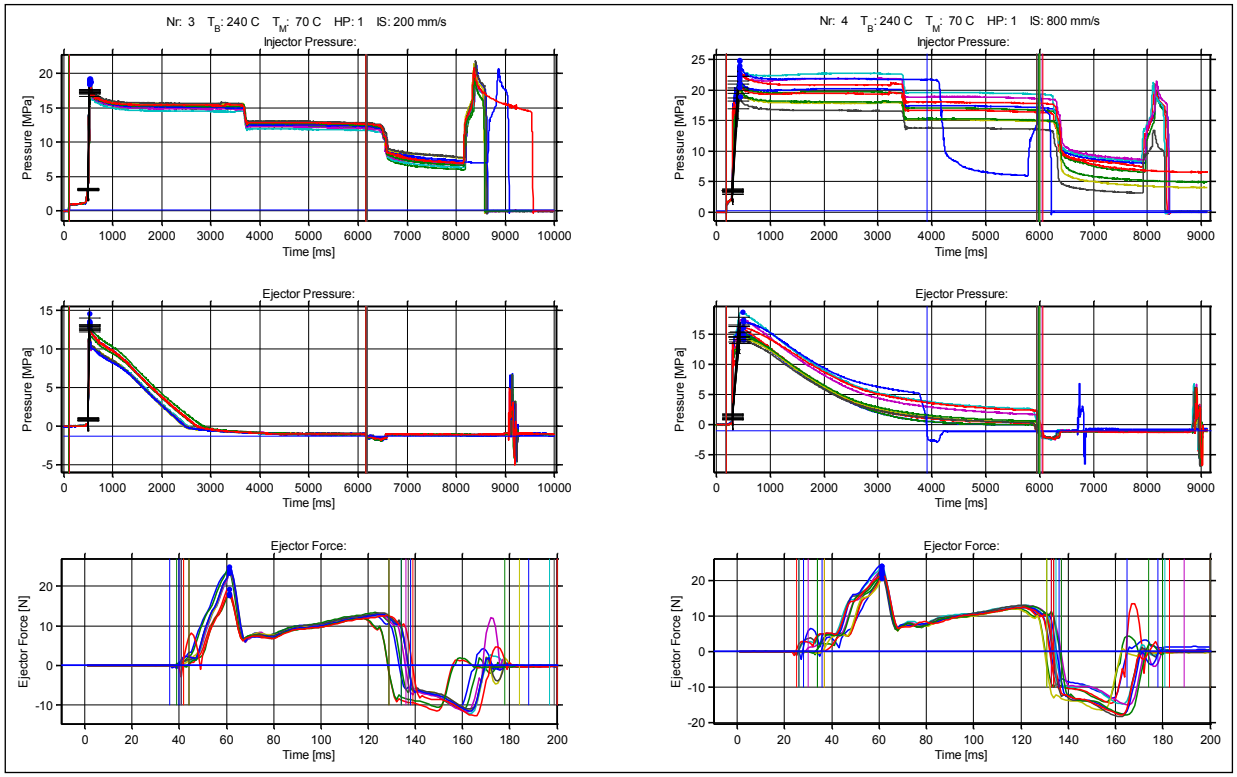
Nr: 3 T_B: 240 C T_M: 70 C HP: 1 IS: 200 mm/s
Injector Pressure:
Pressure [MPa]
Time [ms]
Ejector Pressure:
Pressure [MPa]
Time [ms]
Ejector Force:
Ejector Force [N]
Time [ms]
Nr: 4 T_B: 240 C T_M: 70 C HP: 1 IS: 800 mm/s
Injector Pressure:
Pressure [MPa]
Time [ms]
Ejector Pressure:
Pressure [MPa]
Time [ms]
Ejector Force:
Ejector Force [N]
Time [ms]

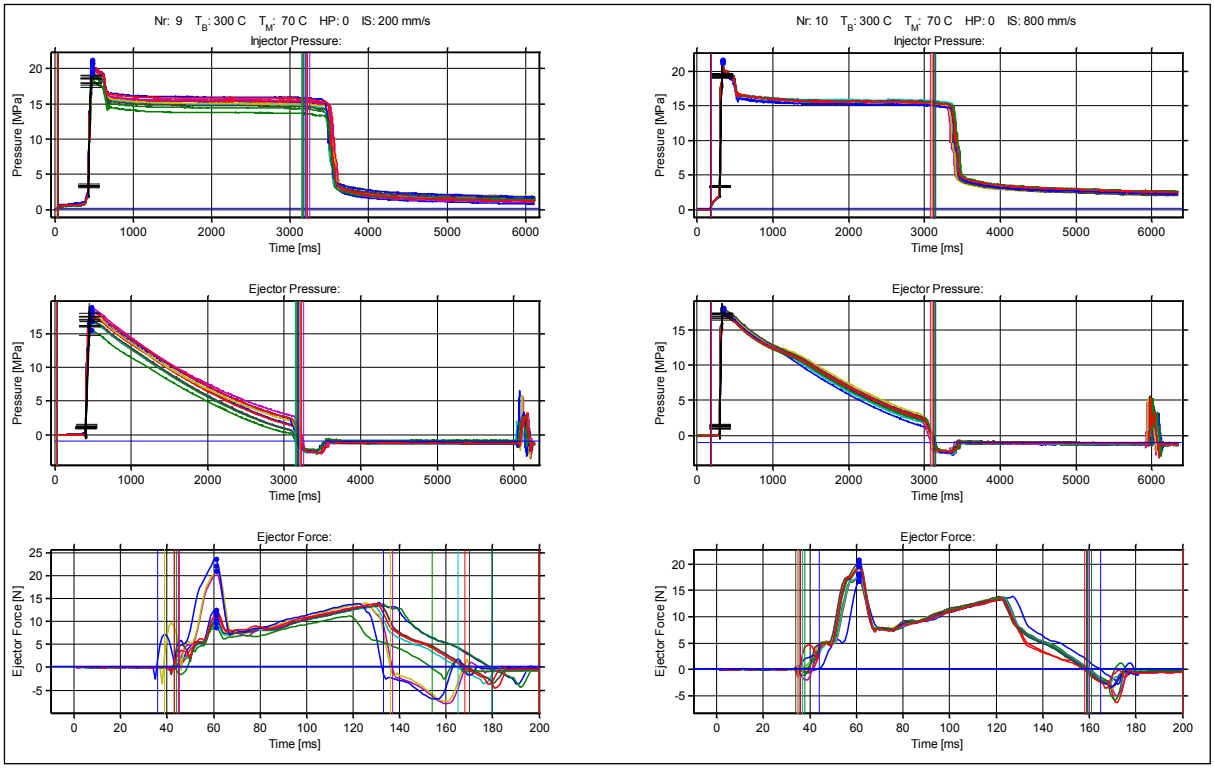
Nr: 9 T_B: 300 C T_M: 70 C HP: 0 IS: 200 mm/s
Injector Pressure:
Pressure [MPa]
Time [ms]
Ejector Pressure:
Pressure [MPa]
Time [ms]
Ejector Force:
Ejector Force [N]
Time [ms]
Nr: 10 T_B: 300 C T_M: 70 C HP: 0 IS: 800 mm/s
Injector Pressure:
Pressure [MPa]
Time [ms]
Ejector Pressure:
Pressure [MPa]
Time [ms]
Ejector Force:
Ejector Force [N]
Time [ms]

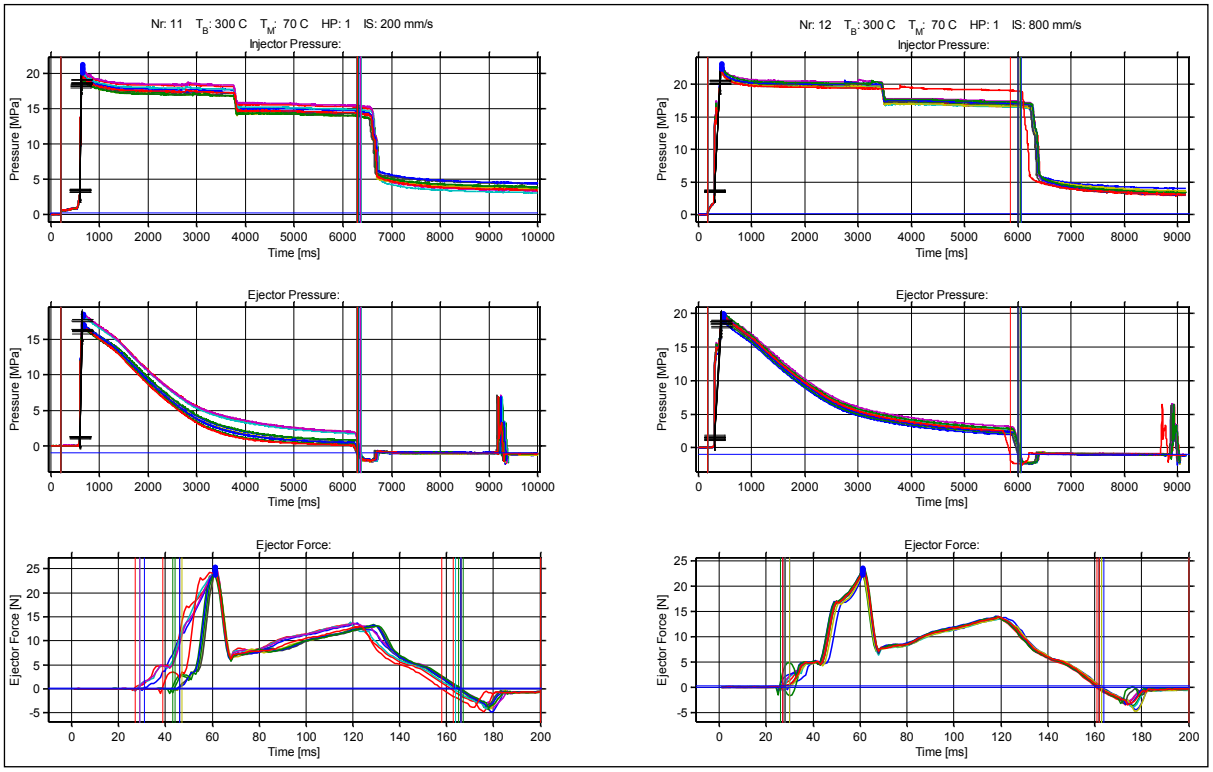
Nr: 11 T_B: 300 C T_M: 70 C HP: 1 IS: 200 mm/s
Injector Pressure:
Pressure [MPa]
Time [ms]
Ejector Pressure:
Pressure [MPa]
Time [ms]
Ejector Force:
Ejector Force [N]
Time [ms]
Nr: 12 T_B: 300 C T_M: 70 C HP: 1 IS: 800 mm/s
Injector Pressure:
Pressure [MPa]
Time [ms]
Ejector Pressure:
Pressure [MPa]
Time [ms]
Ejector Force:
Ejector Force [N]
Time [ms]

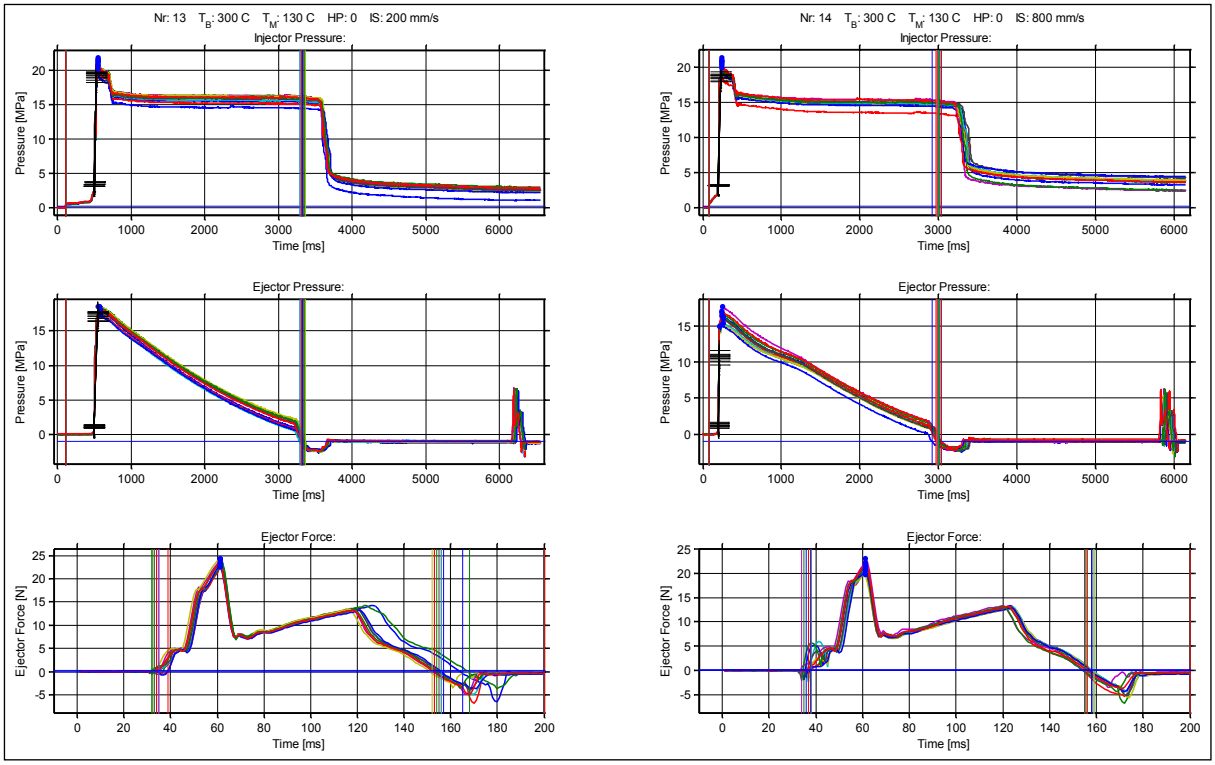
Nr: 13 T_B: 300 C T_M: 130 C HP: 0 IS: 200 mm/s
Injector Pressure:
Pressure [MPa]
Time [ms]
Ejector Pressure:
Pressure [MPa]
Time [ms]
Ejector Force:
Ejector Force [N]
Time [ms]
Nr: 14 T_B: 300 C T_M: 130 C HP: 0 IS: 800 mm/s
Injector Pressure:
Pressure [MPa]
Time [ms]
Ejector Pressure:
Pressure [MPa]
Time [ms]
Ejector Force:
Ejector Force [N]
Time [ms]

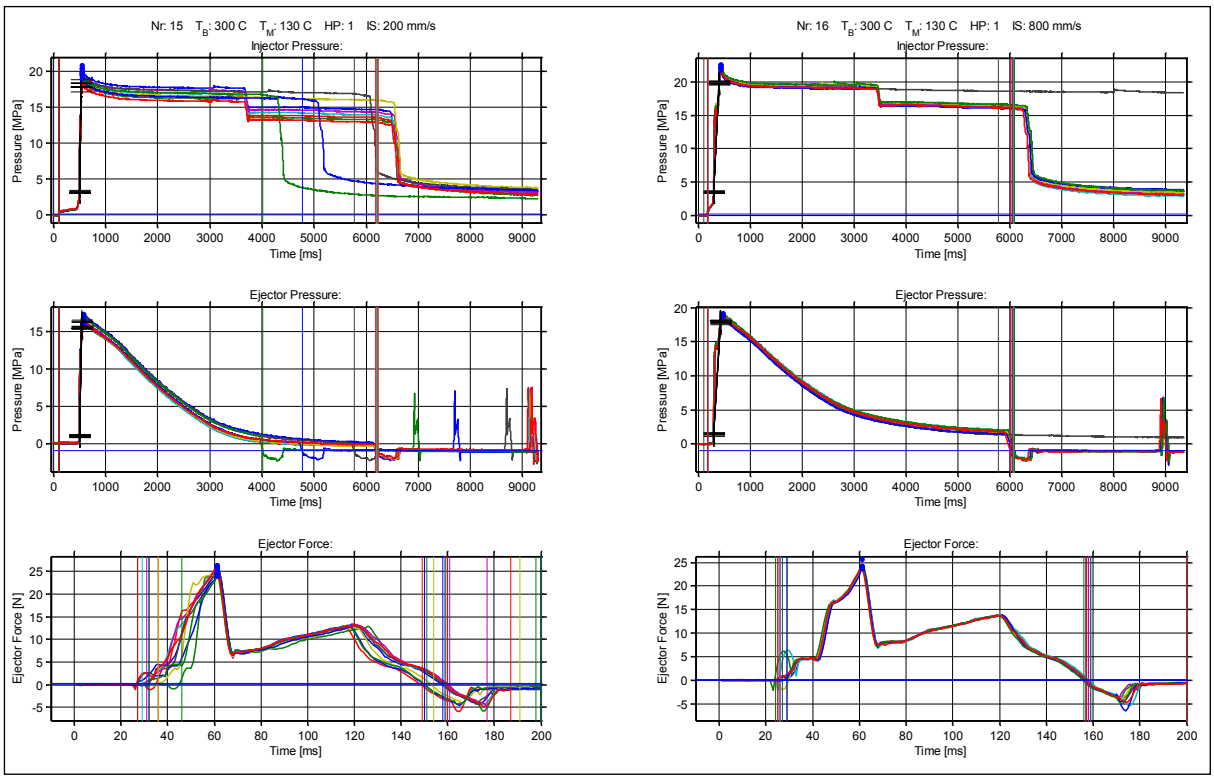
Nr: 15 T_B: 300 C T_M: 130 C HP: 1 IS: 200 mm/s
Injector Pressure:
Pressure [MPa]
Time [ms]
Ejector Pressure:
Pressure [MPa]
Time [ms]
Ejector Force:
Ejector Force [N]
Time [ms]
Nr: 16 T_B: 300 C T_M: 130 C HP: 1 IS: 800 mm/s
Injector Pressure:
Pressure [MPa]
Time [ms]
Ejector Pressure:
Pressure [MPa]
Time [ms]
Ejector Force:
Ejector Force [N]
Time [ms]

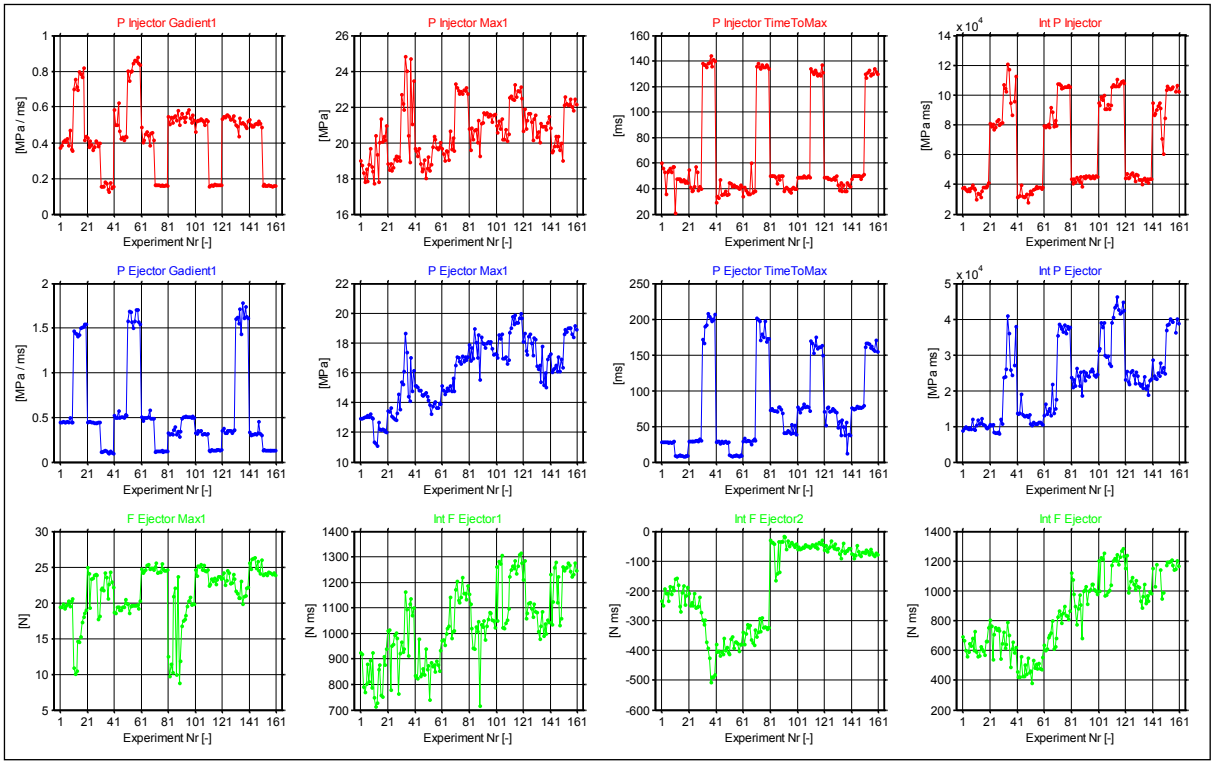

Figure 8-5 Characteristic variables of P_c, P_i and F^e

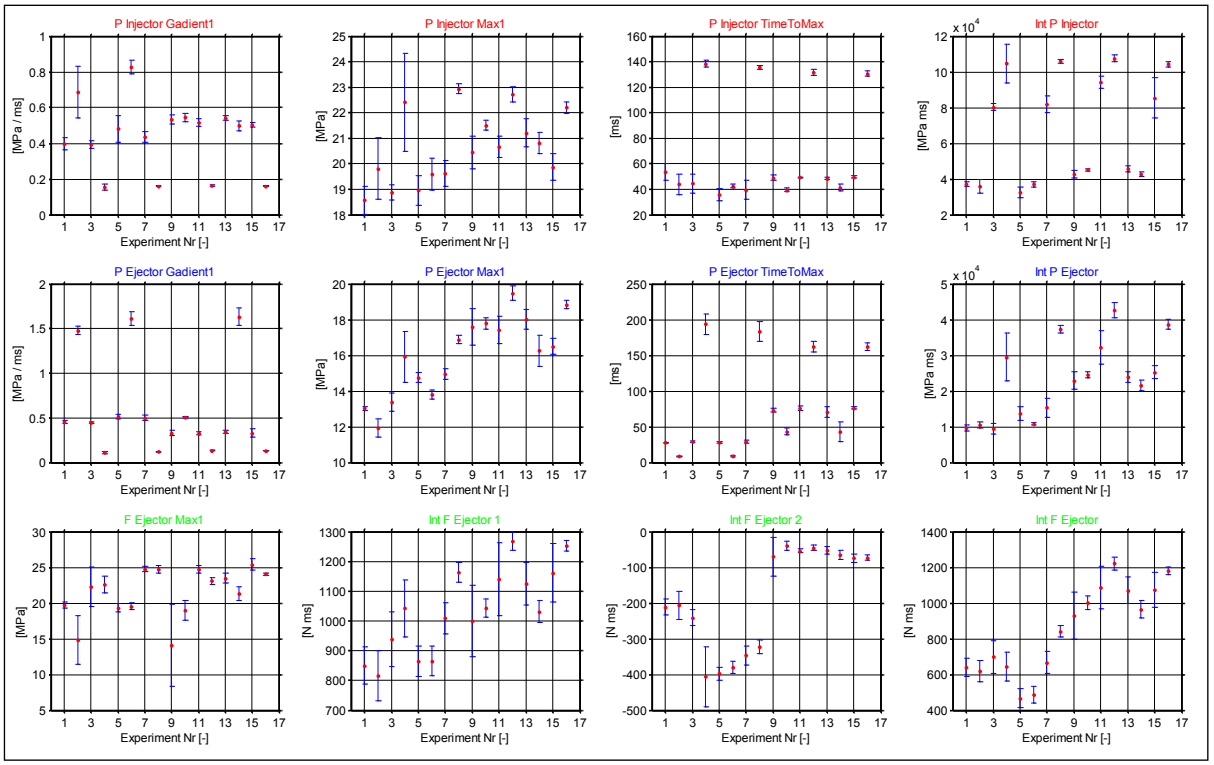

Figure 8-6 Distribution of characteristic variables of P_c, P_i and F^e

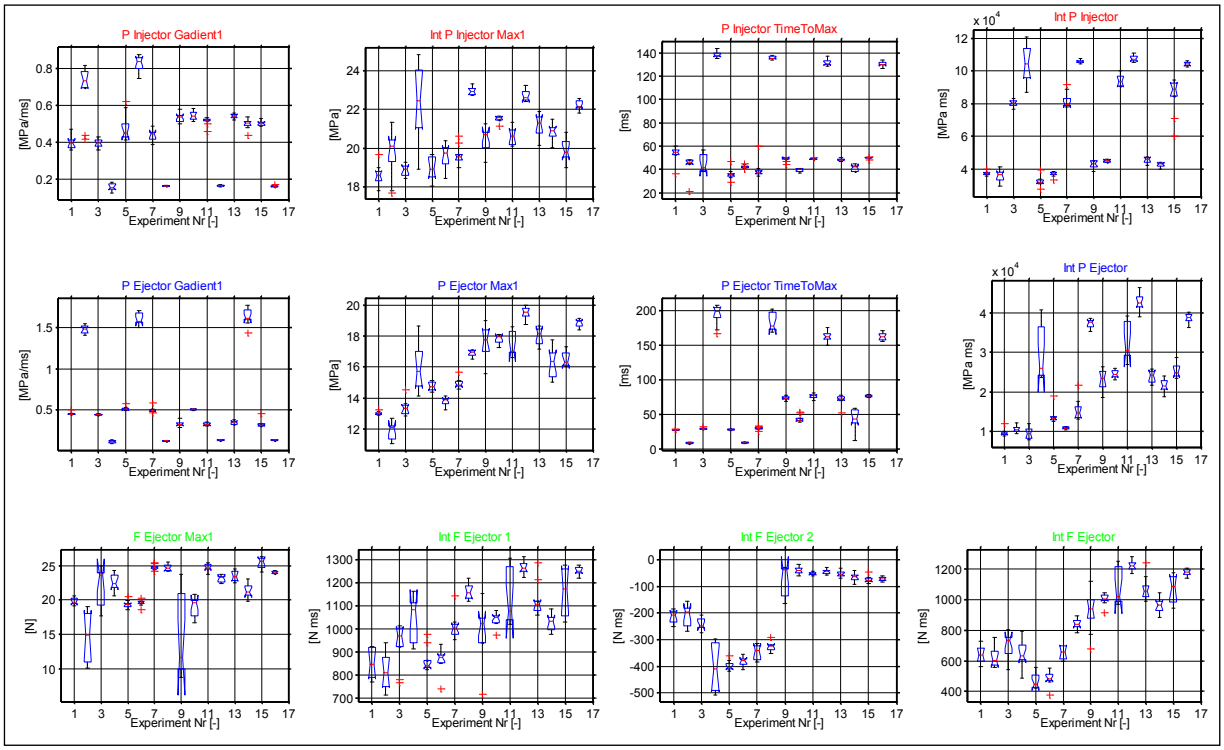

Figure 8-7 ANOOA of characteristic variables of P_c, P_i and F^e

8.3.2 Table of Characteristic Numbers:

	F^e_{max} [N] Maximum Demoulding Force										AVERAGE				
Exp1	19.393	19.436	19.874	19.206	19.53	19.686	20.235	19.54	20.222	20.565	**19.76881**				
Exp2	10.93	10.052	10.451	14.59	14.553	15.213	17.249	18.08	18.519	18.994	**14.86308**				
Exp3	24.952	24.126	19.318	23.393	23.416	23.854	24.021	23.928	17.743	18.132	**22.28843**				
Exp4	21.864	22.042	21.744	24.248	23.578	20.616	22.566	24.26	22.92	22.215	**22.60502**				
Exp5	18.655	18.601	19.367	19.364	18.997	19.012	19.465	19.412	20.518	19.981	**19.33731**				
Exp6	19.854	18.541	19.516	19.643	19.586	19.671	19.661	19.769	19.215	20.223	**19.56792**				
Exp7	24.784	24.205	24.372	24.633	25.311	25.37	24.756	24.86	24.842	24.629	**24.77616**				
Exp8	25.061	25.567	24.226	24.26	24.256	25.479	24.786	24.484	24.527	24.68	**24.73263**				
Exp9	12.53	9.723	11.42	10.318	20.921	22.1	9.98	23.689	8.7575	11.899	**14.13385**				
Exp10	16.731	17.481	17.73	18.195	19.497	20.222	20.777	19.72	19.813	19.881	**19.00475**				
Exp11	24.63	23.751	25.187	25.057	25.378	24.605	25.313	24.542	24.417	24.615	**24.74934**				
Exp12	22.351	22.558	23.364	22.985	23.459	22.605	23.213	23.7	23.645	23.324	**23.1204**				
Exp13	23.483	24.208	22.542	23.16	24.485	24.238	22.761	22.845	24.03	23.346	**23.50987**				
Exp14	21.699	21.278	20.729	20.662	23.042	19.82	20.904	20.959	22.106	22.197	**21.33954**				
Exp15	25.585	24.746	26.097	26.192	26.371	24.787	25.764	24.56	24.045	25.965	**25.41134**	Average	Standard Deviation	Maximum	Minimum
Exp16	23.89	24.008	24.117	23.862	24.314	24.223	NaN	23.959	24.173	23.852	**24.04419**	**21.4533**	**3.444356911**	**25.4113447**	**14.13385244**

	P^c_{work} [MPa ms]– Cavity Pressure work done														
Exp1	8854.8	9392.2	9951.6	9423	9243.9	9672.7	9158.4	11997	9351.8	9097.3	**9614.299**				
Exp2	10319	11754	10770	10907	12170	10619	10334	9623.1	9515	9949.4	**10596.07**				
Exp3	10474	10343	10525	8407.5	8246.3	8103.4	8362.1	7950.5	11980	10802	**9519.463**				
Exp4	23715	24017	25970	40852	35993	25788	24292	NaN	27218	38046	**29543.24**				
Exp5	13722	13539	13710	19024	13267	12946	12822	13030	12556	13298	**13791.2**				
Exp6	10762	10395	11257	10721	10709	10757	11138	11126	10708	10482	**10805.46**				
Exp7	13045	16246	13435	14467	15097	13062	21718	13693	15025	17565	**15335.36**				
Exp8	35359	38681	38046	37445	36483	38429	35992	38076	37435	37752	**37369.87**				
Exp9	23647	20878	23110	21300	26311	24069	21342	25138	18558	25329	**22967.94**				
Exp10	22967	25043	24118	23864	25372	25966	25435	24330	23921	24504	**24552**				
Exp11	31256	31888	39122	37843	39058	29800	29370	29580	27570	26916	**32240.21**				
Exp12	39018	40433	43295	44029	46350	42618	41573	42048	44855	42454	**42667.2**				
Exp13	23047	25356	22472	21763	25126	25742	24384	22029	25130	24179	**23922.85**				
Exp14	22004	21449	21734	20762	23946	20464	21348	18739	22899	23306	**21665.06**				
Exp15	28681	24188	23573	23372	24924	24074	27726	25239	26561	24793	**25313.14**	Average	Standard Deviation	Maximum	Minimum
Exp16	36865	38420	38544	40148	39529	39245	NaN	36362	40152	38816	**38675.67**	**23036.2**	**10907.49645**	**42667.1983**	**9519.463428**

	P^i_{work} [MPa ms]– *Injection* Pressure work done														
Exp1	37811	37920	36567	35543	37128	35660	37824	39878	37454	36722	**37250.74**				
Exp2	29712	34057	33452	31288	35614	38161	37923	38091	39317	41446	**35905.92**				
Exp3	81036	78997	80299	76754	78532	82328	83332	80018	80934	81623	**80385.31**				
Exp4	106970	104474	102425	120718	117129	94932	86878	NaN	96001	112667	**104688.2**				
Exp5	31376	31895	32448	39531	31997	31283	32139	33445	27940	33662	**32571.5**				
Exp6	35783	33541	36576	36989	38803	37599	37938	38118	37214	38245	**37080.55**				
Exp7	79656	78460	79406	80511	78293	91945	88761	79111	83176	79468	**81878.6**				
Exp8	107444	107622	106311	104599	105187	105685	105682	105672	106337	105340	**105987.9**				
Exp9	43734	40541	43989	41809	44943	43001	41617	45194	38638	45260	**42872.66**				
Exp10	44128	45827	45434	45890	44422	44784	45567	44277	45625	45269	**45122.52**				
Exp11	94977	93311	99041	96995	99970	90775	90758	93670	90785	93140	**94342.25**				
Exp12	105526	106869	106294	105920	110784	106176	107358	109066	109742	108288	**107602.3**				
Exp13	44225	47215	44056	44699	46920	47595	45804	42347	46652	46242	**45575.49**				
Exp14	43098	43304	40020	43181	44234	41990	43952	41130	43599	43901	**42840.85**				
Exp15	94619	86770	87766	90057	92898	94761	91486	70956	60364	84812	**85449**	Average	Standard Deviation	Maximum	Minimum
Exp16	103562	105990	104460	103875	104278	105402	NaN	102521	106440	102434	**104329.1**	**67742.7**	**29997.68768**	**107602.272**	**32571.50466**

	P^c_{max} [MPa]- Maximum Cavity Pressure														
Exp1	12.94	12.959	12.991	13.05	13.019	13.141	13.056	13.247	12.965	12.934	**13.03007**				
Exp2	11.355	11.234	11.104	12.701	12.223	12.148	12.216	12.193	12.081	12.014	**11.92693**				
Exp3	13.46	13.405	13.655	13.08	12.988	12.895	12.84	13.3	14.562	13.536	**13.37222**				
Exp4	15.368	15.212	16.087	18.639	17.398	14.402	14.128	17.023	14.788	16.144	**15.91876**				
Exp5	15.156	15.109	15.036	14.812	14.828	14.527	14.489	14.587	14.666	14.404	**14.76142**				
Exp6	14.138	13.875	13.258	13.757	13.932	14.056	13.636	13.648	13.941	13.907	**13.81496**				
Exp7	15.119	14.824	14.576	14.793	14.982	14.835	15.109	14.793	15.665	14.788	**14.94836**				
Exp8	16.512	17.079	17.046	16.769	16.593	17.136	16.755	17.074	16.888	17.057	**16.89095**				
Exp9	17.888	16.819	17.665	16.996	18.97	18.052	17.019	18.536	15.556	18.417	**17.59174**				
Exp10	17.986	17.922	17.681	17.992	18.081	18.011	18.092	17.613	17.245	17.278	**17.79013**				
Exp11	17.201	17.009	18.569	18.286	18.601	16.948	16.958	17.047	16.622	16.859	**17.41009**				
Exp12	18.723	19.018	19.769	19.27	19.88	19.384	19.384	19.688	20.005	19.685	**19.48044**				
Exp13	18.086	18.633	17.503	17.224	18.469	18.589	18.001	17.165	18.373	18.264	**18.03058**				
Exp14	16.471	16.258	16.503	15.386	17.771	15.189	16.023	15.047	16.904	17.113	**16.26651**				
Exp15	17.3	16.042	16.194	16.308	16.516	16.127	17.089	16.106	16.933	16.377	**16.49924**	Average	Standard Deviation	Maximum	Minimum
Exp16	18.627	18.93	18.766	18.997	19.022	19.004	18.588	18.396	19.141	18.914	**18.83841**	**16.0357**	**2.203786792**	**19.4804405**	**11.92693338**

	P^i_{max} [MPa]- Maximum Cavity Pressure														
Exp1	18.998	18.734	18.321	17.796	18.511	17.853	18.808	19.692	18.674	18.385	**18.57721**				
Exp2	17.711	20.415	19.336	17.823	20.003	21.359	20.049	20.359	20.142	20.942	**19.814**				
Exp3	18.847	18.503	18.81	18.439	18.624	19.095	19.272	19.021	19.205	19.011	**18.88262**				
Exp4	22.718	22.175	21.865	24.813	24.029	20.399	18.905	24.708	21.049	23.448	**22.4109**				
Exp5	19.675	19.542	19.263	19.685	18.826	18.418	18.525	19.051	18.031	18.59	**18.96069**				
Exp6	19.214	18.438	18.785	19.756	20.37	20.194	19.73	19.651	19.781	20.02	**19.59405**				
Exp7	19.681	19.394	18.999	19.538	19.503	19.053	20.647	19.629	20.275	19.563	**19.6282**				
Exp8	23.315	23.099	22.925	22.754	22.88	22.74	22.975	22.901	23.083	22.75	**22.94209**				
Exp9	20.768	19.611	20.832	20.178	20.71	20.732	20.034	21.244	19.26	21.089	**20.44562**				
Exp10	21.136	21.67	21.614	21.67	21.475	21.587	21.567	21.159	21.542	21.608	**21.50294**				
Exp11	20.949	20.555	21.193	20.804	21.328	20.206	20.195	20.731	20.102	20.507	**20.65704**				
Exp12	22.54	22.621	22.454	22.41	23.237	22.572	22.923	22.881	23.14	22.48	**22.72587**				
Exp13	20.643	21.901	20.804	21.257	21.654	21.629	21.188	20.14	21.361	21.561	**21.21389**				
Exp14	20.326	20.615	20.043	21.068	20.917	20.904	20.9	20.755	21.121	21.488	**20.81339**				
Exp15	20.811	19.453	19.555	19.81	20.368	19.789	20.379	19.617	19.979	18.983	**19.87425**	Average	Standard Deviation	Maximum	Minimum
Exp16	22.117	22.561	22.188	22.115	22.153	22.434	22.027	21.823	22.449	22.154	**22.20209**	**20.6403**	**1.412298441**	**22.9420939**	**18.57721182**

8.4 List of Publications

8.4.1 Related to this thesis

[1] Scholz, S. G., 2007, "Experimental series to verify the moulding accuracy of microstructures using a variothermal process control via an external inductive heating (DA)," Diplom Ingenieur (DA) Diplomarbeit / Master thesis, RWTH Aachen University.

[2] Scholz, S. G., 2007, "Design and layout of a robot-inductor-system for the variothermal tempering of an injection mould by induction (SA)," Diplom Ingenieur (SA) Studienarbeit, RWTH Aachen University.

[3] Michaeli, W., Klaiber, F., and Scholz, S. G., "Investigations in Variothermal Injection Moulding of Microstructures and Microstructured Surfaces," Proc. 4M 2008, Fourth International Conference on Multi-Material Micro Manufacture, S. Dimov, and W. Menz, eds., Whittles publishing, pp. 253-265.

[4] Griffiths, C. A., Dimov, S. S., Scholz, S. G., Hirshy, H., Tosello, G., Hansen, H. N., and Williams, E., "Cavity Pressure Behaviour in Micro Injection Moulding," Proc. 4M 2010 7th International Conference on Multi -Material Micro Manufacturing, B. Fillon, C. Khan-Malek, and S. Dimov, eds., Research Publishing, pp. 291-294.

[5] Griffiths, C., Dimov, S., Hirshy, H., Scholz, S., Fischer, S., and Spitzbart, M., 2011, "Prototype tooling for producing small series of polymer micro parts," Proceedings of the Institution of Mechanical Engineers, Part B: Journal of Engineering Manufacture, accepted.

[6] Griffiths, C., Dimov, S., Scholz, S., and Tosello, G., "Air Flow and Gassing Potential in Micro-injection Moulding," Proc. 4M 2011 8th International Conference on Multi -Material Micro Manufacturing, H. Kueck, H. Reinecke, and S. Dimov, eds., Research Publishing, pp. 310-314.

[7] Griffiths, C., Dimov, S., Scholz, S., and Tosello, G., 2011, "Influence of injection and cavity pressure on the demoulding force in micro-injection moulding " Journal of Manufacturing Science and Engineering, ASME, submitted.

[8] Griffiths, C. A., Dimov, S. S., Scholz, S., Hirshy, H., and Tosello, G., 2011, "Process Factors Influence on Cavity Pressure Behavior in Microinjection Moulding," Journal of Manufacturing Science and Engineering, 133(3), pp. 031007-031010.

[9] Griffiths, C. A., Dimov, S. S., Scholz, S. G., and Tosello, G., 2011, "Cavity Air Flow Behavior During Filling in Microinjection Molding," Journal of Manufacturing Science and Engineering, 133(1), pp. 011006-011010.

8.4.2 Other publications

[1] Petkov, P. V., Scholz, S. G., and Dimov, S. S., "Strategies for material removal in laser milling," Proc. 4M 2008, Fourth International Conference on Multi-Material Micro Manufacture, S. Dimov, and W. Menz, eds., Whittles Publishing, pp. 249-252.

[2] Brousseau, E., Krohs, F., Dimov, S., Griffiths, C., Scholz, S., Rees, A., and Fatikow, S., "Investigation of a new process chain based on atomic force microscopy scratching," Proc. 4M/ICOMM 2009 - The Global Conference on Micro Manufacture, V. Saile, K. Ehmann, and S. Dimov, eds., The Charlesworth Group pp. 267-270.

[3] Kautt, M., Anson, S., Saile, V., Scholz, S., Fugier, P., Lambertini, V., Abad, E., Dirne, F., Loeschner, H., and Leach, R., "Facilitating open innovation in micro and nano technology by providing open access to a pan-European toolbox called EUMINAfab," Proc. 4M/ICOMM 2009 - The Global Conference on Micro Manufacture, V. Saile, K. Ehmann, and S. Dimov, eds., The Charlesworth Group pp. 11-24.

[4] Scholz, S., Griffiths, C. A., Dimov, S. S., Brousseau, E. B., Lalev, G., and Petkov, P., "New process chains for replicating micro and nano structured surface with bio-mimetic applications," Proc. ANTEC 2009 - Proceedings of the 67th Annual Technical Conference & Exhibition, S. o. P. Engineers, ed., pp. 3021-3027.

[5] Scholz, S., Petkov, P., Brousseau, E., Griffiths, C., Hirshy, H., and Dimov, S., "Process chain for replicating bio inspired micro structured surfaces," Proc. 4M/ICOMM 2009 - The Global Conference on Micro Manufacture, V. Saile, K. Ehmann, and S. Dimov, eds., The Charlesworth Group pp. 271-274.

[6] Velkova, V., Lalev, G., Hirshy, H., Scholz, S., and Dimov, S., "Novel process chain for fabrication of Ni shims," Proc. 4M/ICOMM 2009 - The Global Conference on Micro Manufacture, V. Saile, K. Ehmann, and S. Dimov, eds., The Charlesworth Group pp. 411-414.

[7] Brousseau, E., Scholz, S., and Rees, A., 2010, "Fabrication of 3D Structures using Atomic Force Microscopy scratching," Proc. 4M 2010 7th International Conference on Multi -Material Micro Manufacturing, B. Fillon, C. Khan-Malek, and S. Dimov, eds., Research Publishing, pp. 65-68.

[8] Minev, R., Vella, P., Brousseau, E., Dimov, S., Scholz, S., and Matthews, C., 2010, "Capability Maturity Study of the Horizontal and Vertical Integration of Structuring,Patterning and Characterization MNTs," Proc. 4M 2010 7th International

Conference on Multi -Material Micro Manufacturing, B. Fillon, C. Khan-Malek, and S. Dimov, eds., Research Publishing, pp. 253-256.

[9] Moguedet, M., Bambury, E., Blondiaux, N., Cosgun, D., Dimov, S., Scholz, S., Eigenbrod, H., Fillon, B., Gruber, J., Guttenberg, Z., Halper, J., Juliet, P., Kaller, S., Modrich, K., Pugin, N., Ribeiro, N., Rochowicz, M., Salaun, G., Totzeck, M., and Vuillermoz, P., "Flexible Compression Injection Moulding Platform for Multi-Scale Surface Structures : The IMPRESS FP7 Project," Proc. 4M 2010 7th International Conference on Multi -Material Micro Manufacturing, B. Fillon, C. Khan-Malek, and S. Dimov, eds., Research Publishing, pp. 220-223.

[10] Velkova, V., Lalev, G., Hirshy, H., Scholz, S., Hiitola-KeinÃ¤nen, J., Gold, H., Haase, A., Hast, J., Stadlober, B., and Dimov, S., 2010, "Design and validation of a novel master-making process chain for organic and large area electronics on flexible substrates," Microelectronic Engineering.

[11] Hirshy, H., Lalev, G., Velkova, V., Popov, K., Scholz, S., and Dimov, S., "Master Tool Fabrication for the Replication of Micro and Nano Features," Proc. 4M 2011 8th International Conference on Multi -Material Micro Manufacturing, H. Kueck, H. Reinecke, and S. Dimov, eds., Research Publishing, pp. 317-320.

[12] Lacan, F., Scholz, S., P.V., P., and Dimov, S., "Manufacturing of an Array of Microneedles in a Steel Insert for Micro-injection Moulding Using Laser Milling," Proc. 4M 2011 8th International Conference on Multi -Material Micro Manufacturing, H. Kueck, H. Reinecke, and S. Dimov, eds., Research Publishing, pp. 336-339.

[13] Scholz, S. G., Griffiths, C. A., Dimov, S. S., Brousseau, E. B., Lalev, G., and Petkov, P., 2011, "Manufacturing routes for replicating micro and nano surface structures with bio-mimetic applications," CIRP Journal of Manufacturing Science and Technology, 4(4), pp. 347-356.

[14] Velkova, V., Lalev, G., Hirshy, H., Omar, F., Scholz, S., Minev, E., and Dimov, S., 2011, "Process chain for serial manufacture of 3D micro- and nano-scale structures," CIRP Journal of Manufacturing Science and Technology.

9 REFERENCES

Alting, L.,Kimura, F.,Hansen, H. N. and Bissacco, G. 2003. Micro Engineering. *CIRP Annals - Manufacturing Technology* 52(2), pp. 635-657.

An, C.-C. and Chen, R.-H. 2007. Experimental Study of Demolding Properties on Stereolithography Tooling. *Journal of Manufacturing Science and Engineering* 129(4), pp. 843-847.

An, C. C. and Chen, R. H. 2008. The experimental study on the defects occurrence of SL mold in injection molding. *Journal of Materials Processing Technology* 201(1-3), pp. 706-709.

Attanasio, D. C.,Hopkinson, N.,Kehrberger, R.,Sridhar, A. and Witt, G. 2006. Application and modelling of hybrid stereolithography injection mould tooling. *Virtual and Physical Prototyping* 1(3), pp. 197-206.

Azcarate, S.,Uriarte, L.,Bigot, S.,Bolt, P.,Staemmler, L.,Tosello, G.,Roth, S.,Schoth, A.,Wolfgang, M.,Stefan, D. and Bertrand, F. eds. 2006. *Hybrid tooling: A review of process chains for tooling microfabrication within 4M*. 4M 2006 - Second International Conference on Multi-Material Micro Manufacture. Oxford. Elsevier, pp. 305-308.

Bendada, A.,Derdouri, A.,Lamontagne, M. and Simard, Y. 2004. Analysis of thermal contact resistance between polymer and mold in injection molding. *Applied Thermal Engineering* 24(14-15), pp. 2029-2040.

Bibber, D. M. ed. 2004. *Micro molding challenges*. Chicago, IL. pp. 3703-3711.

Bigot, S.,Ivanov, A. and Popov, K. eds. 2005. *A study of the micro EDM electrode wear*. 4M 2005 - First International Conference on Multi-Material Micro Manufacture. Oxford. Elsevier, pp. 355-358.

Bigot, S.,Minev, R.,Dobrev, T.,Dimov, S. and Matthews, C. eds. 2009. *Function and length scale integration in micro/nano manufacturing*. 4M/ICOMM 2009 - The Global Conference on Micro Manufacture. Karlsruhe, Germany, September 2009. pp. 147-152.

Binet, C.,Heaney, D. F.,Spina, R. and Tricarico, L. 2005. Experimental and numerical analysis of metal injection molded products. *Journal of Materials Processing Technology* 164-165, pp. 1160-1166.

Blanco, A. 2004. Microfluidics made easy. *Plastics Engineering* 60(6), p. 6.

Blattert, C.,Jurischka, R.,Tahhan, I.,Schoth, A.,Kerth, P. and Menz, W. eds. 2005. *Microfluidic blood/plasma separation unit based on microchannel bend structures*. Oahu, HI. pp. 38-41.

Bourdon, R. and Schneider, W. 2002. A Systematic Approach to Microinjection Moulding. *Business Briefing:Medical Device Manufacture & Technology*.

Bralla, J. G. 1999. *Design for Manufacturability Handbook*. McGraw-Hill.

Campanelli, S. L.,Ludovico, A. D.,Bonserio, C.,Cavalluzzi, P. and Cinquepalmi, M. 2007. Experimental analysis of the laser milling process parameters. *Journal of Materials Processing Technology* 191(1-3), pp. 220-223.

Cao, D.,Jiang, J.,Yang, R. and Meng, W. 2006. Fabrication of high-aspect-ratio microscale mold inserts by parallel μEDM. *Microsystem Technologies* 12(9), pp. 839-845.

Chang, R. Y.,Chen, C. H. and Su, K. S. 1996. Modifying the Tait equation with cooling-rate effects to predict the pressure-volume-temperature behaviors of amorphous polymers: modeling and experiments *Polymer Engineering and Science (USA)* 36(13), pp. 1789-1795.

Charmeau, J.-Y.,Chailly, M.,Gilbert, V. and Béreaux, Y. 2008. Influence of mould surface coatings in injection moulding. Application to the ejection stage. *International Journal of Material Forming* 1(0), pp. 699-702.

Chen, C. S.,Chen, S. C.,Liao, W. H.,Chien, R. D. and Lin, S. H. 2010. Micro injection molding of a micro-fluidic platform. *International Communications in Heat and Mass Transfer* 37(9), pp. 1290-1294.

Chua, C. K.,Hong, K. H. and Ho, S. L. 1999. Rapid tooling technology. Part 1. A comparative study. *International Journal of Advanced Manufacturing Technology* 15(8), pp. 604-608.

Clavería, I.,Javierre, C. and Ponz, L. 2005. Method for generation of rheological model to characterize non-conventional injection molding by means of spiral mold. *Journal of Materials Processing Technology* 162-163(SPEC. ISS.), pp. 477-483.

Collins, C. 1999. Monitoring cavity pressure perfects injection molding. *Assembly Automation* 19(3), pp. 197-202.

Colton, J. S.,Crawford, J.,Pham, G. and Rodet, V. 2001. Failure of rapid prototype molds during injection molding. *CIRP Annals - Manufacturing Technology* 50(1), pp. 129-132.

Crawford, R. J. ed. 1990. *Plastics Engineering.* 2nd ed. Pergamon Press.

Dairanieh, I. S.,Haufe, A.,Wolf, H. J. and Mennig, G. 1996. Computer simulation of weld lines in injection molded poly(methyl methacrylate). *Polymer Engineering and Science* 36(15), pp. 2050-2057.

De Grave, A.,Eriksson, T. and Hansen, N. H. eds. 2007. *Demouldability of microstructures in polymer*. 4M 2007 Proceedings of the 3rd International Conference on Multi-material Micro Manufacture. Whittles publishing, pp. 225-228.

Debondue, E.,Fournier, J. E.,Lacrampe, M. F. and Krawczak, P. 2004. Weld-line sensitivity of injected amorphous polymers. *Journal of Applied Polymer Science* 93(2), pp. 644-650.

Debowki, M.,Zhao, J.,Spowage, A. and Glendenning, P. 2003. *Development of techniques and methodologies for micro and sub-micro evaluation of moulded polymer systems*. SIMTech Singapore (Singapore Institute of Manufacturing Technology).

DESMA. 2008. *Desma Formiplast 1k* [Online]. http://www.desma-tec.de/en/machines/micro_injection/pdf/FormicaPlast_1K_E.pdf: DESMA. Available at: [Accessed: 01-06-2011].

Despa, M. S.,Kelly, K. W. and Collier, J. R. 1999. Injection molding of polymeric LIGA HARMs. *Microsystem Technologies* 6(2), pp. 60-66.

Dimov, S. ed. 2005. *4M Network of excellence: An Instrument for Integration of European research in Multi-Material Micro Manufacture* First international conference on Multi-Material Micro Manufacture.

Dimov, S. S.,Matthews, C. W.,Glandfield, A.,Dorrington, P.,Wolfgang, M.,Stefan, D. and Bertrand, F. eds. 2006. *A roadmapping study in Multi-Material Micro Manufacture*. 4M 2006 - Second International Conference on Multi-Material Micro Manufacture. Oxford. Elsevier, pp. xi-xxv.

Dobrev, T.,Dimov, S. S. and Thomas, A. J. 2006. Laser milling: Modelling crater and surface formation. *Proceedings of the Institution of Mechanical Engineers, Part C: Journal of Mechanical Engineering Science* 220(11), pp. 1685-1696.

Ebnesajjad, S. 2003. *Melt Processible Fluroplastic: The Definitive User's Guide*. Plastics Design Library ed. Wiliam Andrew Publishing.

Eloy, J. C. 2008. *Europe is Maintaining its Leadership in MEMS.* International magazine on smart systems technologies. pp. 14-15.

Feynman, R. P. 1959. "There's plenty of Room at the Bottom" presented at the American Physical Society Meeting in Pasadena CA. *reprinted with the permission of Van Nostrand Reinhold in Journal of Micromechenical Systems* 1, pp. 60-66.

Feynman, R. P. 1983. "Infinitisimal Machinery" presented at the Jet Propulsion Labratory on February 23, 1983. *reprinted in Microelectronic systems* 2, pp. 4-14.

Fleischer, J. and Kotschenreuther, J. 2007. The manufacturing of micro molds by conventional and energy-assisted processes. *The International Journal of Advanced Manufacturing Technology* Volume 33(1), pp. 75-85.

Fu, G.,Tor, S. B.,Loh, N. H.,Tay, B. Y. and Hardt, D. E. 2008. The demolding of powder injection molded micro-structures: Analysis, simulation and experiment. *Journal of Micromechanics and Microengineering* 18(7), pp. 1-12.

Gandarias, E.,Dimov, S.,Pham, D. T.,Ivanov, A.,Popov, K.,Lizarralde, R. and Arrazola, P. J. 2006. New methods for tool failure detection in micromilling. *Proceedings of the Institution of Mechanical Engineers, Part B: Journal of Engineering Manufacture* 220(2), pp. 137-144.

Gao, F.,Patterson, W. I. and Kamal, M. R. 1996. Cavity pressure control during the cooling stage in thermoplastic injection molding. *Polymer Engineering and Science* 36(19), pp. 2467-2476.

Giboz, J.,Copponnex, T. and Mele, P. 2007. Microinjection molding of thermoplastic polymers: A review. *Journal of Micromechanics and Microengineering* 17(6), p. 96.

Gornik, C. ed. 2004. *Injection moulding of parts with microstructured surfaces for medical applications*. Macromolecular Symposia. pp. 365-374.

Griffiths, C. A.,Bigot, S.,Brousseau, E.,Worgull, M.,Heckele, M.,Nestler, J. and Auerswald, J. 2010. Investigation of polymer inserts as prototyping tooling for micro injection moulding. *International Journal of Advanced Manufacturing Technology* 47(1-4), pp. 111-123.

Griffiths, C. A.,Dimov, S. S. and Brousseau, E. B. 2008a. Microinjection moulding: The influence of runner systems on flow behaviour and melt fill of multiple microcavities. *Proceedings of the Institution of Mechanical Engineers, Part B: Journal of Engineering Manufacture* 222(9), pp. 1119-1130.

Griffiths, C. A.,Dimov, S. S.,Brousseau, E. B.,Chouquet, C.,Gavillet, J. and Bigot, S. 2009. Investigation of surface treatment effects in micro-injection-moulding. *International Journal of Advanced Manufacturing Technology*, pp. 1-12.

Griffiths, C. A.,Dimov, S. S.,Brousseau, E. B. and Hoyle, R. T. 2007. The effects of tool surface quality in micro-injection moulding. *Journal of Materials Processing Technology* 189(1-3), pp. 418-427.

Griffiths, C. A.,Dimov, S. S.,Brousseau, E. B. and Packianather, M. S. 2008b. The finite element analysis of melt flow behaviour in micro-injection moulding. *Proceedings of the Institution of Mechanical Engineers, Part B: Journal of Engineering Manufacture* 222(9), pp. 1107-1118.

Gui, D. Y.,Ernst, L. J.,Jansen, K. M. B.,Yang, D. G.,Goumans, L.,Bressers, H. J. L. and Janssen, J. H. J. 2008. Effects of molding pressure on the warpage and the viscoelasticities of HVQFN packages. *Journal of Applied Polymer Science* 109(3), pp. 2016-2022.

Haberstroh, E. and Brandt, M. 2002. Determination of Mechanical Properties of Thermoplastics Suitable for Micro Systems. *Macromolecular Materials and Engineering* 287(12), pp. 881-888.

Hansen, H. N. and Theilade, U. A. eds. 2005. *Surface microstructure replication in injection moulding*. 4M 2005, Fourth International Conference on Multi-Material Micro Manufacture. Karsruhe, Germany, 29. June - 1. July 2005. Elsevier Industrial Engeneering Publishing, pp. 91-94.

Harris, R.,Newlyn, H. and Dickens, P. 2002. Selection of mould design variables in direct stereolithography injection mould tooling. *Proceedings of the Institution of Mechanical Engineers, Part B: Journal of Engineering Manufacture* 216(4), pp. 499-505.

Harris, R. A.,Hague, R. J. M. and Dickens, P. M. 2003a. Crystallinity control in parts produced from stereolithography injection mould tooling. *Proceedings of the Institution of Mechanical Engineers, Part L: Journal of Materials: Design and Applications* 217(4), pp. 269-276.

Harris, R. A.,Hague, R. J. M. and Dickens, P. M. 2004. Thermal conditions in stereolithography injection mould tooling and their use for polyether-ether-ketone moulding. *International Journal of Production Research* 42(1), pp. 119-129.

Harris, R. A.,Newlyn, H. A.,Hague, R. J. M. and Dickens, P. M. 2003b. Part shrinkage anomilies from stereolithography injection mould tooling. *International Journal of Machine Tools and Manufacture* 43(9), pp. 879-887.

Heckele, M. and Schomburg, W. K. 2004. Review on micro molding of thermoplastic polymers. *Journal of Micromechanics and Microengineering* 14(3).

Hellmeyer, H. O.,Lixfield, H. D. and Menges, G. 1977. Control of maximum pressure in the injection mould. *Kunstst Ger Plast* 67(4), pp. 4-6.

Heyderman, L. J.,Schift, H.,David, C.,Gobrecht, J. and Schweizer, T. 2000. Flow behaviour of thin polymer films used for hot embossing lithography. *Microelectronic Engineering* 54(3-4), pp. 229-245.

Homes, W. and Kabus, R. 2001. Controlling injection moulding processes in real time. *Kunststoffe Plast Europe* 91(1), pp. 29-30.

Hopkinson, N. and Dickens, P. 1999. Study of ejection forces in the AIM (TM) process. *Materials & Design* 20(2-3), pp. 99-105.

Hopkinson, N. and Dickens, P. 2000a. A comparison between stereolithography and aluminium injection moulding tooling. *Rapid Prototyping Journal* 6(4), pp. 253-258.

Hopkinson, N. and Dickens, P. 2000b. Predicting stereolithography injection mould tool behaviour using models to predict ejection force and tool strength. *International Journal of Production Research* 38(16), pp. 3747-3757.

Hopkinson, N. and Dickens, P. M. 2000c. Using stereolithography tools for injection moulding: research into tensile tool failure and unexpected benefits of the process. *Proceedings of the Institution of Mechanical Engineers, Part B: Journal of Engineering Manufacture* 214(10), pp. 891-899.

Huang, C. K.,Chen, S. W. and Yang, C. T. 2005. Accuracy and mechanical properties of multiparts produced in one mold in microinjection molding. *Polymer Engineering & Science* 45(11), pp. 1471-1478.

Huang, M. C. and Tai, C. C. 2001. The effective factors in the warpage problem of an injection-molded part with a thin shell feature. *Journal of Materials Processing Technology* 110(1), pp. 1-9.

Huang, M. S. 2007. Cavity pressure based grey prediction of the filling-to-packing switchover point for injection molding. *Journal of Materials Processing Technology* 183(2-3), pp. 419-424.

Jena, R. K.,Yue, C. Y. and Anand, L. 2011. Improvement of thermal bond strength and surface properties of Cyclic Olefin Copolymer (COC) based microfluidic device using the photo-grafting technique. *Sensors and Actuators, B: Chemical* 157(2), pp. 518-526.

Jensen, M. F.,McCormack, J. E.,Helbo, B.,Christensen, L. H.,Christensen, T. R. and Geschke, O. 2004. Rapid prototyping of polymer microsystems via excimer laser ablation of polymeric moulds. *Lab on a Chip - Miniaturisation for Chemistry and Biology* 4(4), pp. 391-395.

Kalima, V.,Pietarinen, J.,Siitonen, S.,Immonen, J.,Suvanto, M.,Kuittinen, M.,Mo?nkko?nen, K. and Pakkanen, T. T. 2007. Transparent thermoplastics: Replication of diffractive optical elements using micro-injection molding. *Optical Materials* 30(2), pp. 285-291.

Kao, C. C. and Shih, A. J. 2006. Sub-nanosecond monitoring of micro-hole electrical discharge machining pulses and modeling of discharge ringing. *International Journal of Machine Tools and Manufacture* 46(15), pp. 1996-2008.

Kazmer, D. and Barkan, P. 1997. The process capability of multi-cavity pressure control for the injection molding process. *Polymer Engineering and Science* 37(11), pp. 1880-1895.

Kelly, A. L.,Woodhead, M. and Coates, P. D. 2005. Comparison of injection molding machine performance. *Polymer Engineering & Science* 45(6), pp. 857-865.

Kemmann, O. and Weber, L. 2001. *Simulation of the Micro Injection Molding Process. Specialised molding techniques*. William Andrew Inc.

Kim, J. K.,Song, J. H.,Chung, S. T. and Kwon, T. H. 1997. Morphology and mechanical properties of injection molded articles with weld-lines. *Polymer Engineering & Science* 37(1), pp. 228-241.

Kim, S. M. and Kang, S. 2003. Replication qualities and optical properties of UV-moulded microlens arrays. *Journal of Physics D: Applied Physics* 36, pp. 2451-2456.

Knitter, R.,Bauer, W. and GÃ¶hring, D. 2003. Microfabrication of ceramics by rapid prototyping process chains. *Proceedings of the Institution of Mechanical Engineers, Part C: Journal of Mechanical Engineering Science* 217(1), pp. 41-52.

Kuek, S. C. and Angstadt, D. C. eds. 2007. *Process monitoring in micro-injection molding*. Proceedings of the ASME International Manufacturing Science and Engineering Conference 2007, MSEC2007. Atlanta, GA. pp. 163-170.

Kukla, C.,Loibl, H.,Detter, H. and Hannenheim, W. 1998. *Micro injection moulding – The aims of a project partnership.* Kunstoffe Plast. Europe. September 1998. pp. 6-7.

Kurt, M.,Saban Kamber, O.,Kaynak, Y.,Atakok, G. and Girit, O. 2009. Experimental investigation of plastic injection molding: Assessment of the effects of cavity pressure and mold temperature on the quality of the final products. *Materials and Design* 30(8), pp. 3217-3224.

Kussul, E. M.,Rachkovskij, D. A.,Baidyk, T. N. and Talayev, S. A. 1996. Micromechanical engineering: A basis for the low-cost manufacturing of mechanical microdevices using microequipment. *Journal of Micromechanics and Microengineering* 6(4), pp. 410-425.

Kwak, S.,Kim, T.,Park, S. and Lee, K. 2003. Layout and sizing of ejector pins for injection mould desian using the wavelet transform. *Proceedings of the Institution of Mechanical Engineers, Part B: Journal of Engineering Manufacture* 217(4), pp. 463-473.

Lalev, G.,Petkov, P.,Sykes, N.,Hirshy, H.,Velkova, V.,Dimov, S. and Barrow, D. 2009. Fabrication and validation of fused silica NIL templates incorporating different length scale features. *Microelectronic Engineering* 86(4-6), pp. 705-708.

Lee, H. S. 1997. Finite element analysis for the flow characteristics along the thickness direction in injection molding. *Polymer Engineering & Science* 37(3), pp. 559-567.

Levy, G. N.,Schindel, R. and Kruth, J. P. 2003. Rapid manufacturing and rapid tooling with layer manufacturing (LM) technologies, state of the art and future perspectives. *CIRP Annals - Manufacturing Technology* 52(2), pp. 589-609.

Li, W.,Minev, R.,Dimov, S. and Lalev, G. 2007. Patterning of amorphous and polycrystalline Ni78B14Si8 with a focused-ion-beam. *Applied Surface Science* 253(12), pp. 5404-5410.

Liou, A. C. and Chen, R. H. 2006. Injection molding of polymer micro- and sub-micron structures with high-aspect ratios. *International Journal of Advanced Manufacturing Technology* 28(11-12), pp. 1097-1103.

Liu, S.-J.,Wu, J.-Y.,Chang, J.-H. and Hung, S.-W. 2000. An experimental matrix design to optimize the weldline strength in injection molded parts. *Polymer Engineering & Science* 40(5), pp. 1256-1262.

Luo, S. Y.,Yu, T. H. and Hu, Y. C. 2007. Fabrication of micro nickel/diamond abrasive pellet array lapping tools using a LIGA-like technology. *Journal of Micromechanics and Microengineering* 17(6), pp. 1130-1138.

Madou, M. J. 2001. *Fundamentals of microfabrication: The Science Of Miniaturization*. 2nd ed. CRC Press.

Madou, M. J.,Lee, L. J.,Daunert, S.,Lai, S. and Shih, C.-H. 2001. Design and Fabrication of CD-like Microfluidic Platforms for Diagnostics: Microfluidic Functions. *Biomedical Microdevices* 3(3), pp. 245-254.

Martyn, M. T.,Whiteside, B.,Coates, P. D.,Allan, P. S. and Hornsby, P. eds. 2002. *Studies of the process-property interaction of the micromoulding process*. SPE ANTEC. 2002.

Maruo, S. and Ikuta, K. 2002. Submicron stereolithography for the production of freely movable mechanisms by using single-photon polymerization. *Sensors and Actuators, A: Physical* 100(1), pp. 70-76.

McFarland, A. W.,Poggi, M. A.,Bottomley, L. A. and Colton, J. S. 2004. Injection moulding of high aspect ratio micron-scale thickness polymeric microcantilevers. *Nanotechnology* 15(11), p. 1628.

McFarland, A. W.,Poggi, M. A.,Bottomley, L. A. and Colton, J. S. 2005. Injection-moulded scanning force microscopy probes. *Nanotechnology* 16(8), p. 1249.

McGraw-Hill 2003. *Dictionary of engineering* 2nd ed. The McGraw-Hill Companies Inc.

Menges, G. and Mohren, P. eds. 1993. *How to Make Injection Molds* 2nd ed. Hanser Gardner

Michaeli, W.,Hopmann, C. and Gruber, J. 2004a. Process control in injection moulding. *Prozessregelung beim spritzgieÃŸen* 94(1), pp. 20-24.

Michaeli, W.,Klaiber, F. and Scholz, S. G. eds. 2008. *Investigations in Variothermal Injection Moulding of Microstructures and Microstructured Surfaces*. 4M 2008, Fourth International Conference on Multi-Material Micro Manufacture. Cardiff, UK, September 09-11, 2008. Amsterdam, Netherlands: Whittles publishing, pp. 253-265.

Michaeli, W. and Schreiber, A. eds. 2009. *Advanced Process Control For Injection Molding Based On Cavity Pressure*. ANTEC 2009 - Proceedings of the 67th Annual Technical Conference & Exhibition. Chicago, IL, June 22 - 24. pp. 1704-1708.

Michaeli, W.,Spennemann, A. and GÃ¤rtner, R. 2004b. New plastification concepts for micro injection moulding. *Journal of Polymer Engineering* 24(1-3 SPEC. ISS.), pp. 81-93.

Michaeli, W. and Ziegmann, C. 2003. Micro assembly injection moulding for the generation of hybrid microstructures. *Microsystem Technologies* 9(6-7), pp. 427-430.

Mönkkönen, K.,Pakkanen, T. T.,Hietala, J.,Pääkkönen, E. J.,Pääkkönen, P.,Jääskeläinen, T. and Kaikuranta, T. 2002. Replication of sub-micron features using amorphous thermoplastics. *Polymer Engineering & Science* 42(7), pp. 1600-1608.

Montgomery, D. 2004a. *Design and Analysis of Experiments*. 6h edition ed. Wiley, pp. 1-450.

Montgomery, D. C. 2004b. *Introduction to Statistical Quality Control*. Hoboken, New Jersey: John Wiley & Sons Inc.

Morgan, M. J. 1999. *Engineering Thermodynamics*. Frank Kreith Boca Raton ed. CRC Press LLC.

N.N. 1965. *The principles of injection moulding*. ICI Plastics Technical Service Publication.

Navabpour, P.,Teer, D. G.,Hitt, D. J. and Gilbert, M. 2006. Evaluation of non-stick properties of magnetron-sputtered coatings for moulds used for the processing of polymers. *Surface and Coatings Technology* 201(6), pp. 3802-3809.

Nicoud, J. D. ed. 1995. *Microengineering: When is small too small? Nanoengineering: When is large too large?* Proceedings of the 1995 6th International Symposium on Micro Machine and Human Science. Nagoya, Jpn. IEEE, pp. 1-6.

Niggemann, M.,Ehrfeld, W.,Weber, L.,Günther, R. and Sollböhmer, O. 1999. Miniaturized plastic micro plates for applications in HTS. *Microsystem Technologies* 6(2), pp. 48-53.

Orzechowski, S.,Paris, A. and Dobbin, C. J. B. eds. 1998. *Process monitoring and control system for injection molding using nozzle-based pressure and temperature sensors*. Annual Technical Conference - ANTEC, Conference Proceedings. Atlanta, GA, USA. Soc Plast Eng, pp. 424-430.

Park, J. H.,Yang, K. M. and Kang, K. S. 2005. A quality function deployment methodology with signal and noise ratio for improvement of Wasserman's weights. *The International Journal of Advanced Manufacturing Technology* 26(5), pp. 631-637.

Park, K. and Ahn, J. H. 2004. Design of experiment considering two-way interactions and its application to injection molding processes with numerical analysis. *Journal of Materials Processing Technology* 146(2), pp. 221-227.

Petkov, P. V.,Scholz, S. G. and Dimov, S. S. eds. 2008. *Strategies for material removal in laser milling*. 4M 2008, Fourth International Conference on Multi-Material Micro Manufacture. Cardiff, September 09-11, 2008. Whittles Publishing, pp. 249-252.

Pham, D. T.,Dimov, S. S.,Bigot, S.,Ivanov, A. and Popov, K. 2004. Micro-EDM - Recent developments and research issues. *Journal of Materials Processing Technology* 149(1-3), pp. 50-57.

Pham, D. T.,Ivanov, A.,Bigot, S.,Popov, K. and Dimov, S. 2007a. An investigation of tube and rod electrode wear in micro EDM drilling. *International Journal of Advanced Manufacturing Technology* 33(1-2), pp. 103-109.

Pham, D. T.,Ivanov, A.,Bigot, S.,Popov, K. and Dimov, S. 2007b. A study of micro-electro discharge machining electrode wear. *Proceedings of the Institution of Mechanical Engineers, Part C: Journal of Mechanical Engineering Science* 221(5), pp. 605-612.

Phelan, F. R. 1997. Simulation of the injection process in resin transfer molding. *Polymer Composites* 18(4), pp. 460-476.

Piotter, V.,Mueller, K.,Plewa, K.,Ruprecht, R. and Hausselt, J. 2002. Performance and simulation of thermoplastic micro injection molding. *Microsystem Technologies* 8(6), pp. 387-390.

Pontes, A. J. and Pouzada, A. S. 2004. Ejection force in tubular injection moldings. Part I: Effect of processing conditions. *Polymer Engineering and Science* 44(5), pp. 891-897.

Pontes, A. J.,Pouzada, A. S.,Pantani, R. and Titomanlio, G. 2005. Ejection force of tubular injection moldings. Part II: A prediction model. *Polymer Engineering & Science* 45(3), pp. 325-332.

Popov, K.,Dimov, S.,Pham, D. and Ivanov, A. 2006. Micromilling strategies for machining thin features. *Proceedings of the Institution of Mechanical Engineers, Part C: Journal of Mechanical Engineering Science* 220(11), pp. 1677-1684.

Pouzada, A. S.,Ferreira, E. C. and Pontes, A. J. 2006. Friction properties of moulding thermoplastics. *Polymer Testing* 25(8), pp. 1017-1023.

Quintana, I.,Dobrev, T.,Aranzabe, A. and Lalev, G. eds. 2010. *Laser micromachining of metallic glasses. Investigation of the material response to machining with micro-second and pico-second lasers*. San Francisco, CA.

Rajitha, A.,Iuru, M. and Suresh, A. 2001. Simulation of injection molding into rapid-prototyped molds. *Rapid Prototyping Journal* 7(1), pp. 42-51.

Ratchev, S. and Turitto, M. 2008. *MINAM Strategic Research Agenda – Charting the Future of Micro- and Nanomanufacturing in Europe.* International Magazine on Smart Systems Technologies. pp. 9-10.

Rees, A.,Brousseau, E.,Dimov, S.,Gruber, H. and Paganetti, I. eds. 2008. *Wire electro discharge grinding: surface finish optimisation*. International Conference on Multi-Material Micro Manufacrure. Cardiff, 2008. Whittles Publishing Ltd, pp. 233-237.

Ribeiro Jr, A. S.,Hopkinson, N. and Ahrens, C. H. 2004. Thermal effects on stereolithography tools during injection moulding. *Rapid Prototyping Journal* 10(3), pp. 176-180.

Roopesh, M.,Suresh, A. G. and Fink, B. K. 1999. Use of genetic algorithms to optimize gate and vent locations for the resin transfer molding process. *Polymer Composites* 20(2), pp. 167-178.

Rosochowski, A. and Matuszak, A. 2000. Rapid tooling: the state of the art. *Journal of Materials Processing Technology* 106(1-3), pp. 191-198.

Rötting, O.,Röpke, W.,Becker, H. and Gärtner, C. 2002. Polymer microfabrication technologies. *Microsystem Technologies* 8(1), pp. 32-36.

Ruprecht, R.,Gietzelt, T.,Mueller, K.,Piotter, V. and Hausselt, J. 2002. Injection molding of microstructured components from plastics, metals and ceramics. *Microsystem Technologies* 8(4-5), pp. 351-358.

Saito, T.,Satoh, I. and Kurosaki, Y. 2002. A new concept of active temperature control for an injection molding process using infrared radiation heating. *Polymer Engineering & Science* 42(12), pp. 2418-2429.

Sasaki, T.,Koga, N.,Shirai, K.,Kobayashi, Y. and Toyoshima, A. 2000. An experimental study on ejection forces of injection molding. *Precision Engineering* 24(3), pp. 270-273.

Schnerr, O.,Kudlik, N. and Michaeli, W. eds. 1998. *Self-adaptive closed-loop cavity pressure control for injection moulding*. Annual Technical Conference - ANTEC, Conference Proceedings. Atlanta, GA, USA. Soc Plast Eng, pp. 410-413.

Scholz, S. G. 2007a. *Design and layout of a robot-inductor-system for the variothermal tempering of an injection mould by induction (SA).* Studienarbeit, RWTH Aachen University.

Scholz, S. G. 2007b. *Experimental series to verify the moulding accuracy of microstructures using a variothermal process control via an external inductive heating (DA).* Diplomarbeit / Master thesis, RWTH Aachen University.

Senturia, S. D. ed. 1994. *Feynman revisited*. Micro Electro Mechanical Systems, 1994, MEMS '94, Proceedings, IEEE Workshop on. 1994. pp. 309-312.

Sha, B.,Dimov, S.,Griffiths, C. and Packianather, M. S. 2007a. Investigation of micro-injection moulding: Factors affecting the replication quality. *Journal of Materials Processing Technology* 183(2-3), pp. 284-296.

Sha, B.,Dimov, S.,Griffiths, C. and Packianather, M. S. 2007b. Micro-injection moulding: Factors affecting the achievable aspect ratios. *International Journal of Advanced Manufacturing Technology* 33(1-2), pp. 147-156.

Shen, Y. K.,Chang, C. Y.,Shen, Y. S.,Hsu, S. C. and Wu, M. W. 2008. Analysis for microstructure of microlens arrays on micro-injection molding by numerical simulation. *International Communications in Heat and Mass Transfer* 35(6), pp. 723-727.

Shen, Y. K. and Wu, W. Y. 2002. An Analysis of the three-dimensional micro-injection molding. *International Communications in Heat and Mass Transfer* 29(3), pp. 423-431.

Shen, Y. K.,Yeh, S. L. and Chen, S. H. 2002. Three-dimensional non-newtonian computations of micro injection molding with the finite element method *International Communications in Heat and Mass Transfer* 29(5), pp. 643-652.

Stahl, J. and Koch, F. 2005. The cavity pressure profile must be right. *Der Werkzeuginnendruck-verlauf muss stimmen* 95(9), pp. 133-137.

Standard, I. 1985. Calibration specimens – Stylus instruments – Types, calibration and use of specimens.*ISO 5436-1985*. UK: BS 6393-1987.

Su, Y. C., Shah, J., and Lin, L. 2004. Implementation and analysis of polymetric microstructure replication by micro injection moulding. *Journal of Micromechanics and Microengineering* 14, pp. 415-422.

Tosello, G.,Fillon, B.,Azcarate, S.,Schoth, A.,Mattsson, L.,Griffiths, C.,Staemmler, L. and Bolt, P. J. 2007. Application of different process chains for polymer microfluidics fabrication including hybrid tooling technolgies,standardization and replication: a benchmark investigation within 4M Polymer Division. *4M 2007, Proceedings of third International Conference on Multi-Material Micro Manufacture*, pp. 77-80.

Tosello, G.,Gava, A.,Hansen, H. N. and Lucchetta, G. 2010. Study of process parameters effect on the filling phase of micro-injection moulding using weld lines as flow markers. *International Journal of Advanced Manufacturing Technology* 47(1-4), pp. 81-97.

Tsai, K. M.,Hsieh, C. Y. and Lo, W. C. 2009. A study of the effects of process parameters for injection molding on surface quality of optical lenses. *Journal of Materials Processing Technology* 209(7), pp. 3469-3477.

Tseng, S. C.,Chen, Y. C.,Kuo, C. L. and Shew, B. Y. 2005. A study of integration of LIGA and M-EDM technology on the microinjection molding of ink-jet printers' nozzle plates. *Microsystem Technologies* 12(1-2 SPEC. ISS.), pp. 116-119.

Uhlmann, E.,Piltz, S. and Doll, U. 2005. Machining of micro/miniature dies and moulds by electrical discharge machining--Recent development. *Journal of Materials Processing Technology* 167(2-3), pp. 488-493.

Weber, L.,Ehrfeld, W.,Freimuth, H.,Lacher, M.,Lehr, H. and Pech, B. eds. 1996. *Micromolding: a powerful tool for large-scale production of precise microstructures*. Austin, TX, USA. pp. 156-167.

Whiteside, B. R.,Martyn, M. T.,Coates, P. D.,Greenway, G.,Allen, P. and Hornsby, P. eds. 2003. *Micromoulding: Process characteristics and product properties*. Annual Technical Conference - ANTEC, Conference Proceedings. Nashville, TN. pp. 592-596.

Whiteside, B. R.,Spares, R.,Howell, K.,Martyn, M. T. and Coates, P. D. eds. 2005a. *In-process monitoring and 3d dimensional assessment of micromouldings*. Annual Technical Conference - ANTEC, Conference Proceedings. Boston, MA. pp. 83-87.

Whiteside, B. R.,Spares, R.,Howell, K.,Martyn, M. T. and Coates, P. D. 2005b. Micromoulding: extreme process monitoring and inline product assessment. *Plastics, Rubber and Composites* 34, pp. 380-386.

Wimberger-Friedl, R. ed. 2001. *Injection Molding of Sub-µm Grating Optical Elements* NY: William Andrew Publishing, pp. 78-83.

Worgull, M.,Heckele, M.,Hétu, J. F.,Kabanemi, K. K. and Heckele, M. eds. 2006. *Characterization of Friction during the Demolding of Microstructures Molded by Hot Embossing*. Symposium on Design, Test, Integration and Packaging of MEMS/MOEMS. 2006. TIMA Editions, p. 8 p.

Wu, C. H. and Liang, W. J. 2005. Effects of geometry and injection-molding parameters on weld-line strength. *Polymer Engineering and Science* 45(7), pp. 1021-1030.

Yang, H.,Segal, J.,Turitto, M. and Ratchev, S. eds. 2009. *Rapid manufacturing of micro fluidic devices by microstereolithography*. 4M/ICOMM 2009 - The Global Conference on Micro Manufacture. Karlsruhe, Germany, September 2009. pp. 157-160.

Yang, X.,Xu, C. and Kunieda, M. 2010. Miniaturization of WEDM using electrostatic induction feeding method. *Precision Engineering* 34(2), pp. 279-285.

Yao, D. and Kim, B. 2002. Injection molding high aspect ratio microfeatures. *Journal of Injection Molding Technology* 6(1), pp. 11-17.

Yao, D. and Kim, B. 2004. Scaling Issues in Miniaturization of Injection Molded Parts. *Journal of Manufacturing Science and Engineering* 126(4), pp. 733-739.

Yokoi, H.,Man, X.,Takahashi, T. and Kim, W. K. 2006. Effects of molding conditions on transcription molding of microscale prism patterns using ultra-high-speed injection molding. *Polymer Engineering and Science* 46(9), pp. 1140-1146.

Yokoi, H.,Masuda, N. and Mitsuhata, H. 2002. Visualization analysis of flow front behavior during filling process of injection mold cavity by two-axis tracking system. *Journal of Materials Processing Technology* 130-131, pp. 328-333.

Yoshii, M. and Kuramoto, H. 1994. Experimental study of transcription of minute width grooves in injection moulding. *Polymer Engineering and Science* 34(15), pp. 1211-1218.

Yoshii, M.,Kuramoto, H.,Kawana, T. and Kato, K. 1996. The observation and origin of micro flow marks in the precision injection molding of polycarbonate. *Polymer Engineering & Science* 36(6), pp. 819-826.

Young, W. B. 2005. Effect of process parameters on injection compression molding of pickup lens. *Applied Mathematical Modelling* 29(10), pp. 955-971.

Yuan, S.,Hung, N. P.,Ngoi, B. K. A. and Ali, M. Y. 2003. Development of micro replication process. *Journal of Materials and Manufacturing Processes* 18, pp. 731-751.

Zauner, R. 2006. Micro powder injection moulding. *Microelectronic Engineering* 83(4-9 SPEC. ISS.), pp. 1442-1444.

Zhang, X.,Jiang, X. N. and Sun, C. 1999. Micro-stereolithography of polymeric and ceramic microstructures. *Sensors and Actuators, A: Physical* 77(2), pp. 149-156.

Zhao, J.,Lu, X.,Chen, Y.,Chow, L. K.,Chen, G.,Zhao, W. and Samper, V. 2005. A new liquid crystalline polymer based processing aid and its effects on micro-molding process. *Journal of Materials Processing Technology* 168(2), pp. 308-315.

Zhao, J.,Mayes, R. H.,Chen, G.,Chan, P. S. and Xiong, Z. J. 2003a. Polymer micromould design and micromoulding process. *Plastics, Rubber and Composites* 32, pp. 240-247.

Zhao, J.,Mayes, R. H.,Chen, G.,Xie, H. and Chan, P. S. 2003b. Effects of process parameters on the micro molding process. *Polymer Engineering & Science* 43(9), pp. 1542-1554.

Zhao, R. and Macosko, C. W. 2002 Slip at Molten Polymer Polymer Interfaces. *Journal of Rheology* 46(1), pp. 145-167.

Zheng, R.,Kennedy, P.,Phan-Thien, N. and Fan, X. J. 1999. Thermoviscoelastic simulation of thermally and pressure-induced stresses in injection moulding for the prediction of shrinkage and warpage for fibre-reinforced thermoplastics. *Journal of Non-Newtonian Fluid Mechanics* 84(2-3), pp. 159-190.

Zhou, H. and Li, D. 2006. Integrated simulation of the injection molding process with stereolithography molds. *International Journal of Advanced Manufacturing Technology* 28(1-2), pp. 53-60.